POSITRON ANNIHILATION IN CADMIUM AND ZINC

ANTHONY A. BERRY

B.Sc.(Hons),St.Andrews

A Thesis Submitted for the Degree of

DOCTOR OF PHILOSOPHY

in the

UNIVERSITY OF LONDON

Physics Department

Bedford College

London

1982

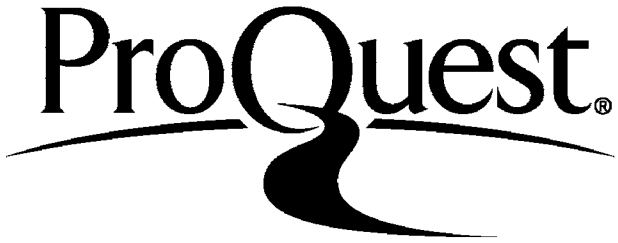

DEDICATION

==========

TO ELIZABETH

ABSTRACT

========

A study of Doppler broadened annihilation quanta arising from the interaction of thermalised positrons with the electrons of metallic lattices has been made.The study embraced single crystal specimens of cadmium and zinc and a deformed polycrystalline specimen of cadmium.A high resolution intrinsic germanium gamme-ray detector was employed.

The single crystal studies were carried out for the [ØØØ1] and [1Ø$\bar{1}$Ø] directions over the temperature range from 4.2K to 58ØK in the case of cadmium and from 4.2K to 6ØØK in the case of zinc.Both these studies reveal anisotropies in the temperature dependencies of the annihilation characteristics derived from the gamma-ray lineshapes.The origin of these anisotropies is discussed with reference to the coefficients of thermal expansion in the relevant directions.Monovacancy formation parameters are deduced for both orientations of each specimen by means of a two state trapping model and by means of a self-trapping model.In the case of cadmium,a comparison is made of the observed anisotropies arising from two distinct specimens.

The study of the deformed specimen of polycrystalline cadmium here presented embraced the temperature range 4.2K to 580K and included a room temperature deformation followed by annealing and a subsequent deformation at liquid nitrogen temperatures.As the annealing subsequent to this latter deformation progressed,observations were made at low temperatures in order to investigate the possible temperature dependence of the positron trapping rate.A convolution procedure based on the superposition of a Gaussian function and an inverted parabola was employed to describe the annihilation lineshapes arising from this specimen in an effort to investigate,by means of the associated zero point motion,the nature of the deformation-induced traps.The results derived from this analysis are discussed.

ACKNOWLEDGEMENTS

==========

I am very grateful to Dr.P.Rice-Evans for his supervision of this work, for his valuable assistance and his encouragement. I should also like to take this opportunity of thanking Professor E.R.Dobbs for his interest in the work.

To Drs.M.Lea, B.Cowan and P.Fozooni, I should like to express my thanks for advice and assistance.

It is a pleasure to acknowledge the generous help of the previous members of the positron group, Drs.I.Chaglar and F.A.el Khangi, who provided much support and valuable assistance.

I should also like to thank Messrs.W.Baldock, A.Betts, J.Sales, F.Greenhough and D.Gower for the technical assistance which they provided throughout this work. I also acknowledge the debt I owe to Messrs.F.Grimes and A.King of the Physics Department workshop for their forbearance and generous assistance. I should also like to express my gratitude to Mrs.S.Pearson and Miss P.Franklyn for administrative support.

I am grateful to the members of the Bedford College computer unit, in particular to Dr.P.Pal for the provision of the facilities of the VAX 11/78Ø on which machine this work was typed and processed; also to Messrs.M.Datko, L.Nodes, G.Rock, C.Kirton and D.Edmiston. I should also like to thank Mr.E.Caesar of the University of London Reactor Centre for his co-operation.

Finally, I should like to thank the SERC for the provision of financial assistance, without which I should have been unable to undertake this work.

INDEX

CHAPTER 3: INVESTIGATION OF DEFECTS BY POSITRON ANNIHILATION ...46

1.1: INTRODUCTION

The existence of the positron was predicted by Dirac [1] and observed experimentally by Anderson [2] in a bubble chamber exposed to cosmic radiation.

An initially energetic positron from a radioactive source on entering condensed matter is rapidly slowed down to thermal energies by collisions with electrons and ions. After a time, which is dependent on the specimen, it annihilates with an electron, the total rest mass of the pair being converted into electromagnetic radiation. The time lapse between the entry of the positron and its subsequent annihilation, the energies and the momenta of these emergent photons are almost entirely dependent on the initial state of the positron-many-electron system.

Early experiments [3] revealed that, in the case of two photon annihilation, the photons are radiated in almost exactly opposite directions. Subsequent more precise measurements [4] determined the extent of this departure from collinearity as 1/137 radians. There are many published reviews of the application of the positron annihilation technique to the study of condensed media, some

examples of which are [5-9].

In some materials, a positron may become bound to an electron to form the positronium atom. The subsequent decay of this atom is determined not only by its interactions with the host medium but also by the possible states of the atom itself.

1.2: POSITRON ANNIHILATION MODES

The probabilities of the various modes of annihilation of slow positron- electron pairs are governed by selection rules drawn from fundamental Quantum Electrodynamics [10]. Conservation of momentum requires that both the one- and three-photon annihilation processes take place only in proximity to a body(quanta or particle) additional to the photons i.e. an electron or nucleus by which the recoil momentum may be absorbed. This requirement reduces the cross-section for these processes relative to that of the two-photon annihilation case. It can be shown from this [7], that the probability of either one- or three-photon annihilation is considerably smaller than that for two-photon annihilation.

For the two-photon process, the annihilation probability per unit time or annihilation rate λ for a non-relativistic positron and a stationary electron is obtained from the cross-section for the event [1]. This yields

$$\lambda = \pi r_o^2 c n_e \qquad 1.1$$

where $\sigma_2 = \frac{\pi r_o^2 c}{v}$ and r_o is the classical electron radius, c the velocity of light, v is the positron velocity, σ_2 the cross-section for two-photon annihilation and n_e the electron density at the positron site. It can be seen that this rate is independent of the positron velocity. Thus, by measuring the mean positron lifetime τ, which is the inverse of the annihilation rate, information can be obtained on the electron density experienced by the positron. The range of values obtained for the mean positron lifetime in metals is 100picoseconds to 500picoseconds [11, 12, 13].

As has been mentioned, the annihilating pair has a non-zero momentum which results in the departure from collinearity of the annihilation photons. This kinetic energy is of the order of a few electron volts. From [7], the extent of the resulting angular departure, $\delta\theta$, is

$$\tan \delta\theta \simeq \delta\theta = \frac{P_T}{M_o c} \qquad 1.3$$

where p_T is the momentum of the positron-electron pair transverse to the direction of emission and m_o, the electron rest mass. Typically $\delta\theta$ is of the order of a few

milliradians and the approximation is valid. Thus, since the positron velocity is negligible, the transverse momentum is dependent only on that of the electron. Measurement of the angular deviation of the photons thus yields information on the momentum distribution of the participating electrons.

The non-zero momentum of the annihlating pair also causes a Doppler shift ΔE, in the energy of the photons. Again from [7], this is given by,

$$\Delta E = \pm \frac{cp_L}{2} \qquad 1.4$$

where p_L is the longitudinal momentum component of the positron-electron pair. Measurement of this broadening of the annihilation line produces information similar to that obtained in angular correlation studies.

1.3: POSITRONIUM FORMATION AND ANNIHILATION

As has briefly been discussed, the bound state of a positron-electron pair i.e. the positronium atom, may be formed by the capture of an electron by a positron. Positronium formation according to [5] is relevant only to those molecular materials in which electron exchange is restricted to individual molecules and the prevailing covalent forces are repulsive.

The Ore-gap model is commonly used to describe the energetics of positronium formation [14]. In this it is stated that the probability of positronium formation is highest when, as a result of its loss of energy on its passage through the material, the positron energy lies within limits between which no other electronic energy transfer process is possible. The capture of an electron by a positron from the medium can only take place when the positron energy, E_p , is greater than the net difference between the ionisation eneregy, E_I , of the medium and the binding energy of the positronium atom, E_B . This binding energy has the value 6.8eV in vacuum but may be less in matter. However, if the positron energy were larger than the ionisation energy, the kinetic energy of the positronium atom formed would be greater than its binding energy and the atom would rapidly break up in collisions. Also, the process of inelastic scattering would compete with that of positronium formation until the energy of the positron were less than E_{EX} , the lowest excitation energy. Thus the formation of positronium is most probable for positron energies in the range,

$$E_{ex} > E_p > E_I - E_B \qquad 1.5$$

This energy range is known as the Ore-gap.

There are two ground states of the positronium atom, parapositronium and orthopositronium. Parapositronium is the singlet ^1S state in which both the orbital angular momentum, l, and the total spin, s, are zero; while orthopositronium, the triplet ^3S state has l=Ø and s=1 .

As a result of its total spin being unity, this latter state cannot decay into two photons [15]. The decay modes are further constrained by the principles of conservation of parity.

From [10], the charge parity of the positron-electron system is given as,

$$C = p_i P_\ell P_S \qquad 1.6$$

wher p_i is the intrinsic parity, which is negative for particle-antiparticle pairs, $p_\ell = (-1)^\ell$ is the spatial parity and p_S, the spin parity$=(-1)^{S+1}$. Hence for the positronium atom,

$$C = (-1)^{\ell+S+2} \qquad 1.7$$

$=+1$ for the singlet state

$=-1$ for the triplet state

Since the charge parity of the photons is negative, we have for a system of n photons,

$$C = (-1)^n \qquad 1.8$$

Thus, from the conservation of charge parity we have the result that the singlet state, parapositronium, decays into an even number of photons while orthopositronium decays into an odd number of quanta. Recalling the conclusions of section 1.2, it follows that parapositronium decays mainly into two photons while the decay of orthopositronium is dominated by three photon emission.

The wave functions of the positronium ground state have the form,

$$\psi(r) = (\pi a^3)^{-\frac{1}{2}} \exp(-r/a) \qquad 1.9$$

where r is the relative co-ordinate and $a = 2h^2/m_o c^2$, is the Bohr radius of positronium which is twice that of hydrogen since the reduced mass is $m_o/2$.

From equation 1.1, we have that,

$$\lambda = \pi r_o^2 c n_e \qquad 1.1$$

This was derived by averaging over four spins while in the case of positronium only one of the states can undergo two-photon decay. Thus, in such a case i.e. for parapositronium, it can be deduced that the decay rate is given by,

$$\lambda_{para} = 4\pi r_o^2 c |\psi(0)|^2 \qquad 1.10$$

where $|\psi(0)|^2 = (\pi a^3)^{-1}$ is the electron density at the positron site. By substitution of values for r_o and a, we obtain the annihilation rate for parapositronium and thus its lifetime:

$$\tau_{para} = \lambda^{-1}_{para} = 123 \text{ picoseconds} \qquad 1.11$$

Similarly, using the relationship for the spin average cross-section for three-photon annihilation [10]:

$$\sigma_3 = \frac{4(\pi^2-9) r_o^2 c\alpha}{3v} \qquad 1.12$$

where α is the fine structure constant $=1/137$, we have:

$$\tau_{ortho} = \lambda^{-1}_{ortho} = (\sigma_3 v n_e)^{-1} \simeq 140 \text{ nanoseconds} \qquad 1.13$$

It can be seen from the relative cross-sections (equations 1.2, 1.12) that the ratio of three- to two-photon annihilation events is $\sim 1/370$. However, the availability of states dictates that the fraction of three-photon events will be larger than predicted by this. Nevertheless, decay from the orthopositronium states is in competition with more rapid mechanisms resulting from interactions of the positronium atom with other electrons and atoms of the medium. Such a mechanism is "pick-off" annihilation in which the positron in the orthopositronium atom undergoes two-photon annihilation with an external electron having anti-parallel spin. Further causes of reduction of the three- to two- photon annihilation ratio include orthopositronium to parapositronium conversion, a process which can be enhanced by the application of a magnetic field.

Chapter 2: POSITRON ANNIHILATION MODES

2.1: POSITRON THERMALISATION AND MOBILITY

Positrons emitted from the radio-isotopes commonly used in the investigation of positron annihilation: ^{64}Cu, ^{22}Na, ^{58}Co, have beta-energy spectra with a maximum value, E(max), of the order of Ø.6MeV (table 2.1). On entry into a solid specimen, the positron will rapidly lose most of its energy, primarily as a result of collisions with the electrons of the medium. Each of such collisions, for positron energies greater than that typically required for the promotion of an electron to an excited state, will result in the positron losing approximately half its initial energy. Thus the time taken for the positron energy to drop to a few electron volts, assuming a distance between collisions of the order of a lattice spacing, can be shown to be approximately $1Ø^{-15}$ seconds. Early work [16], suggested that the time required for the reduction of the positron energy in a metal to thermal values(~Ø.Ø25eV) was approximately 3 picoseconds, which is considerably shorter than experimentally observed positron lifetimes.

Source	Half-Life	E(max) [MeV]	Surface Density (mg/cm^2)
Na-22	2.5y	Ø.54	24
Co-55	18.2h	1.5Ø	1Ø5
Co-58	71.3d	Ø.48	21
Cu-64	12.9h	Ø.65	32
Ge-68	275d	1.9Ø	147

Table 2.1: Commonly used positron sources, their half-lives, energies and surface densities.

The effective temperature of the positron was defined [17] through the study of the momentum distribution of the annihilation photons in the Fermi momentum "cut-off" region of the angular correlation curve. These measurements, made in metals having low electronic densities, provided evidence of thermalisation at temperatures greater than 100K but did not support the early theory for temperatures lower than this. The same study revealed the positron effective mass. The recognition of the fact that the latter stages of the thermalisation process account for almost all of the thermalisation time and the consideration of positron energy loss through the excitation of electron-hole pairs [18] suggested that the thermalisation times were larger and more significant in comparison with the measured lifetimes and, in some low temperature cases, were in excess of the positron lifetime.

A theoretical argument was proposed [19] compatible with the experimental findings of [17] in which the positron annihilates from a non-equilibrium state. However as was indicated in [20] phonon-scattering is an important factor in the expedition of the final stages of positron thermalisation. This theory was supported by the angular correlation measurements [21], in which it was observed that positrons in metals do in fact thermalise before annihilation even at temperatures approaching that of liquid helium.

The effective mass of the positron, m_+^*, can be deduced from experiments such as [17] and is a result of the combination of static positron-lattice interactions (band mass), positron-phonon scattering [22] and positron-electron interactions (many-body mass) [23, 24]. Theoretical predictions of the combined effect of these interactions yield $m_+^*=1.2m$, where m is the rest mass of the electron, for alkali metals [20, 25, 26].

The extent to which a positron penetrates a solid is given [27, 28] by

$$\delta P(x) = \alpha_+ \exp(-\alpha_+ x)\delta x \qquad 2.1$$

where $\delta P(x)$ is the probability that the positron thermalises at a distance between x and $x+\delta x$ from the specimen surface, and α_+ is a mass absorption co-efficient given by

$$\alpha_+ = (16 \pm 1)\frac{\rho}{E_{max}^{1.43}} \qquad 2.2$$

where α_+ has the units cm^{-1}, ρ is the density of the specimen in g cm^{-3} and E(max), the maximum kinetic energy of the positron is in MeV. Thus for a solid specimen, the typical implantation range, $r=(\alpha)^{-1}$, is of the order of a tenth of a millimetre.

The motion of a positron in a solid is determined by its interactions with the electrons and the lattice and by impurity scattering. As a result of experimental difficulties, few direct measurements of the positron mobility in condensed matter exist. The mobility in

germanium has been determined [29] by measurements of the Doppler shift in the energies of the annihilation quanta as a function of the electric field across an intrinsic germanium solid-state detector. The mobility in silicon was determined by the application of a similar technique [30]. The mobility, μ , and the diffusion constant, D, are defined via the Einstein relation,

$$D = \mu . \frac{kT}{e} \qquad 2.3$$

where e is the electronic charge. In most cases, the mobility of a positron in an insulator is a few percent of the electron mobility at a similar temperature.

Observation of positron mobility in metals is prohibitively difficult. Theoretical estimates have been made of the various contributions to the mobility in simple metals [31]. The inverse of the relaxation time corresponding to scattering by conduction electrons near the Fermi surface is given by,

$$(\tau_e)^{-1} = \frac{\pi}{4} \frac{m^*}{m} \frac{(kT)^2}{\hbar E_F} \qquad 2.4$$

where E_F is the Fermi energy. Scattering by acoustic phonons contributes a relaxation time $\bar{\tau}_{ph}$ which is proportional to $(kT)^{-3/2}$ and the relaxation time due to impurity scattering goes with $(kT)^{-1/2}$. The mean free path of a positron in a pure metal is given as,

$$\ell = \left(\frac{3kT}{m^*}\right)^{\frac{1}{2}} \left(\frac{1}{\tau_e} + \frac{1}{\tau_{ph}}\right)^{-1} = \frac{3D}{V} \qquad 2.5$$

where v is the thermal velocity of the positron. The

average diffusion length before annihilation is given as,

$$L = (6D\tau)^{\frac{1}{2}} \qquad 2.6$$

where $\bar{\tau}$ is the positron lifetime. Typical values for these parameters in pure metals are:

$$\bar{\tau}_{ph} \sim 10^{-14} \text{ seconds}, \ \bar{\tau}_{e} \sim 10^{-12} \text{ seconds};$$

$$\mu \sim 20 \text{cm}^2 \text{ v}^{-1} \text{ s}^{-1}; D \sim 0.5 \text{ cm}^2 \text{ s}^{-1}; \qquad \mathcal{D}$$

$$L \sim 3 \times 10^3 \text{ Å}; l \sim 20 \text{ Å}.$$

It can be seen that the mobility is limited by phonon scattering at all practical temperatures and that, because of the insignificance of the electronic contribution, the corresponding diffusion constants are of the same order of magnitude in metals as in insulators.

2.2: POSITRON TECHNIQUES

2.2.1: Positron Lifetimes

The lifetime technique seeks to gauge the electronic density at the site of the annihilation of the positron.

A convenient positron source for lifetime spectroscopy is ^{22}Na which emits a 1.28MeV gamma-ray simultaneous to the emission of a positron. The annihilation process is announced by the emergence of two 511keV photons. A fast-slow coincidence system, figure 2.1,

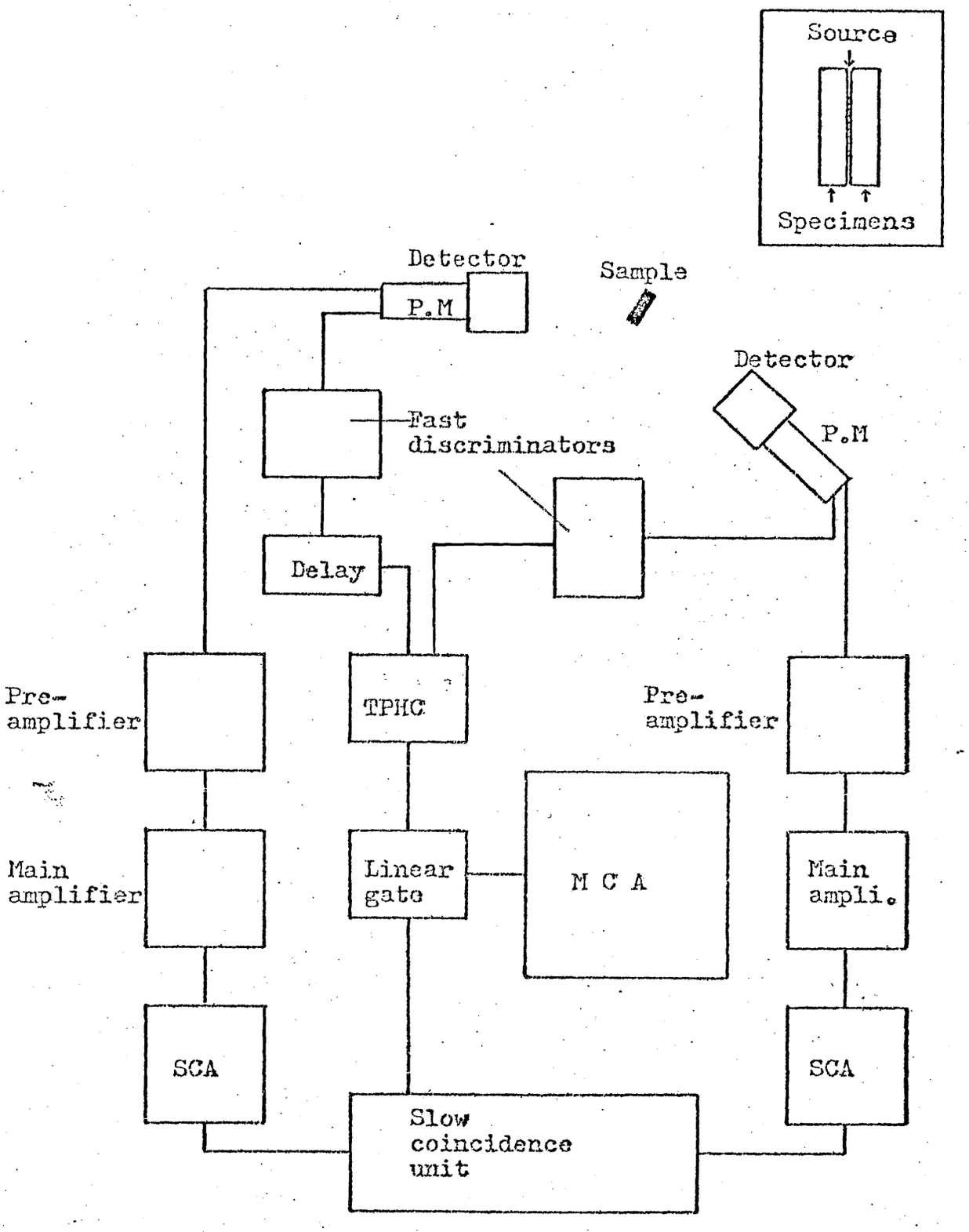

Figure 2.1: A schematic diagram of a typical system for the measurement of positron lifetimes.

records the resulting annihilation time spectrum. Detailed reviews of the technique are given in [32, 33, 34].

The detection system used in the measurement of positron lifetimes consists of a pair of fast plastic scintillators which are coupled to fast photo-multiplier tubes. The two slow channels in such a spectroscopy system each make use of a single channel analyser, the energy window of one channel being set to detect the 1.28MeV gamma-ray while that of the other is focussed on the 511keV photon. Fast signals from the photo-multiplier anodes are processed by timing discriminators to produce well-defined pulses so as to mark accurately the time of occurrence of each detected event. A time to pulse height convertor generates a pulse whose amplitude is proportional to the time delay between a pair of coincident events. This pulse is transferred for storage to a multi-channel analyser through a gate which is driven by coincidences in the slow channel. Thus the event is recorded only if the signals satisfy the energy criteria of the single channel analysers.

Ideally, the random and systematic errors in the measurement process should be much smaller than the measured delays. In practice, the stored spectrum is significantly smeared by such errors and can be regarded as the convolution of the real spectrum with the instrumental resolution function. This intrinsic time resolution function can be closely approximated to by replacing the positron source with one such as ^{60}Co which emits two

simultaneous gamma-rays. Typical values of intrinsic resolutions obtained using commercial lifetime systems are around 200 to 300 picoseconds and an example of the best resolution currently attainable is [35] in which a full width at half maximum of 170 picoseconds is reported. The mechanisms which have significant effect on the limits to which the intrinsic resolution can be reduced are the decay time of the light centres in the scintillators themselves and also the transit time spread of the electrons in the photo-multipliers.

If the lifetime to be measured is large compared with the width of the prompt resolution curve, the distribution of time intervals between events is an exponential decay curve proportional to $\exp(-t/\tau)$. In practice, the finite width of the instrumental time resolution function causes smearing of this decay curve. There are two principal methods of analysis of data from such experiments.

If there are several states from which the positrons annihilate, as in the case of a defected sample, the resulting spectrum is the sum of several exponential decay components, the whole being convoluted with the instrumental resolution function. In order to analyse such a spectrum it is necessary to construct a function from trial decay functions, and then to convolute this with the observed resolution function before fitting to the data in order to obtain the lifetime and relative intensity of each

of the components. The computer programs required for such tasks [36, 37], are large and problems arise in such fitting techniques particularly if the decay values of the components are not very different one from another.

If however, the positron decay can be described by a single component, as in the case of an annealed metal, the lifetime of the positron in the free state is given by the difference between the centroids of the positron decay function and the instrumental resolution function. The precision required for such measurements demands that the electronic stability of such a spectrometer be of a high order [38]. Further uncertainties resulting from annihilation within the source and variations in source-system geometry affect the reliability of the measurements. In this latter respect a procedure by which the prompt and delayed spectra are collected simultaneously, [39], is of significance.

2.2.2: Angular Correlation of Annihilation Radiation

One of the primary interests in positron annihilation has been the study of the two-photon angular correlation [4]. By collecting the coincident counts at 511keV as a function of the angular displacement between the two detectors, information is obtained on the momentum distribution of the centre-of-mass of the annihilating

electron-positron pair. The technique is examined in [6, 40].

If both the electron and the positron are at rest the principles of conservation of energy and momentum demand that, in two- photon annihilation, the gamma-rays are emitted with exactly the same energy, $E_\gamma = m_o c^2$, and in exactly opposite directions with linear momentum, $p_\gamma = m_o c$. If however, the annihilating pair has a non-vanishing linear momentum, the symmetry is lost and the angle between the direction of emission departs from 180°. Recalling equation 1.3, this small angular departure is given by,

$$\delta\theta = \frac{P_T}{M_o c} \qquad 1.3$$

where p_T, is the momentum component transverse to the emission direction of the annihilation photons.

Figure 2.2 illustrates a typical system by which the angular correlation of the two annihilation photons may be measured. The sources employed are of much higher activity (10mCi-1Ci) than those used for either the measurement of positron lifetime or the Doppler broadening of the annihilation linewidth. The commonly used isotopes are ^{22}Na, ^{64}Cu, ^{58}Co and, as can be seen from figure 2.2, the source is remote from the specimen in order to shield the detectors from direct view of the source. Photons resulting from the annihilation of positrons in the specimen are detected by a pair of NaI scintillators, the single channel analyser in each channel being set such that only coincident 511keV photons are counted.

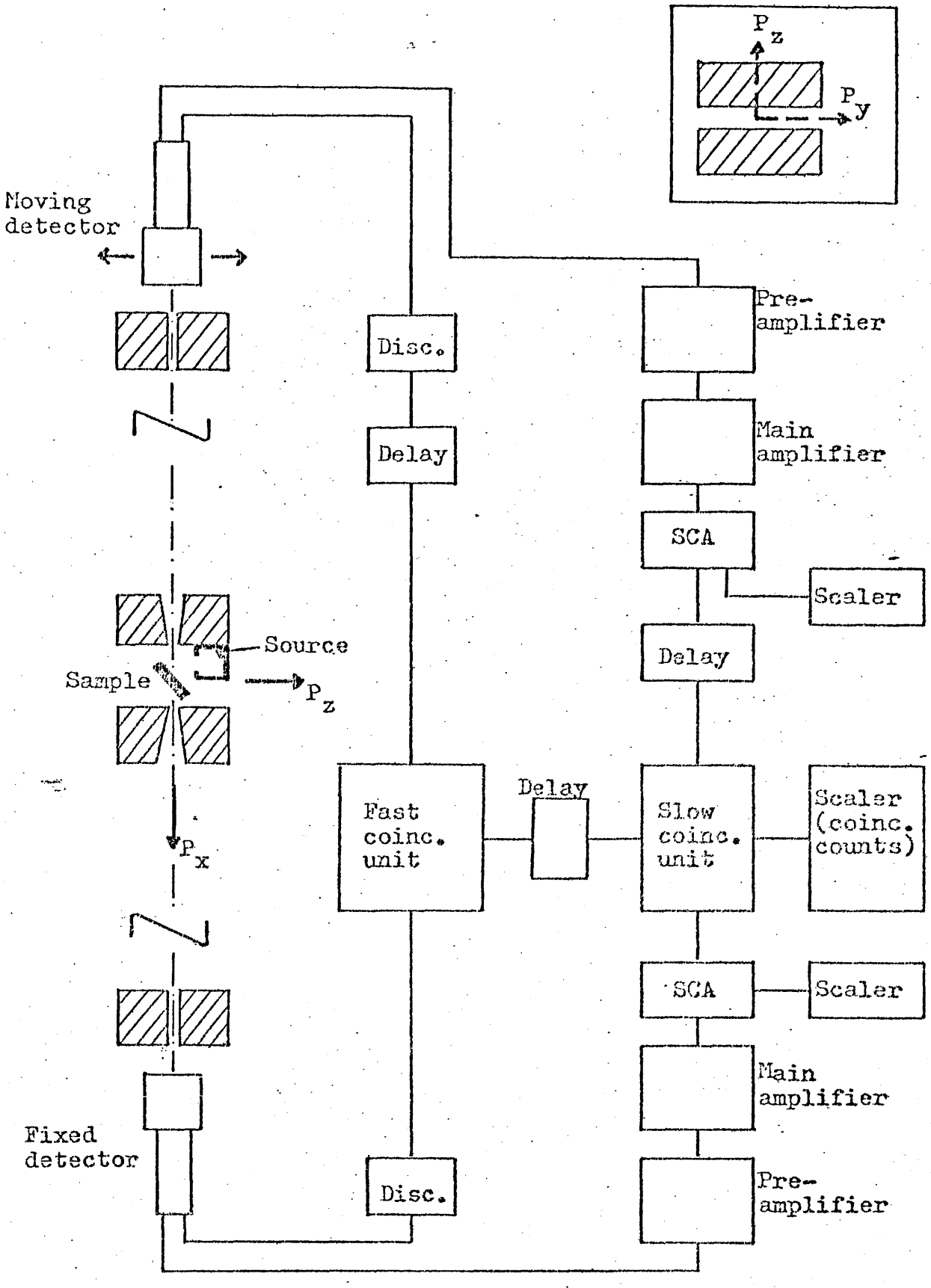

Figure 2.2: A schematic diagram of a typical angular correlation system.

The intrinsic angular resolution of such a system is defined by the lead collimators in front of the detectors. In order to achieve an angular resolution of less than Ø.5mrad, which is typical of angular correlation spectrometers, the distance between the detectors is several metres. An inconvenience of a coincidence technique such as this is the low counting rate, the amelioration of which is partly achieved by making the collimators as long as possible in the x-direction.

This long-slit configuration [41] resolves neither the angular distribution in the x-direction nor the Doppler shift in the y-direction. The counting rate is given by [42],

$$N_z(\theta) = \text{const.} \int_{-\infty}^{\infty} \int_{-\infty}^{\infty} \Gamma(p_x, p_y, m_o c\theta_z)\, dp_x dp_y \qquad 2.7$$

where $\Gamma(p_x, p_y, p_z)$ is the momentum distribution of the annihilating positron-electron pairs in the specimen. If the positron is assumed to be in thermal equilibrium with the specimen and to be in the free state, it has negligible momentum. Thus, the angular correlation curve represents the p_z-distribution of the electrons participating in the annihilation events. Unlike positron lifetime [4, 6, 43], angular correlation curves are almost insensitive to many-body effects, a circumstance which allows for their interpretation by means of the Independent Particle Model, and, as such, they are particularly suitable to studies of momentum densities and Fermi surfaces.

An angular correlation curve can readily be recognized as the sum of two components: an inverted parabola which can be equated to positron annihilation with a gas of free electrons [8] and is a result of positron interaction with the conduction electrons, superimposed on a broader component due to annihilations with core electrons. This latter component is often approximated to by a Gaussian function . The momentum at the Fermi surface can be obtained from the curve at the point at which these two components intersect since there is a cut-off in the valence electron momentum contribution at the Fermi surface. Another application of the technique is that of measuring the peak counting rate, H, as a function of temperature in order to assess the temperature induced changes in the core to valence annihilation ratio [44,45].

More detailed information can be obtained using point detectors which resolve two of the three momentum components according to

$$N(\theta_y,\theta_z) = \text{const.} \int_{-\infty}^{\infty} dp_x \Gamma(p) \qquad 2.8$$

An early design which employed point detectors [46] was successful in extracting more detail but suffered from very poor counting rates. Developments in two-dimensional detector arrays however hold the promise of the optimisation of increased resolution and statistical efficiency.

2.2.3: Doppler Broadening

As discussed in section 1.2, a Doppler shift in the energy of annihilation radiation is caused by the motion of the positron-electron pair. This results in the broadening of the 511keV spectral line and thus this lineshape gives the distribution of the longitudinal component of the annihilating pair. The detailed study of these lineshapes was initially facilitated by the use of Ge(Li) detectors [47, 48] and applied to the investigation of defects in metals by MacKenzie et al [49-51]. An example of the system generally used in Doppler broadening studies is shown in figure 2.3 .

The energy distribution of the annihilation radiation is given by,

$$E = m_o c^2 (1 \pm \frac{Vcm}{c}) \qquad 2.9$$

where v_{cm} is the centre-of-mass velocity of the positron-electron pair. For thermalised positrons annihilating in a gas of free electrons having Fermi velocity, v_F, this distribution is:

$$E = m_o c^2 (1 \pm \frac{V_F}{2c}) \qquad 2.10$$

which is a parabola centred at $E = m_o c^2$. For annihilation with core electrons, because of the fact that on average their velocities are higher, the extent of the resultant

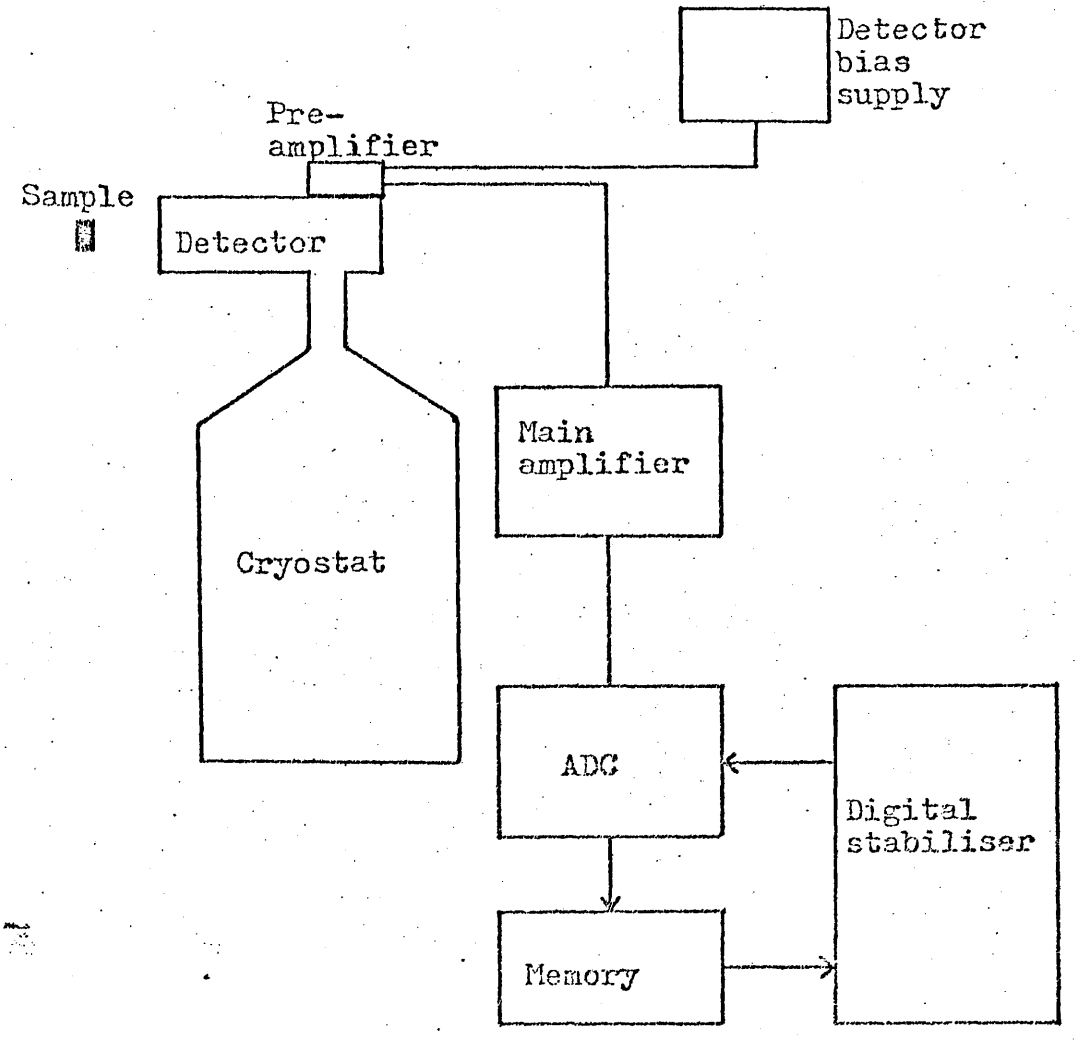

Figure 2.3: A schematic diagram of a typical Doppler broadening system.

broadening of the distribution is greater and, as in the case of angular correlation studies, is usually represented as a Gaussian.

The energy distribution of the 511keV radiation obtained in Doppler broadening studies is equivalent to the angular correlation measurements acquired using the long-slit geometry since both the techniques seek to measure changes in the electron momentum distribution. However the resolution which can be achieved in Doppler broadening studies by the use of even the best available solid-state detectors is considerably inferior to that obtained in angular correlation measurements. The measurements of the two techniques are related by,

$$\delta\theta = 2\,\frac{\Delta E}{m_o c^2} \qquad 2.11$$

Thus, for a solid-state detector having a resolution of 1keV at 511keV, the corresponding angular resolution is approximately 4 mradians i.e. a factor of ten poorer than that of an angular correlation arrangement. A further limitation is the requirement for a high order of electronic stability since even a relatively small drift during measurement in the position of the 511keV line can severely degrade the data obtained.

The Doppler broadening technique has however compensating features. It has the advantage over angular correlation experiments in that the spectrometer is very much simpler, requiring only one detector and no coincidence circuitry. As a result, it allows for rapid data

accumulation with a concomitant improvement in counting statistics. These features compensate at least in part for the poor resolution and for example, in the study of annealing mechanisms, can outweigh the resolution consideration.

As has been indicated, the resolution of the lineshape is inadequate for the study of momentum densities. Computing procedures exist by which the resolution function of the spectrometer, as measured by the system response to a mono-energetic gamma such as ^{85}Sr, can be deconvoluted from the data [52,53]. However, such techniques are costly in terms of computing time and can be unreliable. A more common method of data analysis is the use of one or more of the various lineshape parameters devised for use in Doppler broadening studies [54]. While the values of these parameters are not absolute, the changes in their values can be employed in the study of, for example, changing defect concentrations in a specimen and, as such, are at their most useful in a detailed study of a generally understood phenomenon.

2.3:POSITRON DISTRIBUTION IN METALS

A positron moving in the field of the ions and conduction electrons of a metal will be in the lowest Bloch state [55] with purely thermal momentum . In the vicinity of the atomic cores, the amplitude of the positron wavefunction will be small as a result of the stongly repulsive Coulomb potential acting between the positron and the positive ions. In the region between the atomic sites, however, this amplitude increases rapidly to its maximum.

Thus the positron density distribution has a pronounced "Swiss-cheese" character in that it is relatively uniform in the interstitial regions while exhibiting "holes" around each ion. The magnitude of the repulsive potentials responsible for this distribution prohibit the application of a "nearly free positron" theory to the solution of the wave equation [56]. However, this difficulty can be resolved by the use of a positron pseudo-potential [57,58,59]. From calculations for the case of a positron in a uniform electron gas [60], it is concluded that positron-electron correlation effects are not highly sensitive to changes in electron density and will be insignificant by comparison with the electrostatic potential near the ion cores. The Hartree potential of the ions and the conduction electrons is accordingly thought to be a good

approximation to the positron environment in a perfect metal. This approach may require modification in the case of defected metals in order to take account of positron-electron correlations. This modification in many such cases, can satisfactorily be made by the use of a local density approximation.

Accordingly, for states near the bottom of the lowest energy band, the positron wavefunction can be divided into two components. The first of these represents the strong Coulomb repulsion of the positron from the ions and is independent of both the positron energy and the core environment. This is complemented by a function which corresponds to the positron distribution in the regions between the ion cores and is dependent on both the positron energy and the environment. Calculations have been performed [57,58,59,61] using this model of the ground-state wavefunctions, energies and band-masses of the positron in simple metals.

A rigorous description of the annihilation process requires the solution of a many-body problem even in the case of a perfect metal. As will be discussed, a model in which the conduction electrons of the metal are treated as a homogeneous electron gas yields annihilation parameters close to those observed in both angular correlation and positron lifetime experiments.

2.3.1: Positron Annihilation in an Electron Gas

The Sommerfeld model can be applied to the determination of the parameters of the annihilation of a thermalised positron with a gas of free-electrons. The electron wavefunction is defined as

$$\psi_k(\underline{r}) = V^{-\frac{1}{2}} \exp(i.\underline{k}.\underline{r}) \quad k \leq k_F \qquad 2.12$$

Similarly the wavefunction for a thermalised positron ($\underline{k}=\emptyset$) is

$$\psi_+(\underline{r}) = V^{-\frac{1}{2}} \qquad 2.13$$

From [7] we have that the momentum distribution of the positron-electron pair, obtained by treating the positron and the electron as independent particles is

$$\Gamma(\underline{k}) = \text{const.} \sum_i \left| \int d\underline{r} \exp(-i.\underline{k}.\underline{r}) \psi_-(\underline{r}) \psi_+(\underline{r}) \right|^2 \qquad 2.14$$

Comparison with experiment is facilitated by consideration of the long-slit arrangement of the angular correlation technique . This measures a distribution given by

$$N(p_z)dp_z \alpha \int_{-\infty}^{\infty}\int_{-\infty}^{\infty} \Gamma(\underline{p})dp_x dp_y dp_z \qquad 2.15$$

which, for an isotropic distribution [41], reduces to

$$N(p_z)dp_z \alpha 2\pi \int_{p_z}^{\infty} p\Gamma(p)dpdp_z \qquad 2.16$$

In the case of the momentum distribution of equation 2.7, this is a parabola :

$$N(p_z)dpz \propto (p^2_F - p_z^2)dpz \text{ for } p_z < p_F$$
$$= 0 \qquad \text{for } p_z > p_F \qquad 2.17$$

where p_F is the Fermi momentum.

Such a parabolic component is observed in the angular distribution of many metals. Further, the $p_z=p_F$ cut-offs agree well with the Sommerfeld theory predictions of conduction electron densities [41,62]. An additional feature of the angular distribution is a broad component of roughly Gaussian form which underlies the inverted parabola. This component arises from the more subtle features of the conduction electron momentum distribution and from annihilation with more tightly bound electrons. The latter contribution, usually referred to as core annihilation is believed to be the major contribution to the broad component in the distribution [56,42]. For some metals, often termed simple, the intensity of this broad component is small and, for these cases, conduction electron annihilation accounts for almost all of the events.

The Sommerfeld model is not however equally successful in predicting annihilation rates, i.e. those rates which are obtained by integrating equation 2.17 over p_z. Positron lifetime measurements reveal that the model provides an underestimate of the rates and an overestimate of their sensitivity to average electron densities. In

reality, the presence of a positron in an electron gas draws around itself a cloud of electrons which effectively screens its positive charge. The effect of such positron-electron correlations is to enhance the electron density at the positron site and correspondingly to increase the annihilation rate. Introducing such a density dependent enhancement factor, $\gamma(n)$, to the rate, λ_o, predicted by the Sommerfeld model we have,

$$\lambda = \lambda_o \gamma(n) = \pi r_o^2 cn.\gamma(n) \qquad 2.18$$

where r_o is the classical electron radius. An interpolation formula for this enhancement factor has been suggested [63,28], employment of which yields the new rate,

$$\lambda = \frac{12}{r_s^3} \left(1 + \frac{10+r_s^3}{6}\right) \times 10^9 \qquad 2.19$$

where $r_s = (3/4\pi n)^{1/3}$ is a density parameter given in units of a_o, the Bohr radius and $(12/r_s^3) \times 10^9$ is the rate predicted by the Sommerfeld model for an unenhanced electron gas. The values produced by the use of this formula match those of many-body calculations [64] to within a few percent for the electron density range corresponding to $2 < r_s < 6$, i.e. for metallic electron densities.

2.3.2: Contributions from Core Electron Annihilation

The above treatment considers only annihilation with conduction electrons whereas, in real metals, the overlap of the positron wavefunction with that of the core electrons is non-vanishing. The contribution of the resulting core annihilation to the total rate is particularly large for the transition and noble metals because of their extended d-shells. It has been suggested [65,7] that electron gas theories can be used to calculate this core component by adjusting the valence electron density by the ratio of the annihilation rates corresponding to core, Γ_c , and valence, Γ_v , electrons, viz. :

$$neff = n(1 + {}^{\Gamma_c}/_{\Gamma_v}) \qquad 2.20$$

Estimates of the Γ_c/Γ_v ratio can be obtained from angular correlation curves where $\Gamma_c/\Gamma_v = A_c/A_v$ and A_c, A_v are respectively the areas under the Gaussian and parabolic parts of the curve. Such a separation of the curve is most satisfactorily achieved in simple metals. There are however, difficulties in forming reasonable estimates of A because of the uncertainty which surrounds the contribution of higher momentum components of valence electron annihilations and that which applies to the extrapolation to the origin of the broad component. A proposed solution [65] involves the arbitrary choice of 80% of the measured area as

forming the estimate of A_c. This procedure predicts annihilation rates for the simple metals which are quite close to those observed.

2.3.3: The Effect of Electron-Positron Correlations on Momentum Distributions

The Independent Particle Model, equation 2.14, ignores the effect of electron-positron correlations on the momentum distribution in the homogeneous electron gas. These can be included through a momentum dependent enhancement factor, $\mathcal{E}(\underline{p})$, the most successful calculations of which employ the Green's function for the electron-positron pair [66,67] and yield,

$$\varepsilon(\gamma) = a + b\gamma^2 + c\gamma^4 \qquad 2.21$$

where the reduced momentum $\gamma = p/p_F$ and the constants a,b and c depend on the electron density. This enhancement factor is weakly dependent on momentum and has a relatively small effect on the long-slit angular correlation distribution causing slight broadening of the free-electron parabola. The annihilation rates produced are for cases in which the core component is small, in good agreement with experiment [11] for $r_s \lesssim 5$.

CHAPTER 3: THE INVESTIGATION OF DEFECTS BY POSITRON ANNIHILATION

3.1: LATTICE DEFECTS AND THEIR INVESTIGATION

3.1.1:Point Defects

Point defects in crystals are perturbations of the ideal crystal lattice whose extent in any direction is no greater than a few atomic distances. Such defects may be termed zero-dimensional by contrast with dislocations which are one-dimensional or with grain boundaries which are two-dimensional. In a homogeneous solid, point defects such as vacant sites, self-interstitials and then agglomerates are classified as being intrinsic while those point defects which involve foreign atoms are termed extrinsic. Intrinsic defects are produced by changes in temperature, by plastic deformation or by the displacement of atoms from their lattice sites by energetic radiation.

The study of such lattice defects can be divided into two categories viz. those involving equilibrium and non-equilibrium techniques ; the relative merits of these are discussed in [68,8]. A characteristic feature of equilibrium measurements is that the number of different point defects involved is very small in that the main effects are caused by monovacancies. An approximate interpretation of point defect equilibrium effects in metals utilises this feature by considering only one defect type i.e. monovacancies. However, in some cases, it is necessary to take account of a divacancy contribution to the equilibrium properties although, since this contribution is in the main small in relation to the monovacancy effect, the information obtained on divacancies is less accurate than that for monovacancies.

3.1.2: The Statistical Thermodynamics of the Monovacancy

Concentration

The creation of a vacancy involves the removal of an atom from its lattice site and its replacement at either the crystal surface or at an interstitial site. Consider a crystal having N atoms at constant pressure; the change in Gibbs free energy involved in bringing an atom from a given interior lattice site to a surface site is given by

$$G_{1v}F = H_{1v}F - TS_{1v}F \qquad 3.1$$

where H_{1v}^F is the enthalpy and S_{1v}^F the entropy associated with monovacancy creation and T is the absolute temperature. This change in entropy results from the change in the vibrational frequencies of the lattice when a vacancy is created and does not include the configurational entropy. This latter contribution, in the case of the creation of n vacancies, accounts for the number of ways in which the n vacancies and N atoms may be distributed among the N+n sites, and is given by [68]

$$S = k\ell n \frac{M!}{(M-n)!n!} \qquad 3.2$$

where M=N+ n, the total number of sites available to the defects.

From the total change in the Gibbs free energy, [68], we obtain

$$n = M \exp(-G_{1v}^F/k\tau) \qquad 3.3$$

Introducing the concentration of monovacancies, C_{1v}, we have

$$C_{1v} \equiv \frac{n}{N} = \frac{N+n}{N} \exp(-G_{1v}^F/k\tau) \qquad 3.4$$

to which a good approximation is:

$$C_{1v} = \exp(S_{1v}^F/k)\exp(-H_{1v}^F/k\tau) \qquad 3.5$$

Since in metals the equilibrium vacancy concentrations at the melting temperature, T_m, have values between 10^{-3} and 10^{-4} and both experiments and theoretical estimates suggest that S_{1v}^F is of the order of k, the Boltzmann constant, it follows that, in metals, H_{1v}^F is of

the order $10kT_m$ and hence that

$$T_m S_{1v}^F << H_{1v}^F \qquad 3.6$$

From this and the fact that an analogous relation exists for other point defects, we have that the equilibrium concentration of a point defect is determined mainly by its formation enthalpy. Thus, defects whose formation enthalpies exceed the lowest point defect H^F by several kT_m have equilibrium concentrations which are an order of magnitude smaller than defects with the smaller H^F, provided that their formation entropies are not excessively large. From this, the generality can be drawn that it is unnecessary to consider more than two types of point defect in thermal equilibrium in a metal.

The above relations can be extended to take account of divacancies in which case the total vacancy concentration, C_v, is given by

$$C_v = C_{1v} + C_{2v} \qquad 3.7$$

where, C_{2v}, the concentration of divacancies is given by

$$C_{2v} = \frac{1}{2} z \exp(\Delta S_{2v}/k)\exp(H_{2v}^B/kT)(C_{1v})^2 \qquad 3.8$$

where z is the coordination number of the lattice and the divacancy binding enthalpy is

$$H_{2v}^B = 2H_{1v} - H_{2v} \qquad 3.9$$

and the association entropy of divacancies is given by

$$\Delta S_{2v} = S_{2v} - 2S_{1v} \qquad 3.10$$

3.1.3: Investigation of Lattice Defects

The main weakness of the detection and quantitative experimental investigation of point defects in thermal equilibrium is that they must be carried out at high temperatures since the equilibrium concentration of defects decreases exponentially with decreasing temperature. A general result of this is that there will be a large background contribution whose origin is not associated with the defect or defects of interest. Since the independent determination of these background effects is not possible as a crystal at high temperatures will not be free of defects, this contribution must be determined by extrapolation from low temperatures at which the equilibrium defect concentration is negligible. The uncertainties involved in such a procedure are considerable particularly at high temperatures where anharmonic effects may contribute. Such considerations restrict the utility of equilibrium measurements to cases in which the concentration of point defects is not small compared with that of the ideal crystals.

A further requirement of an equilibrium study of defects is knowledge of the contribution per vacancy to the physical property measured. A technique which solves both of these problems is that of differential dilatometry. In this method comparison of the macroscopic thermal expansion

with that of a unit cell as measured by X-ray determinations of the lattice parameter, in principle, yields V_{lv}^F the formation volume of a monovacancy.

Both the measurement of the change in specimen length, $\Delta\ell/\ell_o$, and that corresponding to the lattice parameter, $\Delta a/a_o$, have the same background since thermal expansion of the lattice causes equal relative changes in each. If no lattice strains were associated with the creation of a lattice vacancy and an associated self-interstitial, the lattice parameters would remain unchanged. This is not the case however and, from [8], for a cubic crystal, the equilibrium defect concentrations can be obtained as a function of temperature by means of the relation

$$3\left(\frac{\Delta\ell}{\ell_o} - \frac{\Delta a}{a_o}\right) = C_v - C_1 \qquad 3.11$$

where C_v is the concentration of vacant sites and C_i that of self-interstitials. Correction terms to this relation for the case of non-cubic crystals have been derived [69] and the technique has been applied to the study of equilibrium defects in metals [70, 71]. From these and similar studies, no evidence of a measurable equilibrium concentration of self-interstitials has been found and thus in equation 3.11 we may assume that $C_i(T) \ll C_v(T)$ and obtain the vacancy contribution from this relation. For metals, $C_v(T_m)$ is found to take values between 2×10^{-4} (Pb, Ag) and 10×10^{-4} (Al).

The determination of vacancy formation enthalpies proceeds from the measurement of the temperature dependence of the total vacancy concentration by means of the definition of an effective formation enthalpy,

$$H^F_{eff} = \frac{\partial(\ell n C_V(T))}{\partial(1/kT)} \qquad 3.12$$

The quantity, $H^F eff$, is however, temperature dependent as a result of two different effects. First, an appreciable contribution from divacancies to $C_V(T)$ leads to estimates of $H^F eff$ which are in excess of H^F_{1V}; for sufficiently low temperatures however $H^F eff$ tends to H^F_{1V}. Second, there is the temperature dependence of H^F_{1V} and S^F_{1V}; the effect of this contribution is thought to be small over the limited temperature range involved [68]. The accuracy with which C_V can be determined from equation 3.11 decreases rapidly with decreasing temperature and is poor if C_V decreases to 10^{-5}. Thus, for most metals, for the temperature range over which the slope of the Arrhenius plot, equation 3.12, may be determined with accuracy that slope, $H^F eff$, will contain a significant divacancy contribution and therefore will be temperature dependent.

An alternative absolute method of studying vacancy concentrations is in principle that of the measurement of the specific heat as a function of temperature by means of calorimetric techniques. In such a study the contribution per vacancy is the vacancy formation enthalpy which, in principle, can be obtained independently from measurements of the temperature dependence. In reality however,

uncertainties regarding the extrapolation to high temperatures of the specific heat of the defect-free material are such that the results obtained are not consistent with those of other techniques.

Other equilibrium techniques include the measurement of tracer diffusion and resonance and relaxation experiments such as NMR, Mossbauer effect or ultrasonic measurements. These methods are reviewed in [72].

A relatively new equilibrium technique is that of positron annihilation. This technique is not capable of determining absolute values of $C_v(T)$ independently but has the merit of allowing the determination of H^F_{iv} in a temperature range for which the concentration of divacancies is negligible. A further feature of the technique is its insensitivity to self-interstitials and as such provides a means of evaluating the assumptions made earlier as to the importance of this defect type on other equilibrium methods such as differential dilatometry. The positron technique will be discussed in the following sections.

3.2: POSITRON INTERACTION WITH DEFECTS AND THE TRAPPING MODEL

3.2.1: Introduction

Subsequent to the first realisation of the sensitivity of the positron annihilation momentum distributions to the effects of changes in both defect concentration and temperature [73, 74], interest in the application to the study of lattice defects of the available positron techniques has grown. Later lifetime studies [75] indicated the suitability of the technique to the study of equilibrium vacancy concentration determinations once the saturation effect of the positron lifetime had been explained by the application of the trapping model.

The simplest version of this model is the two-state trapping model [76,77] in which it is assumed that initially energetic positrons thermalise into free states in the specimen from which they may subsequently annihilate at a rate λ_f or suffer trapping at a rate νC_v before annihilating at the slower rate λ_t. Trapping by vacancies is energetically favourable to the positron because the absence of the positive ion provides an attractive potential. By the same token, the conduction electrons

suffer a repulsive potential at the vacancy site and thus the electron density experienced by a positron localised in a vacancy trap is lower than that for perfect regions of the specimen crystal. For many metals the major contribution to the difference between λ_f and λ_t is the removal of the core electrons and thus the annihilation at vacancy sites results in the narrowing of the annihilation momentum distribution.

3.2.2: The Trapping Model

The annihilation rate for a positron in a stationary state is time-independent and is a reflection of the electron density sampled by the positron in that state. For a system in which a spectrum of quasi-stationary states, s, is available to the positron, each state being characterised by an annihilation rate $\lambda(S)$ with an associated probability given by a suitable normalised distribution function, P(S), the form of the resulting spectrum depends on the persistence $\bar{l}(S)$ of these states relative to the corresponding annihilation lifetimes $(\lambda(S))^{-1}$ If transitions between the available states occur with time independent rates K_{ij} , an initial positron population will decay as

$$n(t) = \sum_{i}^{N} ni(t) \qquad 3.13$$

where the $n_i(t)$ are given by a set of coupled differential equations

$$\frac{dn_i(t)}{dt} + (\lambda_i + K_{ij})n_i(t) = \sum_{j \neq i}^{N} K_{ji} n_j(t) \qquad 3.14$$

and the consequent lifetime spectrum will be of the form

$$I(t) = \sum I_\nu \exp(-\Gamma_\nu t) \qquad 3.15$$

where, in general, I_ν and Γ_ν are complicated functions of λ_i and K_{ij} .

In the simple trapping models [76,77,78] the assumption is made that, at t=Ø, the positrons exist in a common delocalised state from which they either annihilate or make transitions to other states. If further transitions are neglected equation 3.14 can be written

$$\frac{dn_1(t)}{dt} + (\lambda_1 + \sum_{j\neq 1} K_{ij}) n_1(t) = 0$$
$$\frac{dn_j(t)}{dt} + \lambda_j n_j(t) = K_{ij} n_1(t) \qquad 3.16$$

for all $j \neq 1$. Application of the boundary condition $n_j(Ø) = n_o \delta_{ij}$ yields the discrete spectrum

$$n(t) = n_o\left[1 - \sum_{j\neq 1} \frac{K_{ij}}{(\lambda_1 - \lambda_j + \varepsilon)}\right] \exp\left[-(\lambda_1+\varepsilon)t\right] + \sum_{j\neq 1} \frac{n_o K_{ij}}{(\lambda_1 - \lambda_j + \varepsilon)} \exp(-\lambda_j t) \qquad 3.$$

where $\mathcal{E} = \sum_j K_{ij}$. The decay rate of any resolvable component $j \neq 1$ is equal to the annihilation rate in the corresponding state. For the first state, [79], this is given by

$$\lambda_1 = \sum_j I_j \Gamma_j \qquad 3.18$$

Positron trapping effects will be observable in lifetime spectra whenever a K_{ij} is of the same order as λ_1 and λ_j is distinct from λ_1 . If the former condition is satisfied for a sufficiently low concentration of positron

traps, C_j , K_{ij} can be written

$$K_{1j} = \nu_{ij} C_j \qquad 3.19$$

where ν_{ij} is the positron trapping rate per unit defect concentration. Thus changes in C_j can be monitored through the resulting changes in either Γ_1 or the corresponding intensity I_j . By such means the decay rates corresponding to specific traps may be extracted and employed to determine their nature.

However, the investigation of defected materials by positron annihilation techniques normally proceeds from the assumption that the positron exists in either of two states : the Bloch, or delocalised, state or the defect-trapped state. Thus, in this two state case, the set of equations 3.14 reduces to

$$\frac{dnf}{dt} = n_f \lambda_f - n_f \nu C$$

$$\frac{dnt}{dt} = n_f \nu C - n_t \lambda_t \qquad 3.20$$

where use has been made of equation 3.19 in substituting for the trapping rate. making use of the boundary condition that at t=Ø all the positrons are in the free state, the population at a subsequent time is described by

$$n(t) = n_o \left[\frac{\lambda_f - \lambda_t}{\lambda_f - \lambda_t + \nu C} \exp \left[-(\lambda_f + \nu C) t \right] + \frac{\nu C}{\lambda_f - \lambda_t + \nu C} \exp \left(-\lambda_t t \right) \right] \qquad 3.21$$

The mean positron lifetime is given by

$$\tau = \frac{\lambda_t + \nu C}{\lambda_t (\lambda_f + \nu C)} \qquad 3.22$$

which, in terms of the lifetime components can conveniently

be expressed as,

$$\tau = (1-X)\tau_f + X\tau_t \quad \text{where} \quad X = \nu C/(\lambda_f + \nu C) \qquad 3.23$$

3.2.3: Application to Momentum Distributions

Aside from the instrumental contribution, the shape of the angular correlation or Doppler broadening curve depends only on the proportions of annihilations in each state i.e.,

$$N_j = \int_0^\infty \lambda_j n_j(t)\,dt \qquad 3.24$$

If a characteristic of annihilation, F, is a linear function of positron state such that

$$F = \sum_j \frac{F_j N_j}{N_j} = \sum_j F_j P_j \qquad 3.25$$

where P_j is a normalised probability, then its measurement is capable of yielding information on defect concentrations, trapping rates and sites. In addition to the positron lifetime, other such characteristics are the lineshape parameters of positron annihilation momentum spectra, for which an expression similar to equation 3.23 can be written

$$F = (1-x)F_f + XF_t \qquad 3.26$$

where F_f, F_t are shape parameters characteristic of annihilations from the free and trapped states respectively. Thus we can write,

$$\frac{F-F_f}{F_v-F} = \frac{X}{1-X} = \frac{\nu C}{\lambda_f} \qquad 3.27$$

Application of this two-state trapping model result to the case of monovacancy trapping, where F_v denotes a parameter characteristic of such trapping, yields the result,

$$\frac{F-F_f}{F_v-F} = \nu_r \tau_f \exp(S/k) \exp(-{}^{H}1v/_{kT}) \qquad 3.28$$

and provides a means of evaluation of monovacancy formation enthalpies etc. from positron annihilation spectra.

3.3: TEMPERATURE EFFECTS

In addition to the exponential increase in annihilation characteristic predicted by equation 3.28, early positron annihilation experiments revealed a linear temperature dependence in the annihilation parameter at temperatures lower than that at which the exponential behaviour bacame apparent. This "pre-vacancy rise" was attributed to the suggested temperature dependent behaviour of untrapped positrons. It was realised that, in order to facilitate the deduction of reliable vacancy trapping parameters from such experiments, an accurate assessment of the contribution made by this effect at higher temperatures was necessary. As a result of this, much attention has been focussed on the characterisation of the response of untrapped positrons to increasing temperature.

In some early experiments, for both mean lifetime, τ, [61] and angular correlation peak counts, H, [45], this positive slope closely followed the volume thermal expansion of the specimen and accordingly a thermal expansion term was incorporated in the fitting procedures. However, for other metals, the temperature dependence in the pre-vacancy region, while retaining an approximately linear character, was not consistent with thermal expansion, notably for the Doppler broadening lineshape parameter for cadmium [80]. In order to explain these results, a meta-stable "self-trapping" model was proposed [81].

3.3.1: Positron Self-Trapping

In this model [81,82] it is proposed that the presence of a positron deforms the lattice sufficiently to produce a trap similar to a polaron in polar materials i.e. the positron is self-trapped by strong interactions with the acoustic phonons. An elastic continuum model in which the positron is coupled to the lattice dilatation by a deformation potential was used to account for the pre-vacancy behaviour in cadmiun [80]. In this self-trapping, the positron is assumed to localise in an interstitial region and, as a result of its positive charge, to distort its local environment by displacing the metal ions.

It is suggested [82] that the positron will be self-trapped if

$$\frac{Kh^2}{2\pi\varepsilon^2 m} \quad k_{max} < k_o \qquad 3.29$$

where K is an elastic constant of the lattice, ε is a deformation constant [83], m is the positron mass and k_o is of the order of magnitude $2 \times 10^{-7}\,cm^{-1}$. Further, if the condition

$$k_{max} < \frac{2}{3} k_o \qquad 3.30$$

is satisfied, the binding energy in the self-trapped state is positive i.e. the self-trapped state is stable relative to the free state. If however, k(max) lies between $2/3(k_o)$ and k_o ,the self-trapped state has an energy higher than that of the free state by ΔE and is thus metastable with respect to the Bloch state. According to [82] this range of values obtains in metals. Under these conditions, the population of the metastable state is very low for temperatures very much lower than $\Delta E/k$ (where k is the Boltzmann constant) while at temperatures much higher than this, practically all the positrons are in the self-trapped state. between these two limits, the probability of positron self-trapping is given by

$$P_{st} = [1 + B^{-1}T^{1.5}\exp(\Delta E/kT)]^{-1} \qquad 3.31$$

where B is a numerical parameter whose value is such as to make $BT^{-1.5}$ large compared with unity. Separate calculations however, [84,85], suggest that positron self-trapping is unlikely to occur in metals.

3.3.2: Enhanced Thermal Expansion Effect

Irrespective of the possible existence of self-trapped states, the positron spatial distribution for the free state will be affected not only by thermal expansion but also by the temperature-induced vibration of the lattice. Consideration has been given [59] to such effects in which the positron-core electron annihilation rate, λ_c, defined as the overlap of the positron density distribution with that of the core electrons is used as an indicator of the temperature dependence.

As the temperature of the lattice increases, the positron density distribution at the core ,and thus λ_c is reduced by three effects :

(i) as aresult of the thermal expansion of the crystal the positron wavefunction is spread over a larger volume with a concomitant reduction of its amplitude and its overlap with the core;

(ii) a further result of thermal expansion is the enhancement of the redistribution of the positron density from the core to the interstitial regions of the crystal because of the increased separation between the cores;

(iii) the positron density is increased in an interstitial region which is momentarily enlarged because of the lattice vibrations with a resultant drop

in λ_c similar to that of thermal expansion.

However, whereas the shift in mean atomic positions affects the positron distribution in every cell, lattice vibrations can squeeze the positron from a contracted cell into a neighbouring expanded cell. While particularly favourable events must be infrequent for a given temperature, the root mean square displacements are, according to [59], more than an order of magnitude larger than those for the linear thermal expansion effect and are thus capable of causing a significant change in λ_c .

The authors [59] calculated the individual contributions to the change in core electron annihilation rate with temperature and found that the thermal expansion contribution (i)+(ii) is approximately twice that for the "free-volume" effect (i) alone. Further, in all cases so considered apart from sodium and potassium, the effect of lattice vibrations (iii) is larger than those of (i) and (ii) combined, notably so for indium in which they found effect (iii) to be approximately three times the size of (i)+(ii).

The temperature changes in the total annihilation rate predicted by this theory parallel those observed experimentally for simple and noble metals. However, there are features of the pre-vacancy region which are not explained by this model viz. the appearance of an onset temperature for the pre-vacancy rise (see point C in figure

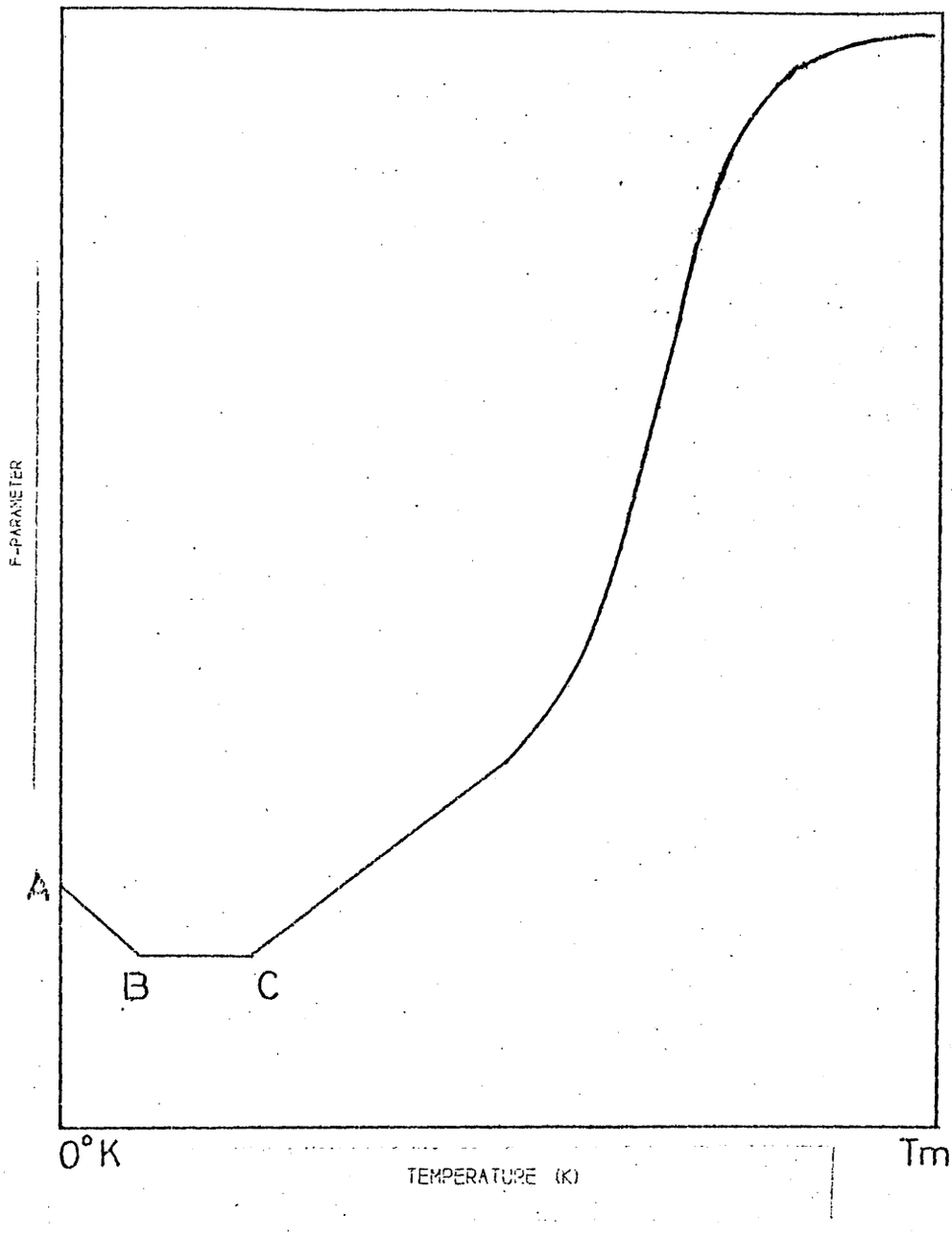

Figure 3.1: An illustration of a typical F-parameter temperature dependence.

3.1) and the existence of a negative temperature dependence at still lower temperatures i.e. at around 5ØK (as shown by the region AB in figure 3.1). The model as discussed above precludes the assessment of onset temperatures. However it is suggested that the combination of a weaker temperature dependence below some temperature characteristic of the phonon spectrum and the weaker temperature dependence of the lattice expansion may account for the observed effect.

The negative temperature dependence observed at low temperatures is unlikely significantly to affect the study of vacancy trapping phenomena. This temperature effect may be the result of positron localisation in weak traps from which the positrons are liberated as the temperature is increased. In the temperature range here mentioned, consideration of thermal energies suggests binding energies of the order of $1Ø^{-2}$ eV for such traps.

3.3.3: Temperature Dependence of the Trapping Rate

The dominant temperature dependence in the vacancy trapping region is that explicit in equation 3.28 . However, in addition to this, there is a possible temperature dependence of the positron-vacancy trapping rate, ν_{iv}. This has been the subject of several theoretical investigations arising from which temperature dependences of $T^{1/2}$ [86,87], T^{0} [88,89,9Ø] and $T^{-1/2}$ [81,83,91] have been

suggested. Experimental evidence is consistent with contemporary theory [92,93,94] in favouring a T^{o} dependence. While the subject is of intrinsic interest, the magnitude of the various suggested dependences is very much weaker than that of monovacancy concentration. For the purposes of vacancy formation enthalpy determinations, deduced values of monovacancy formation enthalpy are relatively insensitive to an inappropriate choice of temperature dependence for the trapping rate [95] within the above mentioned range.

3.3.4: The High Temperature Region

An additional obstacle to the deduction of reliable monovacancy parameters is the uncertainty as to the assignment of a suitable form of temperature dependence to describe the high temperature behaviour of positron annihilation lineshape parameters. Consideration has been given to this high temperature region by various authors but as yet no definite conclusions have been reached . Illustrative of this uncertainty are several works on aluminium.

In [96,97,98], the F-parameter corresponding to trapping by monovacancies was found to have a positive linear temperature dependence half as great again as the thermal expansion coefficient of the lattice. These

findings are in agreement with the predictions of [99,100] that the coefficient of thermal expansion for a vacancy is greater than that for the bulk crystal. To the contrary however it is suggested in [95] that F_v should depend less strongly than F_f on temperature. A contribution to the temperature dependence of F_f is assumed to result from the decrease of the core electron annihilation rate with increasing temperature. It is suggested that, in the case of F_v, the contribution of core electrons to the total annihilation rate is smaller than that for the case of F_f and accordingly that the response to temperature is attenuated. A further reduction in the temperature dependence is expected to result from the fact that the large amplitude of the positron wavefunction allows more freedom for the accomodation of minor changes in density without appreciably changing its overlap with the remaining core electrons. It is concluded [95] that for these reasons F_v should effectively be independent of temperature. Observations which support the temperature independence of F_v have been reported [101,102] . Arguments which indicate a negative coefficient of thermal expansion for a vacancy have also been forwarded [103].

For the W-parameter [96,97] found that the analagous W is independent of temperature and suggest that this results from the increased vibrational amplitudes of the neighbouring ion cores. For the same material however, other workers report a temperature dependence lower than that shown in the pre-vacancy region [104].

In the absence of a generally agreed temperature dependence in this temperature region it is common to allow for several different dependences in the lineshape parameter fitting procedures [105,106,107,108] and to attempt to identify the most suitable by comparison of the respective optimising parameters of the fits obtained. An alternative explanation which has been suggested to account for the anomalous high temperature behaviour involves the creation of divacancies. Again, allowances for this can be made in the fitting function.

However, despite the sophistication of the least squares minimisation routines employed to optimise the parameters of the various models fitted to observations, ambiguities can often arise. For example, the inclusion of a thermal expansion term in F_v tends to increase both the absolute value and the associated uncertainty in the deduced value of monovacancy formation enthalpy. Inclusion of divacancy terms in the computer model has a similar effect on the precision of monovacancy formation enthalpy and, in general, leads to lower returned values of monovacancy formation entropy. These difficulties allow gtreater scope for misinterpretation of the high temperature data than exists at lower temperatures and as such obstruct the resolution of the above mentioned uncertainties.

3.4: THE DETERMINATION OF VACANCY PARAMETERS FROM POSITRON ANNIHILATION DATA

3.4.1: Computer-Aided Fits to the Trapping Model

The determination of vacancy trapping parameters from positron annihilation data proceeds from the trapping model. Equation 3.28 yields

$$\ell n\left[\frac{F-F_f}{F_v-F}\right] = -\frac{H_{1v}}{kT} + \ell n[A] \qquad 3.32$$

where $A=\nu\tau\exp(S/k)$. From this, the monovacancy formation enthalpy can be obtained from the slope of the straight line plot, $\ln(\nu\tau C_v)$ vs. $(1/T)$, while the entropy term is given by the intercept [95,44]. However, the precision of the vacancy parameters deduced from the Arrenhius plot is degraded by the presence of temperature dependences additional to those explicit in equation 3.32 . These terms, which in general are linearly dependent on temperature, cause departures from linearity in the Arrenhius plot at the low and high temperature extremes.

An alternative to this approach is to fit equation 3.28 or a variant thereof to the data. Re-writing equation 3.28 we have

$$F(T) = \frac{F_f + F_{1v} A \exp(-H_{1v}^F/kT)}{1 + A\exp(-H_{1v}^F/kT)} \qquad 3.33$$

Including the self-trapping effect in equation 3.26 we have, on the assumption that trapping by vacancies will always predominate,

$$F = F_{1v}P_{1v} + \{F_f(1-P_{st}) + F_{st}P_{st}\}(1-P_{1v}) \qquad 3.34$$

where F_{1v}, F_{st}, F_f are values of the lineshape parameter characteristic of annihilation in the vacancy-trapped state, the self-trapped state and the free state respectively; and P_{1v}, P_{st} and P_f are the associated probabilities of occurence of each event. This yields

$$F = \frac{F_f + (F_{st} - F_f)\{1 + B^{-1}T^{-1.5}\exp(\varepsilon_o/kT)\}^{-1} + F_{1v}A\exp(-H_{1v}/kT)}{1 + A\exp(-H_{1v}/kT)} \qquad 3.35$$

where

$$B = \pi_j \frac{\nu_j}{\nu_j'} \left(\frac{h^2}{2\pi^2 m_+ k}\right)^{3/2} \frac{1}{\Omega} \qquad 3.36$$

and ε_o is an energy given by

$$\varepsilon_o = \frac{3h^2 K_o^2}{8\pi^2 m_+} - \frac{\varepsilon^2 K_o^3}{2K} \qquad 3.37$$

where ν_j, ν_j' are the vibrational frequencies of the crystal with free or self-trapped positrons, Ω is the atomic volume and K, M_+, k_o, ε are as defined in section 3.3.1.

A more commonly used model than the above is that arising from thermal expansion considerations (sections 3.3.2 and 3.3.4). This can be written

$$F = \frac{F_f^{\,o}(1+\beta T)+F_{1v}^{\,o}(1+\gamma T)A\exp(-H_{1v}/kT)}{1+A\exp(-H_{1v}/kT)} \qquad 3.38$$

where $F_f^{\,o}$, $F_v^{\,o}$ are values of the lineshape parameter at T=0 K corresponding to annihilation from the free and monovacancy trapped states respectively; β , γ are slopes and A is as given above.

Extending equation 3.26 to take account of divacancies we have

$$F = F_f P_f + F_{1v} P_{1v} + F_{2v} P_{2v} \qquad 3.39$$

which yields the model

$$F = \frac{F_f^{\,o}(1+\beta T)+F_{1v}^{\,o}(1+\gamma T)A_{1v}\exp(-H_{1v}/kT)+F_{2v}^{\,o}(1+\gamma T)A_{2v}\exp(-H_{2v}^{\,B}/kT)}{1+A_{1v}\exp(-H_{1v}/kT)+A_{2v}\exp(-H_{2v}^{\,B}/kT)} \qquad 3.40$$

where $H_{2v}^{\,b} = 2H_{1v} - H_{2v}$ and $A_{2v} = (\nu_{2v}\bar{\iota}_f)\frac{z}{2}\exp(S_{2v}^{\,B}/k)$ where z is the coordination number of the crystal.

One or more of the non-linear functions 3.35, 3.38, 3.40 can be fitted to positron annihilation data, using temperature as ordinate, by means of a least squares minimisation routine to yield vacancy formation parameters. Of these models, equation 3.36 is found to yield satisfactory fits more frequently than the others.

3.4.2: Characteristic or Threshold Temperatures

Vacancy parameter values derived from the procedures described above have been evaluated by many workers by means of simple plausibility tests. One such test is that the monovacancy concentration at the melting point $C_{1v}(T_m)$ should be of the order 10^{-4} to 10^{-3}. In addition, many empirical relations between various physical parameters which depend on the binding energy of the lattice atoms have been proposed and verified [110]. Such parameters include T_m, H_{1v}^F, H_{1v}^m (the monovacancy migration enthalpy) and Q (the activation energy for self-diffusion) where Q is given by

$$Q = H_{1v}^F + H_{1v}^m \qquad 3.41$$

Further to this it has been shown that useful information concerning vacancy properties may be contained in a relatively limited portion of the lineshape parameter versus temperature curve where the effect of vacancy trapping on the lineshape parameter first becomes apparent [111, 112]. It is usual to associate with this feature a characteristic or threshold temperature, T_c.

A correlation between the monovacancy formation enthalpy values obtained from conventional analyses of vacancy trapping curves and the characteristic temperatures was first indicated in [111]. Subsequently a linear relationship between T_c and Q was reported [112] which, when used in conjunction with the assumption that

$$H_{1v}^F \simeq Q/2 \qquad 3.42$$

[113], was employed to deduce monovacancy formation enthalpy values from T_c values.

Despite the lack of unanimity over the definition of T_c [111, 112, 110, 114] the relevance to H_{1v}^{f} of a suitably defined T_c can be established. In one of the definitions employed, T_c is given by the intersection of straight line approximations to the pre-vacancy and vacancy trapping parts of the temperature curve. Re-stating the two state trapping model result in terms of a generalised lineshape parameter ,F

$$F = \frac{F_f + F_{1v} A \exp(-H_{1v}/kT)}{1 + A\exp(-H_{1v}/kT)} \qquad 3.33$$

The equation of the straight line approximation to the vacancy trapping region of the curve is given by that of the tangent at the midpoint of this region i.e. where $F(T) = (F_{1v} + F_f)/2$. This tangent can be shown [114] to be represented by

$$F(T) = \frac{(F_{1v}+F_f)}{2} - \frac{(F_{1v}-F_f)}{4} \ln A + \frac{(F_{1v}-F_f)}{4H_{1v}} (\ln A)^2 kT \qquad 3.43$$

T_c is defined as the ordinate at the intersection of equation 3.43 with $F=F_f$. Thus

$$H_{1v}^{F} = \frac{(\ln A)^2}{(\ln A - 2)} kTc = \alpha Tc \qquad 3.44$$

For most metals, $A \sim 10^5$ and thus α is only a weakly varying function of A, where $A = \nu_{1v} \tau_f \exp(S/k)$. Further, it has also been pointed out that, when quantum mechanical transition limited trapping obtains, variations in τ_f tend

to be cancelled by opposing variations in ν_{1v}. Thus, for A in the range 4×10^{4} to 4×10^{5} it follows that

$$H_{1v}^{F} \simeq (14\pm1)kTc \qquad 3.45$$

The generality of this relation is not significantly affected by the inclusion of linear temperature dependences in F_f and F_{1v} [114].

For the low melting point metals there is general agreement between monovacancy formation enthalpy values deduced from the characteristic temperature method and the unconstrained trapping model analysis technique. For other metals however the values obtained from the characteristic temperature method are in general lower than those derived from the trapping model. It is perhaps significant that where differences exist, the T_c-derived values differ by less from values deduced from other techniques than those derived from the trapping model. In the case of the high melting point metals this is perhaps indicative of detrapping effects [115].

In addition to providing an indication of the plausibility of vacancy trapping parameters deduced from the trapping model, the characteristic temperature method is of particular value in studies which embrace a restricted temperature range. In particular, in studies of metals having high melting points it may be necessary for reasons of equipment limitations or in order to minimise the possibility of significant source evaporation, to restrict the highest sample temperature obtained during the

experiment to the extent that the vacancy trapping region is not fully explored. In such cases, the monovacancy formation enthalpy can be deduced given that the temperature range is sufficiently large to enable determination of T_c.

CHAPTER 4: EXPERIMENTAL TECHNIQUES AND EQUIPMENT

4.1: POSITRON ANNIHILATION SPECTROMETER

A schematic diagram of the spectroscopy system used in this study is shown in figure 4.1 . The front-end of the spectrometer is a high resolution intrinsic germanium planar detector which was supplied by Princeton Gamma Tech. In this, a germanium crystal of volume 200 mm^3 and thickness 10 mm is mounted on the end of a cold-finger which is immersed in a liquid nitrogen dewar vessel. The operating bias for the detector crystal is supplied by a Tennelec TC941 high voltage power supply. The detector output is fed into a field effect pre-amplifier a feature of which is an optical reset circuit. An 8 microsecond pulse is periodically generated by this reset circuit to correct for leakage and absorbed-radiation-induced currents in the detector crystal. This pulse is accompanied by an analyser inhibit pulse which gates the analyser off through the anti-coincidence input of the analogue to digital converter during the amplifier recovery from the optical reset. The pre-amplifier output is fed into a Tennelec TC205 amplifier.

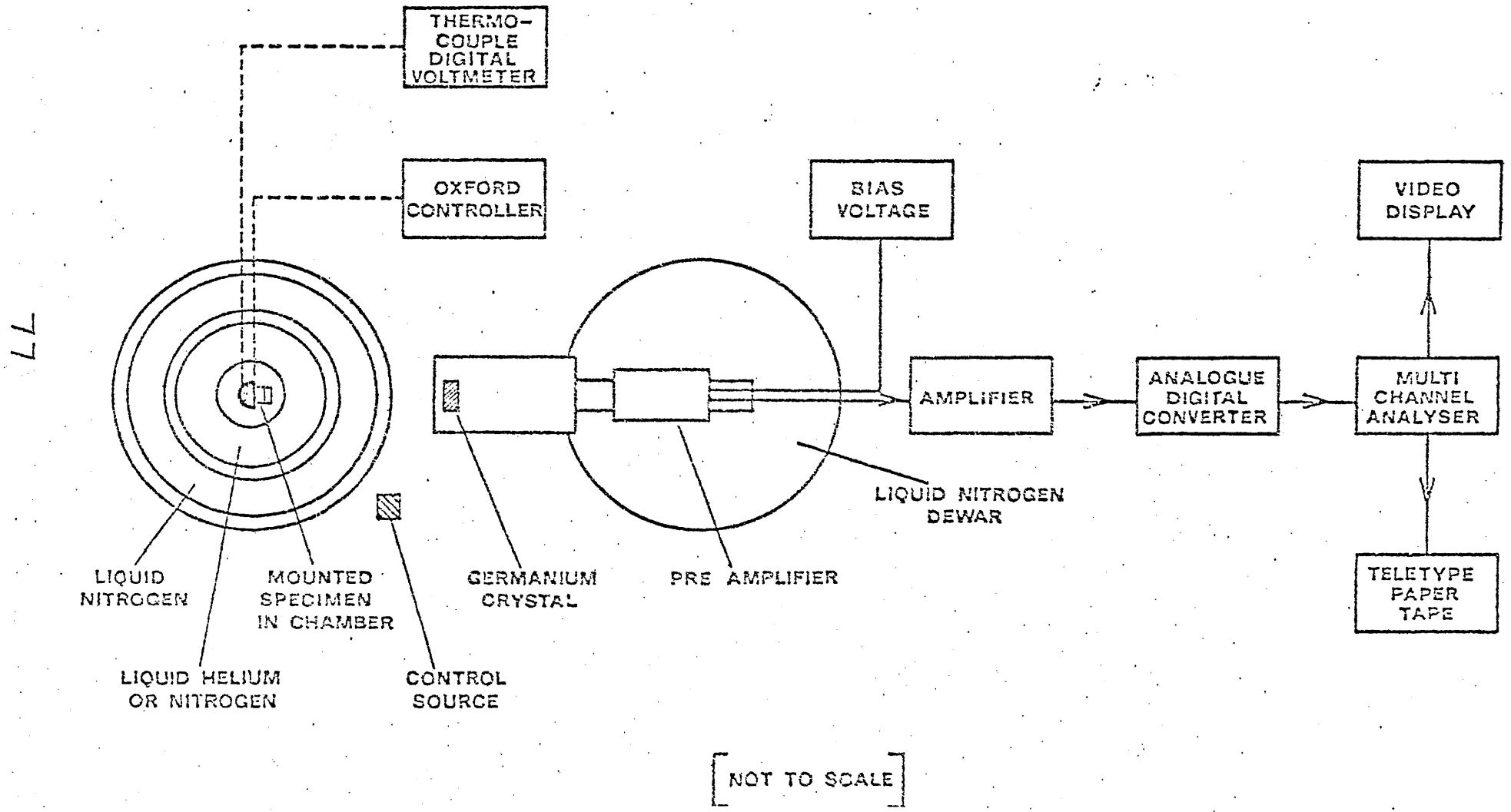

Figure 4.1: A schematic diagram of the Doppler broadening system employed in this study.

Pre-amplifier output pulses (tail pulses) have a very short rise-time, typically less than 100 nanoseconds, and exponential decay-times of around 50 microseconds. In order to reduce problems in amplitude interpretation at the analogue to digital converter consequent on pulse overlap, it is necessary to make a careful choice of the time constants for the main amplifier pulse shaping circuitry. Accordingly, the main amplifier time constants should be chosen to be simultaneously much shorter than the decay time and much longer than the rise time of the pre-amplifier output pulses. The optimum time constant for this spectrometer was found to be 4 microseconds [116].

The output of the main amplifier is then fed into an 8192 channel analogue to digital converter in which the pulses are digitised linearly according to amplitude before being transferred for storage to an 8K Nova-2 computer supplied by Link Systems Ltd. The conversion constant of the analogue to digital converter is 1mV per channel.

During the experiments on single crystal and polycrystalline cadmium, the analogue to digital converter used was a Laben model 8215. This instrument has a pulse conversion time of 4.5 microseconds in excess of the pulse rise time and a quoted gain stability against temperature of 0.0015% per °C. During the single crystal zinc experiment a Canberra model 8080 analogue to digital converter was used. This device has a conversion time of approximately 10 microseconds and a quoted gain stability against temperature

of Ø.ØØ5% per ^{o}C.

4.2: OPERATION OF POSITRON ANNIHILATION SPECTROMETER

4.2.1: Line Stability

An important factor in the stability of any spectrometer is its response to temperature fluctuations of the surrounding environment. Great efforts have been directed towards the minimisation of the effect of such environmental variations by means of spectrum stabilisation instrumentation. The normal method by which improvements in stability are achieved involves the continual adjustment of the spectrum to compensate for observed movements in the position of the peak of interest. In order to facilitate such on line corrections to observed spectra either the observed centroid movement of the spectral line or the change in the ratio of the integrals of two windows disposed about the centroid can be employed.

Measurements of the 497 keV mono-energetic gamma-ray of ^{103}Ru were made simultaneously with those of the annihilation peak and were used throughout the study to monitor the stability of the spectrometer. A lineshape parameter, the G-parameter, similar in conception to those

employed to describe changes in annihilation lineshapes was defined as a measure of the system stability and spectra for which the G-parameter exhibited unacceptable departures from the norm were rejected.

The spectrometer used throughout this study did not incorporate a digital spectrum stabiliser. Instead an alternative approach to the stability problem was adopted i.e. attempts were made to reduce the magnitude of the temperature variations in the vicinity of the spectrometer.

To this end the spectrometer was enclosed within a temperature-stabilised room, figure 4.2, the walls of which, with one exception, were lined with 50mm thick polystyrene sheeting. The exception to this is at point A where an aperture was constructed for the detector in order to reduce the distance between the specimen and the detector. The detector was mounted on rails at this point (in order to facilitate simple adjustments to the count rate where necessary) such that the detector window projected through the wall of the enclosure. At this point the thickness of the polystyrene is 5mm.

Temperature stabilisation within the room was achieved by means of an air-conditioner working at a constant cooling rate placed in opposition to a heater whose power output was a constant 1kW. In addition to these devices a 750watt heater whose output was controlled by means of a mercury-in-glass control thermometer was employed

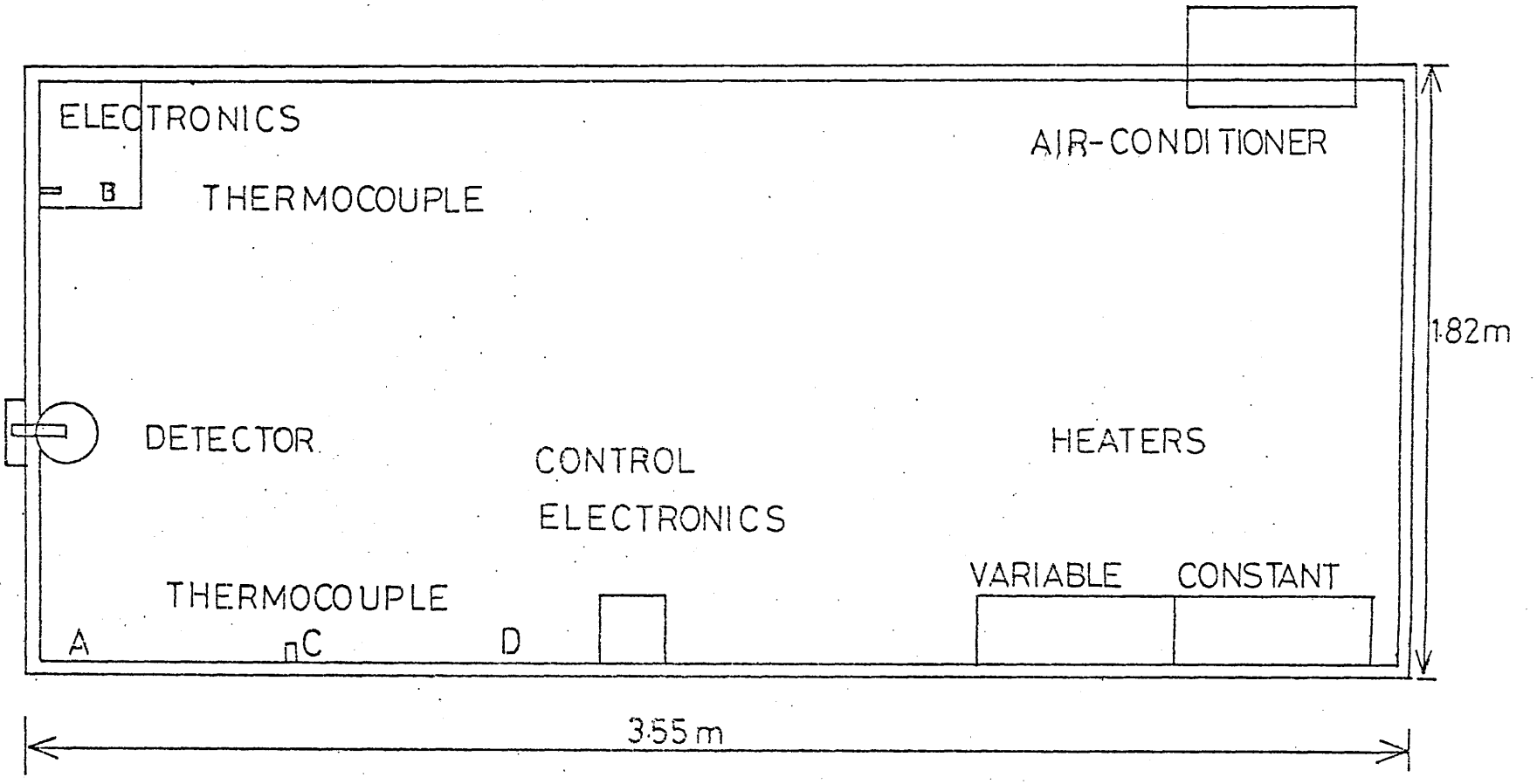

Figure 4.2: A schematic diagram of the temperature-stabilised cage

to raise the ambient temperature as it fell below the control point. In addition to this controlling thermometer, the temperature was also monitored at a point on the spectrometer instrumentation rack (point B) and on the wall opposite (point C) by means of T1-T2 thermocouples and at point D by a mercury-in-glass thermometer.

In order that disturbance of the thermal equilibrium be reduced to a minimum, the enclosed instrumentation was controlled from outside the enclosure via remote control links. A liquid nitrogen supply line was constructed to enable the remote filling of the detector. In addition to this latter provision the accumulation of data was suspended subsequent to filling of the detector dewar in order to ensure a full recovery of the interior equilibrium temperature (typical recovery times were 15-20 minutes).

It was found that the optimum enclosure temperature at which the temperature stabilisation system could be operated on a long-term basis was 20°C. At this ambient temperature, the fluctuations in the temperature of the electronics were less than ±0.15°C.

4.2.2: Detector Filling

It was found, in agreement with the observations of [117], that immediately subsequent to the re-filling of the detector dewar vessel, the centroid stability of the spectrometer was unusually poor. In order to reduce the effect of this detector recovery behaviour on the quality of the data, the operation of the data acquisition system was suspended for a minimum of 60 minutes subsequent to the completion of a liquid nitrogen transfer.

Following the completion of the single crystal cadmium experiment and during the subsequent work, it was observed that, in order to maintain stability of line position, more frequent filling of the detector dewar was necessary. It was concluded that this was an indication of a gradual but progressive degradation of the vacuum jacket on either the dewar vessel or on the detector assembly itself. Subsequent to this observation the detector dewar was filled every 3 days as opposed to the former frequency of 4-5 days. No net degradation in stability was observed as a result of this increased frequency.

4.2.3: Lineshape Correction Techniques

In addition to the on line stability correction techniques described in section 4.2.1., many workers employ off line correction methods. A typical example is that of [118] in which the 477keV mono-energetic gamma-ray of ^{7}Be is used as a control line. In such procedures, the lineshape parameter obtained from observed annihilation spectra are corrected for the observed changes in the reference peaks which are collected simultaneously with the annihilation peaks [118, 117, 119]. In order however that the G-parameter be defined with a precision sufficient to justify the application of such procedures, good counting statistics are required for the control line. A further requirement is that the counting rate be maintained at a constant value since the lineshape is counting-rate dependent. This requirement necessitates the adjustment of the counting-rate during the experiment to compensate for source decay since both of the isotopes commonly used for such purposes (^{7}Be, ^{103}Ru), are short lived.

No attempt was made in this study to employ the control line for correction purposes because of the inadequacy of the reference source counting rate. The rates used however were sufficient to define the reference peak centroid to within $\lesssim 0.1$ channels.

4.2.4: Calibration and Resolution of Spectrometer

In the type of detector here used, an incident photon of gamma radiation expends its energy by the production of free electrons through pair production, the photo-electric effect and the Compton effect. The charge thereby liberated is collected by means of the application of an electric field. Causes of inefficiency in such a detector are trapping by defects and by impurities in the semiconductor crystal. Another contribution to the finite intrinsic resolution of the spectrometer is electronic noise.

In determining the optimum desirable energy dispersion for a spectrometer, a compromise must be made between the dispersal of the spectrum over the largest available range of channels and the statistical accuracy of the resulting contents of each channel. For the spectrometer employed in this work an energy dispersion of approximately 94eV per channel was used.

For each experiment in this study, the intrinsic resolution of the spectrometer was determined through the collection of spectra arising from the mono-energetic 514keV line of ^{85}Sr. Each such spectrum was accumulated over a period of 7200seconds and contained approximately 2.5×10^{6} counts.

The reference spectrum thus obtained was gain shifted such that the centre of the 514keV line appeared in the analyser channel which, under normal operating conditions, corresponded to 511keV, figure 4.3 . The differences observed between these spectra and those collected under normal conditions of gain were within statistical limits [116] and, accordingly all reference spectra were subsequently collected under exactly the same experimental conditions as the positron annihilation spectra.

The effect of the total counting rate on the resolution of the spectrometer is shown in figure 4.4 in which the full width at half maximum of the 514keV gamma-ray is given as a function of the total counting rate. As a compromise between the resolving power and statistical accuracy , a total counting rate of 5000 counts per second was used throughout the experiments in this study. The intrinsic linewidth of the spectrometer at 514keV i.e. the full width at half maximum was found to be 1.15keV under the above conditions of gain and counting rate.

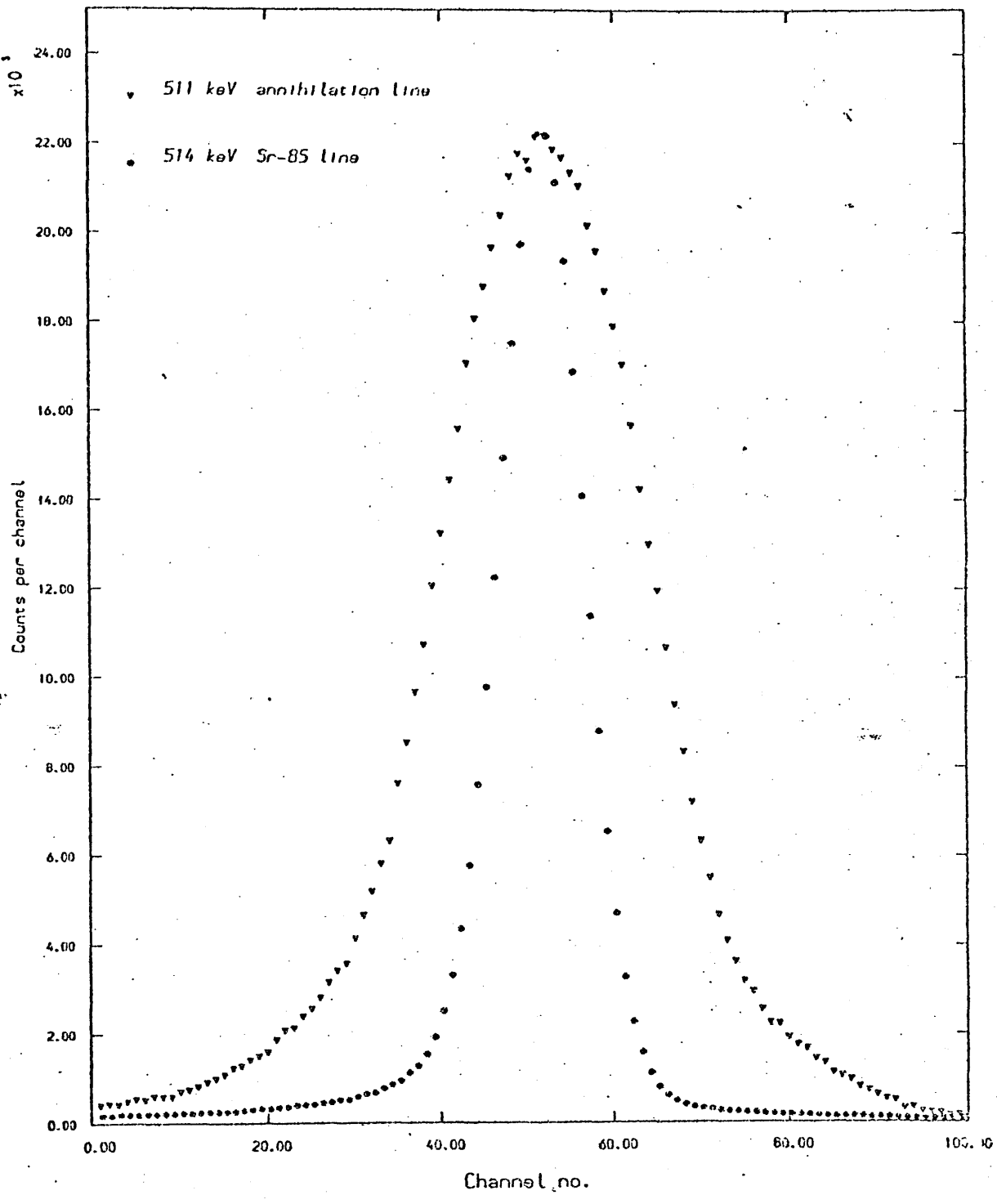

Figure 4.3: The gain shift of the ^{85}Sr gamma-ray to the 511KeV position.

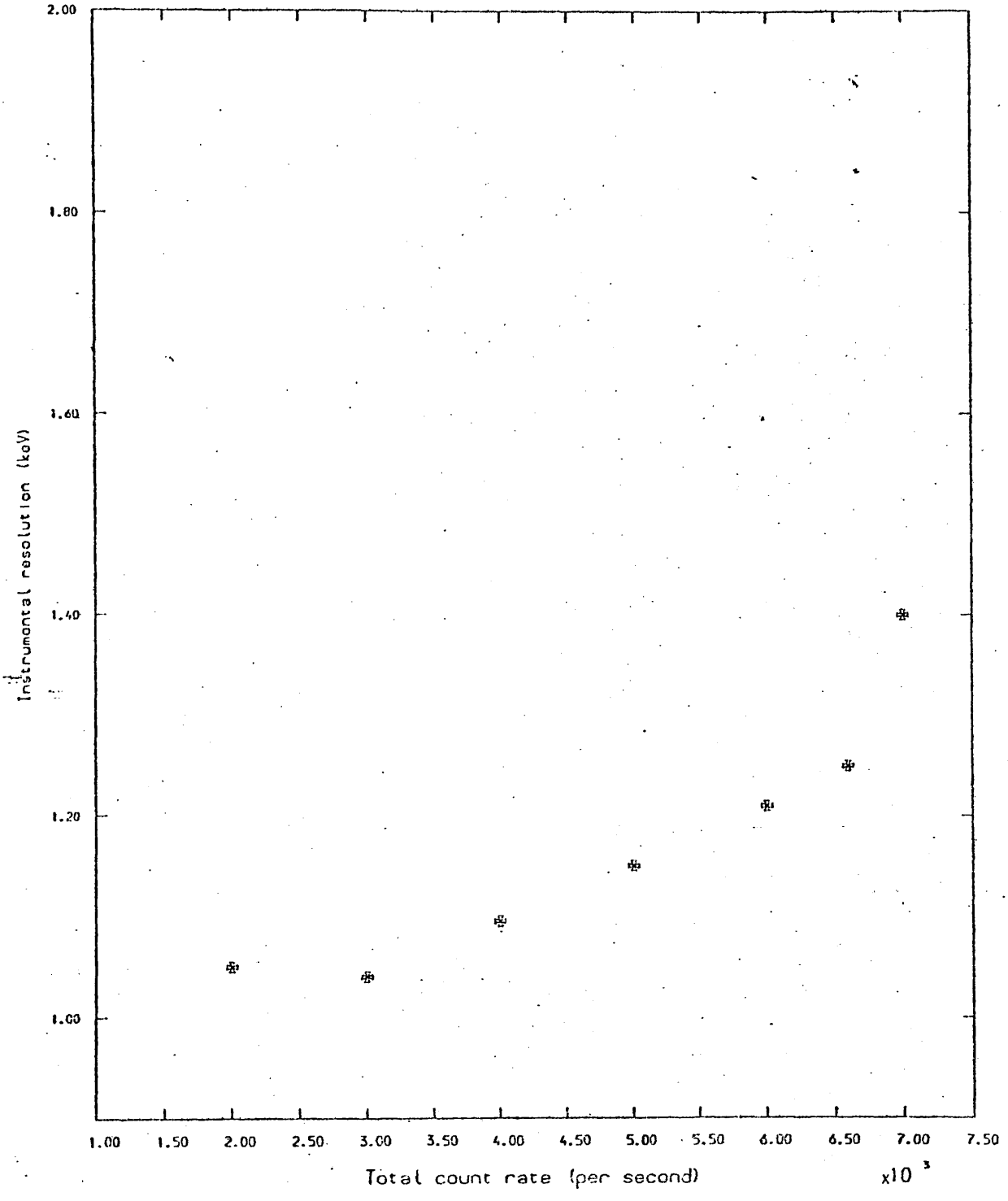

Figure 4.4: The dependence of the system resolution on the total counting rate.

4.3: LOW TEMPERATURE EXPERIMENTS

4.3.1: Low Temperature Cryostat

A low temperature cryostat mounted centrally in the innermost of an arrangement of two concentric Pyrex dewar vessels having outer diameters of 150mm and 90mm respectively, was employed to facilitate measurements of positron annihilation spectra at temperatures between 4.2K and 410K. During such measurements, the specimen was mounted on a copper sample holder of 99.99% (4N) purity. The cryostat is shown in figure 4.5 while the Pyrex dewars are shown in figure 4.6 .

The sample mounted in the cryostat was thermally isolated from the surroundings exterior to the brass chamber by means of an interior vacuum. This was achieved using the conventional technique of an indium wire seal around the flange at the top of the chamber and the use of an Edwards E02 oil vapour diffusion pump of inside diameter 76mm. By the use of such an arrangement pressures of less than 10^{-6} torr were achieved throughout the observations.

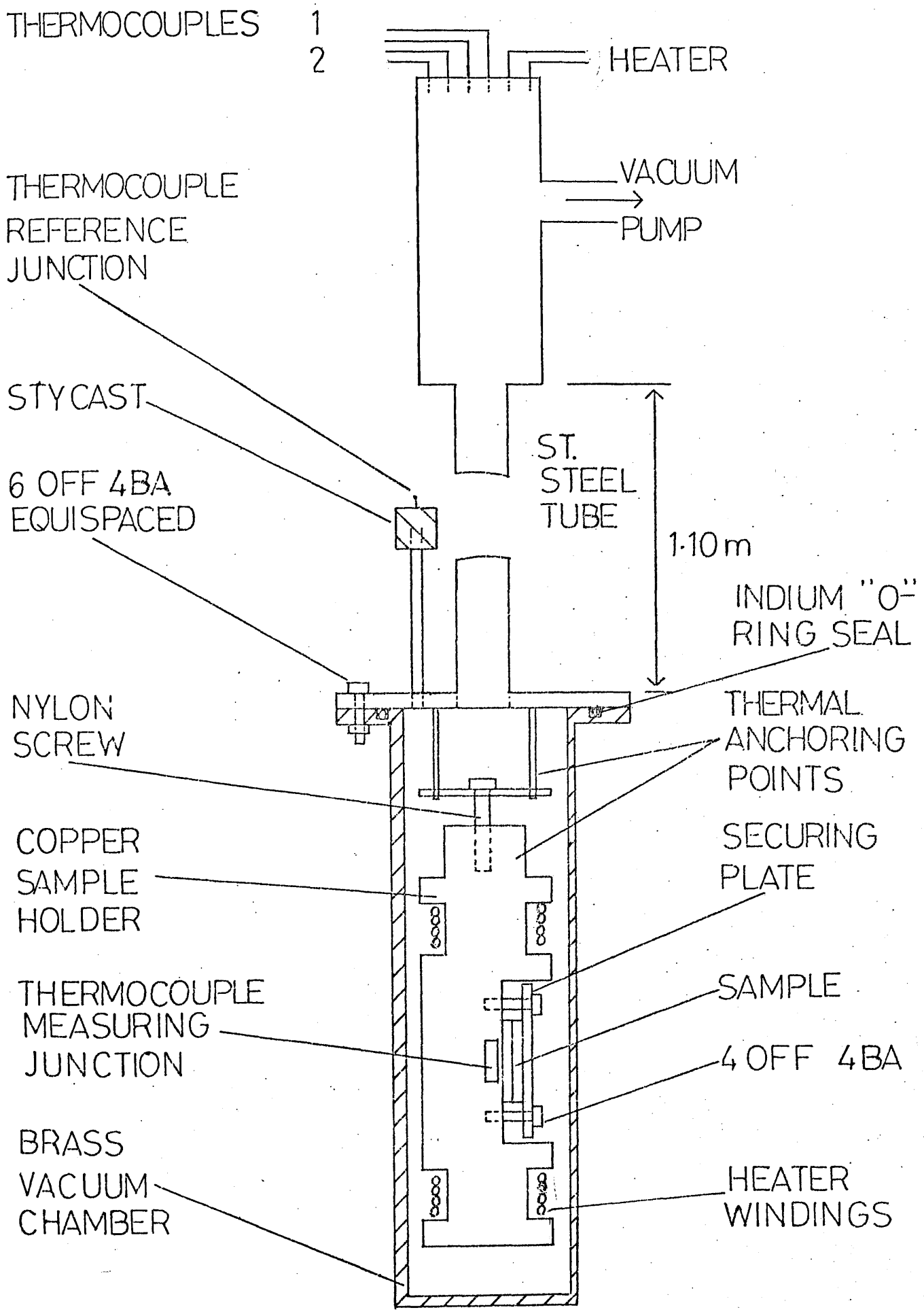

Figure 4.5: A schematic diagram of the low temperature cryostat.

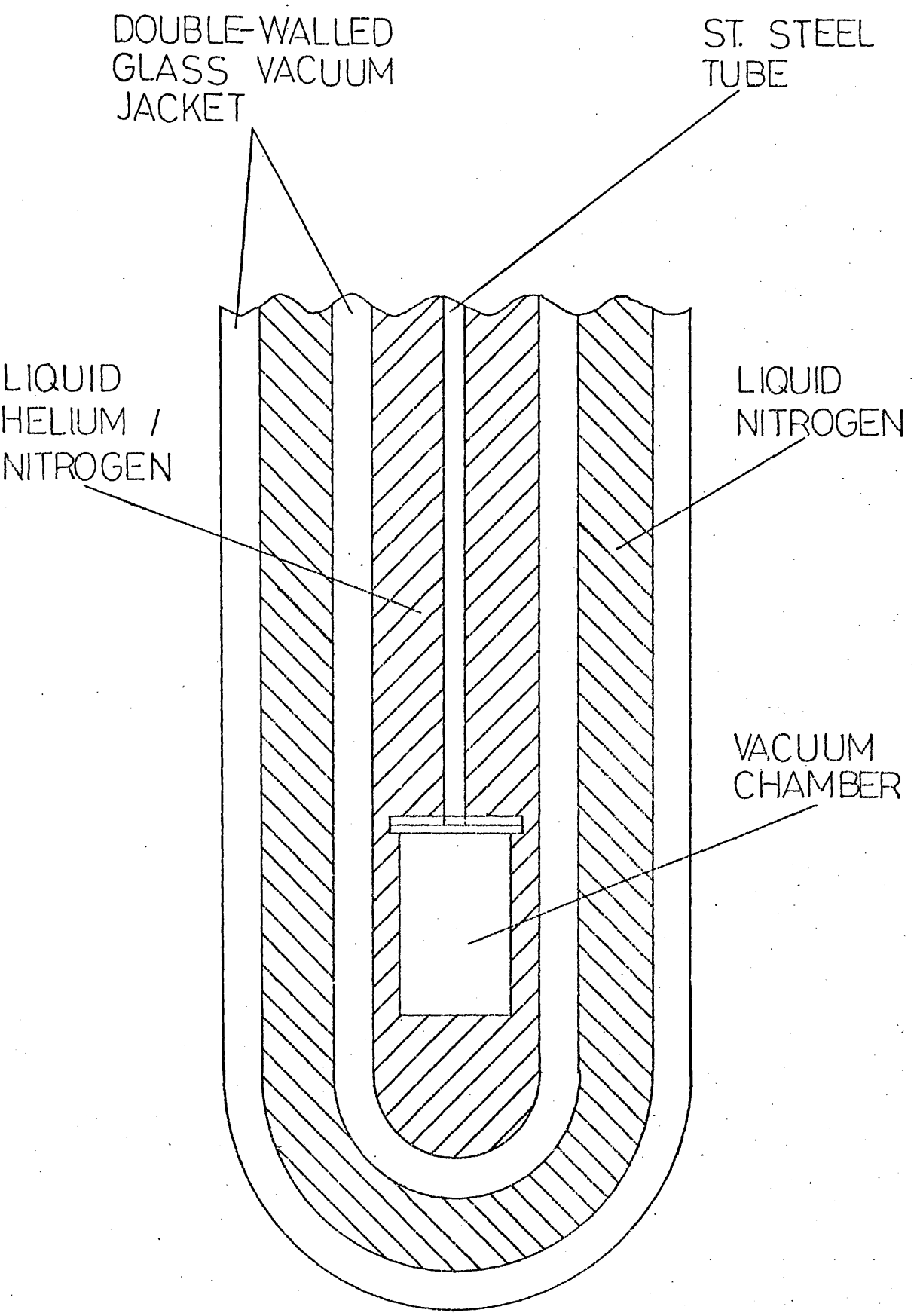

Figure 4.6: A cross-section of the pyrex dewar assembly.

For measurements made in the specimen temperature range from 4.2K to in excess of 80K, the refrigerant used in the inner Pyrex dewar was liquid helium. At sample techniques significantly greater than 80K, the greatly increased boil-off rate makes impracticable the continued use of liquid helium. Therefore, in the temperature range from 80K to 410K, liquid nitrogen was used as refrigerant in the inner dewar. At all times the inner dewar was shielded from the room temperature environment by the outer dewar which contained liquid nitrogen. The pressure in the inner dewar insulating jacket was maintained at 10^{-1} torr while that in the outer dewar jacket was approximately 10^{-6} torr.

4.3.2: Automatic Liquid Nitrogen Dispenser

In order that changes in the level of refrigerant in the dewar vessels did not contribute to variations in the Gamma -ray scattering environment, it was found necessary to prevent the level in either dewar from falling below the half-way mark. A further requirement was that the transfer of either liquid nitrogen or liquid helium take place between counting periods. In general, the outer dewar was replenished at the end of every counting cycle while the inner dewar was recharged with liquid nitrogen every two or three cycles as necessary. On the occassions when liquid helium was used, in general three cycles were completed between transfers.

The need for periodic restoration of refrigerant levels, particularly that of the outer dewar, restricted the accumulation of data and, in order to alleviate this, an automatic liquid nitrogen dispensing system was developed to maintain the liquid nitrogen level in the outer dewar.

Initially this system took the form illustrated in figure 4.7 . In this arrangement the dispensing of liquid nitrogen was controlled such that the level in the outer dewar was maintained between two diodes placed in the outer dewar. When the level in the dewar fell below the lower diode, the solenoid valve was opened and liquid nitrogen was gravity-fed into the object dewar from the overhead storage vessel. The transfer was terminated when the nitrogen level in the outer dewar reached the upper diode. While this arrangement allowed for an extension of data collection it suffered from several faults. Notable among these were:

the small volume of the storage vessel (25 litres);

the need for accurate location of the level monitors in order to guarantee transfer between analysis times;

the occasional failure of the upper level diode to activate, which caused the loss of the contents of the storage vessel;

the tendency for the solenoid valve to freeze in the open position which again caused the loss of liquid nitrogen.

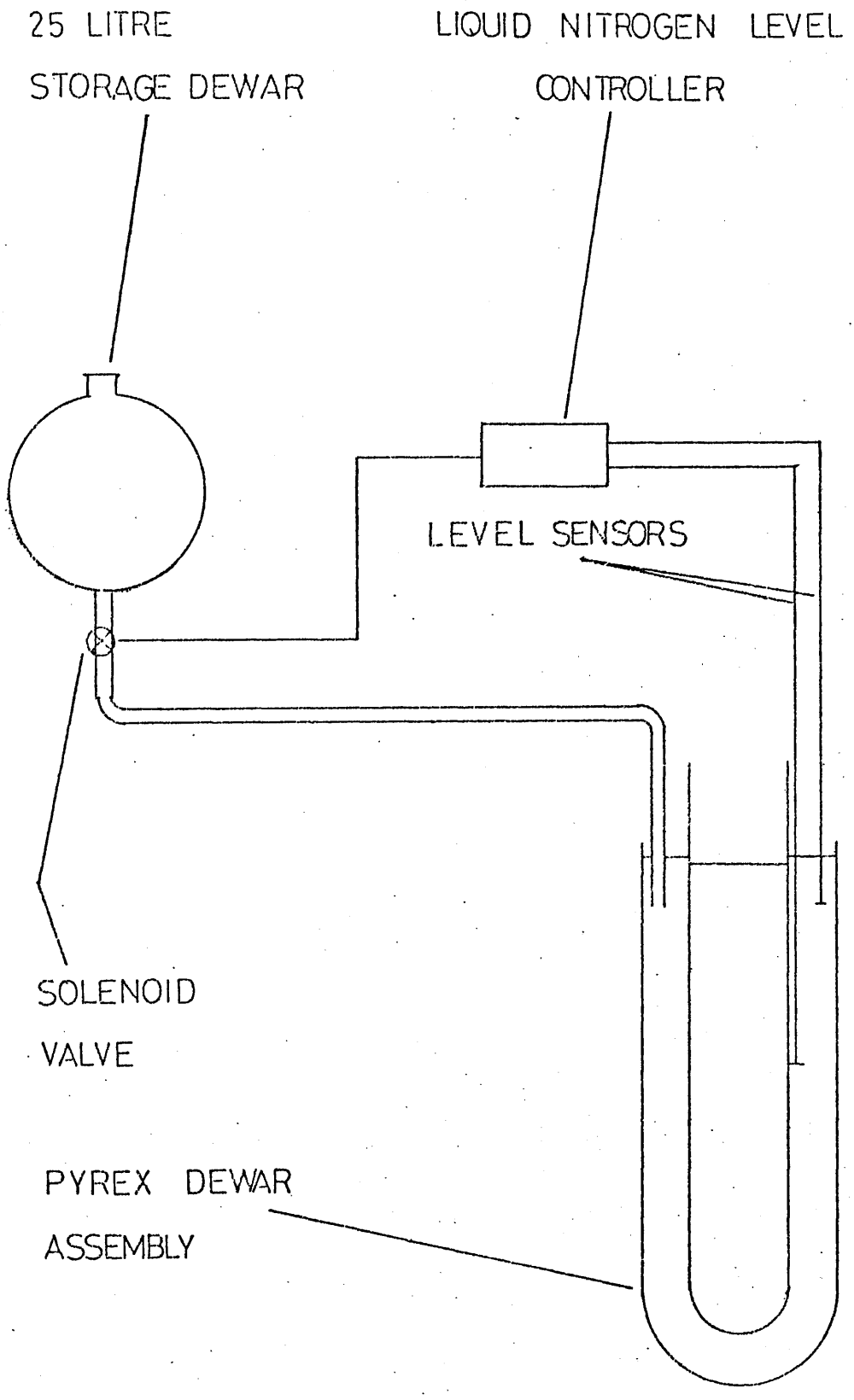

Figure 4.7: A schematic diagram of the early version of the automatic liquid nitrogen dispensing system.

These problems motivated the design of an improved system, illustrated in figure 4.8. In this arrangement the small storage vessel was replaced by a 200 litre self-pressurising dewar. In this, the pressure by which the contents were transferred was maintained by a boil-off system which syphoned a small amount of liquid nitrogen from the bottom of the dewar to a heat exchanger in which the nitrogen evaporated and from which the vapour was fed into the top of the storage vessel. This process continued until the internal pressure reached that required by the user. In the event of over-pressurisation, the excess was vented off. It was found that a pressure of approximately $0.5 Kgcm^{-2}$ within the vessel was sufficient to provide a satisfactory transfer.

As in the earlier version, the transfer was activated by the opening of a solenoid valve; however, in this system two such valves were used in series in order to reduce the possibility of a frozen-open valve leading to the loss of the entire contents of the storage vessel. A further difference between the two systems was the replacement in the later version of the level monitors by a timing mechanism. In this a time controller which was capable of restoring or interrupting the supply voltage at intervals of 15 minutes was employed to turn on a time-delay relay which in turn supplied the solenoid valves. When power was first supplied to the relay a clock was started and the power supply was maintained until the preset delay had elapsed, at which time the solenoid valves closed. A

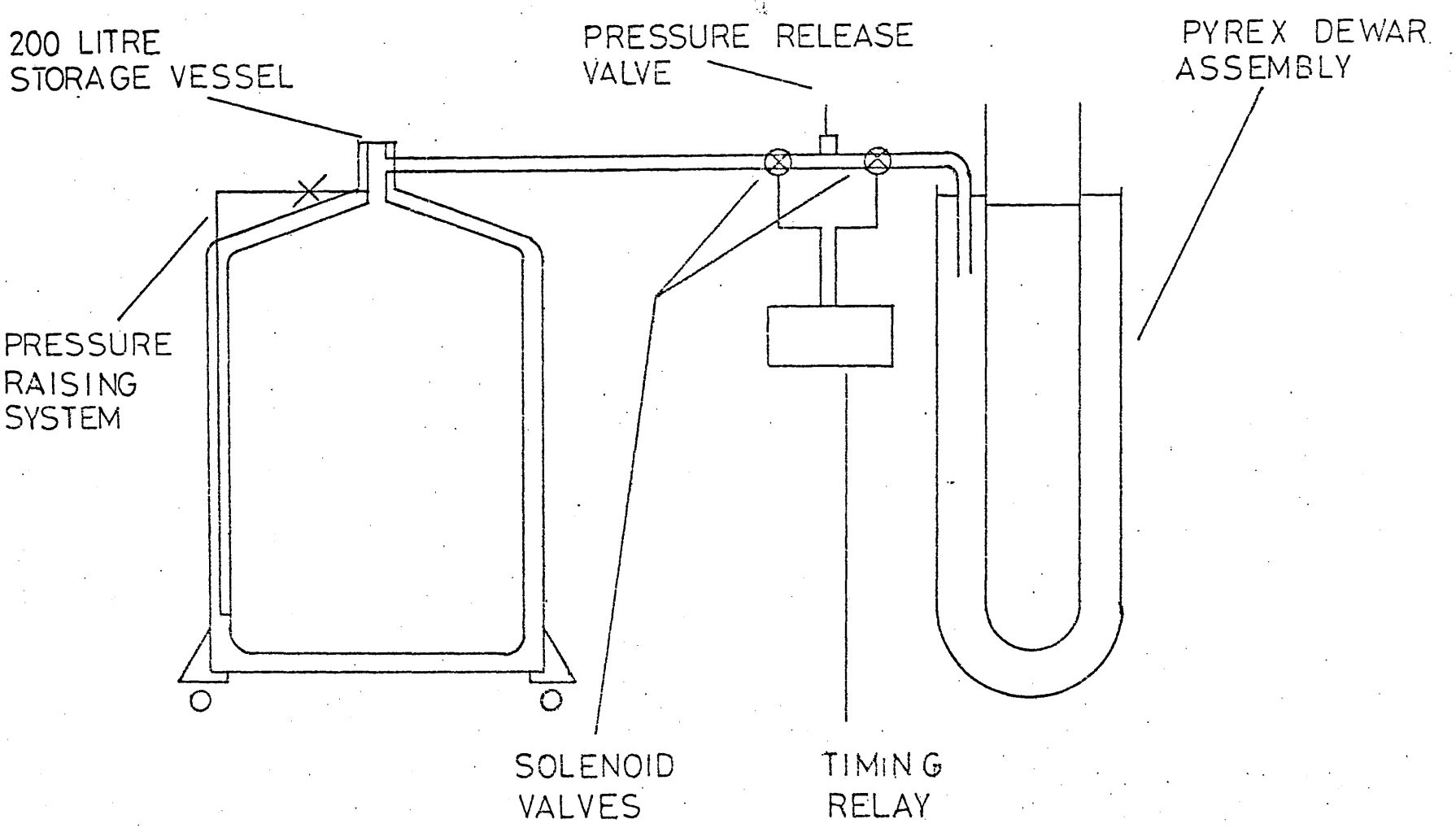

Figure 4.8: A schematic diagram of the final version of the automatic liquid nitrogen dispensing system.

short time later the power was removed from the relay, allowing it to reset in readiness for the start of the next cycle. The timing settings of the system were such that the controller activated the relay only during the dead-time between measurements. The relay was set such that the system was active only for that time required to restore the nitrogen level in the outer dewar to within a few cetimetres of the dewar capacity. It was found that a time of approximately 150 seconds was required to replace that nitrogen which had boiled off during the measurement cycle time.

In order that the expansion of the liquid nitrogen trapped between the solenoid valves did not lead to a rupture of the dispensing tube, a pressure-relief valve was fitted to the supply line between the valves. Using this dispensing system it was possible to maintain the nitrogen levels in both dewars at satisfactory levels for unattended periods in excess of 24 hours.

4.3.3: Temperature Control and Measurement

One obstacle to the maintenance of a constant low temperature in an arrangement such as that described in section 4.3.1 is the leakage of heat from the room temperature environment down the cryostat wiring and vacuum tubing to the sample chamber. The magnitude of this problem

was reduced in this case by the thermal anchoring at low temperatures of the cryostat wiring at a point remote from the specimen.

In order to compensate for the remaining heat leak and to reduce to a reasonable minimum the time taken for the specimen to reach thermal equilibrium with the surrounding liquid refrigerant (viz 4.2 K in the case of helium and 77 K in the case of nitrogen), a small controlled volume of helium exchange gas was injected into the specimen chamber when measurements at these "refrigerant" temperatures were required. Initial upward movement of the sample temperature from these points was achieved by pumping out this exchange gas.

Apart from the above-mentioned exception, the adjustment and regulation of the specimen temperature was effected by the use of a 60Ω heater constructed from a length of enamelled Constantan wire which was wound symmetrically around the sample holder both above and below the specimen mounting position.

The sample temperature was measured by means of a Spec pure Au +0.03At%Fe vs Chromel-P thermocouple, the measuring junction of which was mounted on the copper specimen holder adjacent to the sample mounting point. This thermocouple was calibrated over the temperature range 4.2 to 100 K with the reference junction at 4.2 K and also over the range 77 to 420 K with the reference junction at 77 K.

Control of the sample temperature to within ±Ø.5 K was achieved through the use of a digital temperature controller supplied by Oxford Instruments Ltd. This device seeks to maintain temperature stability by supplying a voltage to the sample heater proportional to the output of a voltage comparator. The two arguments of this comparator are the thermocouple voltage corresponding to the desired temperature and that corresponding to the actual temperature.

In addition to this proportional term, the output of the digital temperature controller was dependent on two further arguments viz a differential term and an integral term. The purpose of these latter two terms was respectively, to damp the rate of temperature adjustment in order to reduce the possibility of overshoot (differential) and, to integrate out small steady state errors between the desired and the measured temperature. In order that the digital temperature controller be well-matched to a particular heating system, it was necessary to optimise the setting of the proportionality constant of the linear term and also the timing constants of the differential and integral terms.

4.4: HIGH TEMPERATURE EXPERIMENTS

4.4.1: High Temperature Vacuum Furnace

A vacuum furnace was employed to facilitate the measurement of positron annihilation spectra at temperatures above 410 K, figure 4.9 . It was found that the illustrated design was convenient for such an application in that its small size allowed for rapid evacuation and ease of handling. A further feature of the design was that it enabled the mounting of the specimen in close proximity to the detector thereby allowing reasonably high counting rates to be attained.

In order that the detector be thermally isolated from the furnace, the heater windings which were situated over the central 200mm of the tube were wrapped in a layer of asbestos insulation ribbon and the central section of the furnace surrounded by a 1mm thick aluminium enclosure.

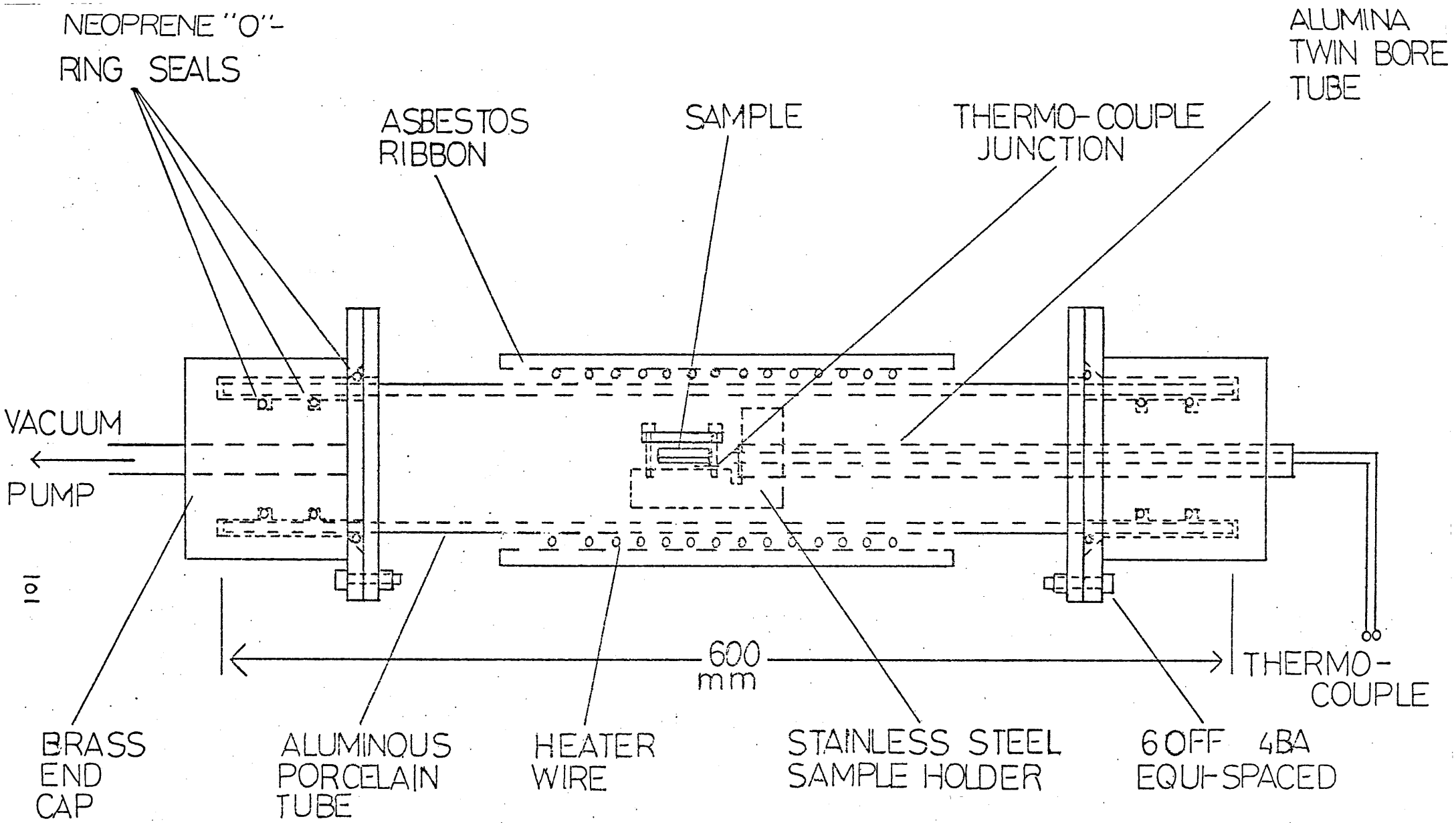

Figure 4.9: A schematic diagram of the high temperature furnace.

4.4.2. Vacuum and Temperature Control

In order that the specimen be secure from the dangers of oxidation and contamination at temperatures up to within a few degrees of its melting point, it was desirable to maintain a good vacuum within the furnace. To achieve this, the ends of the furnace tube were sealed by means of "o" rings within machined brass end-caps and the interior of the furnace evacuated to a pressure of less than 10^{-6} torr by the use of an Edwards E02 oil vapour diffusion pump.

The sample temperature was measured by a nickel-chromium vs nickel-aluminium thermocouple (BS 1827), the measuring junction of which was sandwiched between the specimen and the stainless steel sample holder. The reference junction of this thermocouple was mounted in a solid-state thermocouple reference, bath supplied by Mectron Ltd. The advantage inherent in the use of such a device as opposed to ice is that it maintains a constant temperature of 273 $\pm$ 0.01K without requiring attention.

Control of the sample temperature to within $\pm$0.5 K was achieved by the use of a temperature controller similar to that used in conjunction with the cryostat. However, because of the higher power requirements of this application, the output of the digital temperature

controller was used to control the output of a 3kw power unit supplied by Oxford Instruments Ltd.

4.5: AUTOMATIC TEMPERATURE CONTROLLER

The functions of the spectrometer multi-channel analyser were coordinated with the operation of the temperature control system by the use of a programmable cycle controller. In this, one cycle represents the time taken to adjust the specimen temperature to the desired value plus a constant temperature stabilisation time in addition to the counting time required for the spectrum. The controlling unit was programmed for the length of each experimental cycle and for the temperature increment to be effected between positron annihilation measurements.

On commencement of each cycle this controller activated the transfer of the integrated spectrum from the analyser memory to a teletype while simultaneously initiating the temperature setting procedure. The latter consists of a preset number of microvolt increments or decrements which are transmitted to the "temperature set" arm of the voltage comparator of the digital temperature controller. The time interval between each of these steps is an adjustable parameter and is varied in accordance with the experimental conditions in order to ensure that the sample temperature moves smoothly and without overshoot. On

completion of the temperature setting procedure a 500 second temperature stabilisation period is begun. At the end of this hiatus the transferred spectrum is erased from the analyser memory and the counting cycle restarted.

The controller described above was employed to automate experiments for both high temperature (furnace) and low temperature (cryostat) environments. In the latter case it was necessary, for reasons discussed in section 4.3.2., to synchronise the operation of the automatic dispensing system with the temperature setting period of each experimental cycle.

4.6. RADIOACTIVE SOURCES

Throughout this work the positron emitter used was an a queous solution of carrier-free sodium chloride which was supplied by Amersham International Ltd. (formerly the Radiochemical Centre). The specimen-source sandwiches were prepared by depositing individual drops of the source material onto the centre of one of the specimen slices. Each individual drop was subsequently dried before the application of any further source material.

The gamma-ray reference sources employed (^{103}Ru, ^{85}Sr) were obtained by the irradiation at the University of London Reactor Centre of RuO_2 and $SrCO_3$ respectively.

CHAPTER 5: ANALYSIS TECHNIQUES

5.1: INTRODUCTION

In Doppler broadening studies of positron annihilation, it is convenient to characterise the changes of lineshape through the use of a lineshape parameter. The first such lineshape parameter suggested [49] was the full width at half maximum of the 511KeV peak. The most commonly used lineshape parameter (here called the F-parameter) was proposed as a refinement of this initial parameter [50] and is equivalent to the H-parameter used in angular correlation studies.

The F-parameter is defined as the ratio of two integrals: the integral taken over a small energy range symmetrically disposed about the centroid of the annihilation line, divided by the integral over the whole line. Thus, as the annihilation line becomes narrower, the value of the F-parameter increases. Changes in the relative proportion of core- to valence-electron annihilations are therefore reflected by changes in the F-parameter.

The study of the Doppler broadening of annihilation radiation involves the simultaneous accumulation of data throughout the entire momentum range. As a result, there is considerable scope in the choice of lineshape parameters. Other parameters can be used in addition to or instead of

the peak height or F-parameter.

The W-parameter is a tail or wing parameter, defined as the sum of two symmetrically disposed wing portions of the annihilation line, divided by the integral of the whole line. Other, more complex, parameters are the N-parameter [120] and the parameters derived from Running Integrated Difference Curves [121].

An alternative to the use of lineshape parameters is the deconvolution of the annihilation line. This approach is more complicated than the former and can be both very lengthy and very costly in terms of computing time, particularly if employed on a large scale. Nevertheless, the advantage of this technique resides in its ability to extract momentum information which otherwise would be inaccessible.

5.2: LINESHAPE PARAMETERS

5.2.1: The F-and W-Parameters

As has been mentioned in the previous section, the lineshape parameter F is widely used to characterise Doppler broadening annihilation spectra. The application of this parameter to the study of e.g. a well annealed metal specimen, follows from the assumption that at very low

temperatures all the positrons will annihilate from the free state and the annihilation lineshape will be characteristic of free annihilation. As the specimen temperature is raised, thermally activated defects are introduced and the lineshape begins to narrow as a result of the increasing occurrence of annihilation at defect sites. This process reaches a saturation point when all the positrons annihilate at defects and, at or beyond this temperature, the lineshape is characteristic of defect trapping. At these extremes then, the values of the F-parameter will be characteristic of an annihilation mode.

Also, from the previous section, the F-parameter was defined as the integral taken over a small energy range symmetrically disposed about the annihilation line centroid (n_1), divided by the integral of the whole line (N). This is illustrated in figure 5.1, together with the case for the W-parameter, where

$$W = n_2/N \qquad 5.1$$

An important feature of both the F- and W-parameters is their superpositional property. If various modes of annihilation occur with frequency f_i, each having a lineshape parameter F_i, then the observed F is a linear combination of the individual F_i's,

$$F = \frac{\sum_i f_i F_i}{\sum_i f_i} \qquad 5.2$$

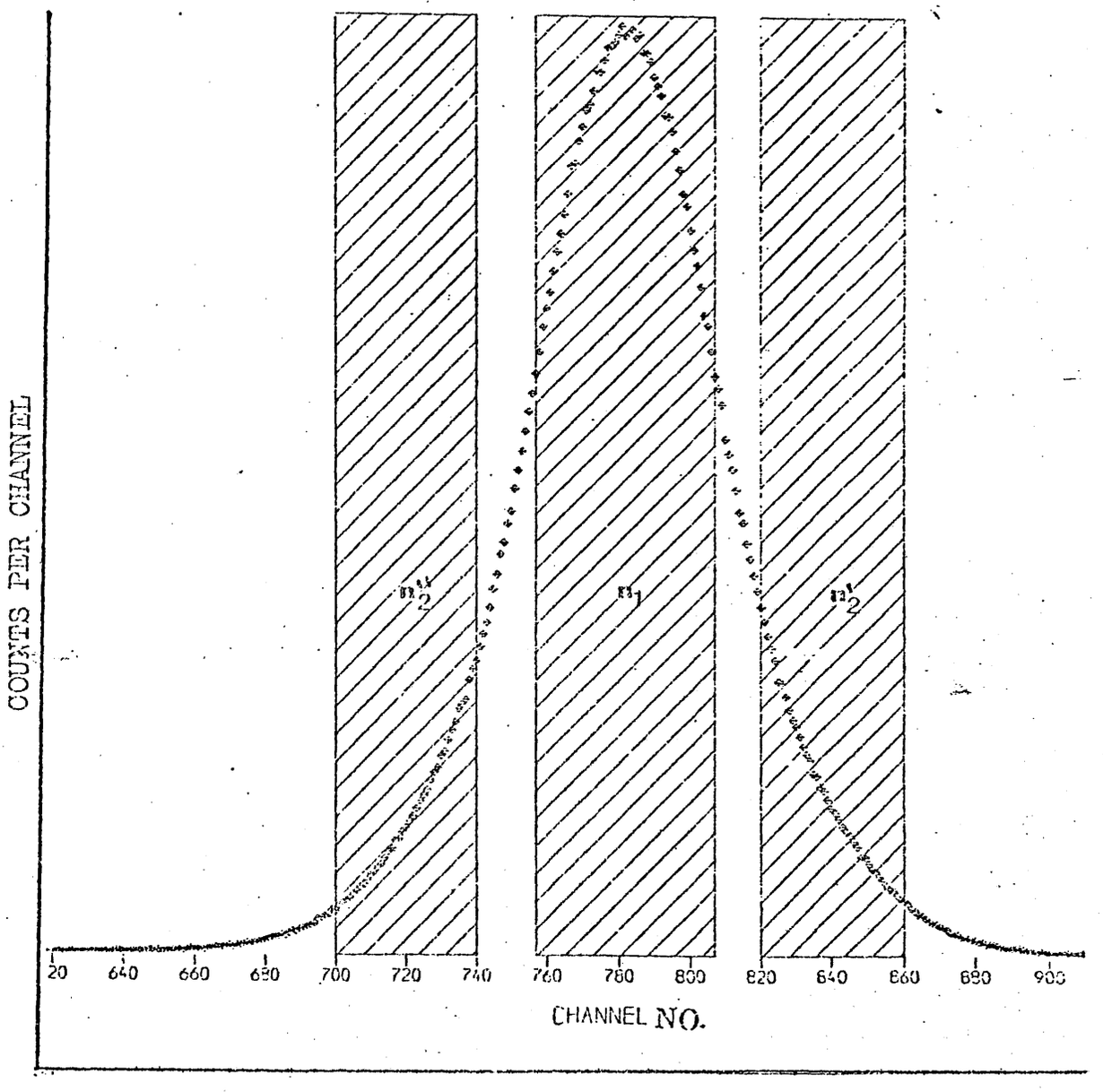

Figure 5.1: An illustration of the definition of the F- and W-parameters.

This property is extremely useful in studies of positron trapping at defects.

5.2.2: Statistical Properties and Sensitivity of Lineshape Parameters

The statistical properties of the F-parameter are determined by the binomial distribution since, in the definition

$$F = \frac{n_1}{N} = p \qquad 5.3$$

there are two classes of events. We therefore have

$$P(n_1) = \binom{N}{n_1} p^{n_1} (1-p)^{N-n_1} \qquad 5.4$$

for $n_1 = 0, 1, 2-N$, and $0 < p < 1$. The measured central intensity therefore has variance

$$V(n_1) = Np(1-p) \qquad 5.5$$

and the standard deviation of the F-parameter is

$$\sigma(n_1/N) = N^{-1.5}[n_1[N-n_1]]^{\frac{1}{2}} \qquad 5.6$$

Thus for a typical value of $F \sim 0.5$, we have $\sigma(F) = \frac{0.5}{\sqrt{N}}$

In order that gain or zero drifts do not introduce fluctuations significant with respect to the statistical error in the lineshape parameter, it is desirable that some sort of spectrometer stabilisation is employed. Such a means of reducing electronic instability is discussed and a

procedure by which the problems caused by instabilities can be alleviated is introduced in [117]. A further correction technique, in which the 478KeV gamma-ray from ^{7}Be is used as a monitor of the energy resolution of the spectrometer, is described in [122]. Also of importance to the success of a lineshape parameterisation is the accurate subtraction of the background underlying the annihilation peak. Such a procedure, employing the complimentary error function, is described in [123, 124].

Before proceeding to the application of the F-parameter to the study of defects in metals, it is necessary to decide upon a convenient width of the central integration region. It is desirable to maximise the response of the lineshape parameter e.g. by reducing the number of channels in the central region. However, in so doing, the statistical counting error is thereby increased. It is therefore necessary to strike a compromise between these two factors. One measure of the sensitivity parameter is the ratio of the change in lineshape parameter over the experimental range of interest to the statistical error (1σ) in the change [54]. This sensitivity can obviously be further enhanced by increases in counting rates or in counting times. However, such enhancements could be negated by the degradation of the spectrometer resolution resulting from higher counting rates or by the increased probability of temperature induced spectrometer instabilities, affecting the quality of the data over longer counting periods. A further complication is that an optimum choice of lineshape definition is not specimen independent since lineshapes arising from metal

samples vary, depending on the mix of valence and core annihilations, the Fermi cut-off and the trapping strength.

The lineshape parameters discussed above can all be used in a straightforward fashion in the trapping model, versions of which were discussed in chapter 3.4.

5.3: CONVOLUTION ANALYSIS

5.3.1: Convolution of Positron Annihilation Lineshapes

The information derived from the study of Doppler broadening of annihilation radiation is, in principle, the same as that available through angular correlation studies. The energy resolution obtained using the Doppler technique is however inferior to that of the angular technique, typically by a factor of approximately ten. The finite resolution of the detector system results in mono-energetic photons being recorded as a distribution over a range of pulse-height channels. The inferiority in resolution of a Ge detector system makes difficult the accurate extraction of information on the momentum distribution of the annihilating electron-positron pairs, as the width of the instrumental resolution function is substantial in comparison with the width of the Doppler broadened annihilation line. Accordingly, precise information about

the momentum distribution is generally more profitably sought by means of the angular correlation technique. Nevertheless, the high source strengths and long data accumulation times which are necessary in the latter technique can negate its inherent advantages. The attractions of the Doppler technique in this respect have been increased by the development of computer programs to deconvolute the intrinsic spectrum from that observed [47, 48, 125, 126, 127, 52,].

The observed annihilation spectrum is the result of the convolution of the true distribution with the response function of the spectrometer. This, after background subtraction, can be written as

$$A(E) = \int_0^\infty I(E^1)R(E-E^1)dE^1 \qquad 5.7$$

where E is the energy of the radiation and is directly related to the spectrum channel number. The intrinsic distribution I(E') can, in principle, be deconvoluted from the observed spectrum A(E) by means of the instrumental resolution function R(E-E').

One of the first deconvolution procedures suggested [47] involved the matrix equation

$$S = X.R \qquad 5.8$$

where the rectangular matrix R was the resolution spectrum recorded using the 514KeV gamma-ray of ^{85}Sr, X was the ideal spectrum and S the synthetic spectrum. An arbitrary distribution for X was assumed and the synthetic spectrum was produced. The value of

$$\chi^2 = \sum_i \frac{(S_i-A_i)^2}{A_i} \qquad 5.9$$

was then calculated where A was the observed spectrum. The components of X were then modified and a new chi-squared produced for comparison with the earlier value. The ideal spectrum, corresponding to the minimised value of chi-squared was thus found. An alternative approach, adopted in [48], involved the representation of the resolution function as the sum of two Gaussians fitted to the resolution data by a least squares method. This analytic resolution function was then convoluted with a final energy distribution in functional form, and the final distribution modified until agreement was reached between experimental and calculated spectra.

Later methods [126, 127, 52, 53] combined the model-independent approach [47] with the analytic method [48]. Typical of these techniques is [126] in which the ideal spectrum obtained from the iterative technique was fitted by means of a least squares routine to an analytic model. A new trial function was then constructed from the best analytical fit and the deconvolution procedure repeated until minimisation of both the deconvoluted and analytical spectrum was produced.

In the model-dependent convolution technique, it is necessary to construct a trial analytical function to describe the intrinsic distribution. The optimum value of each of the variables of this function are then determined by means of a least squares fitting routine. The function most often assumed to describe positron annihilation in annealed metals is the concentric sum of an inverted

parabola and a Gaussian distribution. The parabolic component is a representation of positron annihilation with conduction electrons, while the Gaussian function approximates to the core electron annihilation [128, 129]. The intrinsic distribution can then be written

$$(x) = A\exp\left[-\frac{(x-\bar{x})^2}{2B^2}\right] + C\left[1 - \frac{(x-\bar{x})^2}{2D^2}\right] \quad \text{for} \left|x-\bar{x}\right| \leqslant 2\tfrac{1}{2}D \qquad 5.10a$$

$$(x) = 2A\exp\left[-\frac{(x-\bar{x})^2}{2B^2}\right] \quad \text{for} \left|x-\bar{x}\right| > 2\tfrac{1}{2}D \qquad 5.10b$$

where x is the channel number, $\bar{x}$ is the common centroid of the parabola and Gaussian and A,B,C,D, are respectively the height and width of the Gaussian and the height and width of the parabola. The synthetic spectrum is then calculated as

$$S(i) = \frac{1}{N}\sum_{j=1}^{n} I(i)R(i-j) \quad \text{for } i = 1.....n \qquad 5.11$$

where

$$N = \sum_{i=-n}^{n} R(i) \qquad 5.12$$

and the resolution function R is defined over (2n+1) channels. The optimum value of each of the five variables of equations 5.10 is determined by a least squares fit of S(i) to the experimentally obtained A(i).

In this work, the procedure adopted was one of pure convolution embodied in the program CURFIT. The resolution function employed was the spectrum arising from the 514KeV gamma-ray of ^{85}Sr recorded over 150 channels. This was normalised and convoluted with a nine-variable analytical distribution, five of the parameters of which were those explicit in equations 5.10, the other four variables being

those of a third order polynomial which was used to describe the background underlying the peak. The synthetic spectrum thus produced was fitted to the observed annihilation profile by the least squares minimisation routine E04FBF supplied by NAG. An example of such a fitting is shown in figure 5.2 . The analytical description of the annihilation lineshape here employed relies on the assumption that the core electron momentum distribution is, to a good approximation, Gaussian and also takes no account of the higher momentum components of the conduction electron distribution. Despite the simplicity of the description employed, typical values of the reduced chi-squared are in the range 0.9 to 1.3.

Having determined the optimum values of the variables of equations 5.10, the intensities of the conduction and core electron components can then be calculated. If this convolution procedure is performed for spectra recorded over a range of temperatures, the percentage contribution of the parabola to the whole can be displayed as a function of temperature. An example of the variation of the parabola percentage with temperature is shown in figure 5.3. It can be seen that this variation is similar to the temperature variation of the F-parameter in its response to trapping probability.

There are, however, limitations to the successful application of the deconvolution technique. In cases where the width of one component approaches that of the resolution function, or where one component of the spectrum is very

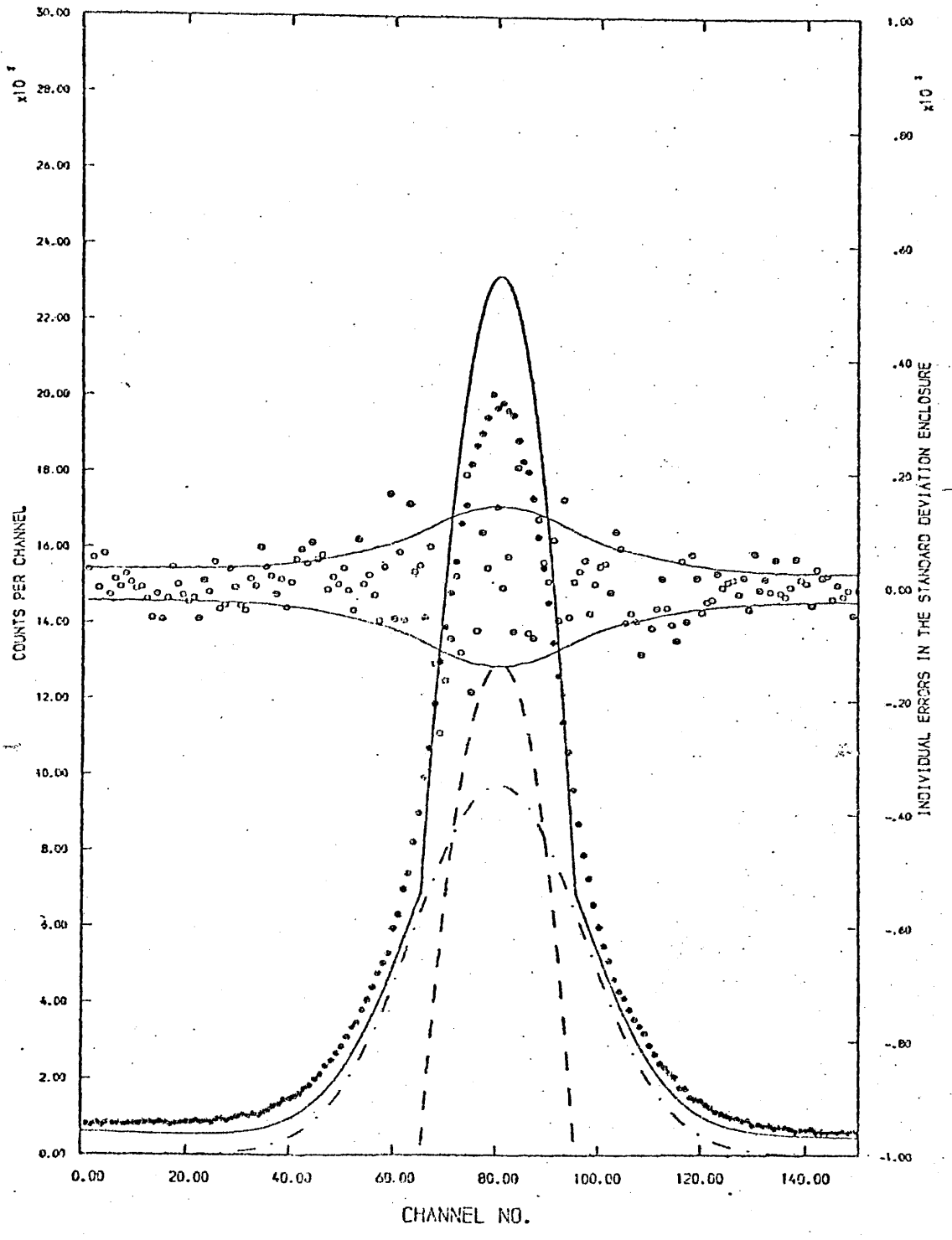

Figure 5.2: The application of the convolution technique a positron annihilation spectrum. The example shown arises from single crystal cadmium.

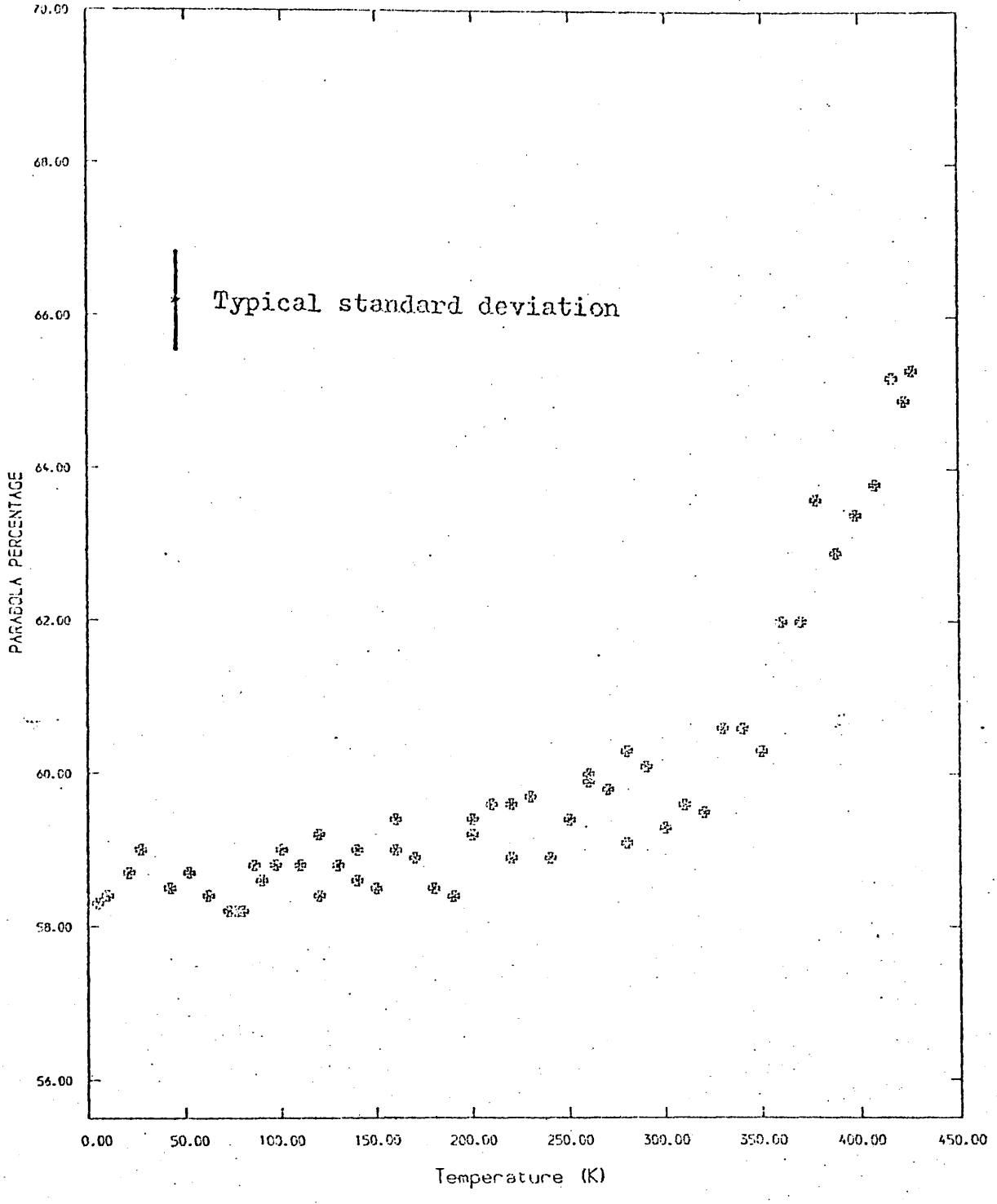

Figure 5.3: An example of the temperature variation of the parabola percentage.

much weaker than the other (~10% of the total intensity), the annihilation spectrum cannot adequately be resolved and , in such cases, the starting values assigned to the variables in the model can influence the optimised values produced by the fitting routine.

5.3.2: Convolution of Positron Annihilation

Lineshapes for Defected Metals

The analytical distribution used to describe positron annihilation in an annealed metal is found to be inadequate when applied to metals exhibiting strong trapping effects [130]. It is thought, on consideration of the Uncertainty Principle, that this inadequacy is a result of the increase in the momentum of the positron, concomitant to its localisation in a trap. In order to take account of the significant contribution of the trapped positron to the momentum of the annihilating pair, it was suggested [130] that an additional function be introduced into the convolution procedure. The motion of the trapped positron was assumed to be that of an harmonic oscillator in its ground state, the momentum distribution of which is Gaussian. The width of this Gaussian will then, in principle, provide a measure of the zero-point energy, E_p, with respect to the bottom of the positron trap,

$$Ep = 3\left(\frac{4\sigma^2}{m_o c^2}\right) \qquad 5.13$$

where σ is the standard deviation of the positron Gaussian.

An effective resolution function, R', is obtained by convoluting the experimentally obtained resolution function with the positron Gaussian and using the resultant function in the convolution procedure in place of the observed resolution function. It is , however, not practicable to introduce the width of the positron Gaussian as a freely floating variable in the minimisation procedure. Instead, the standard deviation of the Gaussian is supplied by the user. Typically, the value of σ is increased from zero in small steps by the user at the end of each minimisation. By this means, a plot of the reduced chi-squared versus σ can be produced, figure 5.4 , and from the value of σ corresponding to the minimum chi-squared, a measure of the trapping strength obtained.

This method of analysis of defected metal specimens results in significant improvements in the accuracy of the value of the reduced chi-squared. However, the information obtained from what can be a very lengthy computing task is only a crude measure of the trapping strength of the relevant defect. This technique, or variations thereon, has been employed to study positron trapping in various types of defect [126,131,132,133,134].

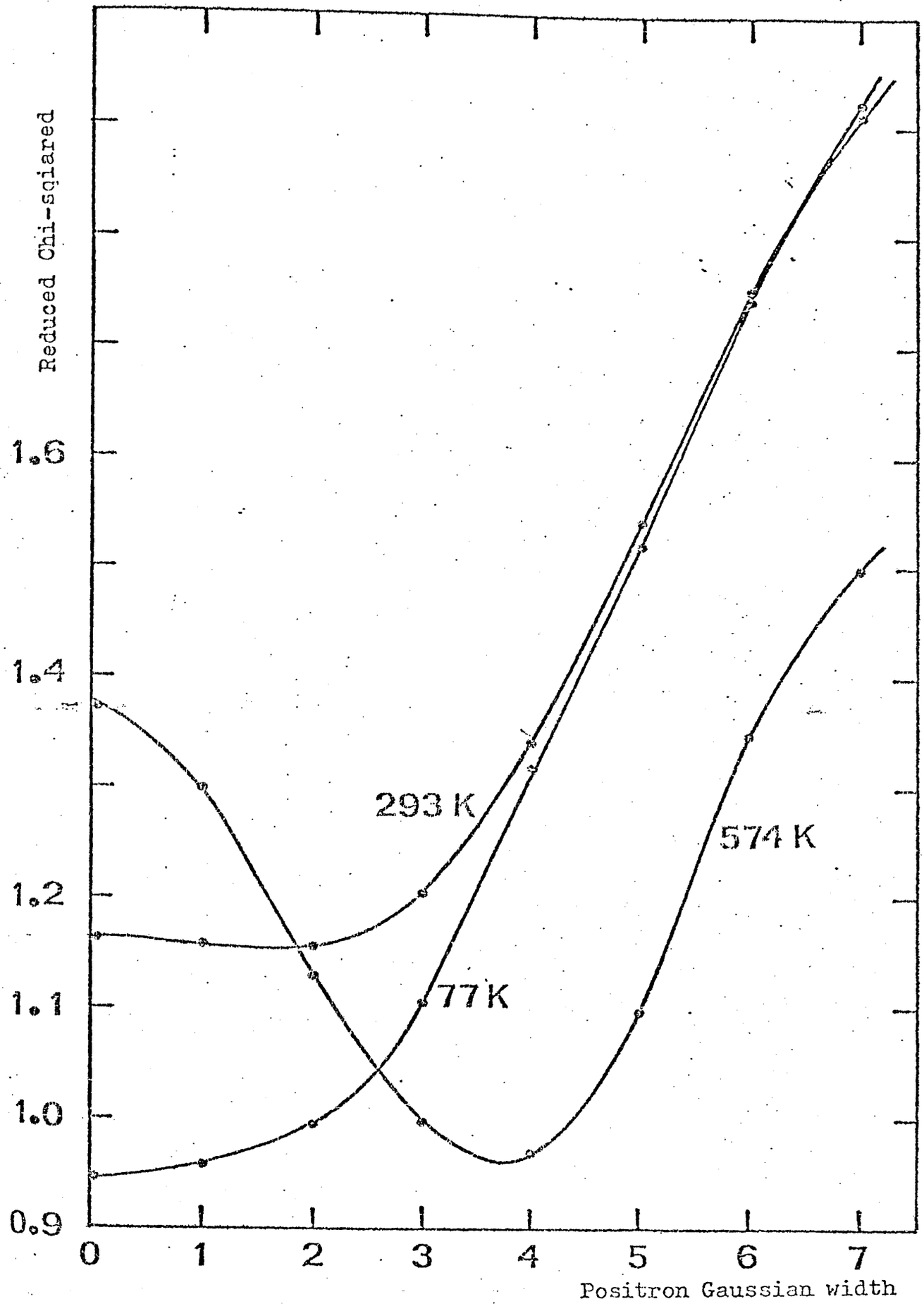

Figure 5.4: An example of the variation of the reduced chi-squared with .

CHAPTER 6: POSITRON ANNIHILATION IN SINGLE CRYSTAL CADMIUM

6.1 : INTRODUCTION

The S-shape which characterises the temperature variation of positron annihilation parameters above the vacancy threshold is explained by the two-state trapping model. This model forms the basis for the determination of monovacancy formation parameters and concentrations from positron annihilation experiments. Observations at lower temperatures in cadmium and other metals have, however, provided evidence of additional anomalous temperature dependences which cast doubt on the precision of vacancy parameters deduced using the trapping model. The uncertainty as to the extrapolation of this pre-vacancy effect into the vacancy region is perhaps greatest for cadmium.

Early angular correlation studies on cadmium [95] revealed an approximately linear temperature dependence in the peak count parameter over the temperature range 100K to 300K. The magnitude of this slope was greater than that expected to arise from the thermal expansion of the lattice and, in order to account for this disparity, a model in which phonon effects were included was proposed [56,7]. Subsequent Doppler broadening studies were reported [80] in

which was revealed the presence of three main regions in the temperature dependence of the positron annihilation characters for cadmium. Thermal expansion was here assumed to dominate, up to approximately 220K, while a new and non-linear equilibrium effect was proposed to account for an enhanced temperature dependence for $220K < T < 370K$. The vacancy region was identified as commencing at 370K .

The intermediate temperature region was later interpreted in terms of the meta-stable self-trapping of positrons [81]. Later, angular correlation peak height experiments supported this description [23] and an examination of the angular distributions of photons suggested that positrons were indeed localised at 330K, which was consistent with the predictions of the self-trapping theory. While further confirmation of this interpretation came from both lifetime [135] and Doppler broadening studies [136], experimental evidence did not consistently support this model [24,137], and indeed it was not supported by theoretical studies [85,84].

The most widely accepted explanation for the pre-vacancy effect includes contributions from volume thermal expansion and from lattice vibrations [59]. In this model it is proposed that the reduction with increasing temperature in the overlap between the positron and core electron wavefunctions which result from both of these approximately linear effects accounts for the magnitude of the observed pre-vacancy rise.

Crucial to the accuracy of vacancy parameters derived from the application of the trapping model, is the appropriate extrapolation of the sub-vacancy temperature dependences into the vacancy region. Unfortunately, the lack of inter-laboratory agreement with respect to the pre-vacancy rise in cadmium has prevented the ultimate resolution of a universally applicable temperature dependence for the region. It is perhaps this uncertainty which is reflected in the inconsistencies of reported monovacancy formation enthalpies for cadmium [95,44].

A further uncertainty is that associated with the magnitude of the slope in the pre-vacancy region and the speculation that this was a result of anisotropic thermal expansion [138]. Such anisotropies were believed to be the cause of wide variations in the pre-vacancy slope arising from polycrystalline and single crystal specimens of cadmium observed by the Bedford College group [136,139,140]. The present orientational study of single crystal specimens of cadmium was prompted by these observations and by those of [166] in which an orientational effect was reported in the coincidence counting rate for a single crystal specimen of cadmium.

6.2: EXPERIMENTAL DESCRIPTION

Two rectangular slices, having dimensions 19 X 18 X 4.5 mm were cut by means of a spark-erosion technique from a rod of 99.999% (5N) purity single crystal cadmium. The crystal, which was supplied by Metal Crystals Ltd., had been grown with the hexagonal axis [ØØØ1] parallel to the axis of the rod. It was verified by means of X-ray photography that the [ØØØ1] direction was normal to the faces of the slices and that the [1$\bar{1}$ØØ] direction was parallel to the longer edges (see figure 6.1). This disposition of the crystallographic axes was chosen in order to facilitate the study of annihilation spectra along both of these directions by means of a simple rotation of 9Ø° of the sample holder. The faces of the slices were then polished, again using a spark-erosion technique, during which process an estimated Ø.25 mm was removed from each slice. The specimens were then chemically polished in 35% nitric acid. Subsequent to thorough rinsing in de-ionised water, the slices were dried and mounted in the vacuum furnace where they were annealed for 26 hours at a temperature of 5ØØK under a pressure of less than $1Ø^{-6}$ torr. On completion of this process, the temperature of the specimens was reduced slowly (<1 degree per minute) to room temperature. The specimens were then chemically polished in 35% nitric acid until a good visual surface finish was

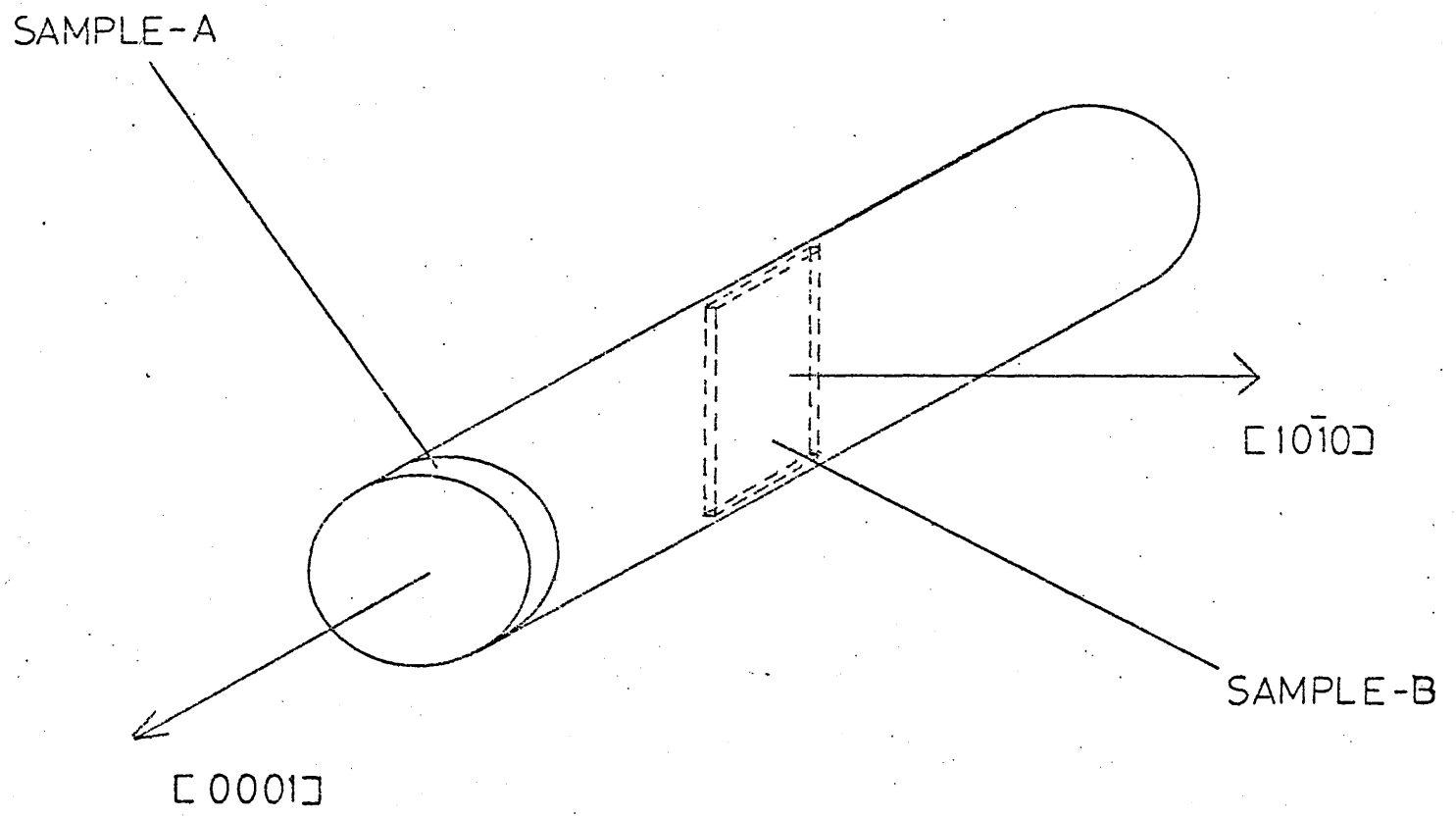

Figure 6.1: An illustration of the disposition of the crystallographic axes with respect to the single crystal cadmium rod.

produced and thoroughly rinsed in de-ionised water.

Approximately 80 microcuries of carrier-free $^{22}NaCl$ in a queous solution was then deposited and evaporated onto the centre of one of the specimen slices, such that the diameter of the source was no greater than 3 mm. A specimen-source sandwich was constructed by aligning the second prepared slice on top of the source carrier such that the [10$\bar{1}$0] directions of the slices were mutually parallel. The sandwich was then encapsulated in a wrapping of thin aluminium foil and the prepared sample mounted on the low temperature cryostat. The cryostat assembly was then placed in front of the detector such that the [0001] direction of the specimen was parallel to the detector axis. The sample-detector distance was approximately 15 cm and the detector crystal subtended an angle of approximately 0.01 sr at the specimen.

Annihilation spectra were recorded at temperature increments of approximately 10K between 4.2K and 400K for the [0001] direction. At each point the specimen temperature stability was better than $\pm$0.1K. On completion of this cycle of measurements, the cryostat insert was rotated by 90° such that the [10$\bar{1}$0] direction was parallel to the detector axis, and a similar series of measurements performed for this orientation. The specimen was then removed from the cryostat and mounted in the furnace where the temperature range 293K to 580K was covered, again in steps of approximately 10K for both directions. At all

times the pressure in the cryostat was less than 10^{-6} torr.

Each spectrum was collected simultaneously with a ^{103}Ru reference peak at a total counting rate of 5000 cps. Over the two-hour counting time used at each temperature, the 511keV spectrum contained approximately 900,000 counts.

6.3: LINESHAPE PARAMETER ANALYSIS

Prior to the computation of the lineshape parameter, all the spectra were subjected to a background subtraction procedure which employs the complementary error function [124]. The width of the central region chosen to define the F-parameter was 15 channels. The energy dispersion, as obtained from the calibration of the spectrometer, was 0.0943 keV per channel. The temperature variation of the F-parameter in the case of radiation emitted in the [0001] direction is shown in figure 6.2, while that corresponding to the $[10\bar{1}0]$ direction is shown in figure 6.3 [141]. Average statistical errors (2σ), as defined in chapter 5.2.2, are for the [0001] direction, 0.0010 and for the $[10\bar{1}0]$ direction, 0.0011 .

As can be seen from both of these figures, the temperature dependence of the lineshape parameter can, in accordance with that observed in earlier reported studies, [80,23,135,142,140], be divided into three regions. For

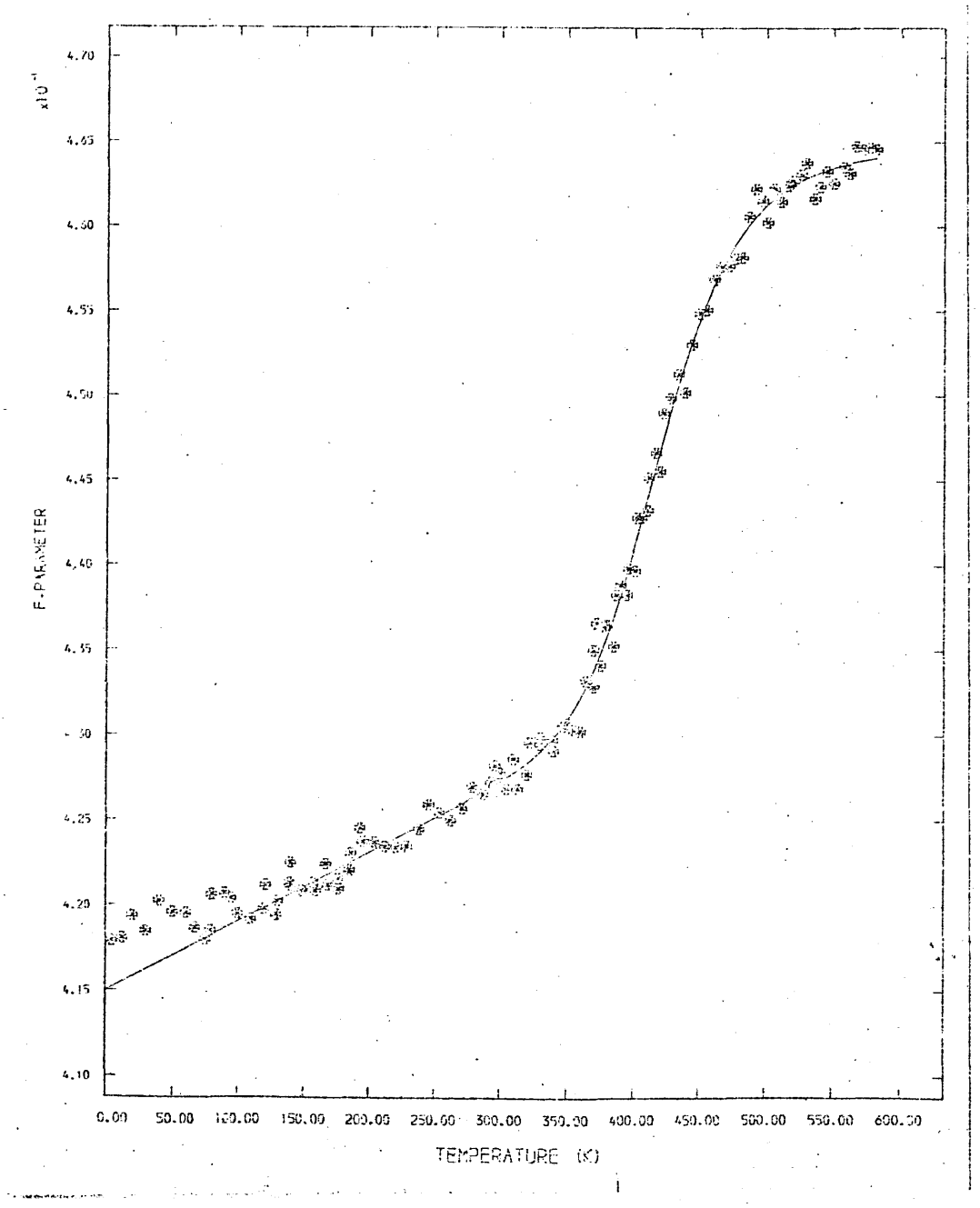

Figure 6.2: The temperature variation of the F-parameter for the [0001] direction of single crystal cadmium.

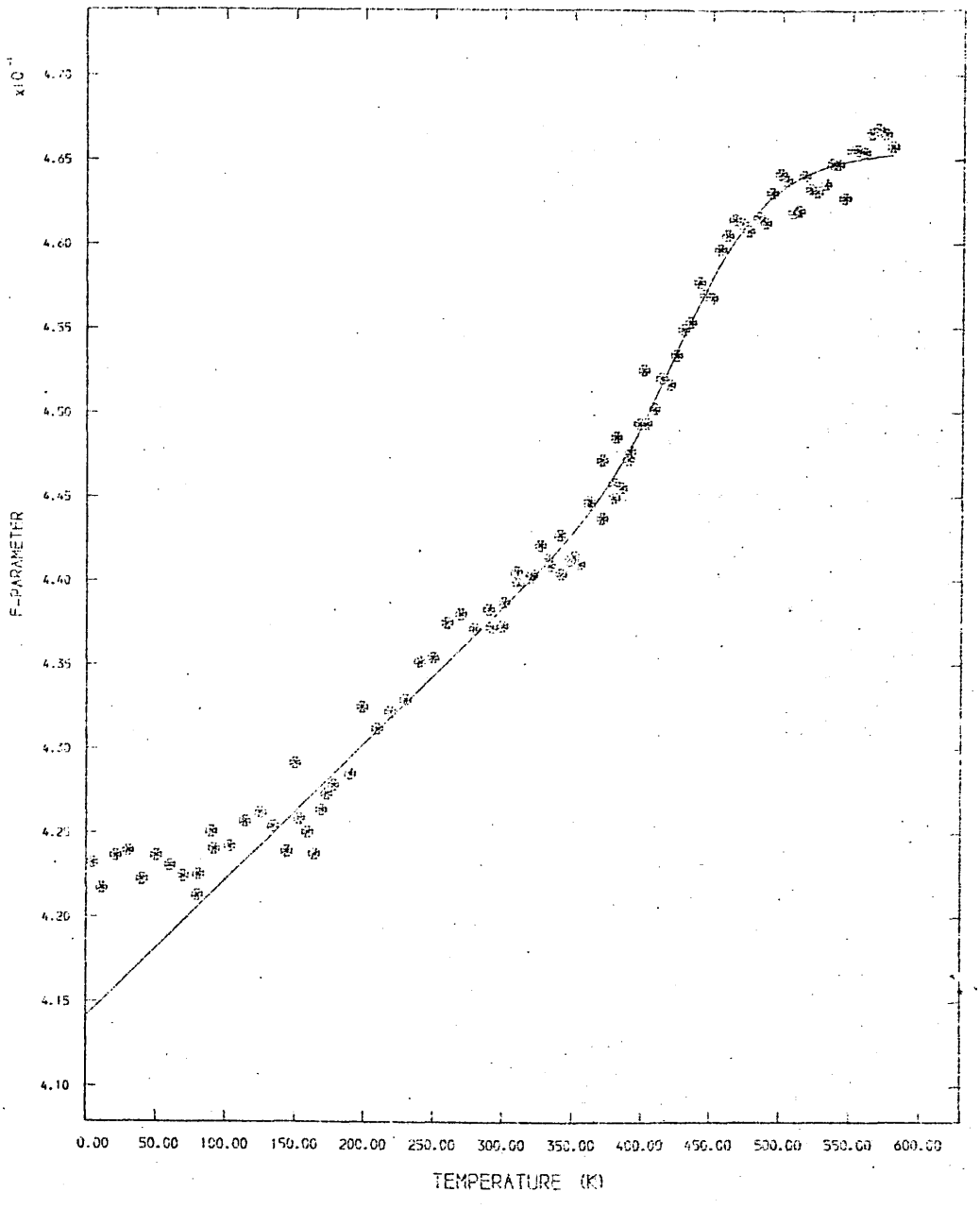

Figure 6.3: The temperature variation of the F-parameter for the [1$\bar{0}$10] direction of single crystal cadmium.

T < 150K, the temperature dependence is characterised by a relatively weak positive slope. For 150 > T > 370K, a stronger linear dependece on temperature is observed while for T > 370K, the vacancy trapping effect is observed. There is no general consensus as to the precise values of these transition temperatures however those here observed are in general agreement with those previously reported.

The initial analysis was as follows. The "linear-rise" model of equation 3.38 with $\gamma=0$ was used in a least squares minimisation routine to fit the temperature dependences of the lineshape parameter for both orientations above 150K. This model is,

$$F = \frac{F_o(1+\beta T)+F_{1v}A\exp(-H_{1v}/kT)}{1+A\exp(-H_{1v}/kT)} \qquad 6.1$$

The solid lines in figures 6.2 and 6.3 have their origin in these fittings, the optimum values obtained from which are listed in table 6.1 . Also included in the table are values deduced for monovacancy formation entropy and monovacancy concentration at the melting temperature deduced from the fitting on the basis of reported values [110] for the free positron lifetime (190 ps) and the specific trapping rate of positrons at vacancies ($\mu=2.5\times10^{14}$ s^{-1}).

It was noted that the vacancy formation entropies deduced from these results were higher than others previously reported [110] and that the vacancy concentration at the melting temperature in the [0001] direction appears to be approximately twice that for the [10$\bar{1}$0] direction.

Temperature range of fitting (K)	149-582 (90)	150-579 (81)
H_{IV} (eV)	0.51±.01	0.53±.01
$A \times 10^{-5}$	9.58±4.50	8.12±2.49
$\beta \times 10^{4}$ (K^{-1})	0.97±.05	1.94±.06
S_{IV} (k)	3.0	2.8
$C_{IV}(T_m) \times 10^{4}$	10.3	5.7

Table 6.1: Fitting parameters derived from initial "linear-rise" model study of single crystal cadmium.

The most striking feature to emerge from these data however, is that the magnitude of the pre-vacancy slope, $\beta = \Delta F/(F_o \Delta T)$ depends strongly on the direction of emission of the annihilation radiation with respect to the crystal lattice. Another possible directional effect is the suggestion for the $[10\bar{1}0]$ direction of a plateau at the top of the pre-vacancy region. Similar plateaux have been reported for cadmium [114,136]. This plateau is not apparent for the [0001] direction. A further feature of these curves is the apparent discontinuity in the pre-vacancy behaviour. It appears that, as the temperature is reduced below approximately 150K, a second and weaker temperature dependence is revealed. Further annealings and subsequent re-examination of this pre-vacancy behaviour revealed no hysteresis. This suggests that these slopes can be interpreted in terms of equilibrium effects. A recent comparison [167] of data arising from three independent orientational studies of single crystal cadmium (one of which is presented here) confirms this effect.

An explanation of the orientational effect in the pre-vacancy region in terms of anisotropies in the thermal expansion of cadmium seems at first sight to be attractive. However, the co-efficients of linear thermal expansion ($0.54 \times 10^{-4} K^{-1}$ and $0.20 \times 10^{-4} K^{-1}$) [143] along the c, [0001], and a, [1120], axes respectively, bear approximately the reverse relationship to that exhibited by the pre-vacancy slopes, $\beta[0001] = 0.97 \times 10^{-4} K^{-1}$ and $\beta[10\bar{1}0] = 1.94 \times 10^{-4} K^{-1}$. (Unfortunately, no reported value of the thermal expansion

co-efficient along the [10$\bar{1}$0] direction has been found and here the co-efficient for the [11$\bar{2}$0] direction has been employed.)

One possible, although unlikely, contribution to this observed effect was thought to be the result of changing sample-detector geometries caused by the rotation of the sample through 90°. It was expected that such changes in the geometry would result in different photon scattering behaviour from the sample and the surrounding fixtures. In an effort to determine the magnitude of any such effect and to investigate the repeatability of the slopes obtained, it was decided to undertake another orientational study of cadmium. It was desirable, in this instance, that the sample-detector geometries be complementary with respect to the crystallographic orientations, to those previously obtaining.

6.4: EXPERIMENTAL DESCRIPTION: SAMPLE-B

Two circular slices, having diameter 18 mm and thickness 2.5 mm, were cut by means of a spark-erosion technique from the same rod of 99.999% (5N) purity single crystal cadmium as was used in single crystal cadmium-A. In this case, however, the [10$\bar{1}$0] axis was normal to the faces of the slices i.e. the discs were cut from a plane orthogonal to that of the earlier specimens, see figure

6.1 . The crystallographic orientations were confirmed using X-ray photography and the edge of each slice marked by means of the spark-erosion wire to indicate this direction. In this configuration, the [10$\bar{1}$0] direction is parallel to the detector axis when the sample face is parallel to the detector window, while the [0001] direction is parallel to the detector axis when the sample edge is aligned with the detector face. The polishing of this sample proceeded as for the earlier specimen. In the interests of simplicity, the earlier specimen will hereafter be referred to as sample-A, while the second specimen will be referred to as sample-B.

Approximately 100 microcuries of carrier-free $^{22}NaCl$ in aqueous solution was then deposited and evaporated onto the centre of one of the specimen slices, the dimensions of the source being similar to those for sample-A. As for the earlier sample a specimen-source sandwich was constructed, care being taken to align the [0001] axes. The sandwich was then encapsulated in a wrapping of thin aluminium foil and the prepared sample mounted on the low temperature cryostat insert such that the [10$\bar{1}$0] direction of the specimen was parallel to the detector axis. The sample-detector distances were similar to those for sample-A.

As the primary interest of this study was the pre-vacancy behaviour above 150K, no measurements were made at liquid helium temperatures. Annihilation spectra for both orientations were recorded at temperature increments of approximately 10K over the range 80K to 400K in the cryostat and, using similar increments, between 294K and 580K in the furnace. The counting conditions were similar to those for sample-A.

6.5: LINESHAPE PARAMETER ANALYSIS

The data arising from sample-B were background subtracted as in the case of the earlier data and the lineshape parameter computed using the same definition as that employed earlier. The F-parameter versus temperature curves were then normalised in the temperature overlap region between the cryostat and furnace measurements (from 294K to 400K). This procedure was necessary in order to take account of variations in photon scattering caused by the change in sample chambers. The average statistical errors (2σ) for sample-B, as defined in chapter 5.2.2, are for the $[10\bar{1}0]$ direction, 0.0010 and for the [0001] direction, 0.0011 .

It was decided to re-analyse the data from cadmium-A in parallel with that from sample-B and, because of the suggested plateau observed for the [1$\bar{0}$10] direction of sample-A (section 6.3), to widen the analysis procedure to include the possibility of positron self-trapping. In addition, two separate temperature dependences were allowed for in the vacancy trapping region. Accordingly, each of the four data sets was analysed in terms of three proposed temperature dependences, viz:

(a) the "linear-rise" model with $\chi = 0$ (equation 6.1),

(b) the "linear-rise" model with $\chi \neq 0$ (equation 3.38) and

(c) the "self-trapping" model (equation 3.35).

The temperature variation of the F-parameter and the optimum values of the fitting paramaters and derived constants obtained from the least squares analysis in terms of the three models, are given for the [0001] and [1$\bar{0}$10] directions of each sample. They are listed in the order: sample-A [0001], figure 6.4 and table 6.2; sample-A [1$\bar{0}$10], figure 6.5 and table 6.3; sample-B [1$\bar{0}$10], figure 6.6 and table 6.4; sample-B [0001], figure 6.7 and table 6.5 . The solid lines in the figures represent the best fit to each set of data; however, the suitability of each of the above models will be discussed for each of the four data sets.

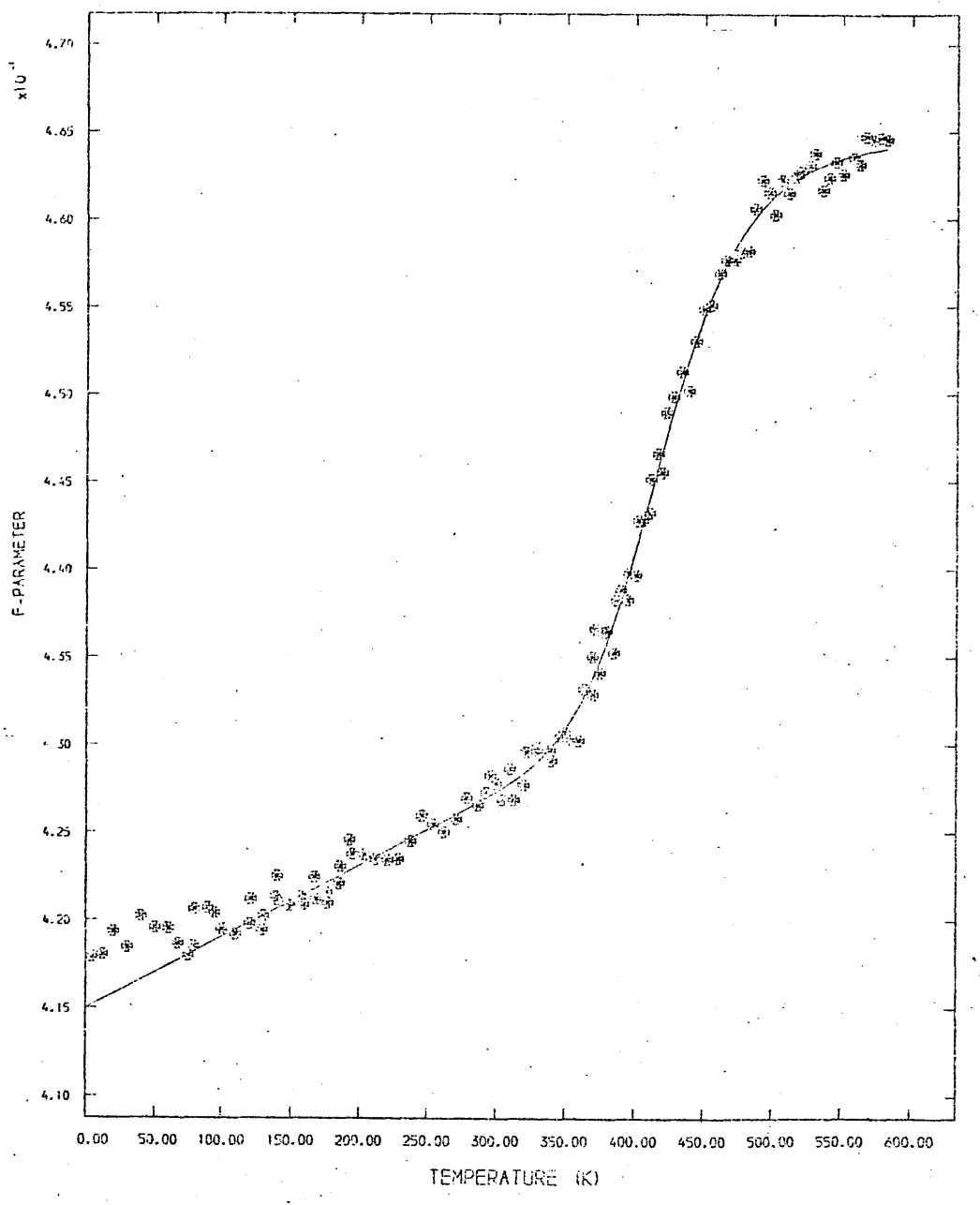

Figure 6.4: The temperature variation of the F-parameter for the 0001 direction of single crystal cadmium, sample-A.

	equation 6.1	equation 3.38	equation 3.35
Temperature range of fitting (K)	149-582 (90)	150-579 (81)	4.2-582 (112)
H_{IV} (eV)	0.51±.02	0.54±.002	0.46±.02
$A \times 10^{-5}$	9.55±4.52	30.94±2.53	3.24±1.29
$\beta \times 10^{4} (K^{-1})$	0.98±.05	1.01±.04	---
$\gamma \times 10^{4} (K^{-1})$	---	0.36±.10	---
$B \times 10^{-5} (K^{-3/2})$	---	---	6.58±4.38
ε_o (eV)	---	---	0.10±.01
S_{IV} (k)	3.0	4.2	1.9
$C_{IV}(T_m) \times 10^{4}$	10.3	16.1	8.7
SSQ/N	2.315	2.265	2.464
Chi-squared	2.451	2.427	2.603

Table 6.2: single crystal cadmium sample-A [0001]: optimum values of fitting parameters.

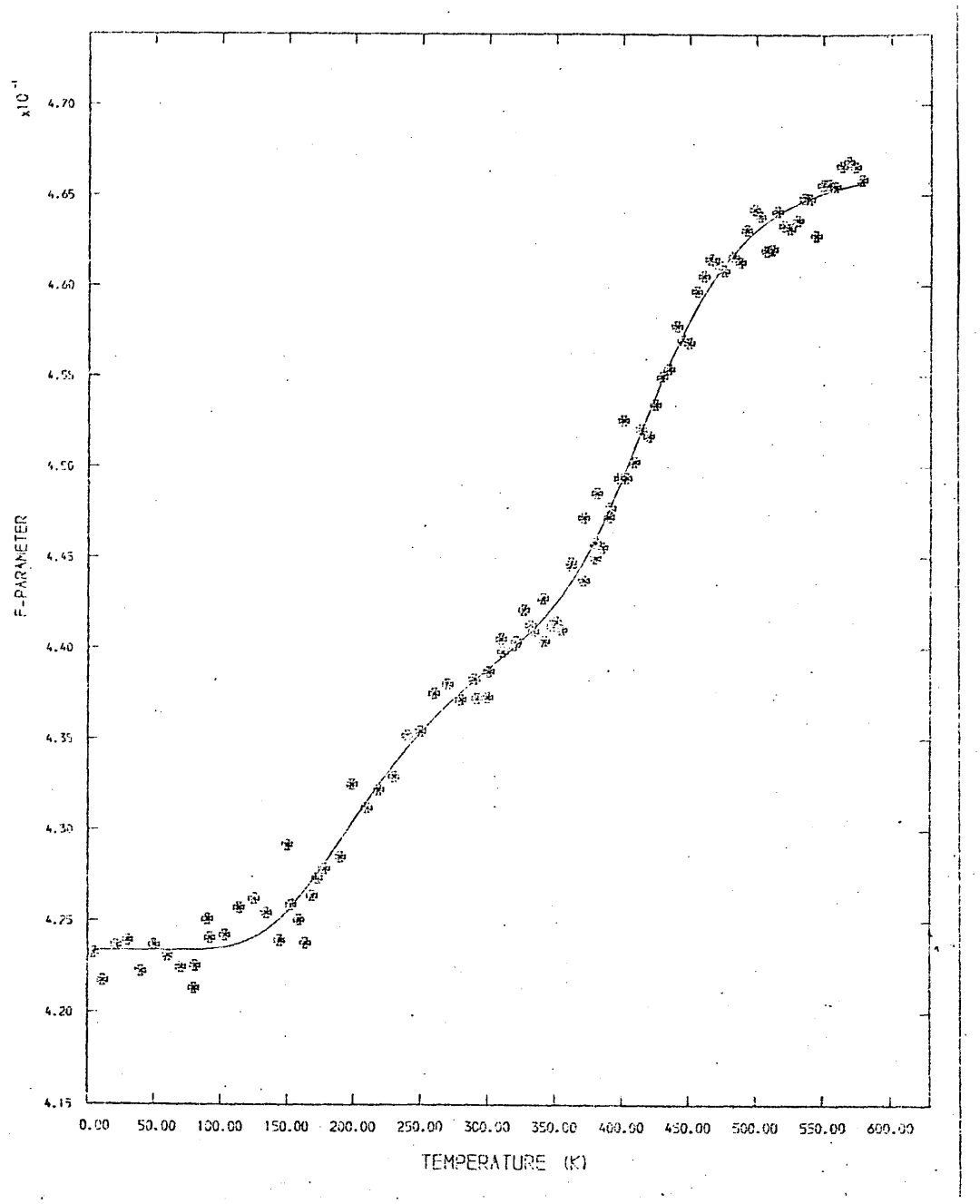

Figure 6.5: The temperature variation of the F-parameter for the [10$\bar{1}$0] direction of single crystal cadmium ,sample-A.

	equation 6.1	equation 3.38	equation 3.35
Temperature range of fitting (K)	150-579 (90)	150-579 (81)	4.2-579 (112)
H_{IV} (eV)	0.53±.01	0.69±.01	0.44±.03
$A \times 10^{-5}$	8.76±2.51	1275.5±3.1	1.50±0.98
$\beta \times 10^{4}$ (K^{-1})	1.95±.06	1.99±.05	---
$\gamma \times 10^{4}$ (K^{-1})	---	0.81±.14	---
$B \times 10^{-5}$ ($K^{-3/2}$)	---	---	2.43±2.45
ξ_o (eV)	---	---	0.10±.01
S_{IV} (k)	2.9	7.9	1.2
$C_{IV}(T_m) \times 10^{4}$	5.8	34.8	5.7
SSQ/N	4.017	3.646	3.406
Chi-squared	4.282	3.938	3.668

Table 6.3: single crystal cadmium sample-A [10$\bar{1}$0]: optimum values of fitting parameters.

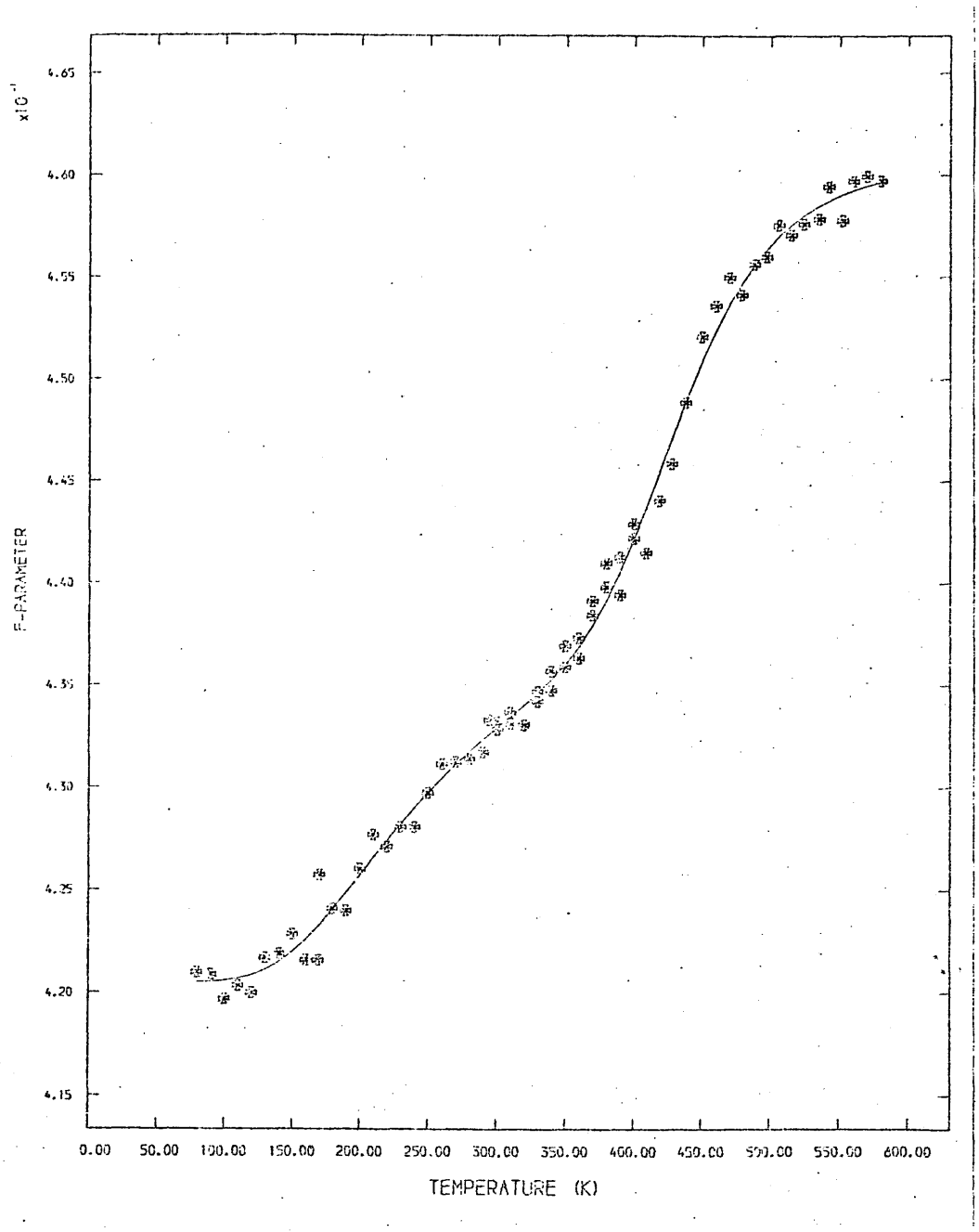

Figure 6.6: The temperature variation of the F-parameter for the [10$\bar{1}$0] direction of single crystal cadmium ,sample-B.

	equation 6.1	equation 3.38	equation 3.35
Temperature range of fitting (K)	150-580 (58)	150-580 (58)	80-580 (112)
H_{IV} (eV)	0.59±.02	0.75±.01	0.46±.02
$A \times 10^{-5}$	38.63±18.26	4064.8±82.6	1.80±1.00
$\beta \times 10^{4}$ (K^{-1})	1.68±.04	1.72±.04	---
$\gamma \times 10^{4}$ (K^{-1})	---	0.64±.15	---
$B \times 10^{-5}$ ($K^{-3/2}$)	---	---	1.68±0.23
ε_o (eV)	---	---	0.10±.004
S_{IV} (k)	4.4	9.1	1.3
$C_{IV}(T_m) \times 10^{4}$	7.7	35.7	5.1
SSQ/N	2.463	2.328	2.314
Chi-squared	2.695	2.597	2.593

Table 6.4: single crystal cadmium sample-B [10$\bar{1}$0]: optimum values of fitting parameters.

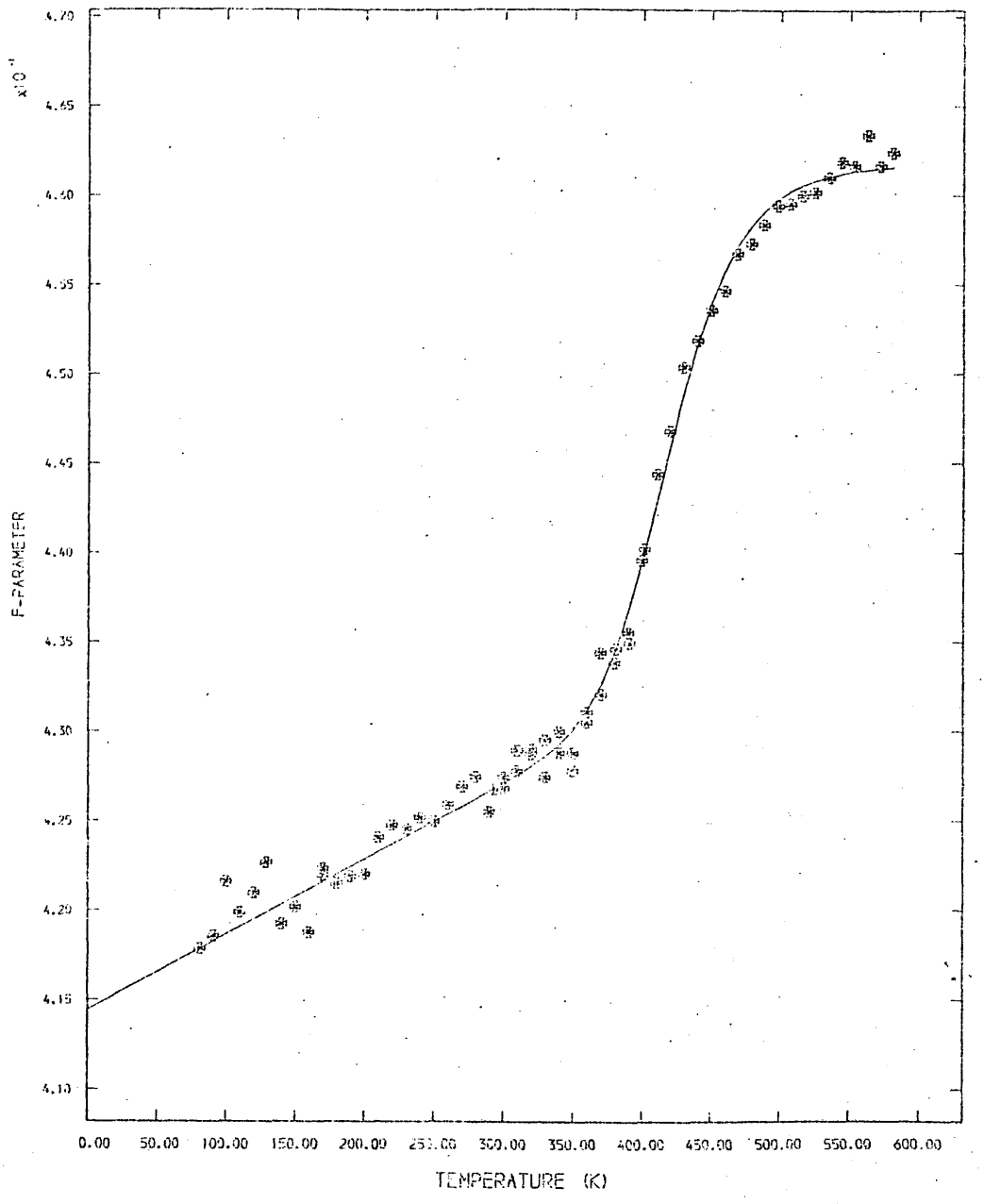

Figure 6.7: The temperature variation of the F-parameter for the [0001] direction of single crystal cadmium ,sample-B.

	equation 6.1	equation 3.38	equation 3.35
Temperature range of fitting (K)	150-581 (58)	150-581 (58)	80-581 (65)
H_{IV} (eV)	0.61±.02	0.81±.003	0.56±.004
$A \times 10^{-5}$	172.2±108.8	79518.±173.	50.96±1.99
$\beta \times 10^{4} (K^{-1})$	1.01	1.10±.04	---
$\gamma \times 10^{4} (K^{-1})$	---	1.04±.10	---
$B \times 10^{-5} (K^{-3/2})$	---	---	38.33±1.92
$\mathcal{E}_{o}$ (eV)	---	---	0.14±.003
S_{IV} (k)	5.9	12.0	4.7
$C_{IV}(T_m) \times 10^{4}$	24.7	225.0	20.6
SSQ/N	2.172	1.601	2.196
Chi-squared	2.377	1.786	2.461

Table 6.5: single crystal cadmium sample-B [0001]: optimum values of fitting parameters.

From table 6.2 it can be seen that for the [ØØØ1] direction of sample-A, the inclusion of the high temperature slope, γ, does not significantly improve the quality of the fit as measured by reduced chi-squared. This is the sum of the squared residuals between fit and data divided by the number of data points considered. As a consequence of this inclusion, the values of H_{IV}, S_{IV} and C_{IV} obtained are significantly higher relative to model (a). This phenomenon had been observed in previous Doppler broadening studies in cadmium [144]. The improvement thus obtained in the fit is not sufficient to endorse unequivocally the validity of $\gamma \neq 0$ in this case, particularly in the light of the rather large uncertainty associated with the value of γ derived from this fit. Also on grounds of quality of fit, the attempted explanation of the pre-vacancy rise in terms of positron self-trapping appears to be inferior to that of the "linear-rise" model. This is to be expected in view of the absence of a plateau for this direction.

Consideration of table 6.3 reveals that, in contrast to the situation obtaining for the [ØØØ1] direction, for the [1$\bar{1}$ØØ] direction the "self-trapping" model as embodied in equation 3.35 seems to provide a more satisfactory fit to the temperature dependence than either of the "linear-rise" models.

For the case of data arising from the [1$\bar{0}$1$\bar{0}$] direction of sample-B, table 6.4, the situation is less clear-cut. While the value of reduced chi-squared for equation 3.35 is lower than for the other models, the improvement is less convincing than for sample-A, particularly with respect to the case of $\gamma \neq 0$. This perhaps is not surprising as the "plateau" is less pronounced here than for sample-A, perhaps to the point of vanishing. The vacancy parameters are, however, more plausibly in accord with generally accepted values and are also very similar to those obtained for sample-A.

In table 6.5 are listed the parameters obtained for the fitting of the three moodels to data arising from the [0001] direction for sample-B. Here, the "self-trapping" model seems less well-suited, on the basis of the sum of squares, than either of the "linear-rise" models. On purely statistical grounds, the most acceptable fit is provided by the model for which $\gamma \neq 0$. However, the vacancy parameters yielded both by this model and that of equation 6.1 are dramatically higher than the generally accepted values for cadmium. In an effort to investigate the possibility of this representing local and not true minima, a model similar to equation 6.1 but having a fixed value of H_{IV} was fitted to these data. It was expected that H_{IV} was a thermodynamic quantity and accordingly, the fixed value chosen for H_{IV} was that obtained for the [0001] direction of sample-A viz.: H_{IV} =0.506 eV. A plot of this fit is shown superimposed on the data in figure 6.8 . The

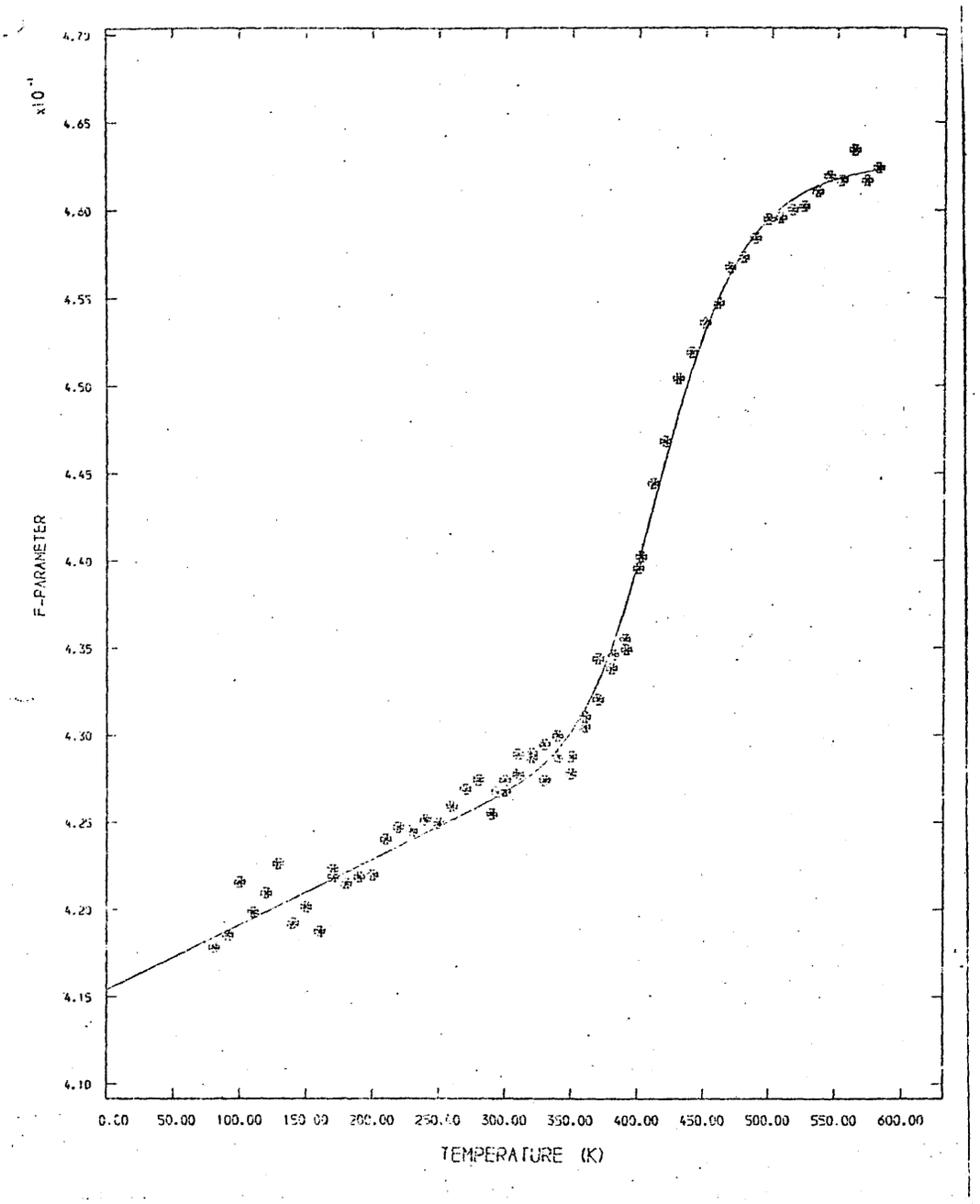

Figure 6.8: The temperature variation of the F-parameter for the [0001] direction of single crystal cadmium ,sample-B. H_{IV}=0.506eV=constant.

value of the reduced chi-squared obtained for this fit was 2.762 c.f. 2.377 for equation 6.1 with H_{IV} a freely floating parameter. The values for the other parameters were closer to expectation. These values are listed below:

H_{IV} =Ø.5Ø6 eV=constant $C_{IV}(T_m)\times 10^{4}$=1Ø.624

$A\times 10^{-5}$=9.9ØØ ± Ø.48Ø S(k)=3.Ø37

$\beta\times 10^{4}$ (K^{-1})=Ø.9Ø2 + Ø.Ø54

The values of A and thus S_{IV} and $C_{IV}(T_m)$ resulting from this constrained fit are more in line with reported values than the earlier obtained values and are only very slightly different from those obtained from the sample-A data. This, however, cannot of itself be taken as prima facie justification for the procedure or as confirmation of the values thereby derived. Nevertheless, inspection of figures 6.7 and 6.8 reveals that, in the vacancy trapping region, the temperature dependence described by the constrained fit more closely agrees with the data than does the unconstrained fit. The increased chi-squared for this constrained fit can therefore be seen as the product of increased residuals between fit and data in the pre-vacancy region.

A comparison of the fitting parameters derived from the unconstrained fits to the data arising from the two [ØØØ1] studies reveals discrepancies between monovacancy formation parameters. A possible explanation of this is specimen dependence. Such a dependence might result from the presence of residual defects in one of the specimens.

The reduced temperature dependence of the F-parameter for sample-B, $\Delta F = 0.48$ c.f.$\Delta F = 0.50$ for sample-A, might indicate that defects which had survived annealing in this specimen result in positron trapping at low temperatures with the result that the magnitude of the apparent pre-vacancy slope is reduced. Such a circumstance might go some way towards explaining the reduction in slope in the $[10\bar{1}0]$ direction of sample-A. However, for the [0001] direction, the relationship is reversed, tables 6.2,6.5 .

In any case it is not obvious that an underestimate of the assumed linear free positron response to temperature would result in the observed higher values of H_{IV} in the second specimen. Such a reduction in pre-vacancy slope would increase the relative contribution of vacancy trapping to the overall change in the F-parameter and would accordingly lead to lower values of H_{IV} and not the higher values observed. It is possible to remove the disparity between monovacancy formation enthalpy values for the [0001] direction of single crystal cadmium by postulating a non-linear extraploation into the vacancy region of the pre-vacancy behaviour.

6.6: DISCUSSION OF RESULTS

6.6.1: Vacancy Parameters

The vacancy parameters obtained from the lineshape parameter analysis can be summarised as follows: for the [ØØØ1] direction of cadmium, the "linear-rise" model gave H_{1V} = Ø.51±.Ø2 eV, S_{1V} = 3.Ø k and $C_{1V}(T_m)$ = 1Ø.3X1Ø$^{-4}$ for sample-A; and H_{1V} = Ø.51 eV, S_{1V} = 3.Ø k and $C_{1V}(T_m)$ = 1Ø.6X1Ø$^{-4}$ for sample-B. The values obtained for the [ØØØ1] direction of sample-B cannot however be taken as confirmation of those for sample-A because they were obtained by constraining the least squares fitting procedure. For the [1Ø$\bar{1}$Ø] direction, the "self-trapping" model of equation 3.35 was found to provide a more satisfactory fit than the "linear-rise" model and, from this, the following values were obtained: H_{1V} = Ø.44±.Ø3 eV, S_{1V} = 1.2 k and $C_{1V}(T_m)$ = 5.7X1Ø$^{-4}$ for sample-A; and H_{1V} = Ø.46±.Ø2 eV, S_{1V} = 1.3 k and $C_{1V}(T_m)$ = 5.1X1Ø$^{-4}$ for sample-B. The values of S_{1V} and $C_{1V}(T_m)$ quoted in the above were obtained by assuming reported values for the free positron lifetime and specific trapping rate at vacancies [11Ø].

Reported values of the monovacancy formation enthalpy for cadmium cover a wide range. Differential dilatometry experiments [145] yield Ø.4Ø eV while Ø.42 eV was obtained from quenching studies [146]. Both of these results differ widely from the value of Ø.59 eV predicted in a theoretical study [147]. Estimates derived from positron annihilation studies cover a similar range. Angular correlation studies have variously yielded Ø.39 eV [44] and Ø.52 eV [95] while a value of Ø.41 eV has been reported as having resulted from lifetime studies [8]. Values originating from Doppler broadening studies have been reported which span the range Ø.4Ø eV [132] to Ø.57 eV [144]. The characteristic temperature correlation technique has been applied to positron annihilation data to yield Ø.45 eV [112].

Discussion of the monovacancy formation entropy is less often found in the literature, perhaps as a result of the rather large associated uncertainties in the deduced values, typically $\sim$2Ø%. However, values arising from differential dilatometry of 1.1 k, [11Ø] and from angular correlation of 3.3 k, [111] have been reported. Values of the monovacancy concentration have been reported from differential dilatometry, 5.6×10^{-4} [145], positron annihilation, $16.Ø\times10^{-4}$ and from electrical resistivity measurements, $3Ø.Ø\times10^{-4}$ [111].

The monovacancy formation enthalpies here obtained fall approximately centrally in the range of reported values. However, the deduced values are seen to be dependent on the crystallographic orientation of the specimen with respect to the relevant direction of photon emission. Such a dependence contradicts the thermodynamic quality of the formation enthalpy and, as such, is unsatisfactory. Perhaps of more significance is the fact that these two distinct values originate from two distinct subtractions of the pre-vacancy behaviour of the lineshape parameter.

It is obviously incorrect to suppose that the "self-trapping" model may reasonably be taken to describe the temperature variation of the lineshape parameter for the $[10\bar{1}0]$ direction while simultaneously holding that the "linear-rise" model is more suitable for the [0001] behaviour. If one were to require an unambiguous description of the temperature variation of the lineshape parameter in cadmium then clearly preference must be given to the "self-trapping" model as the "linear-rise" model is incapable of rendering the pre-vacancy plateau.

The application of the characteristic temperature technique to these data is illustrative of the model dependence of the monovacancy formation enthalpy. This analysis yields, for the [0001] direction: sample-A, $H_{1V} = 0.47$ eV, sample-B, $H_{1V} = 0.47$ eV; while for the $[10\bar{1}0]$ direction: sample-A, $H_{1V} = 0.48$ eV, sample-B, $H_{1V} = 0.49$ eV.

The conformity exhibited by these values suggests that, for cadmium, the nature of the pre-vacancy temperature dependence assumed in the trapping model is influential in determining the value of the monovacancy formation enthalpy so derived.

6.6.2: Pre-Vacancy Region

As was discussed above, this study has revealed significant differences in the pre-vacancy behaviour of the lineshape parameter as measured for the [0001] and [10$\bar{1}$0] directions in single crystal cadmium. The initial analysis, employing a "linear-rise" model to characterise the temperature variation, revealed that the magnitude of the pre-vacancy slope in the [10$\bar{1}$0] direction was approximately double that for the [0001] direction. These values were shown to be repeatable within experimental accuracy cf [0001] sample-A, $\beta = 0.98 \pm .05 \times 10^{-4} K^{-1}$; [0001] sample-B, $\beta = 0.90 \pm .05 \times 10^{-4} K^{-1}$; [10$\bar{1}$0] sample-A, $\beta = 1.95 \pm .06 \times 10^{-4} K^{-1}$; [10$\bar{1}$0] sample-B, $\beta = 1.68 \pm .04 \times 10^{-4} K^{-1}$. The discrepancy between the two [10$\bar{1}$0] slopes is thought not to reflect the effect of changes in the source-detector geometry, nor is it thought that this is caused by differences between the two specimens. It is thought more plausible that this is a reflection of the relative inadequacy of the "linear-rise" model for this direction.

In common with earlier positron annihilation studies of cadmium [80,23,135,142,140], the data arising from this study can be divided into three temperature regions. For temperatures greater than 350K, vacancy trapping dominates. For temperatures between 350K and 150K, a strong and approximately linear temperature dependence is exhibited. At temperatures below 150K, a region of weak or zero temperature dependence is observed. These pre-vacancy effects are found to be stable against annealing and are thus thought to be representative of equilibrium conditions.

A more recent Doppler broadening orientational study on a single crystal of cadmium revealed directional effects similar to those presented here [148]. Direct comparison with the pre-vacancy slopes therein obtained cannot be made because of the definition dependence of the lineshape parameter and also because the orientations chosen in the latter work were distinct from those here employed. However, the existence of a pre-vacancy plateau for a direction similar to $[10\bar{1}0]$ was remarked [148], although the "self-trapping" model was not employed because of the lack of precision of the data. A futher recent observation of this pre-vacancy plateau has been reported for lifetime studies of a polycrystalline specimen of cadmium [149].

6.6.3: The Nature of the Pre-Vacancy Behaviour in Cadmium

An explanation of the origin of the orientational differences in magnitude of the pre-vacancy slopes touches upon the origin of the pre-vacancy rise itself. It is to be expected that the effects of thermal expansion and lattice vibration will combine to cause an increase in the F-parameter with temperature [59]. The thermal expansion is, to a reasonable approximation, linear and exhibits marked anisotropies in the case of cadmium. However, the relationship between the co-efficients of thermal expansion along the c- and a-axes respectively, is the reverse of that observed between the pre-vacancy slopes, section 6.3, cf $\alpha[0001] = 0.54 \times 10^{-4} K^{-1}$ and $\alpha[11\bar{2}0] = 0.20 \times 10^{-4} K^{-1}$ [143]. If the thermal expansion and lattice vibration effects indeed combine to produce the observed orientational dependence, and if the effect of lattice vibrations is assumed to be comparable in magnitude with that of thermal expansion [59], the relevant phonon spectra must exhibit anisotropies of a larger magnitude than those of the thermal expansion co-efficients.

Evidence has been presented which suggests that there are indeed marked anisotropies in the phonon spectra of the h.c.p. metals, zinc and cadmium [15Ø]. These anisotropies result from the departure of the axial ratio, c/a, from the "ideal" value $\sqrt{8/3}$ cf for cadmium, c/a at low temperatures = 1.885 [151]. It is reported that the frequency of vibrations along the c-axis is about one half of those in the basal plane. Although the precise implications of this on the magnitude of the phonon contribution as computed in [59] are not clear, this vibrational anisotropy would go some way towards explaining the observed orientational differences in magnitude of the pre-vacancy slope.

While such arguments may be deployed to explain the magnitude of the pre-vacancy rise, they do not account for the observation of a plateau in the $[1Ø\bar{1}Ø]$ direction. However, it is expected that some of the observed effect in the pre-vacancy region does indeed result from the combined effects of thermal expansion and lattice vibrations. As has been discussed, the "self-trapping" model provided the more satisfactory fits to the data arising from the $[1Ø\bar{1}Ø]$ direction. It is important to note however that this agreement does not represent unambiguous proof of the model. The plateau could equally be interpreted instead as a thermally activated process, and the region up to the plateau fitted using a two-state trapping model similar to that generally employed for the entire temperature range. No such treatment was attempted for these data; however, a

reported value of the activation energy arising from the application of this thermal activation model to similar single crystal cadmium data is Ø.Ø8 ± .Ø2 eV [148].

Another possible interpretation of the anisotropic pre-vacancy behaviour is positron trapping in defects which survive annealing. Such an explanation would require these defects to be preferentially oriented, for example dislocations lying in the [ØØØ1] slip planes; and, in addition, to possess a temperature dependent positron trapping rate.

The results and analyses here presented, while not completely successful in resolving the origin of the anisotropies in the temperature dependence of the lineshape parameter for cadmium, reveal inadequacies in the conventional interpretation or application of the trapping model. The values of vacancy parameters derived from positron annihilation experiments via the trapping model are sensitive to the assumptions made as to the temperature dependence of the lineshape parameter in the pre-vacancy region and, where such uncertainty exists concerning the nature of this dependence, no great confidence can be invested in the deduced values. Accordingly the deduction of reliable monovacancy formation enthalpies from positron annihilation experiments must await the development of a directionally sensitive theoretical model for the temperature dependent annihilation of positrons in metals.

6.7: CONVOLUTION ANALYSIS

6.7.1: Inverted Parabola plus Gaussian Model

In addition to the lineshape parameter analyses previously reported, each of the spectra arising from each of the four studies was analysed by means of the convolution technique discussed in chapter 5.3.1 . The results obtained from each study for the Gaussian width (GW) and the parabola width (PW) are presented as follows: sample-A [ØØØ1], figures 6.9 and 6.1Ø respectively; sample-A [1Ø$\bar{1}$Ø], figures 6.11 and 6.12 respectively; sample-B [1Ø$\bar{1}$Ø], figures 6.13 and 6.14 respectively; sample-B [ØØØ1], figures 6.15 and 6.16 respectively.

The temperature at which vacancy effects are first noticeable in the temperature dependence of the lineshape parameter is taken as a reference point for the interpretation of changes in GW and PW. This temperature is taken as 35ØK, good agreement being obtained for this for all four lineshape temperature variations. The temperature variations of the Gaussian width for the four studies figures 6.9, 6.11, 6.13 and 6.15, seem to indicate a negative linear dependence on temperature which, at approximately 35ØK is superseded by a much stronger negative

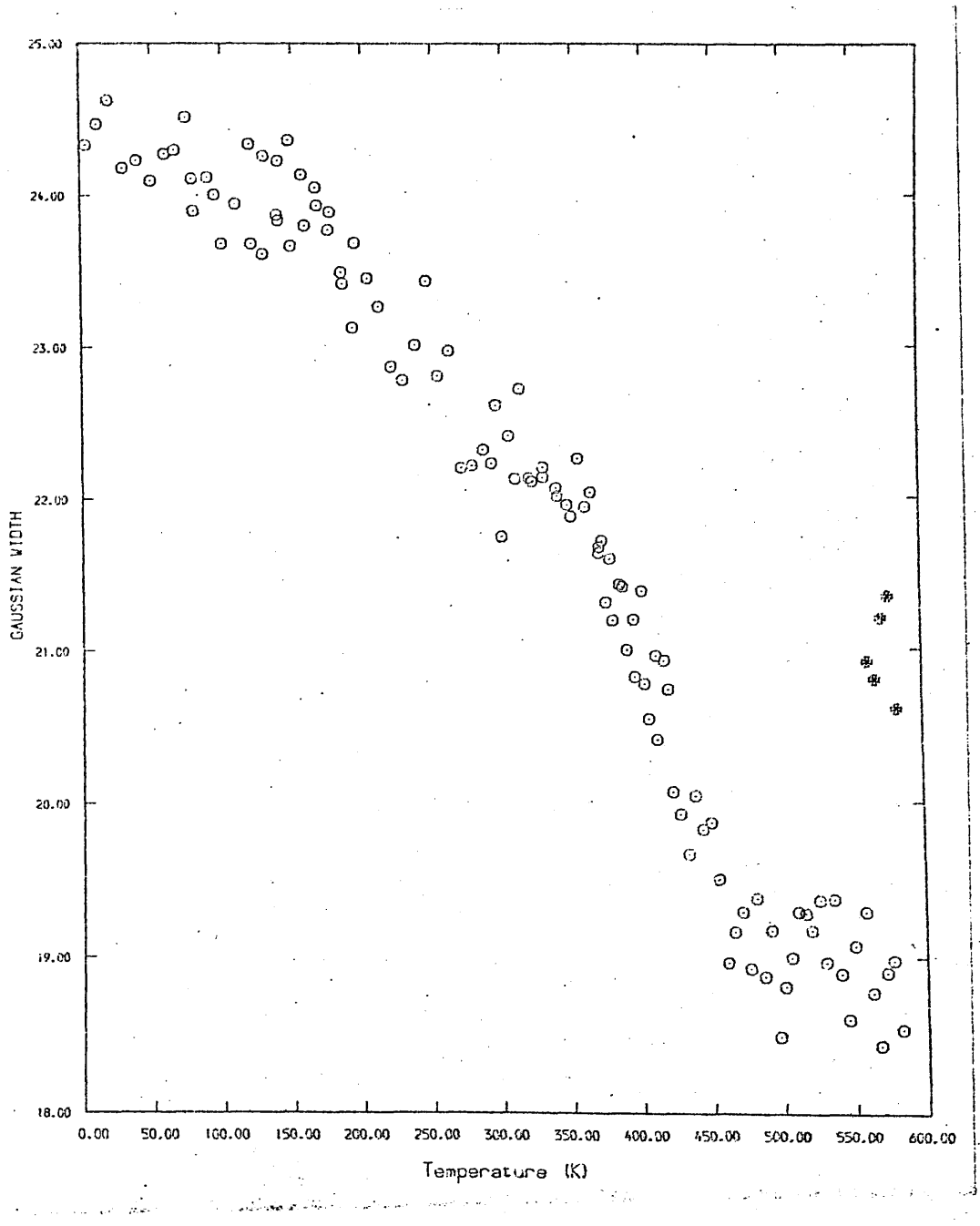

Figure 6.9: The temperature variation of the GAUSSIAN WIDTH for the [0001] direction of single crystal cadmium ,sample-A.

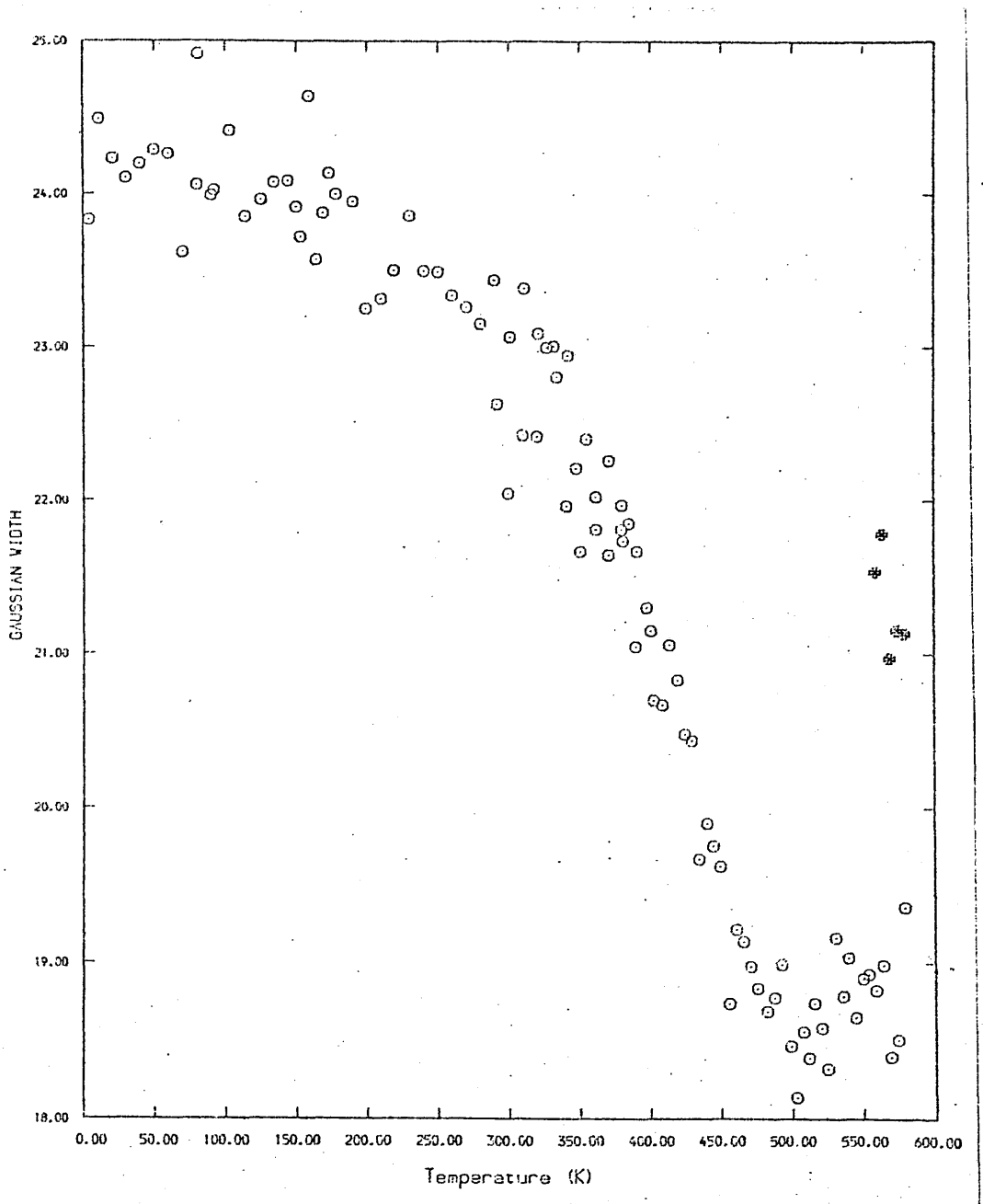

Figure 6.10: The temperature variation of the GAUSSIAN WIDTH for the [10$\bar{1}$0] direction of single crystal cadmium ,sample-A.

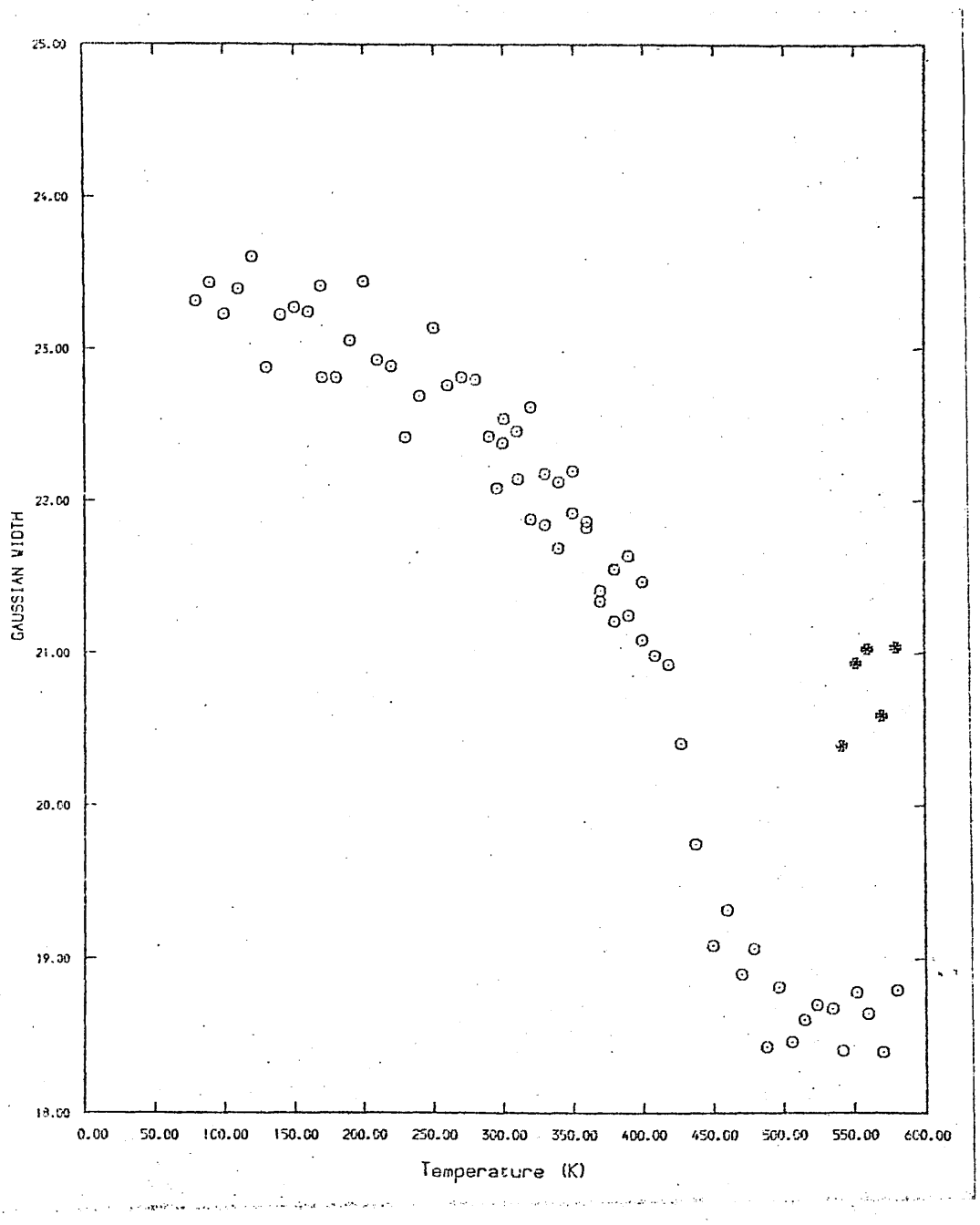

Figure 6.11: The temperature variation of the GAUSSIAN WIDTH for the [1$\bar{0}$10] direction of single crystal cadmium ,sample-B.

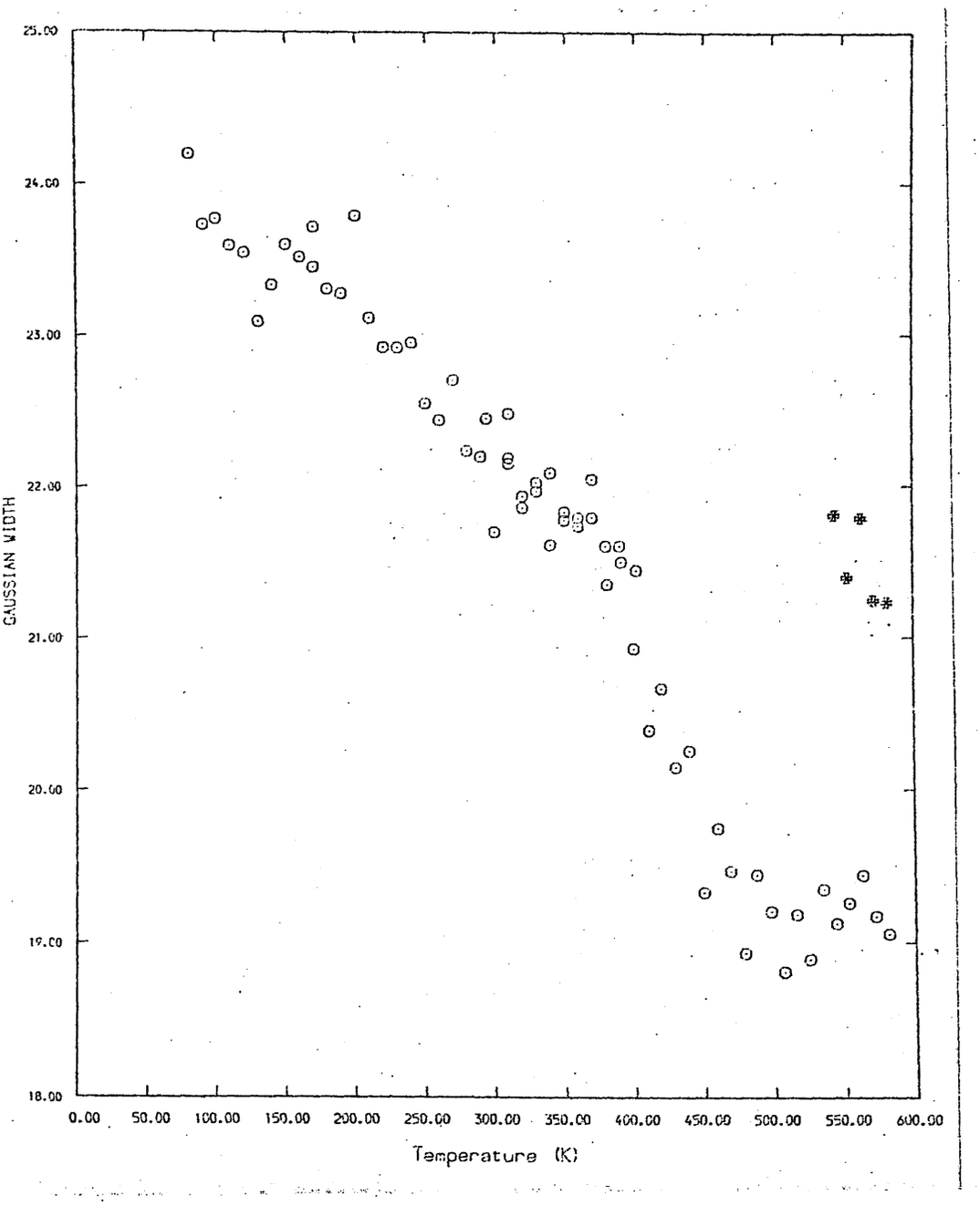

Figure 6.12: The temperature variation of the GAUSSIAN WIDTH for the [0001] direction of single crystal cadmium ,sample-B.

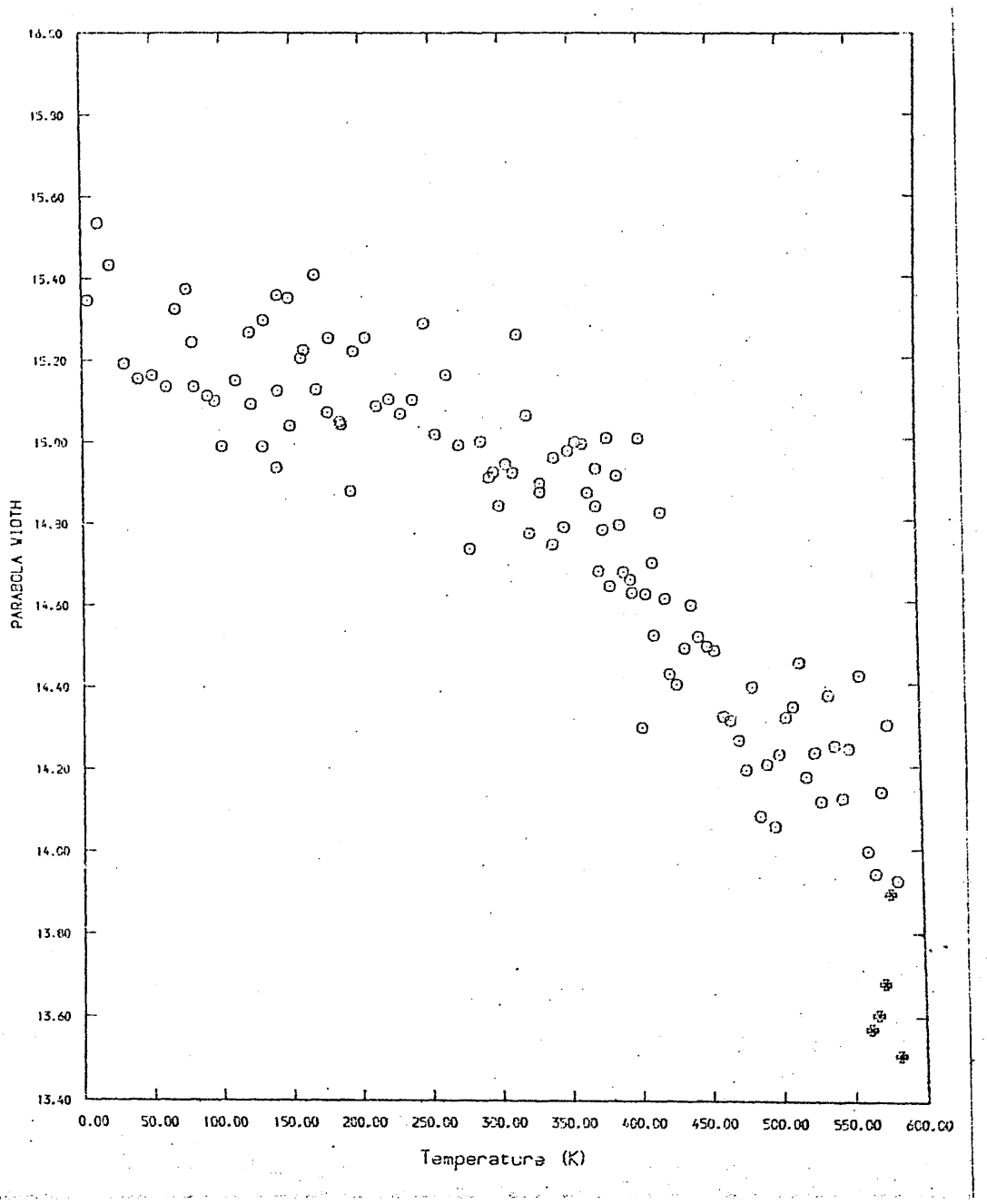

Figure 6.13: The temperature variation of the PARABOLA WIDTH for the [0001] direction of single crystal cadmium ,sample-A.

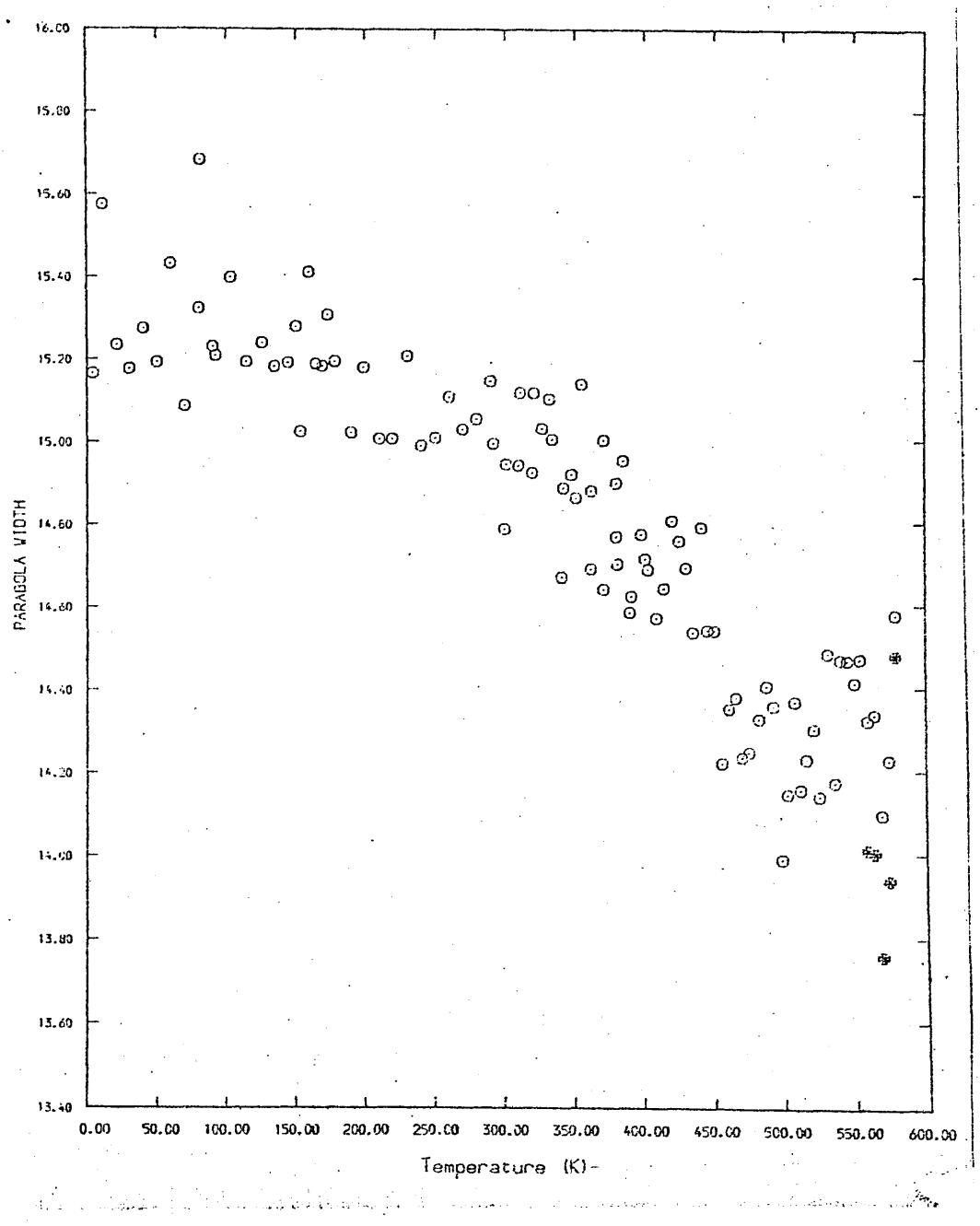

Figure 6.14: The temperature variation of the PARABOLA WIDTH for the 1010 direction of single crystal cadmium, sample-A.

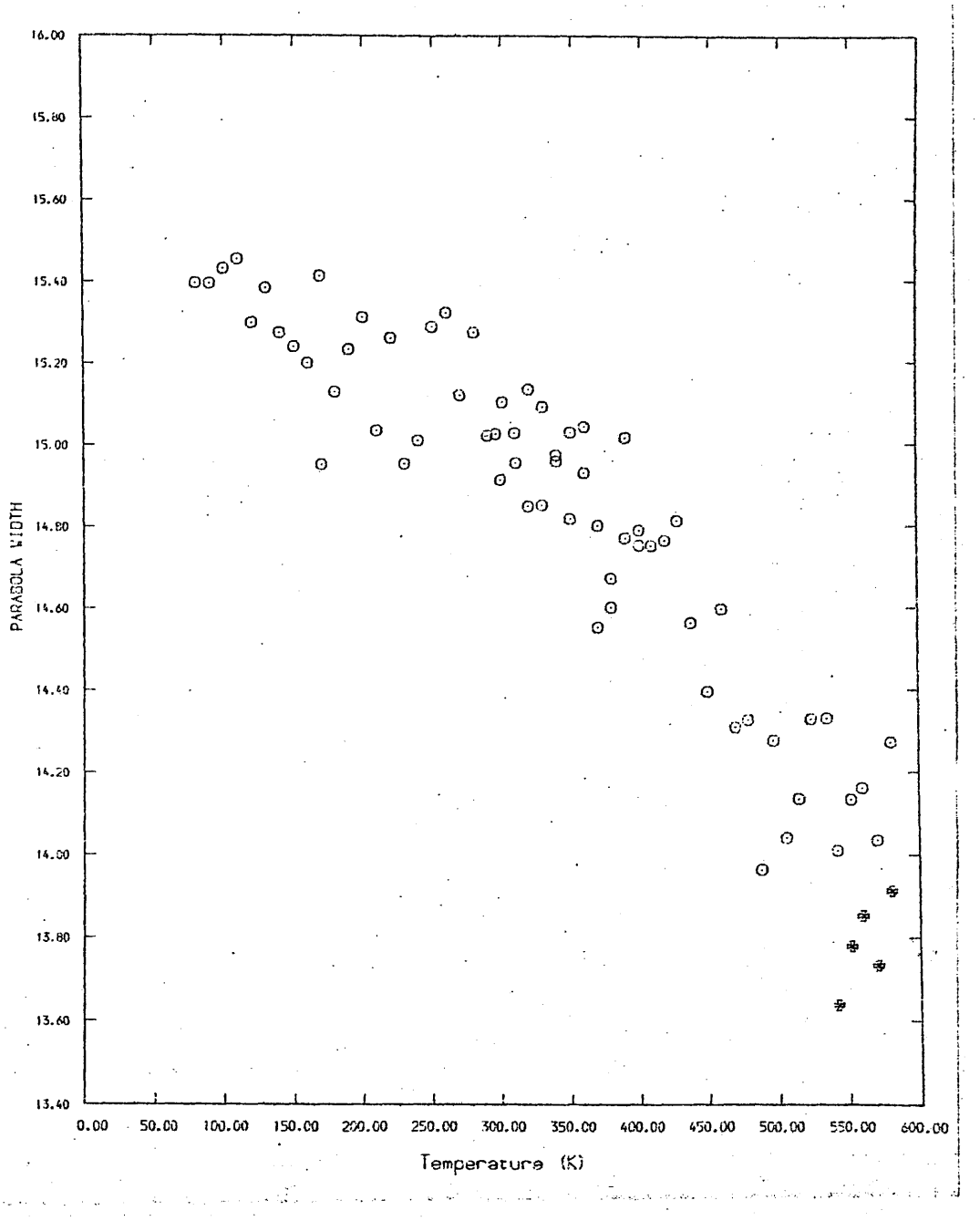

Figure 6.15: The temperature variation of the PARABOLA WIDTH for the [10$\bar{1}$0] direction of single crystal cadmium ,sample-B.

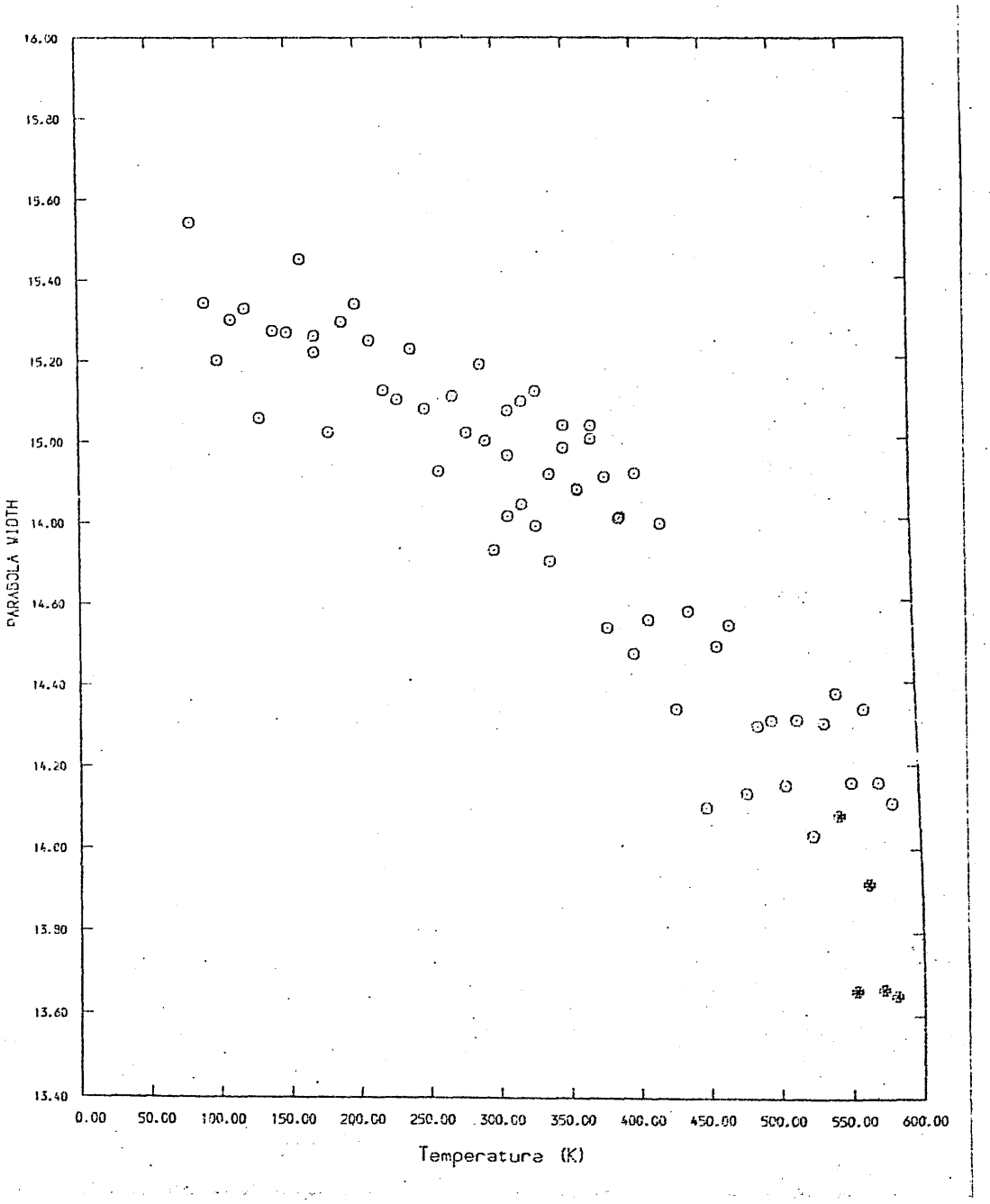

Figure 6.16: The temperature variation of the PARABOLA WIDTH for the [ØØØ1] direction of single crystal cadmium ,sample-B.

dependence. The reduction observed in GW between 350K and 500K is approximately double that which occurs over the temperature range between 150K and 350K. It is to be expected that the inclusion in the model of the zero-point broadening function described in chapter 5.3.2 would result in a temperature dependence of the Gaussian width at these temperatures which is attenuated with respect to that obtained for this simpler convolution model.

The percentage decrease here observed in the parabola width with temperature (figures 6.10, 6.12, 6.14, 6.16) is, approximately one third of that observed for the Gaussian. Again it is noticeable that the temperature dependence exhibited is larger between 350K and 500K than for lower temperatures. The average parabola width at low temperatures is 15.3 channels and is consistent for all four studies. This width corresponds to a Fermi energy of 7.99 eV which is in fair agreement with the accepted value of 7.47 eV [152,153].

The percentage contribution of the parabola to the total area under the annihilation line is shown as a function of temperature for sample-A [0001], sample-A [10$\bar{1}$0], sample-B [10$\bar{1}$0] and sample-B [0001] in figures 6.17, 6.18, 6.19 and 6.20 respectively. The parabola percentage is a measure of annihilations with conduction electrons and is expected to correlate to the F-parameter. The temperature variations of the parabola percentage here presented exhibit large uncertainties and,

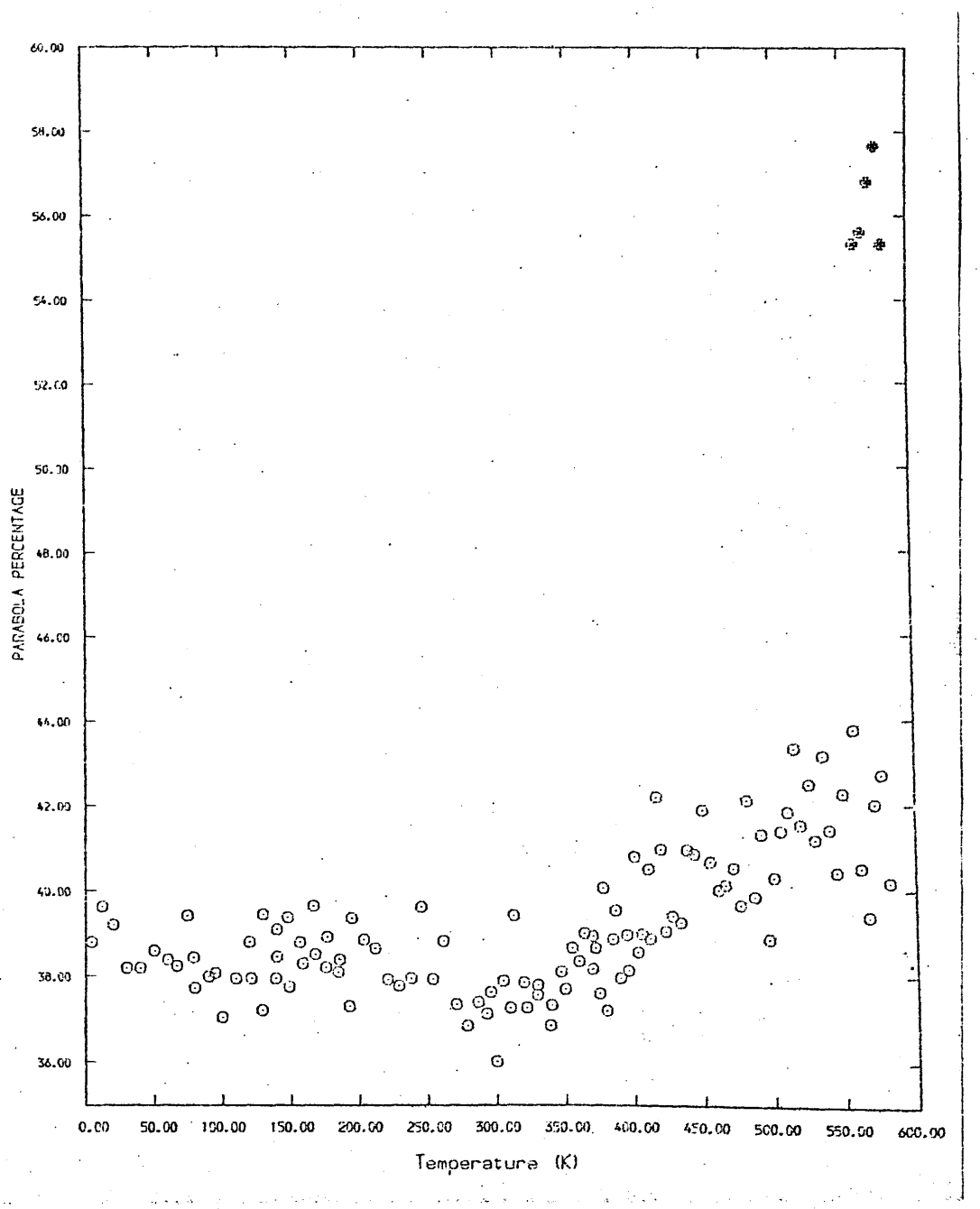

Figure 6.17: The temperature variation of the PARABOLA PERCENTAGE for the [0001] direction of single crystal cadmium ,sample-A.

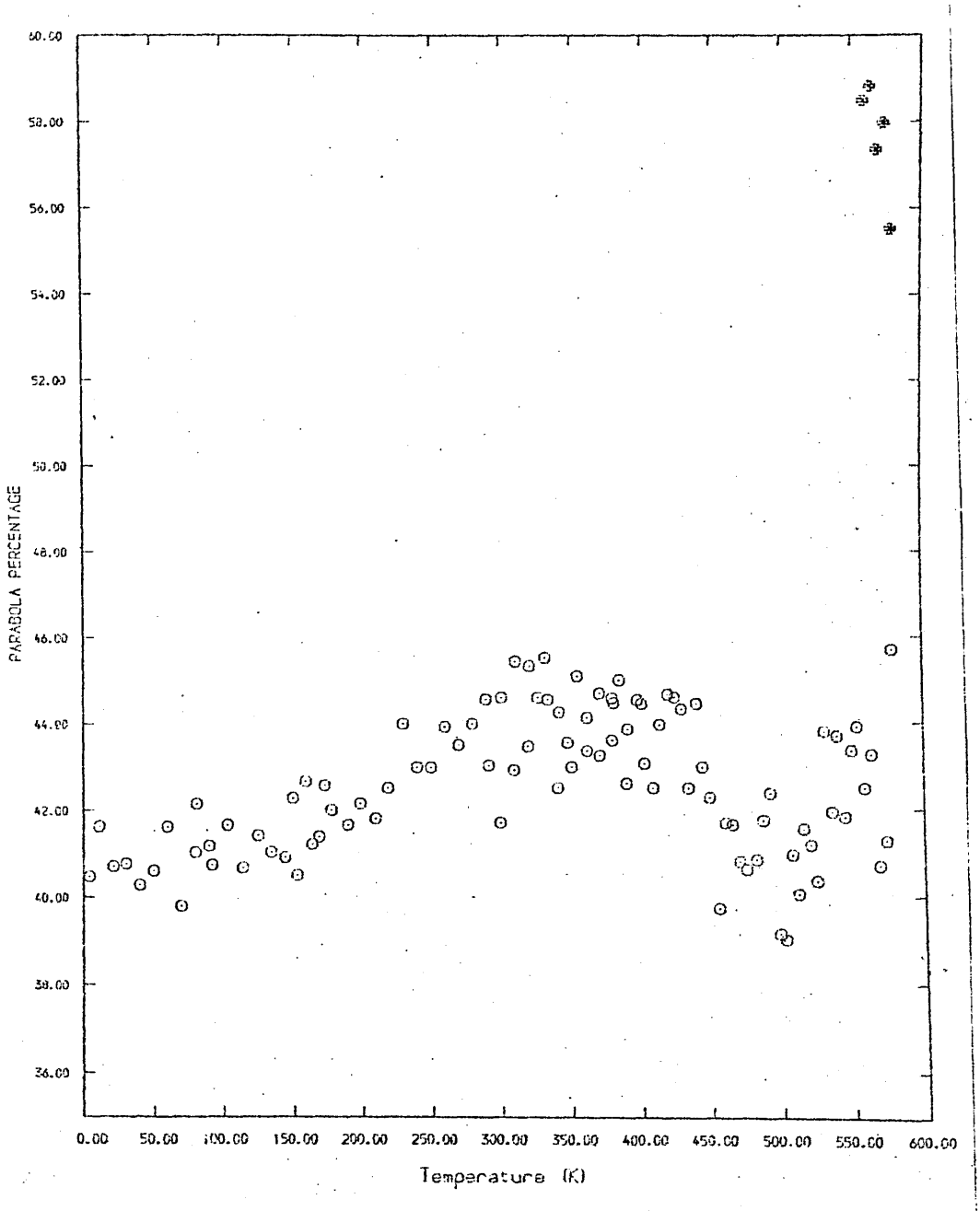

Figure 6.18: The temperature variation of the PARABOLA PERCENTAGE for the [10$\bar{1}$0] direction of single crystal cadmium ,sample-A.

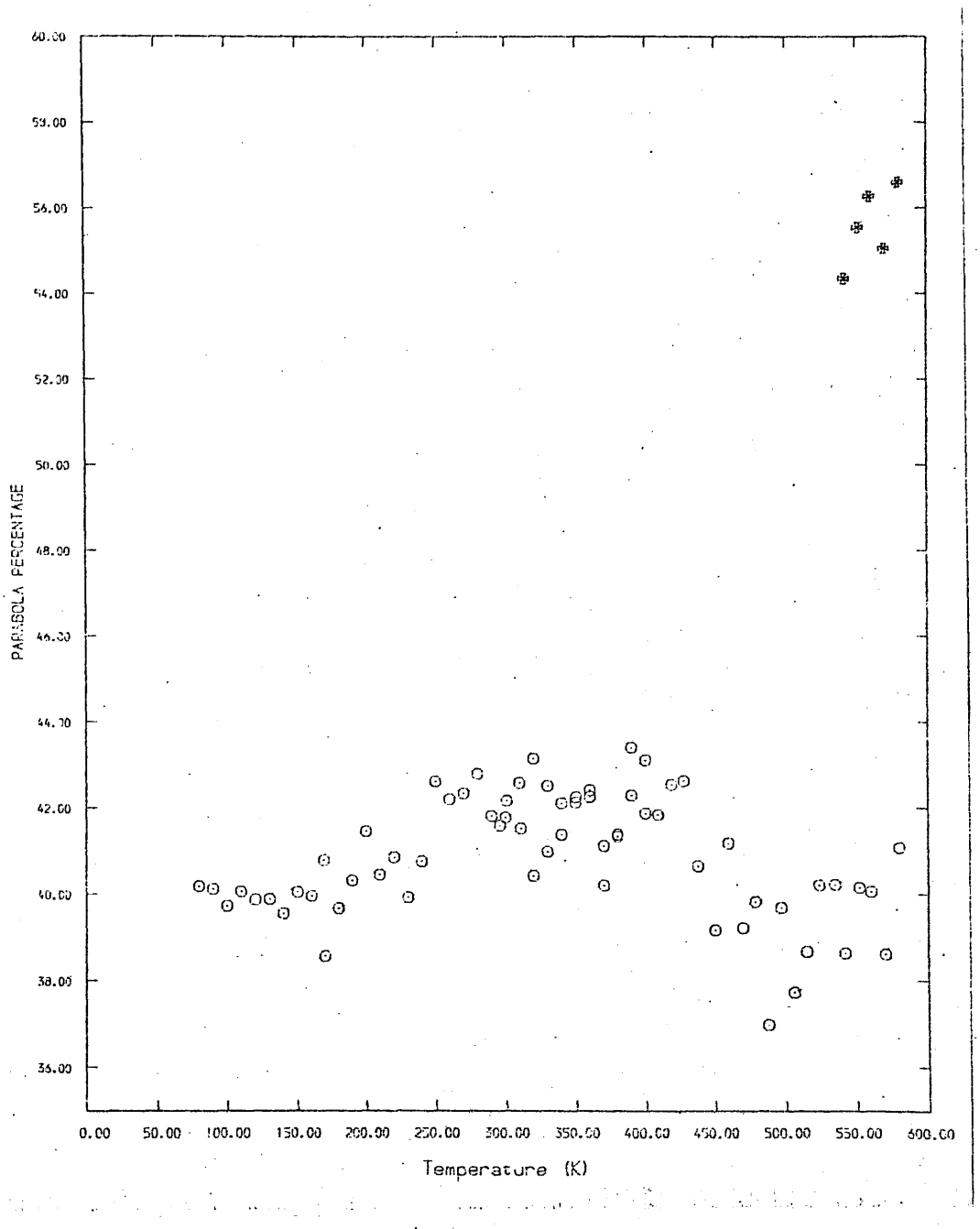

Figure 6.19: The temperature variation of the PARABOLA PERCENTAGE for the [1$\bar{0}$10] direction of single crystal cadmium ,sample-B.

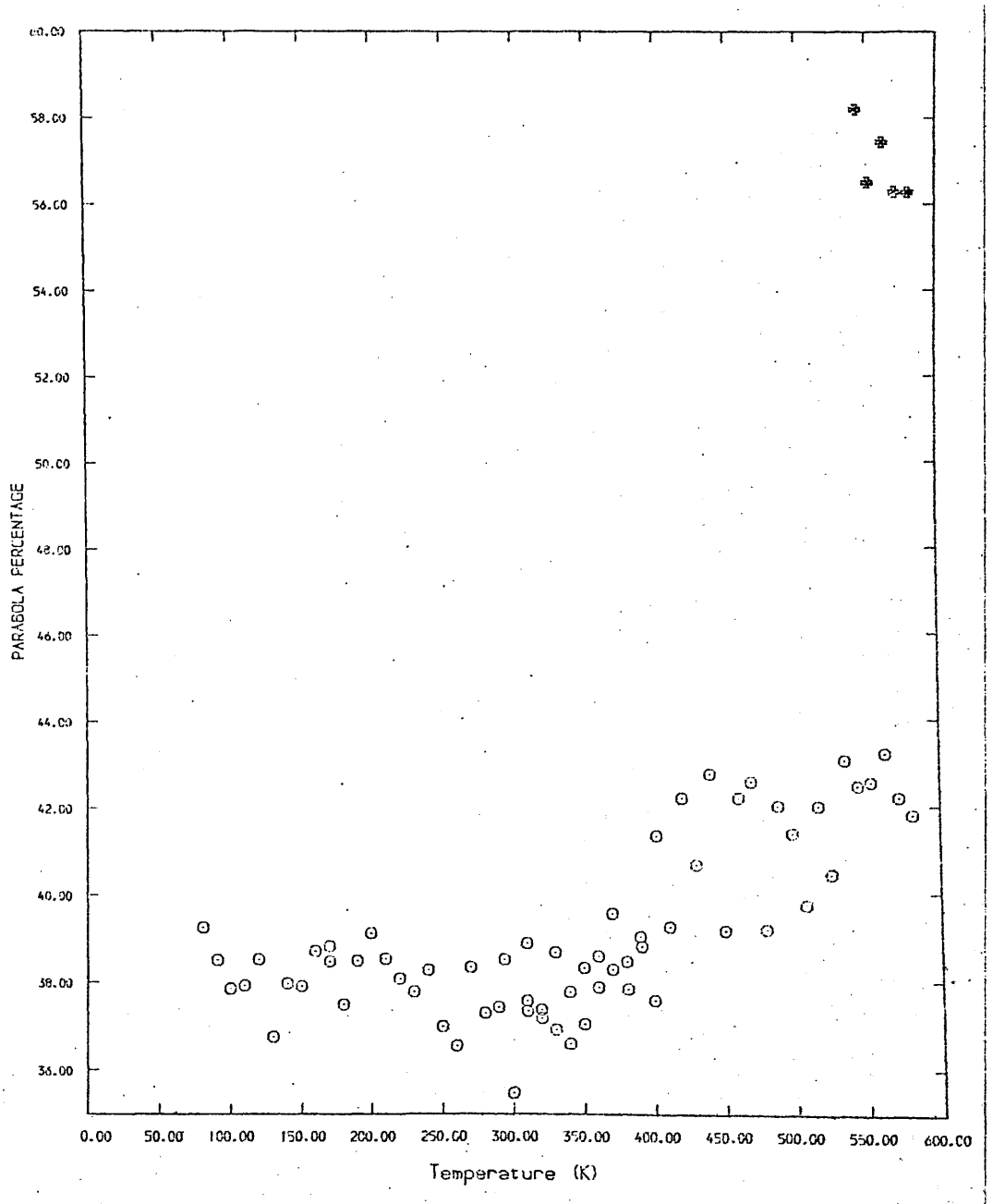

Figure 6.20: The temperature variation of the PARABOLA PERCENTAGE for the [0001] direction of single crystal cadmium ,sample-B.

in the vacancy trapping region (above 400K) for the [10$\bar{1}$0] directions indicate a decrease rather than the increase shown by the lineshape parameter. It is thought that the large scatter exhibited by these curves may be attributable to variations in photon scattering caused by the removal of the specimen from the cryostat to furnace. This suggested explanation is supported by the enhanced scatter present in the Gaussian and parabola widths for the relevant temperature cross-over region (290K-400K).

Notwithstanding the magnitude of these uncertainties, the temperature variation of the parabola percentage for both examples of the [10$\bar{1}$0] direction appear to be quite distinct from those of the [0001] direction. Making allowance for the scattering-induced uncertainties, the c-axis studies indicate an approximately temperature independent parabola percentage of 38 % for temperatures up to 350K, thereafter increasing to around 44 %. these values are in qualitative agreement with previously reported values for cadmium [126,59,132]. For the [10$\bar{1}$0] direction, both of the studies indicate a rise up to 350K: from 40 % to 46 % for sample-A and 40 % to 44 % for sample-B. As the temperature is further increased the parabola percentage drops to close to its low temperature value at the melting temperature. These discrepancies were thought to be a reflection of the inadequacies of the simple inverted parabola plus Gaussian model when applied to the case of positron annihilation from the vacancy trapped state.

6.7.2: Zero Point Motion Analysis

Time did not allow for the application of zero-point motion analysis technique to all of the spectra collected during this study; however such investigations were conducted for sample spectra in the low, pre-vacancy and vacancy temperature regions for each of the four sections of the study. The extension of this analysis to other than the vacancy region was embarked upon, despite the anticipated unsuitability of the model to the case of partial trapping, in order to investigate the orientational dependence and the possibility of trapping in the lower temperature regions.

The contribution of the positron to the momentum of the annihilating pair is included via a Gaussian broadening function, and the determination of the optimum width, σ, of this Gaussian function proceeds from a study of the effect on chi-squared of changes in σ. When this technique was applied, the anomalies in the temperature variation of the parabola percentage in the [1$\bar{0}$1$\bar{0}$] direction are removed. The parabola percentage values derived from the inclusion of the positron zero-point motion are plotted in figures 6.17, 6.18, 6.19, 6.20 respectively. In these figures, the new values of parabola percentage corresponding to the minimum value of chi-squared versus σ, are marked by

a plotting character distinct from that used for the earlier results (which correspond to σ =Ø). The values of the Gaussian and parabola widths corresponding to these optimum zero-point motion fits are also included where appropriate in figures 6.9 to 6.16 . Again, these points are marked by means of a different character to that used for the σ=Ø points.

For the [ØØØ1] direction the results indicate that for sample-A the parabola percentage increases from about 38 % at low temperatures to approximately 56 % at high temperatures while for sample-B between the same temperatures the parabola percentage varies from 38.5 % to 57 %. Comparable variations for the [1Ø$\bar{1}$Ø] direction are 41 % to 57.5 % for sample-A and 4Ø % to 55.5 % for sample-B. All four studies indicate similar positron zero-point broadenings corresponding to a minimum in chi-squared at σ= 4 in the temperature region 56ØK to 58ØK . An example of variation of chi-squared with for this temperature region is shown for each of the four studies in figure 6.21 . This finding is in agreement with a similar study of vacancy trapping in cadmium [136,139]. For an explanation of the reduced chi-squared values shown in this and the following two figures, see appendix.

A similar degree of concord was exhibited by the low temperature (~1ØØK) points studied, examples of which are illustrated in figure 6.22 . At these temperatures, the relationships indicate that σ=Ø provides the optimum fit to

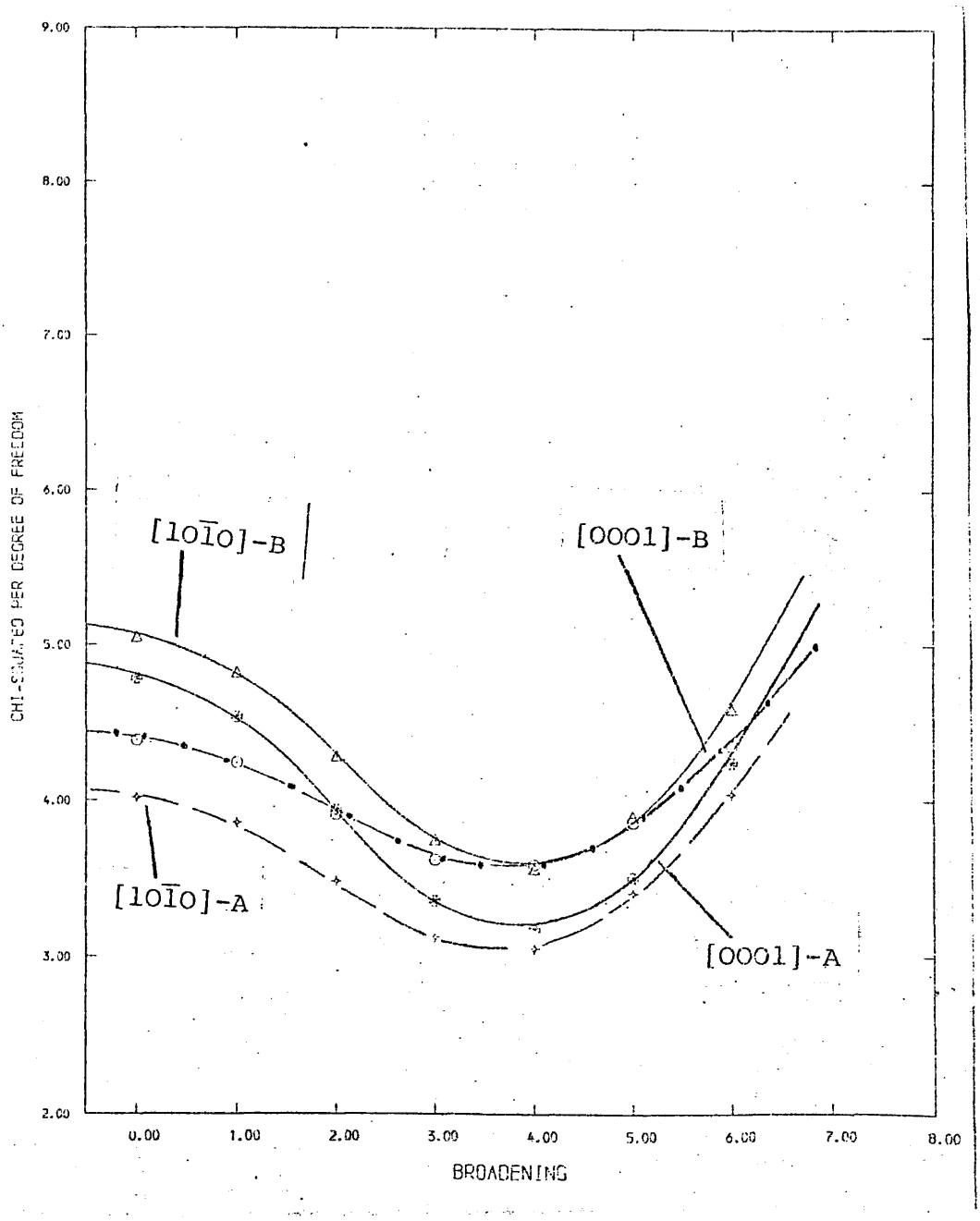

Figure 6.21:The variation of CHI-SQUARED with positron GAUSSIAN WIDTH for the high temperature region of the four studies of single crystal cadmium.

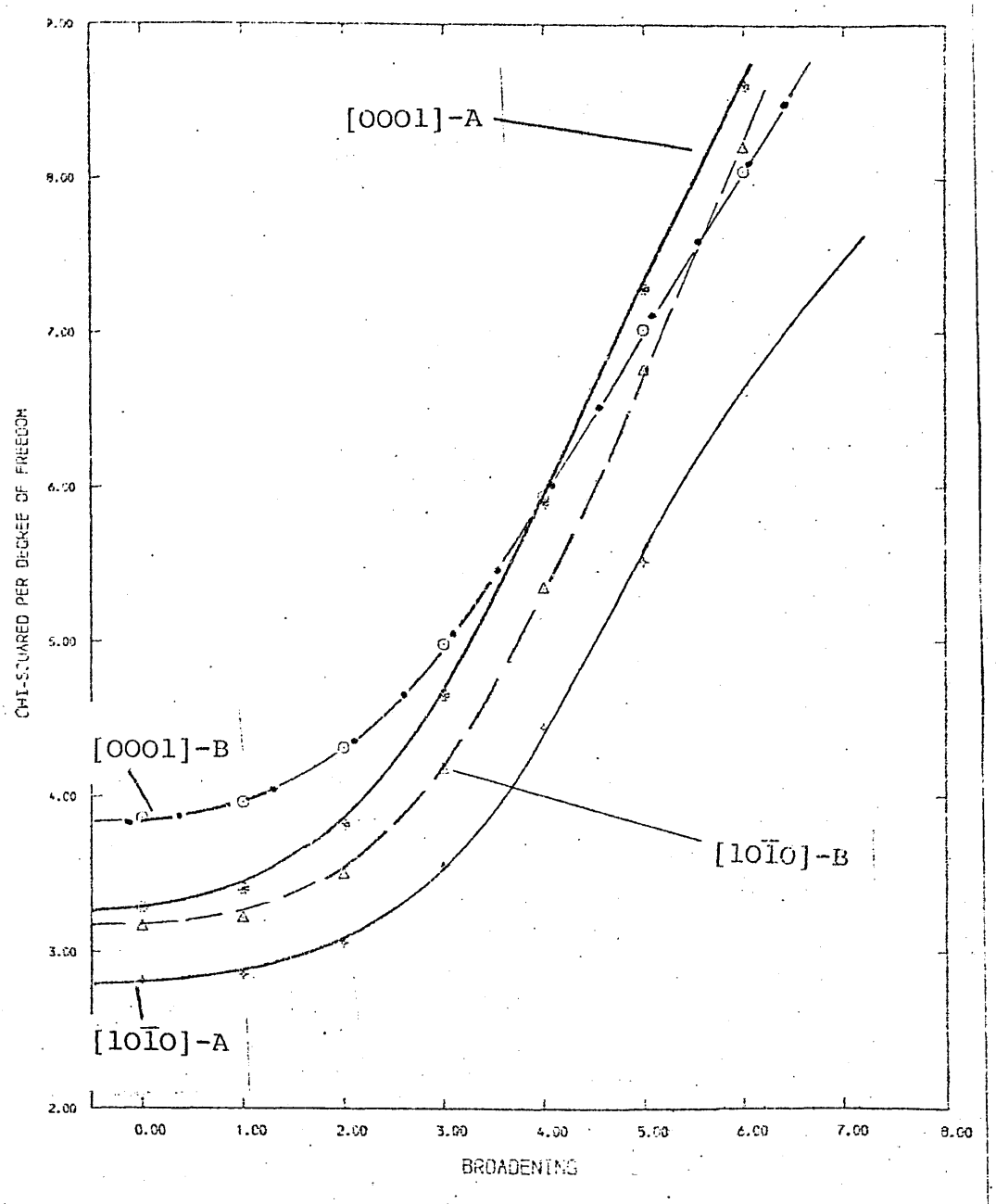

Figure 6.22:The variation of CHI-SQUARED with positron GAUSSIAN WIDTH for the low temperature region of the four studies of single crystal cadmium.

the data. This indicates that no positron trapping is revealed by this technique within the accuracy of the positron broadening widths here employed.

No clear picture emerged from the zero-point broadening analysis in the pre-vacancy region (~310K): there being no consensus between the optimum value of σ suggested by the individual chi-squared versus σ relationships. It was not thought profitable, in the analysis of these four studies , to attempt to distinguish between the results derived from individual spectra; instead, for each of the studies, an average chi-squared versus σ relationship was computed. These relationships are illustrated in figure 6.23 and as can be seen, the suggested minima are shallow, a circumstance which contributed to the uncertainty over the assignment of an optimum σ for the individual spectra.

From these relationships emerges the fact that for both [0001] studies, the optimum fit corresponds to σ=0 and for both [10$\bar{1}$0] studies, σ=1 . Some indication of an orientational effect is suggested here however the respective minima are not well defined and, as a result, no definite conclusions can be drawn.

In the absence of clear minima, some method of characterisation of the chi-squared versus σ relationship is required. Here, the choice has been made of the change in which separates the optimum value of σ from that at which

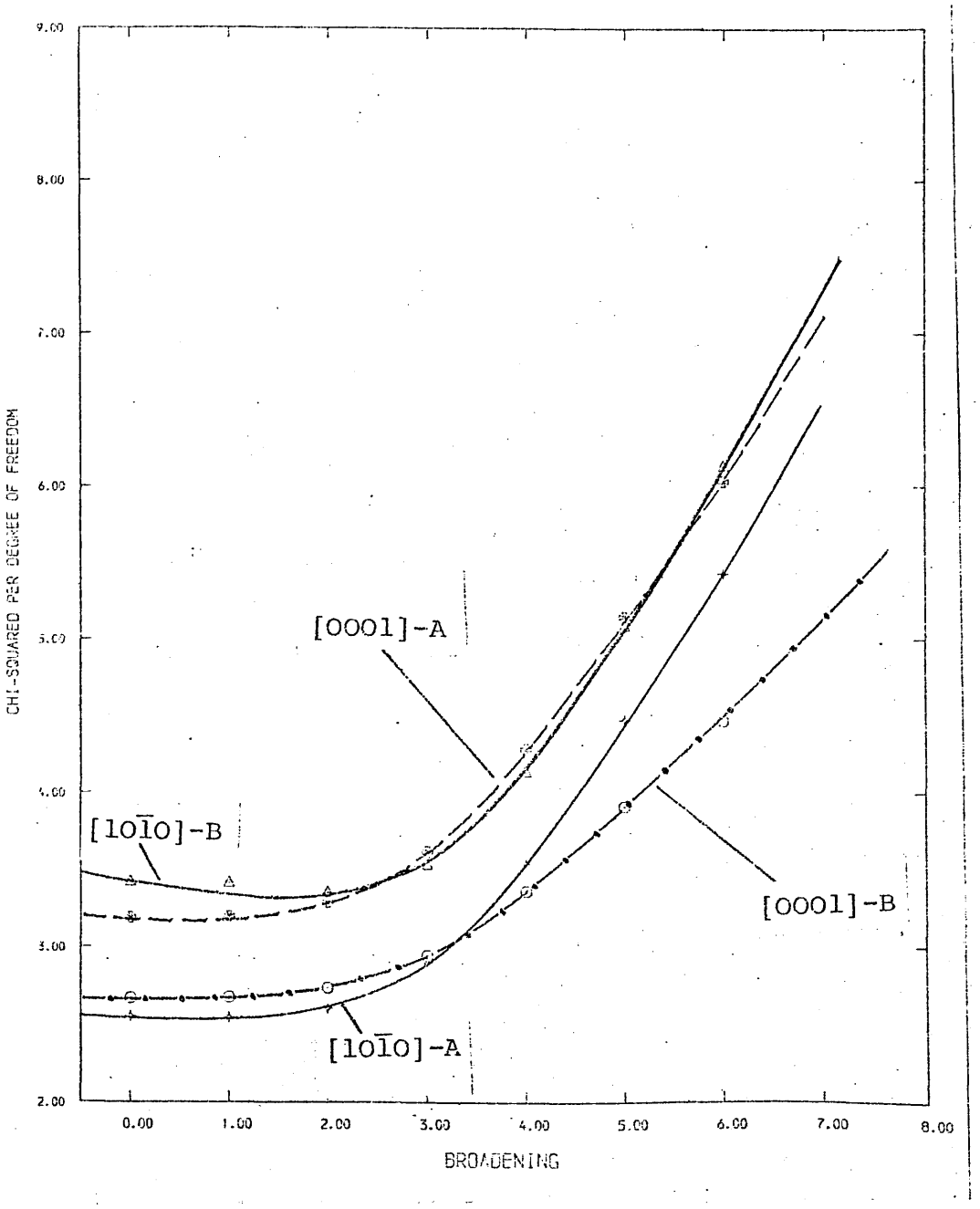

Figure 6.23:The variation of CHI-SQUARED with positron GAUSSIAN WIDTH for the pre-vacancy region of the four studies of single crystal cadmium.

the chi-squared value has increased by 30 % from its minimum value. It is thought that such a characterisation is appropriate to the analysis of the pre-vacancy region for which it has generally been assumed that positrons annihilate from the free state. Application of this parameterisation to the relationships illustrated in figure 6.22 yields, for the [0001] studies: sample-A, $\Delta\sigma$=3.7; sample-B, $\Delta\sigma$=4.2 . For the [10$\bar{1}$0] direction the respective values are 2.6 and 3.3 . Again no clear orientational effect is observed.

On the basis of this convolution model, some evidence of positron localisation at T =~310K exists, and perhaps to a slightly greater extent for the [10$\bar{1}$0] direction than for the hexagonal axis. However, the crudity of the model and the relatively small number of spectra studied do not permit certainty in the matter of positron localisation in the pre-vacancy region of cadmium.

6.7.3: Partial Trapping Analysis

This lack of uniformity for either direction exposes further inadequacies in the convolution model used. The inclusion of the positron broadening function is useful in cases where close to 100 % trapping obtains; however, when a significant proportion of the annihilations take place from the free state, a less than satisfactory description

results. A model which takes account of this "partial trapping" domain is, in principle, simple to construct. Such a model can be broken down into two components representing free and trapped annihilations respectively. Each of the components would contain an inverted parabola and a Gaussian; however, the trapped component alone would possess an additional positron broadening function. The model representing the background subtracted intrinsic distribution can be constructed as follows:

$$(x) = \left[P_T \ (\text{parabola} + \text{Gaussian})_T * \ ZPM\right] + \left[(1-P_T)(\text{parabola} + \text{Gaussian})_F\right] \qquad 6.2$$

where the subscripts T,F refer to trapped and free annihilations respectively, p is a probability, * represents convolution and ZPM is the positron broadening function. This model, when complemented by a description of the background requires that fourteen free parameters be used in the fitting procedure; by contrast, the present model requires only nine. Unfortunately, the least squares minimisation routine at present available at Bedford College is not capable of finding reliable minima as a function of so many variables. At the present then, efforts to construct a "partial trapping" model along the above lines are limited by our minimisation routine.

In an effort to circumvent this difficulty an alternative procedure, which was developed in collaboration with Drs. I.Chaglar and F.A.el Khangi, was attempted.

In order to reduce the number of variables employed in the fitting procedure, it was decided to fix the values of the parameters of the Gaussian and inverted parabola. Values of these parameters were determined from spectra collected at the extremes of the experimental temperature range by means of the simple convolution model for the low temperature spectra, and one which included a zero-point broadening function for the high temperature extreme. An inherent assumption of this technique is that 100 % positron trapping obtains in this latter case. A new variable p_F, which represents the fraction of free annihilations, was then introduced into the minimisation procedure to allow for the variation of the relative intensities of the free and trapped components for temperatures intermediate to the above mentioned extremes.

This analysis technique was applied to the spectra arising from the [0001] direction of sample-A. In figure 6.24 is illustrated the temperature variation of the free annihilation fraction, p_F, and in figure 6.25, the temperature variation of the reduced chi-squared obtained from these fits. It can be seen from the former figure that, at temperatures approaching 0K, approximately 90 % of the positrons annihilate from the free state while for the vacancy threshold temperature (~350K) this value has dropped to 70 %. At temperatures close to the melting point, the free percentage is found to be 20 %. From figure 6.24, it can be seen that the value of the reduced chi-squared approaches unity in the temperature range 350K to 500K

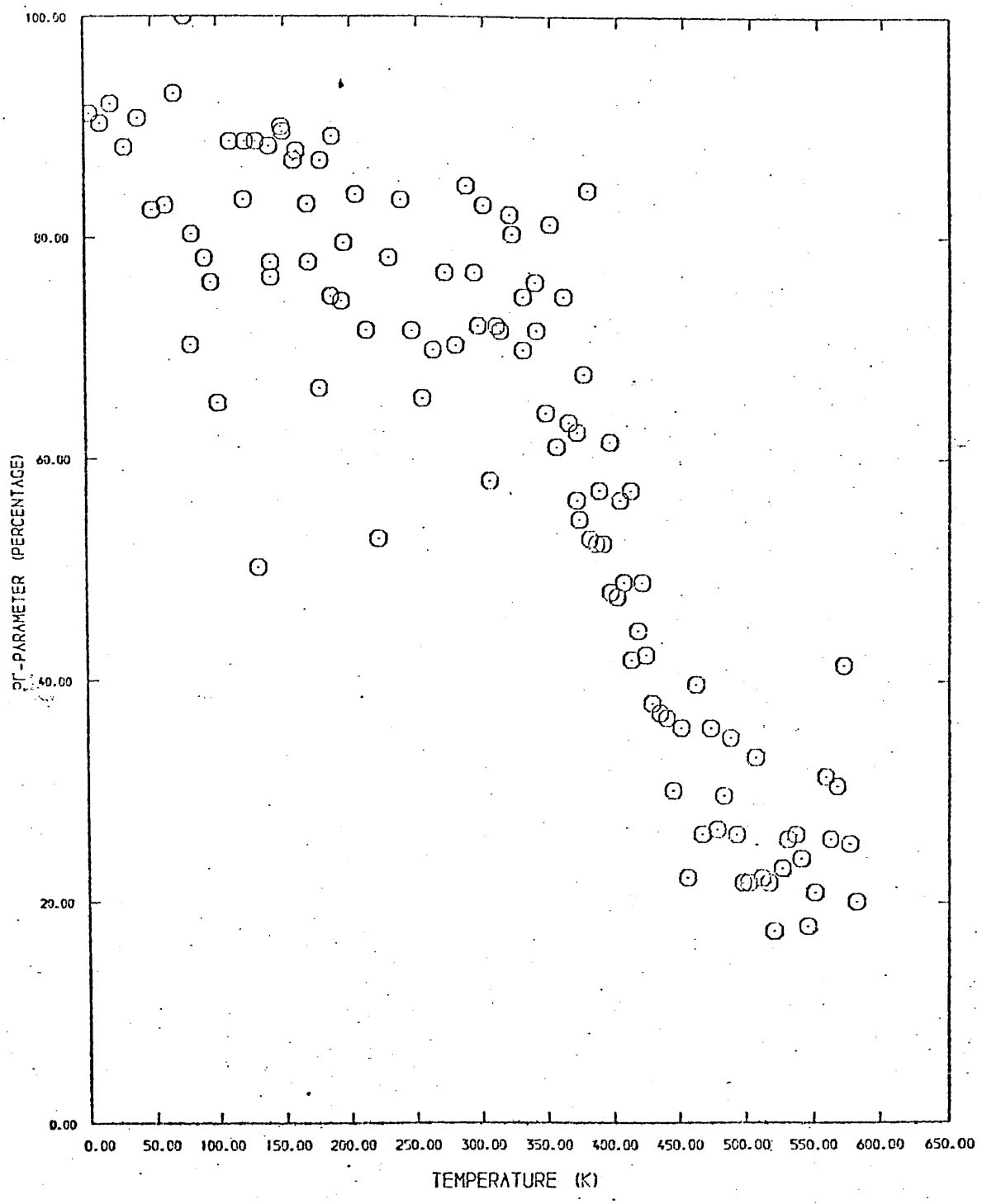

Figure 6.24:The temperature variation of the free annihilation fraction, p , for the [0001] direction of sample-A.

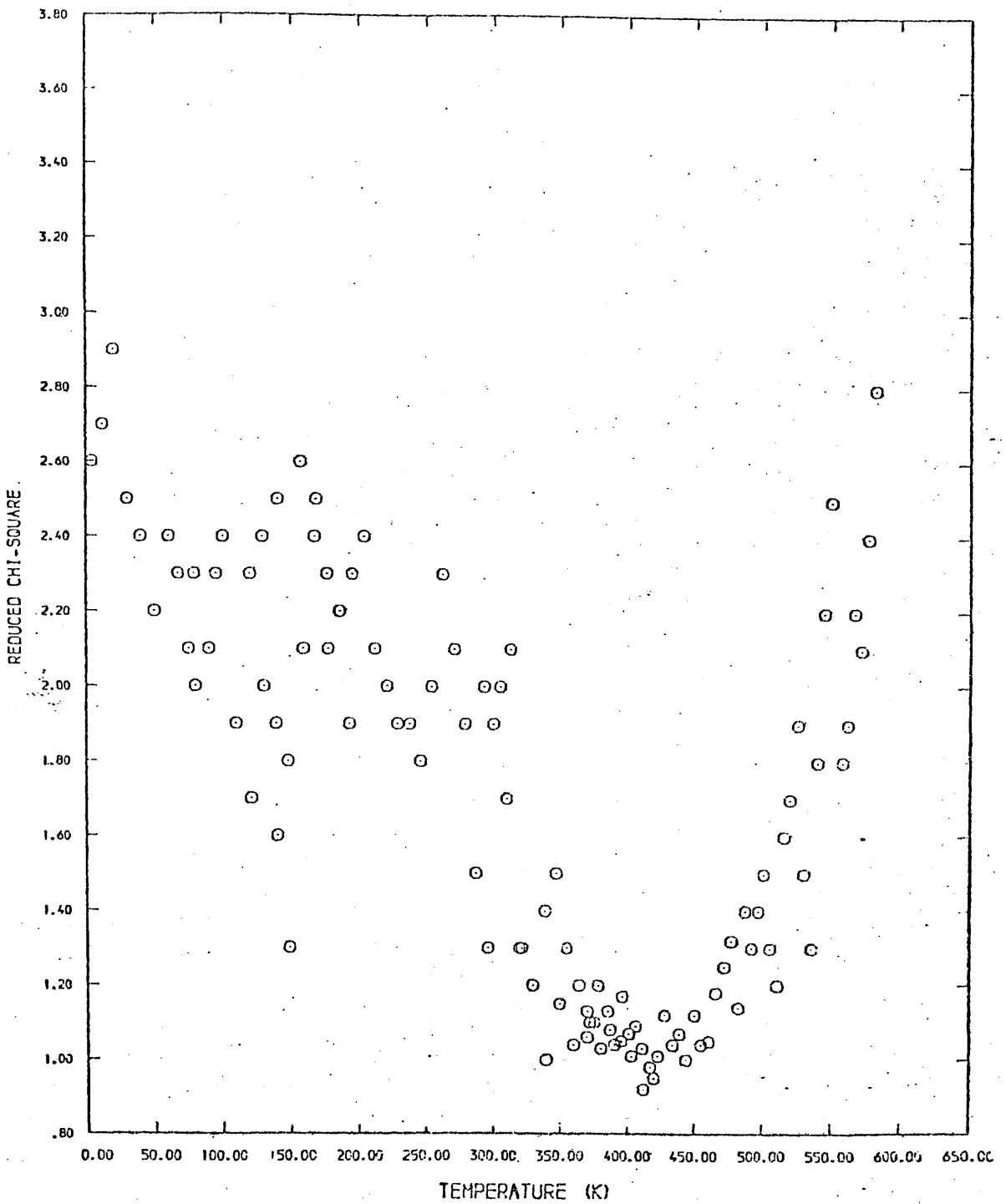

Figure 6.25:The temperature variation of the reduced chi-squared obtained from partial trapping fits to the [0001] direction of sample-A.

however, for other than this region, poorer fits are obtained.

Contributions to the large scatter exhibited by the p_F values are thought to arise from the inability of the least squares minimisation routine to reproduce faithfully narrow or weak (< 20 % of the total intensity) components in the annihilation spectrum. A further possible inadequacy may be that of the broadening function employed for the trapped lineshape. Also, no allowance was made for temperature dependences in the parameters which characterise the trapped positron lineshape. Such a dependence has been reported [133] and provisionally attributed to the temperature dependent electronic structure of vacancies and to the contraction of the Fermi surface.

Despite the difficuties here encountered the development of a partial trapping convolution technique holds the promise of significant enhancements in the analysis of Doppler broadening lineshapes. Notable amongst these is the opportunity for the definition of a lineshape parameter independent of energy and equipment. The parabola percentage of either the free or trapped component, is potentially such a definition independent parameter. Further benefits of a successful partial trapping analysis would be the facility for defect characterisation offered by the functions employed to describe the trapped component and the potential for deriving the monovacancy formation enthalpy from a few points of a $\ln[(p_F)/(1-p_F)]$ versus $(1/kT)$

relationship.

CHAPTER 7: POSITRON ANNIHILATION IN SINGLE CRYSTAL ZINC

7.1: INTRODUCTION

In the preceding chapter evidence was presented of anisotropies in positron annihilation parameters derived from specimens of the hexagonal metal cadmium. It was expected that zinc, which also crystallises in the h.c.p. structure, would exhibit anisotropies similar to those of cadmium. Evidence of such anisotropies had been revealed as the result of angular correlation studies [154]. These data were later interpreted as being the result of the strong enhancement of the annihilation probability in the lenses formed by the intersection of the Fermi surface with BMC surfaces [155]. Such an explanation might have been less plausible had the effect of orientation on the temperature dependence of a positron annihilation parameter been studied. The investigation of the effect of orientation in the temperature dependence of the lineshape parameter was therefore extended to single crystal specimens of zinc.

7.2: EXPERIMENTAL DESCRIPTION

Two rectangular slices, having dimensions 17 X 16 X 3 mm were cut by means of a spark-erosion technique from a rod of 99.999% (5N) purity single crystal zinc supplied by Metal Crystals Ltd. . The cutting of these specimens was performed such that the [ØØØ1] direction was normal to the faces of each slice and the [1Ø$\bar{1}$Ø] direction was parallel to the shorter sides. A spark-planing technique was then employed to remove 2ØØμm from both faces of each slice. The specimens were then chemically polished in 35% nitric acid until a good visual appearance was produced and subsequently thoroughly rinsed in de-ionised water.

The orientation of the crystal lattice with respect to the edges of the specimen slices was verified by means of X-ray photography. The specimens were then electro-polished in a 5Ø:5Ø solution of orthophosphoric acid and ethyl alcohol [156] . After thorough rinsing in de-ionised water the specimens were dried and mounted in the vacuum furnace where they were annealed for 26 hours at a temperature of 6ØØK under a pressure of less than 10^{-6} torr. On completion of this process, the temperature of the specimens was reduced slowly (<1 degree per minute) to room temperature. The specimens were then chemically polished in

35% nitric acid until a good visual finish was produced and thoroughly rinsed in de-ionised water.

Approximately 100 microcuries of carrier-free ^{22}Nacl in acqueous solution was then deposited and evaporated onto the centre of one of the specimen slices, such that the diameter of the source was no greater than 3 mm. A specimen-source sandwich was constructed by aligning the second prepared slice on top of the source carrier such that the $[10\bar{1}0]$ directions of the slices were mutually parallel. The sandwich was then encapsulated in a wrapping of thin aluminium foil and the prepared sample mounted on the low temperature cryostat. The cryostat assembly was then evacuated and the dewars filled with liquid nitrogen. The sample was allowed to cool initially to 77K and subsequently to 4.2K.

The cryostat assembly was placed in front of the detector such that the [0001] direction of the specimen was parallel to the detector axis. The sample-detector distance was approximately 15 cm and the detector crystal subtended an angle of approximately 0.01 sr at the specimen.

Annihilation spectra were recorded at temperature increments of approximately 10K between 4.2K and 400K for the [0001] direction. At each point the specimen temperature stability was better than ±0.1K. On completion of this cycle of measurements, the cryostat insert was rotated by 90° such that the $[10\bar{1}0]$ direction was parallel

to the detector axis and a similar measurement cycle performed for this orientation.

In the case of the furnace measurements it was decided not to follow the normal practice of making positron annihilation measurements up to temperatures within a few degrees of the specimen melting temperature, 693K for zinc. This decision was taken because of the reported likelihood of contamination hazards [134] arising from the evaporation of the NaCl positron source at the low pressures used, $\sim 10^{-6}$ torr. In order to minimise the risk of any such contamination, the highest temperature attained during this measurement cycle was 601K.

Each spectrum was collected simultaneously with a ^{103}Ru reference peak at a total counting rate of 5000 cps. Over the two-hour counting time used at each temperature, the 511keV spectrum contained approximately 900,000 counts. All the measurements made on zinc were performed using a Canberra 8080 analogue to digital converter, in place of the Laben 8192 used for cadmium.

7.3: LINESHAPE PARAMETER ANALYSIS

Prior to the computation of the lineshape parameter, all the spectra were subjected to a background subtraction procedure which employs the complementary error function [124]. The width of the central region chosen to define the F-parameter was 15 channels. The energy dispersion as obtained from the calibration of the spectrometer was 0.0938 keV per channel. The F-parameter versus temperature curves were then normalised in the temperature overlap region between the cryostat and furnace measurements (from 294K to 400K). This procedure was necessary in order to take account of variations in photon scattering caused by the change in sample chambers. The temperature variation of the F-parameter in the case of radiation emitted in the [0001] direction is shown in figure 7.1, while that corresponding to the [10$\bar{1}$0] direction is shown in figure 7.2 [141]. Average statistical errors (2σ), as defined in section 5.2.2, are for the [0001] direction, 0.0010 and for the [10$\bar{1}$0] direction, 0.0011 .

In a similar fashion to the cadmium data, the data arising from each orientation of zinc were analysed in terms of three proposed temperature dependences, viz:

(a) the "linear-rise" model with $\gamma = 0$ (equation 6.1),

(b) the "linear-rise" model with $\gamma \neq 0$ (equation 3.38)

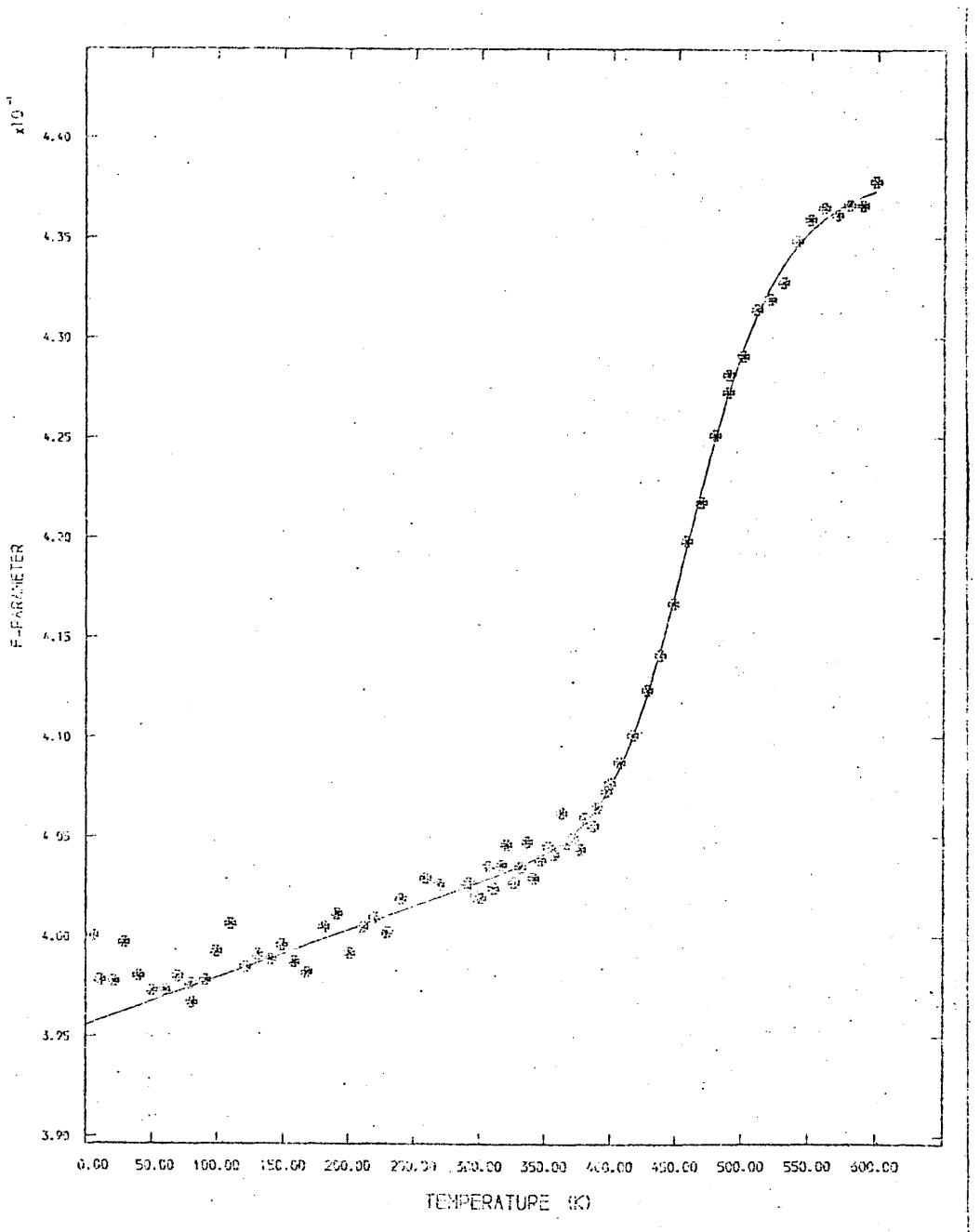

Figure 7.1: The temperature variation of the F-parameter for the [0001] direction of single crystal zinc.

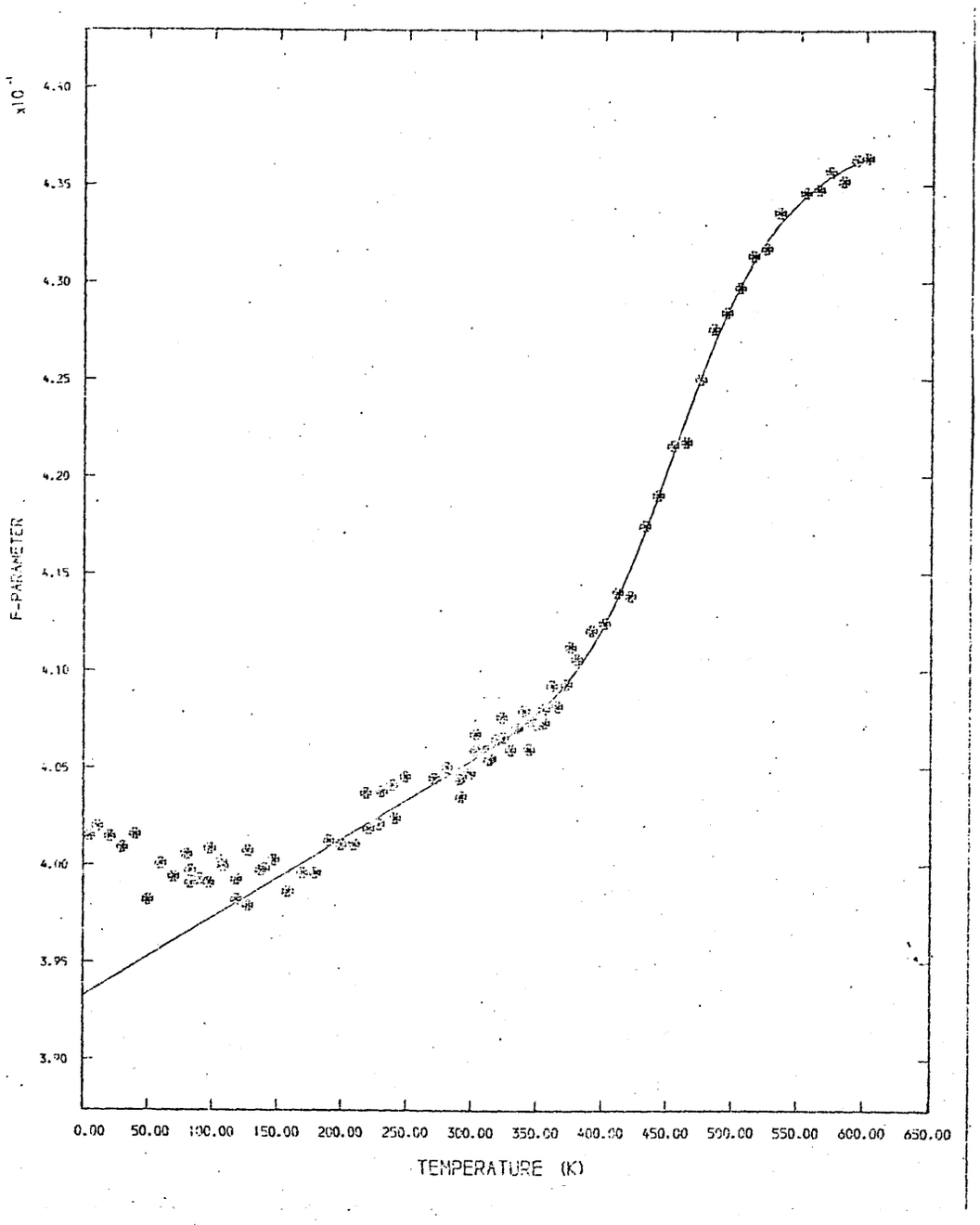

Figure 7.2: The temperature variation of the F-parameter for the [10$\bar{1}$0] direction of single crystal zinc.

and

(c) the "self-trapping" model (equation 3.35).

Each of the above models was fitted to the data sets by means of a least squares minimisation routine. In the cases of models (a) and (b), the region below 150K was excluded from the minimisation calculations in order that the low temperature slope did not interfere with the determination of the pre-vacancy behaviour. The optimum values of the fitting parameters obtained from each of the three models, are given for the [0001] direction in table 7.1 and, for the [10$\bar{1}$0] direction in table 7.2 . Also included in the tables are values for the monovacancy formation entropy and the monovacancy concentration. These latter values were deduced from the fits by assuming typical values for the specific trapping rate of positrons at vacancies (2.4×10^{14} s^{-1}) and for the free positron lifetime (175 ps) [110]. The solid lines in the figures represent the best fit to each set of data; however, the suitability of each of the above models will be discussed for each of the data sets.

From table 7.1 it can be seen that, for the [0001] direction, the inclusion of the high temperature slope, χ, does not significantly improve the quality of the fit as measured by the reduced chi-squared. The improvement thus obtained in the fit is not sufficient to endorse unequivocally the validity of $\chi \neq 0$ in this case, particularly in the light of the rather large uncertainty associated with the value of χ derived from this fit. Also on grounds of quality of fit, the attempted explanation of the pre-vacancy

	equation 6.1	equation 3.38	equation 3.35
Temperature range of fitting (K)	149-599 (57)	149-599 (57)	4.2-599 (73)
H_{IV} (eV)	Ø.59±.ØØ3	Ø.61±.Ø1	Ø.55±.Ø1
$A\chi10^{-5}$	23.69±1.84	36.6Ø±12.31	8.14±2.21
$\beta\chi10^{4}(K^{-1})$	Ø.6Ø±.Ø3	Ø.61±.Ø3	---
$\gamma\chi10^{4}(K^{-1})$	---	Ø.22±.18	---
$B\chi10^{-5}(K^{-3/2})$	---	---	14.1Ø±2.1Ø
$\mathcal{E}_o$ (eV)	---	---	Ø.12±.ØØ3
S_{IV} (k)	4.Ø	4.5	3.Ø
$C_{IV}(T_m)\chi10^{4}$	26.9	32.9	2Ø.6
SSQ/N	1.473	1.465	1.747
Chi-squared	1.614	1.637	1.9Ø4

Table 7.1: single crystal zinc [ØØØ1]:
optimum values of fitting parameters.

	equation 6.1	equation 3.38	equation 3.35
Temperature range of fitting (K)	147-601 (64)	147-601 (64)	4.2-601 (86)
H_{IV}(eV)	0.48±.02	0.45±.02	0.46±.02
$A\times10^{-5}$	1.31±.062	0.53±.24	.79±.35
$\beta\times10^{4}(K^{-1})$	1.02±.04	1.00±.04	---
$\gamma\times10^{4}(K^{-1})$	---	-0.52±.30	---
$B\times10^{-5}(K^{-3/2})$	---	---	1.75±.39
ε_o (eV)	---	---	0.10±.01
S_{IV} (k)	1.1	0.2	0.6
$C_{IV}(T_m)\times10^{4}$	9.7	6.2	9.2
SSQ/N	2.084	2.063	2.377
Chi-squared	2.260	2.277	2.556

Table 7.2: single crystal zinc [10$\bar{1}$0]:
optimum values of fitting parameters.

rise in terms of positron self-trapping appears to be less satisfactory than in the case of cadmium. This is not surprising in view of the absence of a pre-vacancy plateau.

A similar situation prevails for the [10$\bar{1}$0] direction. A very small improvement in the reduced chi-squared is achieved by the inclusion of $\gamma \neq 0$ in the "linear-rise" model; however the fitting here obtained suggests a negative co-efficient in contrast to the positive value obtained for [0001]. Again the uncertainty associated with this slope is high. As a result of this large uncertainty in γ, the $\gamma = 0$ version of the "linear-rise" model was assumed. It can also be seen from table 7.2 that the "self-trapping" model does not provide a good fit to the data.

The difficulty encountered over the assignment of a meaningful value to the high temperature slope, γ, is thought to reflect the absence of datum points in the temperature range 600K to 690K . A similar investigation of single crystal zinc [167] in which measurements of the angular correlation peak count parameter were made up to the melting temperature confirms this assumption.

7.4: DISCUSSION OF RESULTS

A comparison of columns (a) of tables 7.1 and 7.2 reveals anisotropies in the temperature dependence of the lineshape parameter for single crystal zinc which are similar to those previously observed for single crystal cadmium. For the $[10\bar{1}0]$ crystallographic orientation of cadmium it was found that the "self-trapping" model provided a closer fit to the data than did the "linear-rise" model. This was not the case however for the same direction in zinc, both directions for this metal being better described by the "linear-rise" model. A similar finding has recently been reported [157] as resulting from a Doppler broadening study of the [0001] and $[11\bar{2}0]$ directions of single crystal zinc.

A further difference between the zinc and cadmium data lies in the relationship between the deduced monovacancy formation enthalpies, tables 7.1 and 7.2 . When the results of similar models are compared in the case of cadmium, columns (a) of tables 6.3 and 6.4 for example, similar enthalpy values are obtained for the two directions. However, in the present case , tables 7.1 and 7.2, the difference between the enthalpy values is much larger than that normally attributable to uncertainties in the fitting viz., [0001] $H_{1V} = 0.594 \pm .003$ eV, $[10\bar{1}0]$ $H_{1V} = 0.48 \pm .02$ eV.

7.4.1: Pre-Vacancy Region

The pre-vacancy slopes deduced in this study bear a relationship similar to slopes deduced in a recent study [157]. In this latter work an analysis technique was employed in which the assumed linear response to temperature of the free positron was isolated from the vacancy effect. Despite the fact that the resultant temperature dependences of the lineshape parameter show departures from linearity in the pre-vacancy region, a linear relationship was fitted to these generated data, whence the relationship $\beta[11\bar{2}0] = 2.1 \times \beta[0001]$ was derived. Direct comparisons between these values and those obtained here is further obstructed by the non-uniqueness of the lineshape parameter definition and by the lack of identity of the relevant basal plane orientations. A further impediment to such a comparison is the restricted temperature range over which the reported study was conducted. The fact that annihilation spectra were not studied below a temperature of 183K may have increased the uncertainty associated with the deduced slopes. Nevertheless, in essence, the data from these two studies are in agreement as to the directionally dependent nature of the pre-vacancy rise.

It was suggested, for cadmium, that a possible contributory cause of the apparent reversal of the pre-vacancy rise with respect to the thermal expansion co-efficients was the anisotropy of the phonon spectrum. The axial ratio of zinc is less extreme than that of cadmium, c/a(Zn) = 1.851 cf c/a(Cd) = 1.886, nevertheless, similar anisotropies of lattice dynamics are exhibited by zinc [150,158]. In this case however, the reversal of the thermal expansion and pre-vacancy slope relationships is even more striking viz. α(c-axis)=0.61X10^{-4} K^{-1}, α(a-axis)=0.14X10^{-4} K^{-1} whereas we had β (c-axis)=0.60X10^{-4} K^{-1}, β [10$\bar{1}$0]=1.02X10^{-4} K^{-1}. It seems unlikely on the present understanding of the effect of lattice vibrations on the lineshape parameter, that the directional dependence of the pre-vacancy region could be imputed to the reported [150,158] anisotropies of the phonon spectra alone.

7.4.2: Vacancy Parameters

As in the case of cadmium, reported values of the monovacancy formation enthalpy cover a wide range. Quenching experiments yield H_{1V} = 0.45 eV [159] whereas several values have been reported as resulting from macroscopic and lattice thermal expansion viz. H_{1V} = 0.50 eV [160], H_{1V} = 0.44 eV [161], H_{1V} = 0.52 eV [162] and H_{1V} = 0.53 eV [163]. Early positron annihilation experiments yielded H_{1V} = 0.54 eV [44]. The angular

correlation data from this same study was later reanalysed, initially to produce H_{IV} = Ø.56 eV [164]and later H_{IV} = Ø.48 eV [112], the latter result being the product of characteristic temperature considerations. A value of H_{IV} = Ø.42 eV was deduced from Doppler broadening experiments [116].

While the initial value derived from angular correlation experiments appears to agree reasonably well with other reported values, the study whence it was deduced was not extended below room temperature and, as a result, no account of the pre-vacancy behaviour was taken. The limited temperature range encompassed might explain the variation in the values eventually deduced from this study.

The disagreement between the two deduced monovacancy formation enthalpies in this study is striking, tables 7.1 and 7.2 . No such disagreement between the two directions of cadmium was obvious, nor was there any in the values deduced from a similar orientational study of zinc [157]. The values obtained in the latter work were $H_{IV}[ØØØ1]$=Ø.51±.Ø2 eV and $H_{IV}[11\bar{2}Ø]$=Ø.5Ø±.Ø2 eV. In the same study, a value deduced from positron lifetime data was presented as H_{IV} = Ø.51 ± .Ø1 eV. These values were deduced from studies which extended from 183K to 568K. Those of the present study were collected from 4.2K to 6ØØK. As has previously been mentioned, the application of the trapping model to data which are incomplete in temperature regions which bear sensitively on the value of the deduced

parameters can lead to confusion.

A characteristic temperature analysis technique (section 4.3.2) was also applied to the Doppler broadening data [157] and, here, a slight difference between the two deduced values was observed, viz.: [ØØØ1] (T_t=389K), H_{IV}=Ø.52±.Ø6 eV; [11$\bar{2}$Ø] (T_t=375K), H_{IV}=Ø.47±.Ø6 eV. The application of this analysis technique to the present zinc data produces, for the [1Ø$\bar{1}$Ø] direction a value similar to that deduced from the trapping model analysis, H_{IV}=Ø.49±.Ø5 eV(T_t=385K). However the corresponding value obtained for the hexagonal axis is H_{IV} = Ø.51±.Ø5 eV(T_t=4Ø5K), very different from that deduced by means of the more conventional technique and in closer agreement with that for the [1Ø$\bar{1}$Ø] direction.

Perhaps the most striking aspect of this is that while the characteristic temperature produces essentially similar values, those deduced from the trapping model bear no such similarity. In an effort to investigate this anomaly, further measurements of the Doppler broadened lineshape were made for both directions of this specimen of single crystal zinc. These measurements were restricted to the temperature region from 292K to 6ØØK and took place under the same experimental conditions as for the previous measurements. The lineshape parameters thus obtained after background subtraction were normalised to the earlier cryostat measurements in the appropriate temperature region and the resultant temperature dependence of the lineshape

parameter analysed by means of the three models previously employed.

Again it was found that optimum fits were achieved by means of the "linear-rise" model with $\chi=0$. The values derived from these fits are presented in table 7.3 . It can be seen that the data arising from these later studies produce monovacancy formation enthalpies consistent with those earlier deduced and therefore indicate that the disparity between the derived enthalpies is an artefact of the interpretation of the trapping model. It is believed that this disagreement is attributable to the inadequacy of the currently employed trapping model to predict the directional dependence of the pre-vacancy rise.

In an attempt to identify the origin of this present anomaly, the data arising from the later study of the [0001] direction of single crystal zinc were analysed by means of a constrained model similar to that discussed in section 6.5 . Here a constant value of $H_{1V}=0.51eV$ (i.e. that obtained for the $[10\bar{1}0]$ direction was employed). The value of the reduced chi-squared obtained was 2.007 c.f. 1.597 for the corresponding unconstrained fit. The values obtained for the fitting parameters were:

$$H_{1V}=0.51=\text{constant}$$

$$A\times10^{-5}=2.59\pm0.10$$

$$\beta\times10^{4}\,(K^{-1})=0.52\pm.04$$

Temperature range of fitting (K)	149-598 (56)	147-600 (56)
H_{IV} (eV)	0.62±.01	0.53±.01
$A \times 10^{-5}$	37.86±4.42	5.57±3.00
$\beta \times 10^{4}$ (K^{-1})	0.63±.03	1.03±.04
S_{IV} (k)	4.5	2.6
$C_{IV}(T_m) \times 10^{4}$	29.7	18.2
SSQ/N	1.484	2.188
Chi-squared	1.628	2.450

Table 7.3: Fitting parameters derived from later "linear-rise" model study of single crystal zinc.

Inspection of the above values and those of table 7.3 shows that as a result of fixing H_{IV}, the nature of the fit in the pre-vacancy region is affected. A comparison of these two fits reveals that the residuals between fit and data in the vacancy region are of similar magnitude. The increased values reflected in the reduced chi-squared for the constrained fit are therefore seen as originating from the pre-vacancy region.Thus the effect of an assumed thermodynamic monovacancy formation enthalpy is to degrade the agreement between the data and the "linear-rise" model in the pre-vacancy region. If such a degradation is accepted, the difference in the magnitude of the pre-vacancy slopes is enhanced.

A more recent orientational study [167] of single crystal zinc in which measurements were extended to temperatures close to the melting point is interesting in respect of the results arising from the application of the "linear-rise" model. The initial analysis followed in this latter work utilised equation 6.1 . Distinct monovacancy formation enthalpy values arose for the [ØØØ1] and [1Ø$\bar{1}$Ø] directions from the application of the trapping model however, the characteristic temperature technique yielded a thermodynamic value of H_{IV}=Ø.52 eV when applied to these same data. A further trapping model analysis of this work, this time by means of equation 3.38 again yielded a thermodynamic monovacancy formation enthalpy, however the value obtained on this occasion was H_{IV}=Ø.6Ø eV.

The extension of measurements to temperatures close to the melting point is here seen to result in the significantly increased facility of the least squares minimisation routine to identify a high temperature slope, χ. On the inclusion of such a vacancy parameter temperature dependence in the fitting procedure, in the case of this latter work [167], the orientation dependence of the monovacancy formation enthalpy is seen to be resolved. Accordingly, it is thought that the lack of agreement between the monovacancy formation enthalpy values obtained in this present work is, at least in part, a result of the absence of measurements at temperatures in excess of 600K.

7.5: CONVOLUTION ANALYSIS

7.5.1: Inverted Parabola plus Gaussian Model

In addition to the lineshape parameter analysis of the previous section each of the positron annihilation spectra arising from this study was analysed by means of the convolution technique discussed in section 5.3.1 . The results obtained for the Gaussian width and parabola width of the [0001] direction of single crystal zinc are presented as functions of temperature in figures 7.3 and 7.4 respectively. Those resulting from the study of the $[10\bar{1}0]$ direction are presented in figures 7.5 and 7.6 respectively.

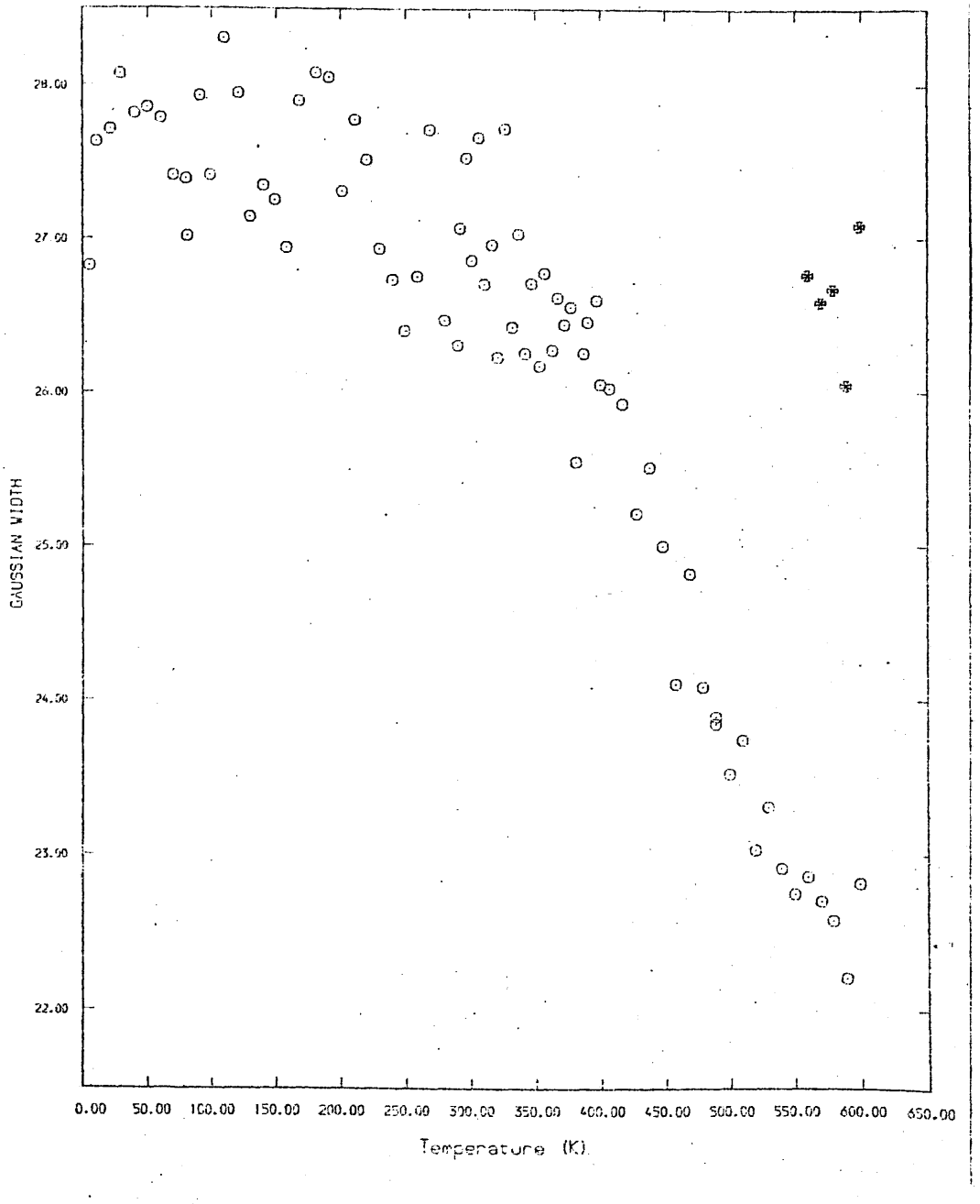

Figure 7.3: The temperature variation of the GAUSSIAN WIDTH for the [0001] direction of single crystal zinc.

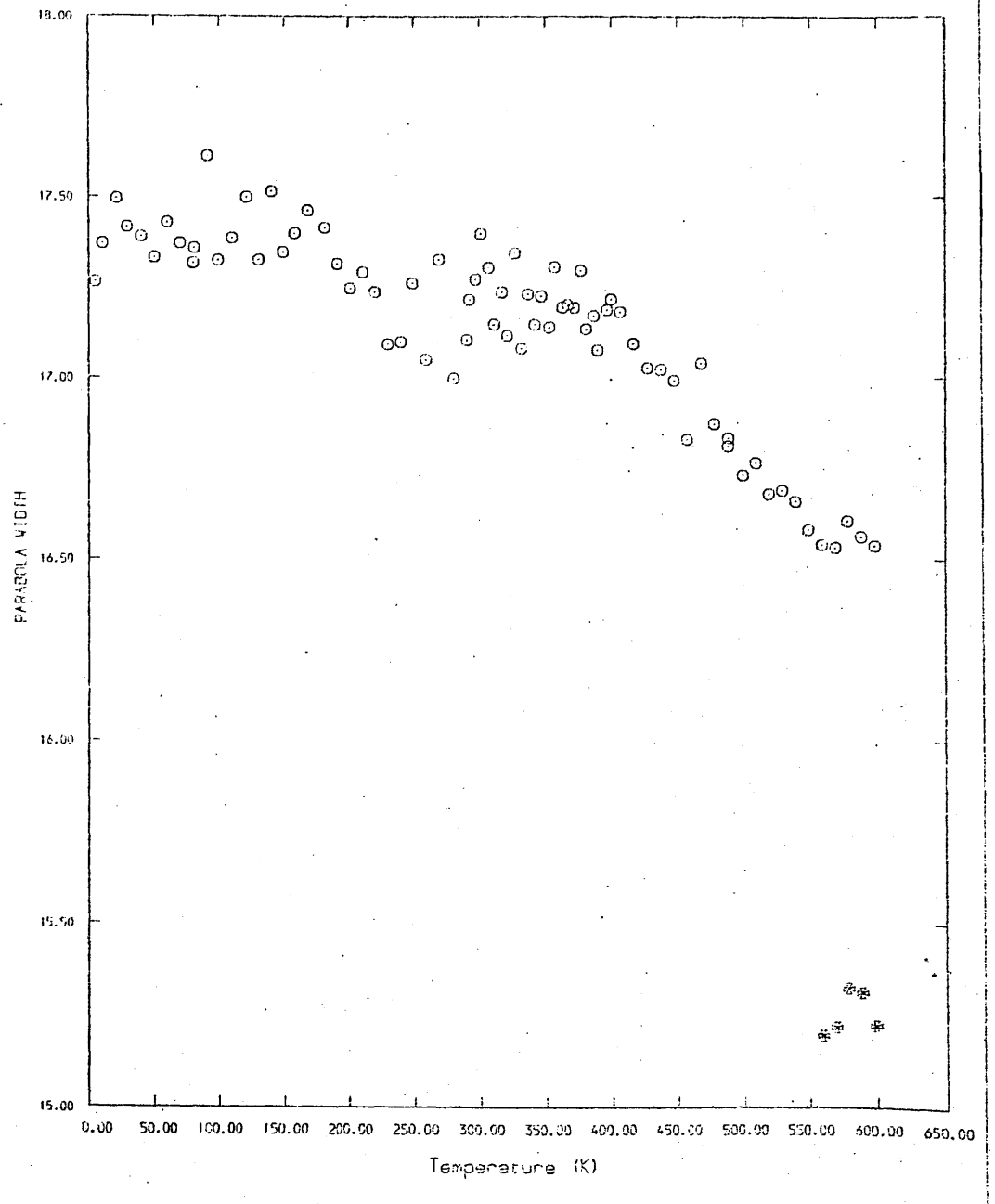

Figure 7.4: The temperature variation of the PARABOLA WIDTH for the [0001] direction of single crystal zinc.

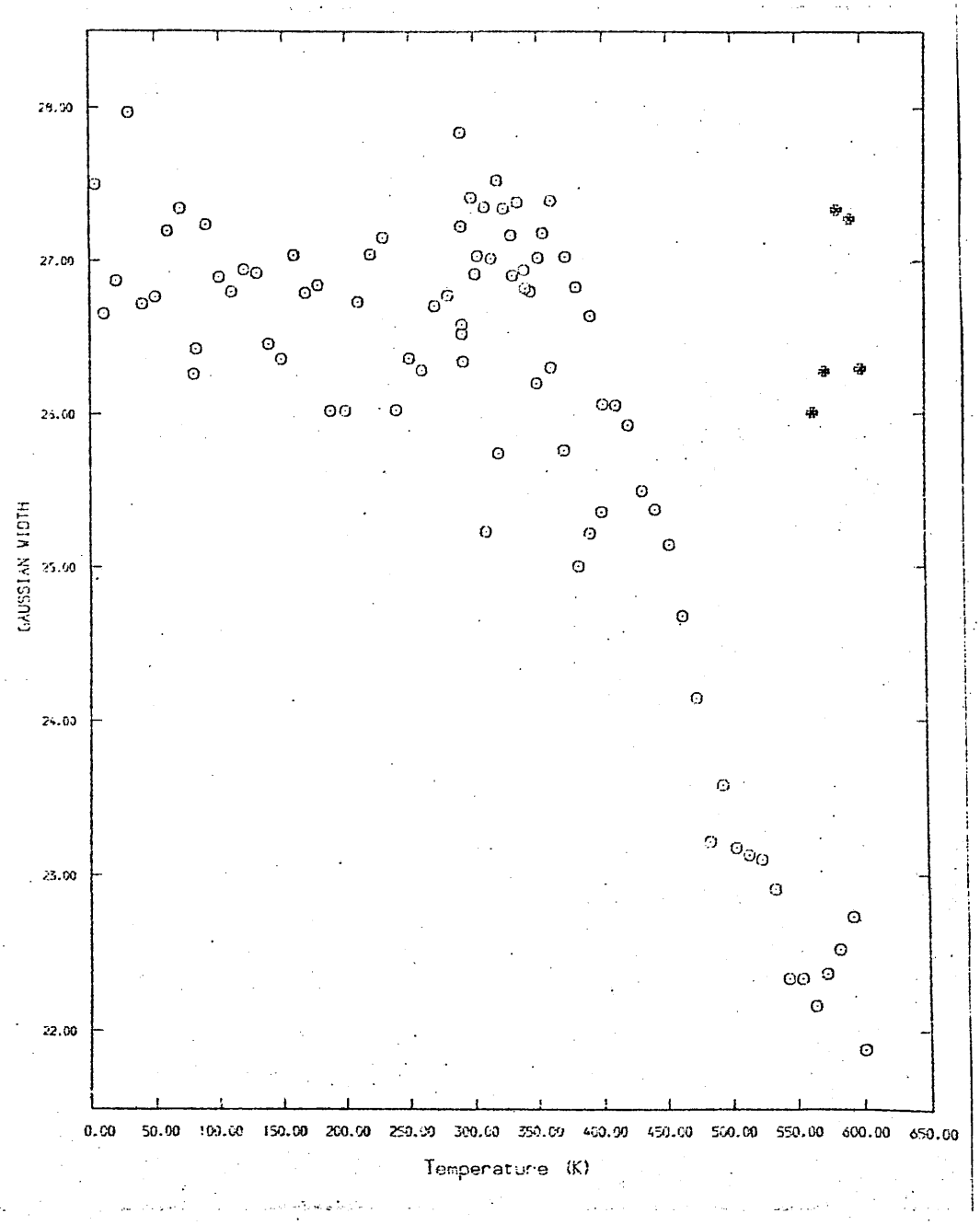

Figure 7.5: The temperature variation of the GAUSSIAN WIDTH for the [10$\bar{1}$0] direction of single crystal zinc.

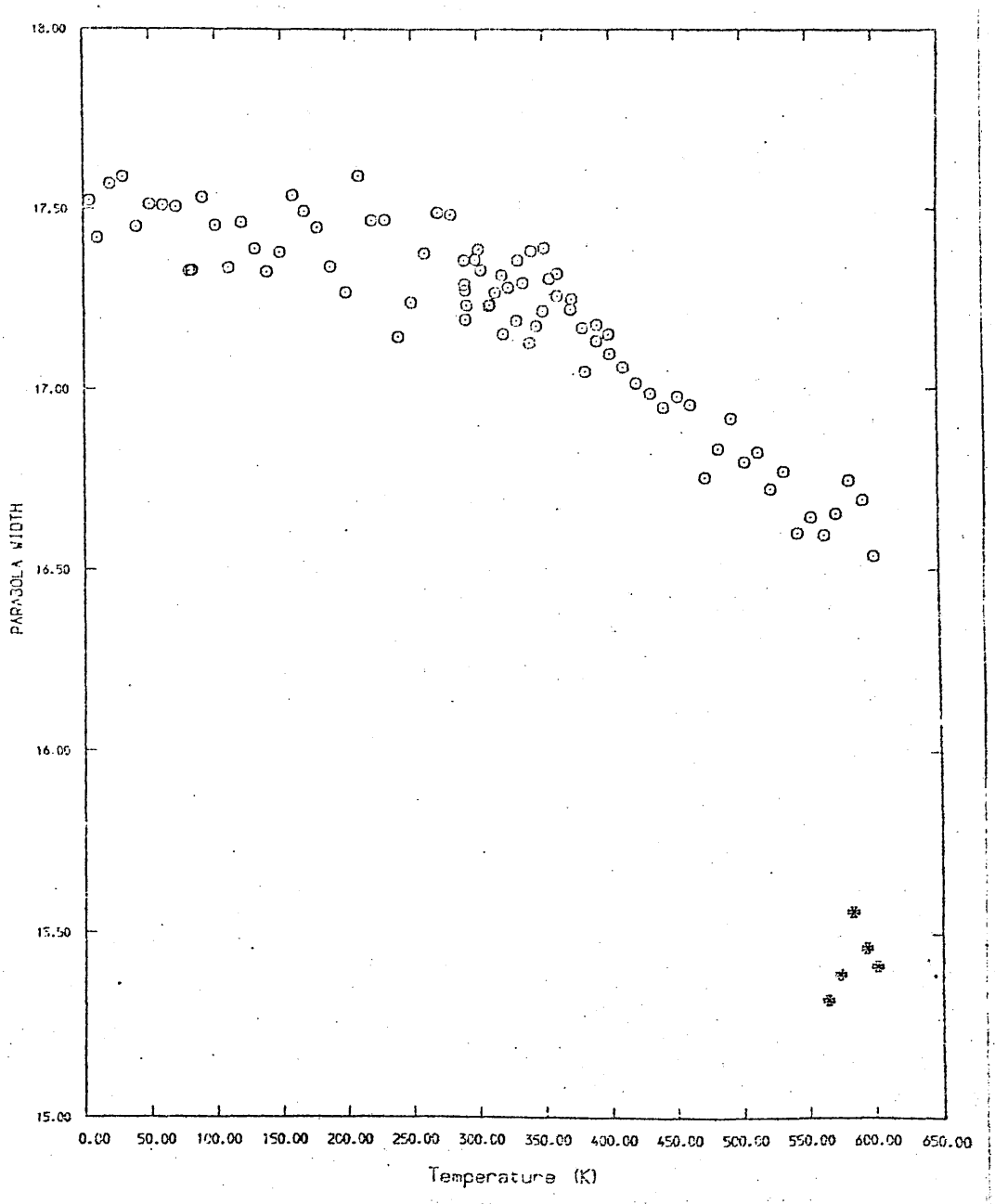

Figure 7.6: The temperature variation of the PARABOLA WIDTH for the [10$\bar{1}$0] direction of single crystal zinc.

As in the cadmium study, the temperature at which vacancy effects are first noticeable in the temperature dependence of the lineshape parameter is taken as being a convenient reference point for the interpretation of changes in the Gaussian and parabola widths. This measuring point is taken to be 400K although it would appear from the relevant figures(7.3 to 7.6) that the break occurs at ~ 380K for the $[10\bar{1}0]$ direction and at ~ 400K for the hexagonal axis. This break is characterised by the onset of a negative temperature dependence much stronger than that exhibited at lower temperatures.

For both orientations, figures 7.3 and 7.5, the reduction in Gaussian width over the temperature region below 400K is approximately one third of that observed between 400K and 600K. The parabola width for both crystallographic directions exhibits a weaker temperature dependence than that of the Gaussian, figures 7.4 and 7.6 respectively. Here also however, the negative temperature dependence is much stronger at temperatures above 400K. The average parabola width at low temperatures is 17.5 channels the same value resulting from both orientations. This width corresponds to a Fermi energy of 10.53 eV which is in reasonable agreement with the accepted value of 9.47 eV.

The percentage contribution of the parabola to the total area under the annihilation line is shown as a function of temperature for the [0001] direction in figure 7.7 and for the $[10\bar{1}0]$ direction in figure 7.8 . The

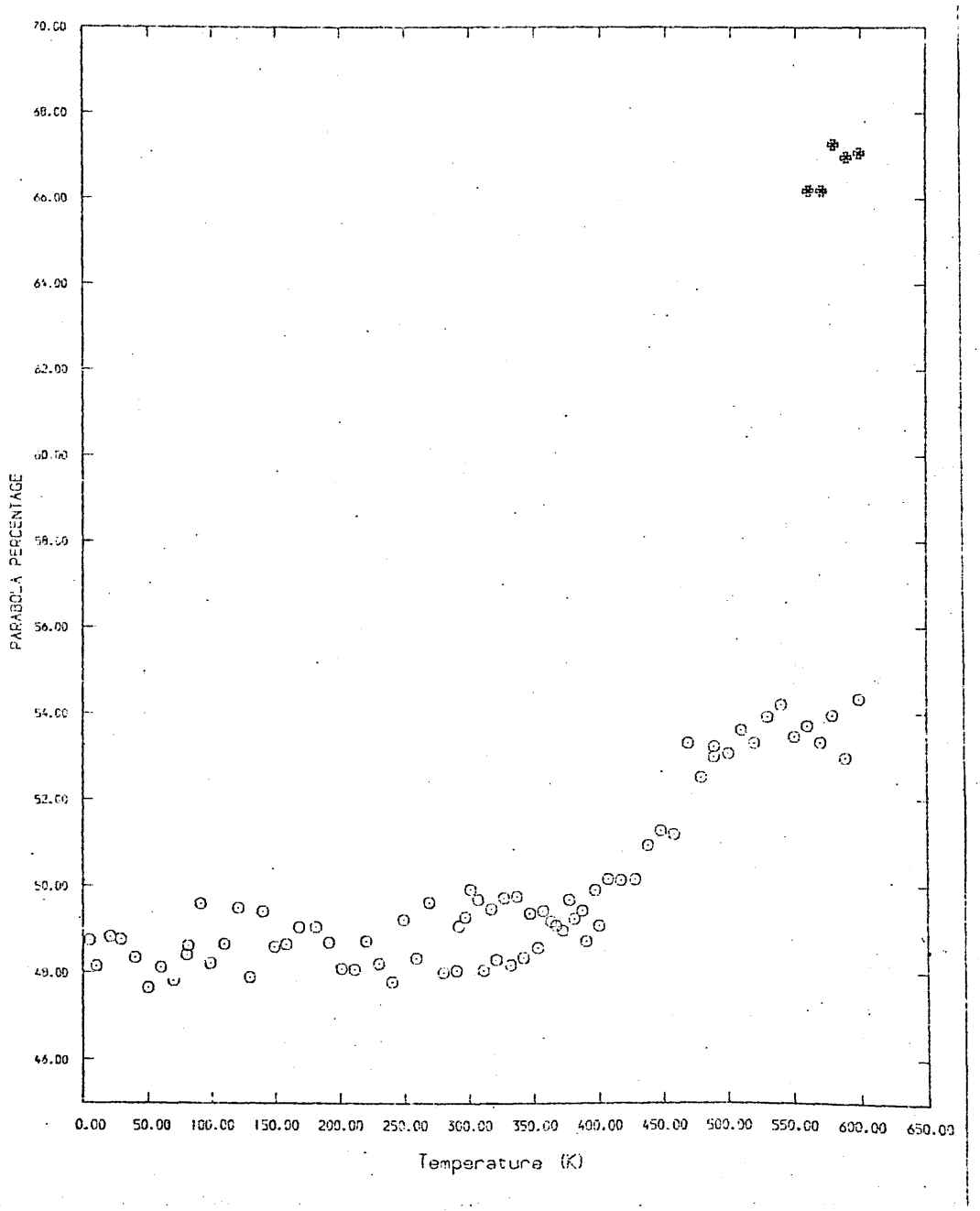

Figure 7.7: The temperature variation of the PARABOLA PERCENTAGE for the 0001 direction of single crystal zinc.

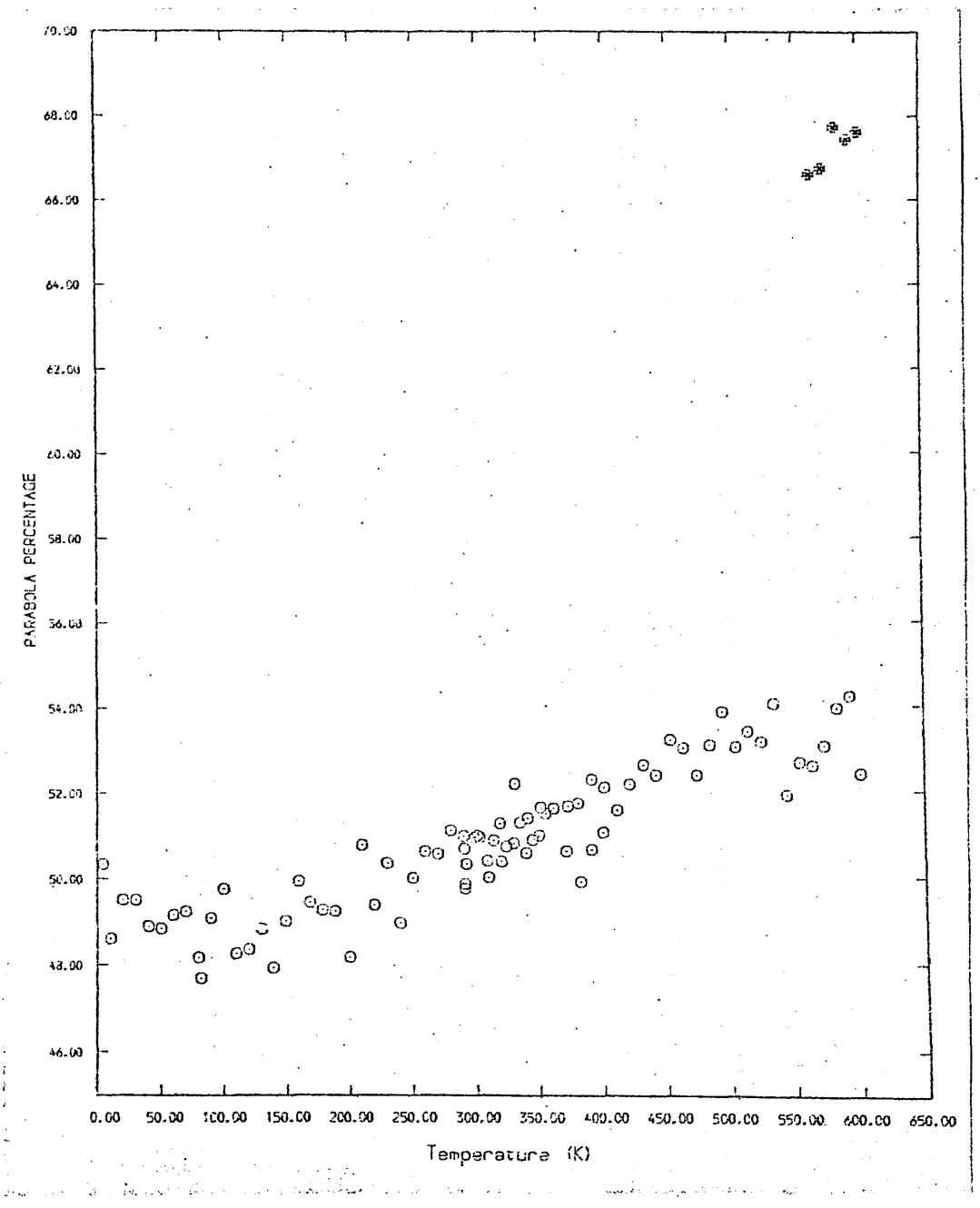

Figure 7.8: The temperature variation of the PARABOLA PERCENTAGE for the [1$\bar{1}$0] direction of single crystal zinc.

relationship between the parabola percentage and temperature for the [ØØØ1] direction is very similar to that for the F-parameter. The parabola percentage increases from a value of approximately 48 % at 4.2K to 56 % at 6ØØK. For the [1Ø$\bar{1}$Ø] direction the parabola percentage behaviour is less similar to that of the corresponding F-parameter. However, on the basis of this graph, the parabola percentage increases from approximately 49 % at 4.2K to 55 % at 6ØØK. The nature of the values derived from such a convolution study makes dangerous the extraction of any definite conclusions, however, the differences between the temperature dependences of the parabola percentage for the two directions may be significant. Such conclusions cannot be drawn on these results. The inclusion of a positron broadening function in the convolution procedure may reveal more definite indications regarding the conduction electron participation.

7.5.2: Zero point Motion Analysis

Again exigencies of time prevented the application of the zero-point motion analysis technique to all of the collected spectra. Sample spectra from the low, pre-vacancy and high temperature regions for both orientations were however investigated by means of this technique. In figures 7.7 and 7.8, the new values of parabola percentage corresponding to the minimum values of chi-squared versus $\bar{\sigma}$,

are marked by a plotting character distinct from that used for the earlier results (which correspond to σ=Ø). The values of the Gaussian and parabola widths corresponding to these optimum zero-point motion fits are also included where appropriate in figures 7.3 to 7.6 . Again, these points are marked by means of a different character to that used for the σ=Ø points.

For the [ØØØ1] direction the results indicate that the parabola percentage increases from 48 % at low temperatures to 67 % at high temperatures while for the [1Ø$\bar{1}$Ø] direction sample-B between the same temperatures, the parabola percentage varies from 49 % to 67 %. Both of the studies indicate similar positron zero-point broadenings corresponding to a minimum in chi-squared at σ = 5 in the temperature region 56ØK to 6ØØK. Had a study been made of spectra corresponding to higher temperatures, a higher optimum value of σ might have resulted. An example of the variation of chi-squared with σ , for this temperature region for each of the two studies of single crystal zinc, is shown in figure 7.9 . A similar agreement was observed for the low temperature (~25K) points studied, examples of which are illustrated in figure 7.1Ø . At these temperatures, the relationships indicate that σ=Ø provides the optimum fit to the data and thus are in accordance with the earlier observations for single crystal cadmium.

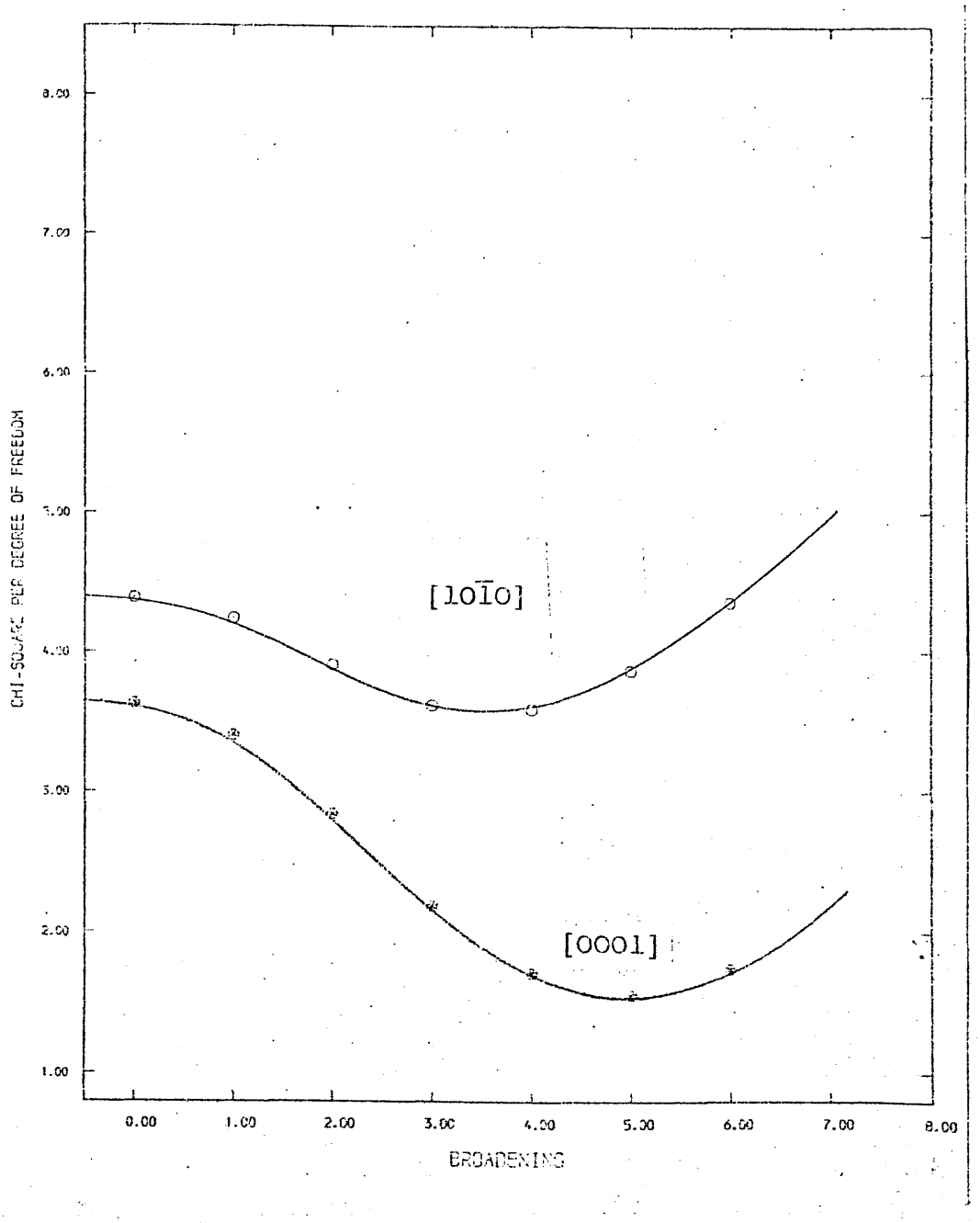

Figure 7.9: The variation of CHI-SQUARED with positron GAUSSIAN WIDTH for the high temperature region of the two studies of single crystal zinc.

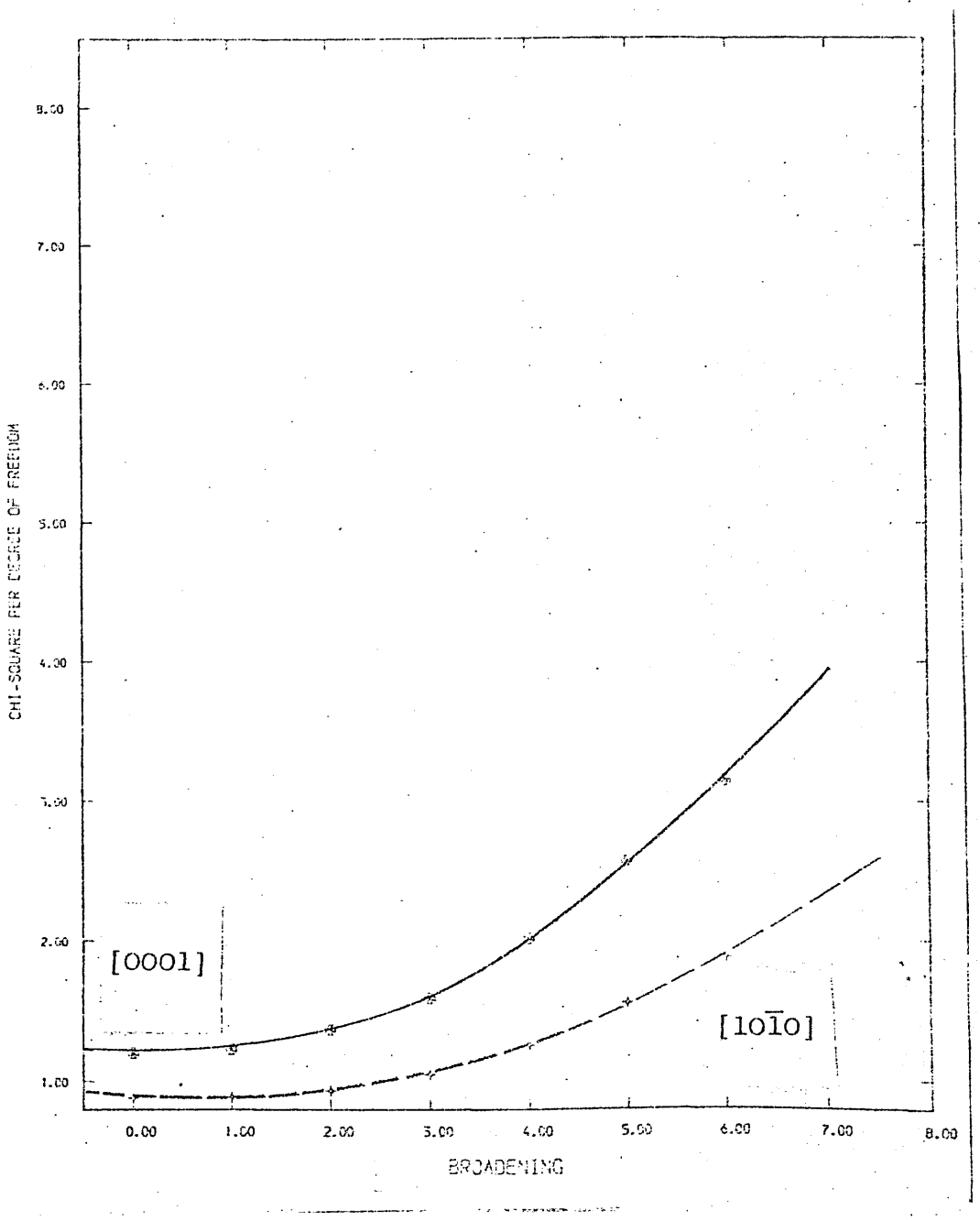

Figure 7.10: The variation of CHI-SQUARED with positron GAUSSIAN WIDTH for the low temperature region of the two studies of single crystal zinc.

As was found for single crystal cadmium, the individual spectra studied in the pre-vacancy region (~350K) of single crystal zinc, did not yield an unique optimum value of σ . However, as for single crystal cadmium, the evidence points towards there being more pre-vacancy positron localisation in the $[10\bar{1}0]$ direction of single crystal zinc than in the hexagonal axis. However, the crudity of the model as applied to the pre-vacancy region does not facilitate the drawing of definite conclusions in this matter. Again, because of the variation of optimum positron broadening function widths obtained, an average chi-squared versus relationship was computed for each of the orientations of single crystal zinc. These are illustrated in figure 7.11 . As can be seen from this figure, the minima in the reduced chi-squared versus σ relationships are not particularly well defined.

Application of the parameterisation technique employed in section 6.7.2 to these, yield for the [0001] direction the change in σ which separates the optimum value of σ from the width at which the chi-squared value has increased from its minimum by 30 % $\Delta\sigma$=2.1 . For the $[10\bar{1}0]$ direction the corresponding value is $\Delta\sigma$=2.1 .

In the case of single crystal cadmium, the $[10\bar{1}0]$ direction yielded a $\Delta\sigma$ generally smaller than that for the hexagonal axis. In the case of single crystal zinc, similar values result from this analysis while, on the basis of the pre-vacancy relationships derived for the two metals, it

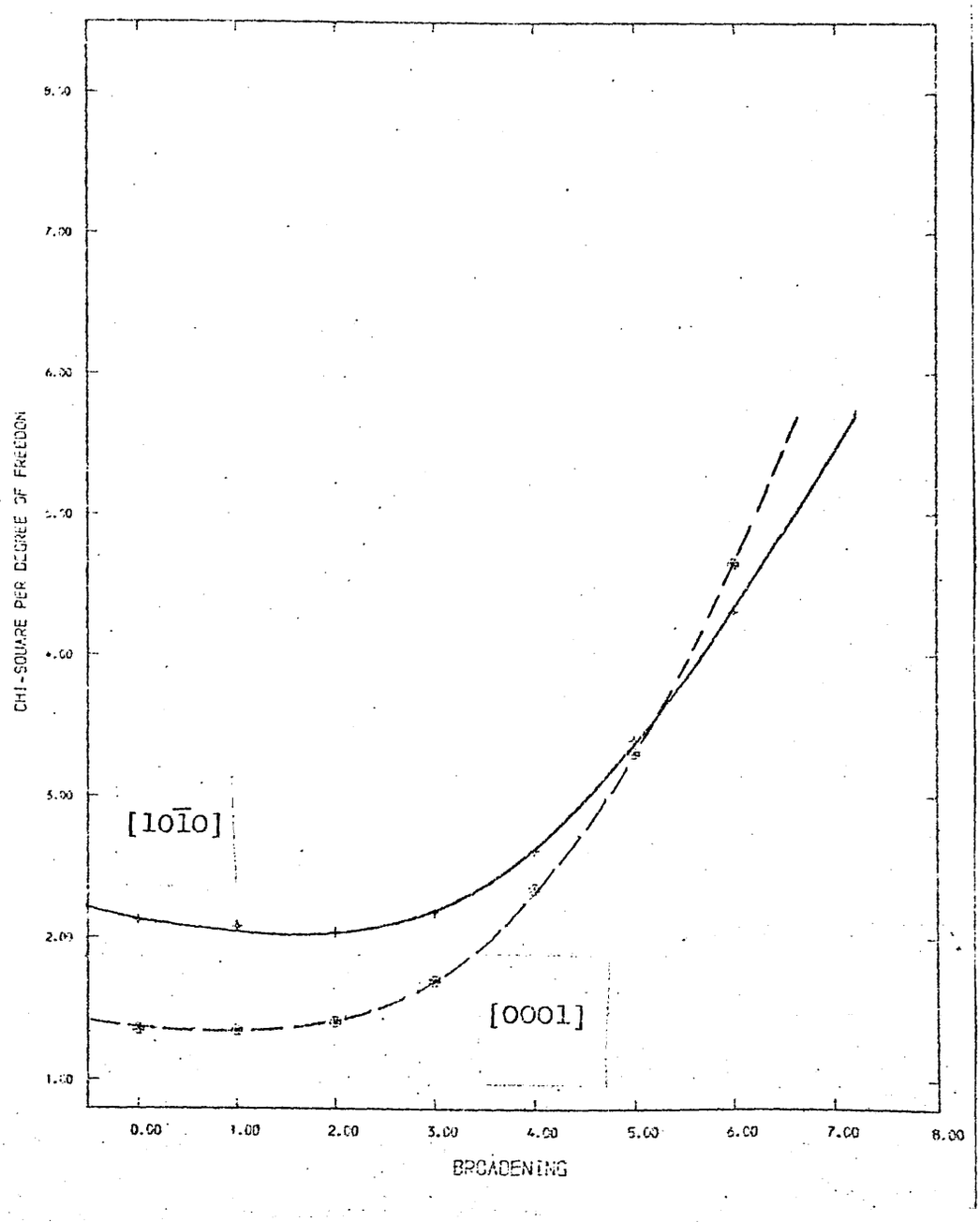

Figure 7.11: The variation of CHI-SQUARED with positron GAUSSIAN WIDTH for the pre-vacancy region of the two studies of single crystal zinc.

might have been expected that qualitatively similar findings would result for the two metals. This evidence is perhaps more indicative of the crudity of the application of integer steps in $\bar{\sigma}$ to the pre-vacancy region than of distinctions between the pre-vacancy behaviour of the h.c.p. metals zinc and cadmium.

CHAPTER 8: POSITRON ANNIHILATION IN POLYCRYSTALLINE CADMIUM

8.1: INTRODUCTION

Following the work on deformed specimens of polycrystalline cadmium contained in [139,133] and the work of [165], it was decided to embark upon a new investigation of the effect of room temperature and low temperature deformations on the positron annihilation lineshape parameter of this material.

8.2: EXPERIMENTAL DESCRIPTION

Two discs having diameter 8 mm and thickness 4.5 mm were cut from a rod of 99.9999% (6N) purity polycrystalline cadmium supplied by Koch-Light Laboratories Ltd. The discs were then compressed in a hydraulic press to produce a resultant average diameter of 11.Ø mm and thickness 2.2 mm. The specimens were then annealed for 24 hours at a temperature of 5ØØK under a pressure of less than $1Ø^{-6}$ torr. On removal from the vacuum furnace, the discs were then chemically polished in 35% nitric acid after which process they were thoroughly rinsed in de-ionised water.

Approximately 150 microcuries of carrier-free ^{22}Nacl in acqueous solution was then deposited and evaporated onto the centre of one of the specimen slices, such that the diameter of the source was no greater than 4 mm. A specimen-source sandwich was constructed and then encapsulated in a wrapping of thin aluminium foil. The specimen-source sandwich was returned to the hydraulic press and the thickness reduced by approximately 21 % under room temperature conditions. The specimen was then mounted on the low temperature cryostat. The cryostat was then evacuated and the dewars filled with liquid nitrogen. The sample was allowed to pre-cool to 77K and, on the transferral of liquid helium to the inner dewar, the sample was cooled to 4.2K .

Annihilation spectra were recorded at temperature increments of approximately 10K between 4.2K and 409K . For each measurement, the specimen temperature stability was better than $\pm$0.1K. After completion of this series of measurements, the specimen temperature was maintained at 409K for 18 hours in order to allow annealing to take place. During this period, several annihilation spectra were recorded.

The specimen temperature was then allowed to decrease slowly (< 1K per minute) in order to allow for the recording of the lineshape parameter temperature variation for the annealed case. Annihilation spectra were recorded at temperature increments of approximately 15K between 4.2K

and 409K . On completion of this second cycle of measurements, the specimen temperature was again slowly reduced to approximately 77K and several annihilation spectra recorded. The differences observed between the lineshape parameters calculated at the beginning and end of this measurement cycle were within statistical limits (2σ). This suggests that no further annealing took place during the second cycle and that this is representative of the annealed metal.

The specimen was then removed from the cryostat, immersed in a bath of liquid nitrogen and mounted on the hydraulic press. The specimen was then subjected to a thickness reduction of approximately 34 % before being transferred to the cryostat. Care was taken at all times during the liquid nitrogen temperature deformation and subsequent removal, to ensure that the specimen was fully submerged in liquid nitrogen. The cryostat was then sealed and replaced in the dewar assembly. The cryostat was evacuated and the sample temperature allowed to drop to 4.2 K. From the time that the specimen was mounted on the cryostat, its temperature was monitored by means of a thermocouple. Over the duration of the process, approximately one hour, the highest value attained by the specimen temperature was 100K .

Annihilation spectra were recorded at temperature increments of approximately 10K over the temperature range from 4.2K and 410K . Again at each point, the specimen temperature stability was better than $\pm$ 0.1 K. On five occasions during this measurement cycle from 4.2K to 410K, the specimen heater was disconnected and the specimen cooled to temperatures close to 80K at which temperatures a minimum of two annihilation spectra were recorded. The temperatures from which this cooling took place were 101K, 158K, 219K, 274K and 348K.

On completion of the liquid nitrogen temperature deformation cycle, the specimen was removed from the low temperature cryostat and mounted in the vacuum furnace. A series of ten annihilation spectra were then recorded over a period of 22 hours after which time the specimen temperature was raised to 503K . This temperature was maintained for 18 hours during which time a further eight spectra were recorded. No significant variation with time was observed in either of the two sets of spectra, a finding which suggests that the effects of the liquid nitrogen temperature deformation had been completely annealed out. The sample temperature was then slowly reduced to 292K and annihilation spectra recorded at temperature increments of approximately 10K between 292K and 592K . It was observed that the value of the lineshape parameters obtained subsequent to the 503K anneal were in good agreement with those obtained on commencement of the furnace measurement cycle and accordingly it is assumed that the annealing was indeed

complete.

Throughout these measurements, each spectrum was collected simultaneously with a ^{103}Ru reference peak at a total counting rate of 5000 cps. Over the two-hour counting period used at each temperature, the 511keV spectrum contained approximately 850,000 counts. The width of the central region chosen to define the F-parameter was 15 channels where each channel, as determined from the calibration of the spectrometer, represents an energy of 0.0938 eV.

8.3: LINESHAPE PARAMETER ANALYSIS

Initially, all the data arising from this study were background subtracted by means of the technique described in chapters 6 and 7. It was found however, in this case, that the benefits of such a subtraction were outweighed by enhanced fluctuations in the background subtracted F-parameter attendant on worsening statistics. Accordingly it was decided to employ non-background subtracted data throughout this study. As before the width of the central region chosen to define the F-parameter was 15 channels. The energy dispersion as obtained from the calibration of the spectrometer was 0.0943 keV per channel.

8.3.1: Annealed Polycrystalline Cadmium

The temperature variation of the lineshape parameter for the annealed specimen is shown in figure 8.1 . Average statistical errors (2σ), as defined in section 5.2.2, associated with these F-parameter values are 0.0011 .

In common with earlier reports,[140,168,149], the low temperature behaviour of the lineshape parameter for polycrystalline cadmium is distinct from that of single crystal specimens in respect of its negative temperature dependence at temperatures below 50K. This phenomenon was initially interpreted [169] as thermal detrapping from grain boundaries. However, other possible explanations are the temperature dependence of the trapping rate [132] or indirect positron trapping into deep traps, i.e. vacancies, via contiguous grain boundaries from which thermal detrapping can occur [168].

The lineshape parameter data from this study were analysed in terms of three proposed temperature dependences viz.:

(a) the "linear-rise" model with $\gamma=0$, equation 6.1,

(b) the "self-trapping" model, equation 3.38 and

(c) a two-trap model given by

$$F = \frac{F_o+F_dA_d \exp(-H_d/kT)+F_{1v}A_{1v} \exp(-H_{1v}/kT)}{1+A_d \exp(-H_d/kT)+A_{1v} \exp(-H_{1v}/kT)} \qquad 8.1$$

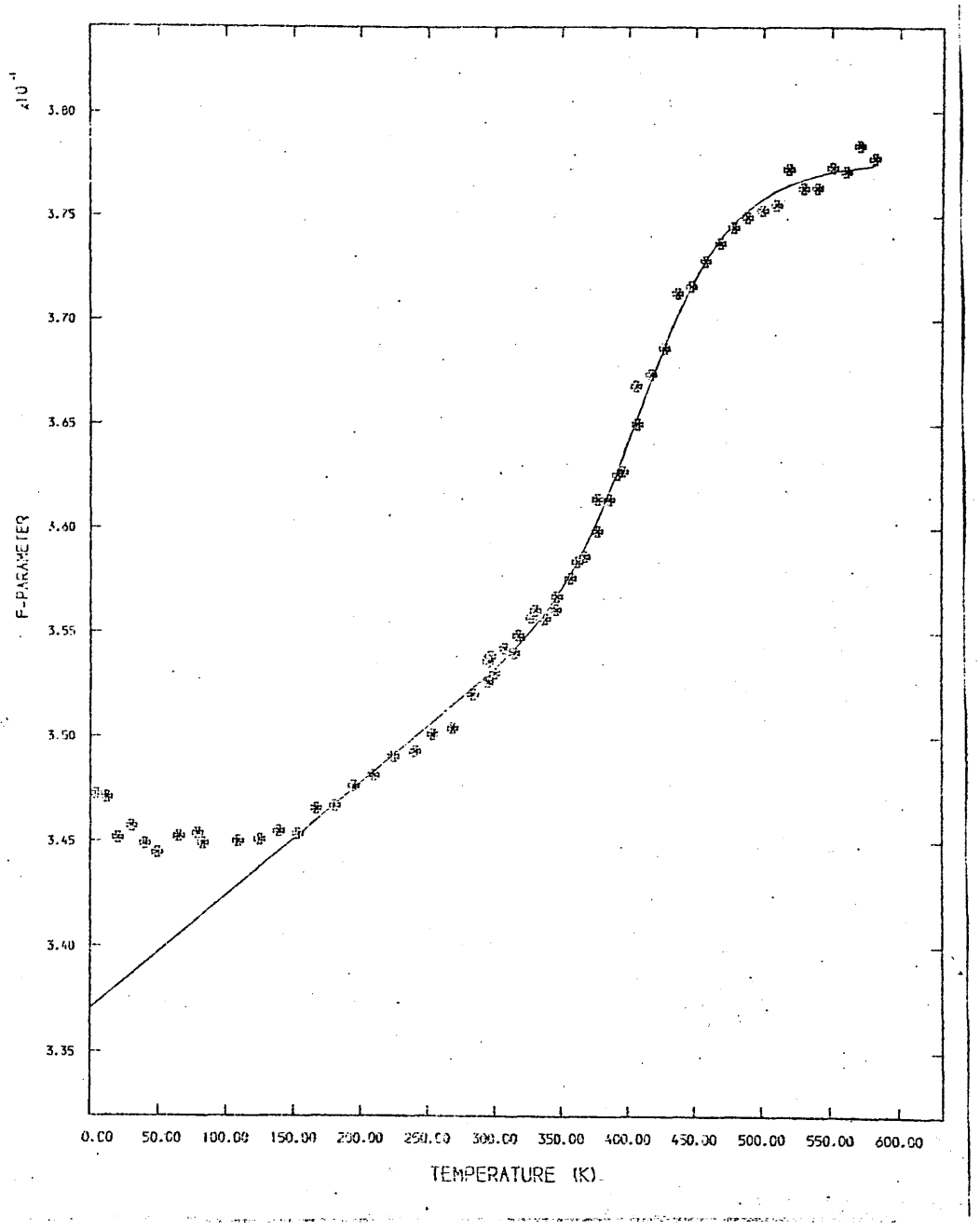

Figure 8.1: The temperature variation of the F-parameter for the annealed specimen of polycrtstalline cadmium.

where the terms F_D, A_D and H_D relate to positron pre-vacancy trapping. Each of the above models was fitted to the data by means of a least squares minimisation routine. In the case of model (a), the temperature region below 150K was excluded from the minimisation calculations. The optimum values of the fitting parameters are given in table 8.1.

As can be seen from the table, models (b) and (c) have associated values of the reduced chi-squared superior to that for the "linear-rise" model. However, the value of F_{St} associated with the self-trapping fit indicates that the trapping spaces of positron self-trapping are deeper than those of vacancy trapping. This is inconsistent with the interpretation of this localisation effect and, accordingly, it is concluded that this fit is not physically meaningful. While the value of chi-squred associated with the fit to equation 8.1 is superior to those of the other two models, it is not clear how this can be interpreted. Thus the interpretation of the pre-vacancy region in terms of the "linear-rise" model, despite the appearance of non-linearities in the temperature dependence of the lineshape parameter for polycrystalline cadmium seems, in this case, to provide the optimum fit to the data. Accordingly, the solid line shown on figure 8.1 is derived from this fit. However, the reservations expressed earlier concerning the "linear-rise" model interpretation of the pre-vacancy region in single crystal cadmium and zinc must also apply to polycrystalline cadmium.

	equation 6.1	equation 3.38	equation 8.1
Temperature range of fitting (K)	153-582 (49)	20-582 (58)	20-582 (58)
H_{IV}(eV)	0.47±.03	0.49±.02	0.53±.002
$A X 10^{-5}$	3.37±2.88	6.37±3.43	38.87±10.29
$\beta X 10^{4} (K^{-1})$	1.59±.06	---	---
Fx	---	0.433	0.371
$B X 10^{-5} (K^{-3/2})$	---	0.23±.12	---
$\mathcal{E}_o$(eV)	---	0.098±.004	0.079±.005
S_{IV}(k)	2.0	2.6	4.4
$C_{IV}(T_M) X 10^{4}$	7.3	9.3	24.8
SSQ/N	1.250	0.883	0.880
Chi-squared	1.393	1.004	1.001

Table 8.1: Polycrystalline cadmium: optimum values of fitting parameters.(x=st for equation 3.38 while for equation 8.1, x=d)

The magnitude of the pre-vacancy slope, β, as given by the "linear-rise" fit is $1.59X10^{-4}K^{-1}$. Average values of this slope obtained from the earlier single crystal studies are [0001] $\bar{\beta}=0.94X10^{-4}K^{-1}$, [10$\bar{1}$0] $\bar{\beta}=1.82X10^{-4}K^{-1}$. These latter values however were derived from background subtracted data unlike that of the present study. If non-background subtracted single crystal data are used, we have that: [0001] $\bar{\beta}=0.92X10^{-4}K^{-1}$, [10$\bar{1}$0] $\bar{\beta}=1.73X10^{-4}K^{-1}$. While normally it is not possible to make a direct comparison of slope values deduced from different studies, the approximate identity which exists between the lineshape parameter definitions used in these two studies and the identity of material allows for some comment. It can be seen that the pre-vacancy slope derived from the polycrystalline data is intermediate in value to those of the single crystal experiments. This is consistent with the expectation that, in the polycrystalline case, the random orientation of the crystallites will lead to the averaging of the observed characteristics.

The monovacancy formation enthalpy value deduced from the present data by means of the "linear-rise" model is $H_{1V}=0.47\pm.03$eV. This value can again be seen to be intermediate to the average values deduced from the earlier single crystal studies: [0001], $\bar{H}_{1V}=0.51\pm.02$eV from the "linear-rise" model and [10$\bar{1}$0], $\bar{H}_{1V}=0.45\pm.02$eV from the "self-trapping" model. Similar analysis treatments were applied to a polycrystalline cadmium specimen in an earlier

reported study [132] to yield, H_{IV}=Ø.56±.Ø2eV for the "linear-rise" model and H_{IV}=Ø.54±.Ø2eV for the "self-trapping" model. It is not clear whether the discrepancies between the results derived from these two polycrystalline studies can reasonably be attributed to differences in stock material and in specimen treatment.

8.3.2: Specimen Deformed at Liquid Nitrogen Temperature

The temperature variation of the lineshape parameter for the liquid nitrogen temperature deformed specimen is shown in figure 8.2 superimposed on those for the annealed and room temperature deformed specimens. The average statistical error (2σ), as defined in section 5.2.2, associated with these F-parameter values are Ø.ØØ11 .

In the temperature region extending from 4.2K to approximately 12ØK, the F-parameter shows no strong temperature dependence. The negative slope exhibited by the first "return" measurement (1ØlK-8ØK) indicates that no significant annealing has taken place up to this point. However, the limited temperature range here encompassed and the small change observed in the F-parameter do not provide sufficient evidence to endorse the apparent negative temperature dependence of the effective trapping rate exhibited by the active positron trap in this region.

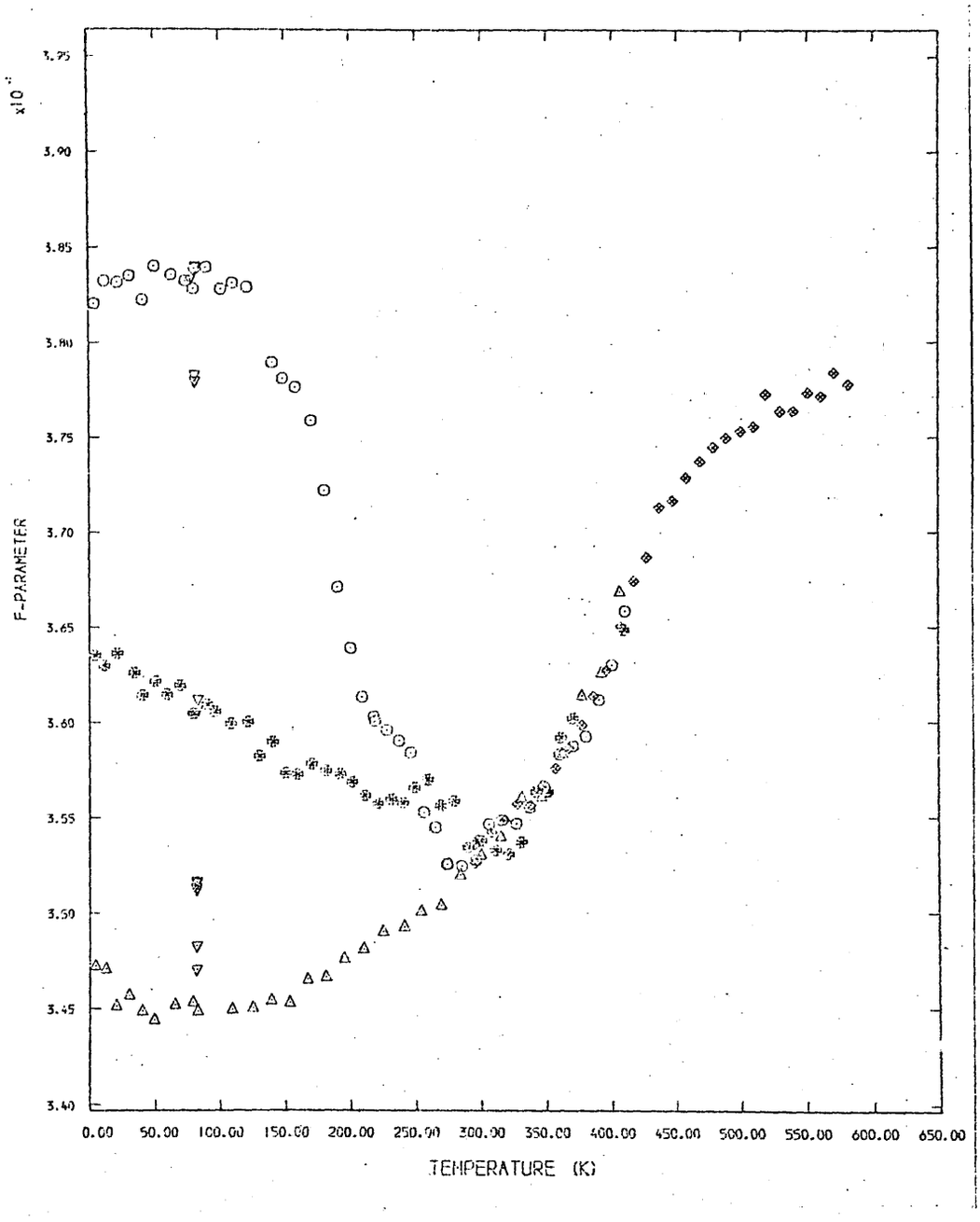

Figure 8.2: The temperature variation of the F-parameter for the specimens of polycrtstalline cadmium deformed at liquid nitrogen and room temperatures.

From 120K to approximately 160K, the F-parameter is seen to drop in a sharp fashion and, at the higher end of this temperature range, there is a suggestion of a "knee". A "return" measurement taken at 158K again reveals a possible negative temperature dependence. Here, the observed change in the value of the lineshape parameter is smaller than that exhibited by the earlier "return" measurement. This suggests that unless the temperature dependence of the effective trapping rate is very complex, the earlier measurement represents an over-estimate of the effect.

Over the temperature range extending from 160K to approximately 250K, the F-parameter value is seen to have a negative temperature dependence stronger that that previously observed and again, the existence of a "knee" is suggested, this time for $220<T<250K$. The negative temperature dependence revealed by the "return" measurement from 219K has a similar slope to that observed from 158K viz.: (158-81K) $\beta = 1.61 \times 10^{-4} K^{-1}$, (219-82K) $\beta = 1.65 \times 10^{-4} K^{-1}$. As the temperature is raised from 250K to approximately 300K, the F-parameter is seen to approach the annealed line and, at temperatures in excess of 300K, the temperature dependence exhibited agrees well with that of the annealed specimen. The reduction in the value of the F-parameter from 250K is less steep than that seen between 160K and 250K and, as evidenced by the "return" measurement from 274K, the sign of the apparent temperature dependence is reversed. A further "return" measurement, taken from 348K, indicates

that the low temperature behaviour of the specimen is now approaching that of the annealed sample.

In accordance with similar studies of the effect of plastic deformation at liquid nitrogen temperatures on the temperature dependence of the lineshape parameter in cadmium [139,165], the spectra arising from this investigation indicates that no significant annealing took place between 4.2K and 120K. There is however no more than fair agreement between the relevant temperature ranges in these three works. This is thought to reflect differences in stock material, handling and deformation treatment between the three studies. As was mentioned earlier, the magnitude of the apparent negative temperature dependence revealed by the first "return" measurement is thought to be an over-estimate. The observed increase in the F-parameter on reducing the specimen temperature from 101K to 80K is 0.0008 while two standard deviations in the parameter is 0.0011 .

From figure 8.2, it can be seen that the "knee" which occurs at 150K in the temperature dependence of the lineshape parameter for the liquid nitrogen temperature deformed specimen has an F-parameter value which is in very close agreement with that observed at 580K for the annealed specimen. This latter value is normally attributed to saturation trapping in monovacancies. The coincidence of F-parameter values here observed accordingly leads one to propose that the dominant process at 150K in this deformed

specimen is positron trapping at monovacancies and that the higher values of the F-parameter observed at lower temperatures are indicative of positron trapping in traps deeper than monovacancies e.g.vacancy clusters. A similar phenomenon was noticed in [165] for low temperature 10 % and 20 % compressions of polycrystalline specimens of cadmium. The temperature at which the onset of this behaviour was observed is, however, distinct from that of the present study viz.: annealing of this defect was suggested as commencing at 138K. It is thought that the disagreement over this onset temperature is a manifestation of differences in stock material and of specimen treatment.

The behaviour of the lineshape parameter over the temperature range 160K to 250K is similar to that exhibited for a similarly deformed cadmium specimen [132]. The agreement between the F-parameter at 150K and that at 580K previously mentioned is consistent with the interpretation of this effect as the migration of vacancy-like defects which, as the temperature appropaches 250K, permits positron trapping in shallower traps whose influence extends from 250K to 300K. A "return" measurement taken from 219K reveals an apparent negative temperature dependence similar in magnitude to that observed from 158K viz.: $1.65 \times 10^{-4} K^{-1}$ (219K to 82K) c.f. $1.61 \times 10^{-4} K^{-1}$ (158-81K). It appears that these two "return" measurement temperatures lie in the same, vacancy dominated, region of the temperature dependence and, when these two slopes are taken together, a possible negative temperature dependence of the

specific positron-vacancy trapping rate is suggested between 80K and 220K.

In the temperature range from 250K to approximately 300K, the F-parameter is seen to drop less sharply than previously and, at approximately 300K to join the annealed line. Thereafter the lineshape parameter behaves in a fashion similar to that of the annealed specimen. This behaviour is similar to that observed in [165] and is thought , in agreement with [165,170] to be the result of the re-arrangement of dislocations. The temperature dependence revealed by the "return" measurement from 274K is weakly positive and is thought to be an average of the temperature dependences intrinsic to the behaviour of the annealed specimen and of annihilation in dislocations .

8.3.3: Specimen Deformed at Room Temperature

The temperature variation of the lineshape parameter for the room temperature deformed specimen is shown in figure 8.2 together with those for the annealed and liquid nitrogen temperature deformed specimen. As before, the average statistical error (2σ), as defined in section 5.2.2, associated with each point is 0.0011 . The temperature dependence here obtained is distinct from that observed in [132]. However the deformation here employed (21 %) is considerably more severe than that of the earlier

work (7 %). Here the lineshape parameter shows a negative temperature dependence which appears to be effective from 4.2K to 310K at which temperature the deformed line joins the annealed line. It is particularly interesting to note that between 290K, at which temperature the specimen was deformed, and 4.2K, the F-parameter rises from 0.353 to 0.363.

The temperature dependence of the lineshape parameter for the room temperature deformed specimen over the temperature range 4.2K to 150K is reminiscent of that observed over the temperature range 100K to approximately 225K in [165] and attributed to thermal detrapping from grain boundaries for a deformed specimen of polycrystalline cadmium. This latter sample was compressed by 10 % at liquid nitrogen temperature and subsequently warmed to 360K. The increase observed in the F-parameter in the present work as the sample is cooled from 290K to 4.2K is however larger than that reported in [165]. It is thought that this additional increase in the F-parameter is here caused by a dislocation population which did not suffer significant re-arrangement over the three hours taken to reduce the specimen temperature from the deformation temperature (292K) to 200K and which forms the dominant trapping mechanisms from 150K to 310K. It is suggested however that as the temperature was raised beyond 200K, these dislocations do indeed begin to re-arrange themselves such that, at 310K the temperature dependence of the lineshape parameter joins that of the annealed line and , as the temperature is further

increased, the temperature dependence exhibited is similar to that of the annealed specimen.

These findings are however not in total agreement with [132,168]. In the latter work, the polycrystalline specimen was subjected to a 50 % compression at room temperature followed by annealing for 48 hours at 375K. The resultant low temperature lifetime spectra were found to yield a component whose lifetime corresponded to vacancy trapping and whose intensity was found to be negatively dependent on temperature principally over the temperature range 10K to 50K. It was suggested that this behaviour was the result of indirect trapping into vacancies via dislocations from which thermal detrapping occurred. In [132], for a 7 % compression at 290K, the lineshape parameter exhibited temperature independence bewteen 290K and 50K below which temperature a strong negative temperature dependence was observed, similar to but of greater magnitude than the low temperature effect observed in annealed polycrystalline specimens. This effect was interpreted by recourse to arguments similar to those of [168]. Both of these reports however differ from the present data and also from [165] in respect of the extent of the temperature ranges over which the low temperature effect persists. The conclusions of [132,165] are however in qualitative agreement with [168] as to the supposed role of indirect positron trapping via grain boundaries at low temperatures in polycrystalline specimens.

It is thought that the discrepancies which are apparent between the temperature ranges of this low temperature effect in [165,132,168] and the present work are the result of the variation in the deformation and annealing conditions of the three specimens and of different impurity concentrations. The temperature range is smallest in [168] in which the sample was annealed for 48 hours at 375K; a similar temperature range was reported in [132] after a less severe room temperature deform. In [165], a short time was spent at 360K, after which it was found that the low temperature effect extended over the range 100K to 225K. In the present work, while the temperature range of this effect is similar to that of [165], the magnitude of the change in the lineshape parameter is larger. The plateau extending from approximately 150K to 200K which is apparent in the present data suggests saturation trapping in a defect shallower than that noticed below 150K. The onset of a decline from this plateau as the temperature is increased beyond 200K suggests, in agreement with [132,170], that these defects may be dislocations which have survived the short annealing period immediately subsequent to the deformation. The apparent absence of such dislocations in either of [165,168] is thought to be a reflection of the increased recrystallisation time allowed in these particular studies, [165]360K, [168] 375K.

In so far as the lineshape parameter is seen to decrease with increasing temperature from 4.2K to 150K, the present data are in agreement with [165,132,168]. The non-identity of the temperature ranges presumed to characterise this effect and the presence of a higher trapping background underlying this effect in the present work is thought to reflect variations in specimen treatment particularly in respect of annealing. The annealing treatment afforded the specimen in [132] is however similar to that employed in the present study, nevertheless the extent of the compressions employed were significantly different. It is thought that the distinct nature of the resultant lineshape parameter temperature dependences observed is a reflection of these deformation details and of differences in stock materials.

8.4: CONVOLUTION ANALYSIS

Several specimen spectra arising from this study of polycrystalline cadmium were analysed by means of the convolution technique discussed in section 5.3.2 . The convolution model employed was that of equations 5.10 with the inclusion of a Gaussian function to describe the positron zero-point motion. A plot of the reduced chi-squared against σ, the width of the positron broadening function, was produced for each of the considered spectra.

Four temperature regions of this study were analysed by means of this technique. For the annealed specimen, eight spectra in the low temperature(4.2-79K) region and nine spectra in the high temperature(500-582K) were studied. For the liquid nitrogen temperature deformed sample nine spectra in the low temperature range (4.2-81K) were so analysed and, for the room temperature deformed specimen, thirty-two spectra over the temperature range (4.2-300K) were studied.

8.4.1: Annealed Cadmium

Each of the eight low temperature (4.2-79K) spectra studied for this specimen indicate that $\sigma=0$ provides the optimum fit to the data. Examples of the variation of the reduced chi-squared with σ are shown in figure 8.3 for spectra recorded at 4.2K and at 79K. Given the rather large steps with which σ was varied, no great precision can be attached to this optimum value however, these results do indicate that the optimum value of σ lies between 0 and 1 and that perhaps σ is at least close to zero. No detectable temperature dependence was observed in these spectra, this is perhaps again a reflection of the large σ increments here employed. It seems unlikely on the evidence of these data that positron trapping in deep traps occurs at low temperatures in annealed specimens of polycrystalline cadmium.

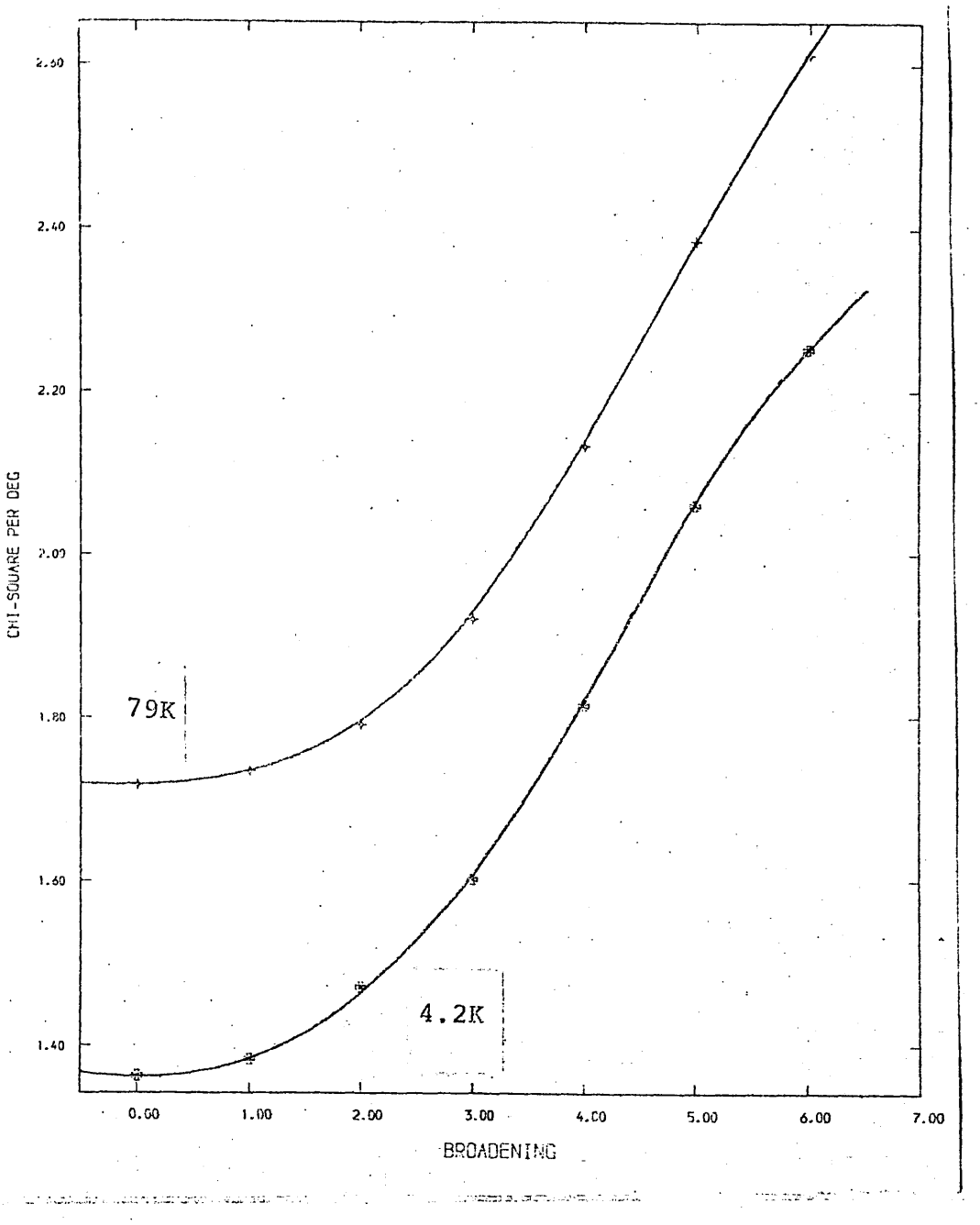

Figure 8.3: The variation of CHI-SQUARED with positron GAUSSIAN WIDTH for the low temperature region of the annealed poly-crystalline specimen of cadmium.

In the high temperature region (500-580K), nine spectra were analysed. Again a high degree of concord was exhibited between the individual reduced chi-squared versus σ relationships. Examples of those arising from spectra recorded at 500K and at 571K are illustrated in figure 8.4 . In accordance with the earlier single crystal studies, the optimum σ for the vacancy trapping region is given here as σ=4 although again with no great precision. It is felt that $\sigma \rightarrow 4$.

8.4.2: Specimen Deformed at Liquid Nitrogen Temperature

Nine spectra in the temperature region 4.2K to 81K were studied for this specimen. The reduced chi-squared versus relationships thereby obtained appear to exhibit no dependence on temperature. This is consistent with the apparent temperature independence of the lineshape parameter. However, the minima in these relationships appear to be sharper than those corresponding to vacancy trapping and appear to suggest an optimum value of σ generally larger than those of figure 8.4 . An example of the reduced chi-squared versus σ relationship for this specimen at T=4.2K is illustrated in figure 8.5 together with a specimen relationship for vacancy trapping (T=571K). Average Guassian and parabola parameters for this low temperature region are respectively GW: 21.0channels,PW: 13.6channels,parabola percentage:

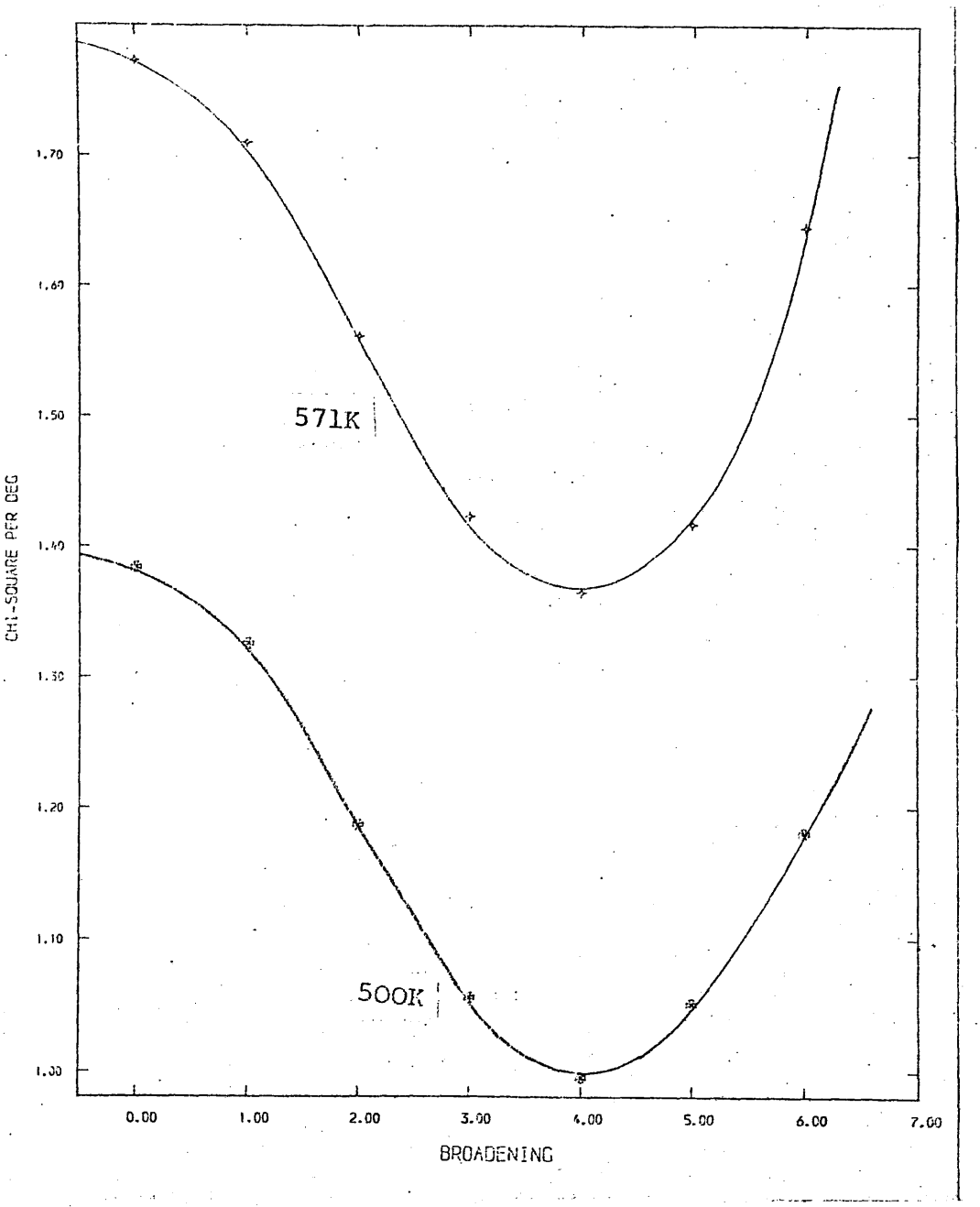

Figure 8.4: The variation of CHI-SQUARED with positron GAUSSIAN WIDTH for the high temperature region of the annealed polycrystalline specimen of cadmium.

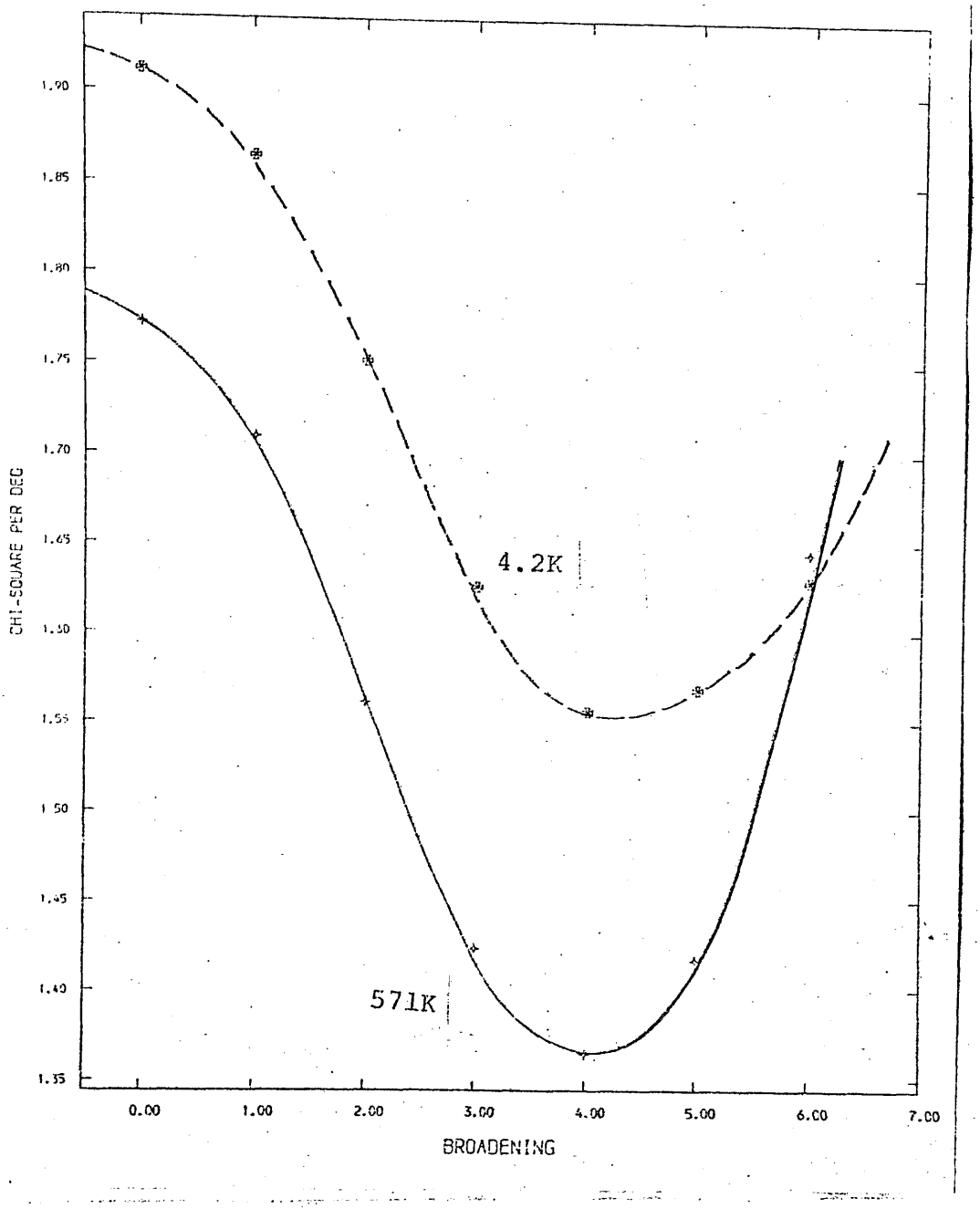

Figure 8.5: The variation of CHI-SQUARED with positron GAUSSIAN WIDTH for low temperatures of the specimen of polycrystalline cadmium deformed at liquid nitrogen temperature together with that arising from the annealed specimen at 571K.

58.3 %; and GW: 21.5channels, PW: 13.8channels, parabola percentage: 57.Ø %. The increased parabolic component observed for the liquid nitrogen temperature deformed specimen together with the suggested higher optimum values of σ, suggest that stronger positron trapping than that of vacancies obtains in the low temperature region.

8.4.3: Specimen Deformed at Room Temperature

The convolution technique was applied to spectra arising from the room temperature deformed specimen over the temperature range 4.2K to 3ØØK, in all thirty-two spectra were analysed. The resultant reduced chi-squared versus σ relationships appear to fall into three broad categories. For the low temperature region extending from 4.2K to approximately 13ØK, the minima produced are well-defined and typically correspond to σ=3. In the temperature range 14ØK-2ØØK, the relationships encompass a smaller range of chi-squared and, generally indicate that σ=2 provides the optimum fit to the data. As the temperature is raised above 2ØØK, the minima become progressively shallower and here, typical optimum values of σ are 1.5 . In figure 8.6 is illustrated a specimen reduced chi-squared versus σ relationship for a spectrum recorded at 5ØK, while in figure 8.7 spectra recorded at 159K and 259K are shown. These arise from spectra recorded at 5ØK, 159K and 259K.

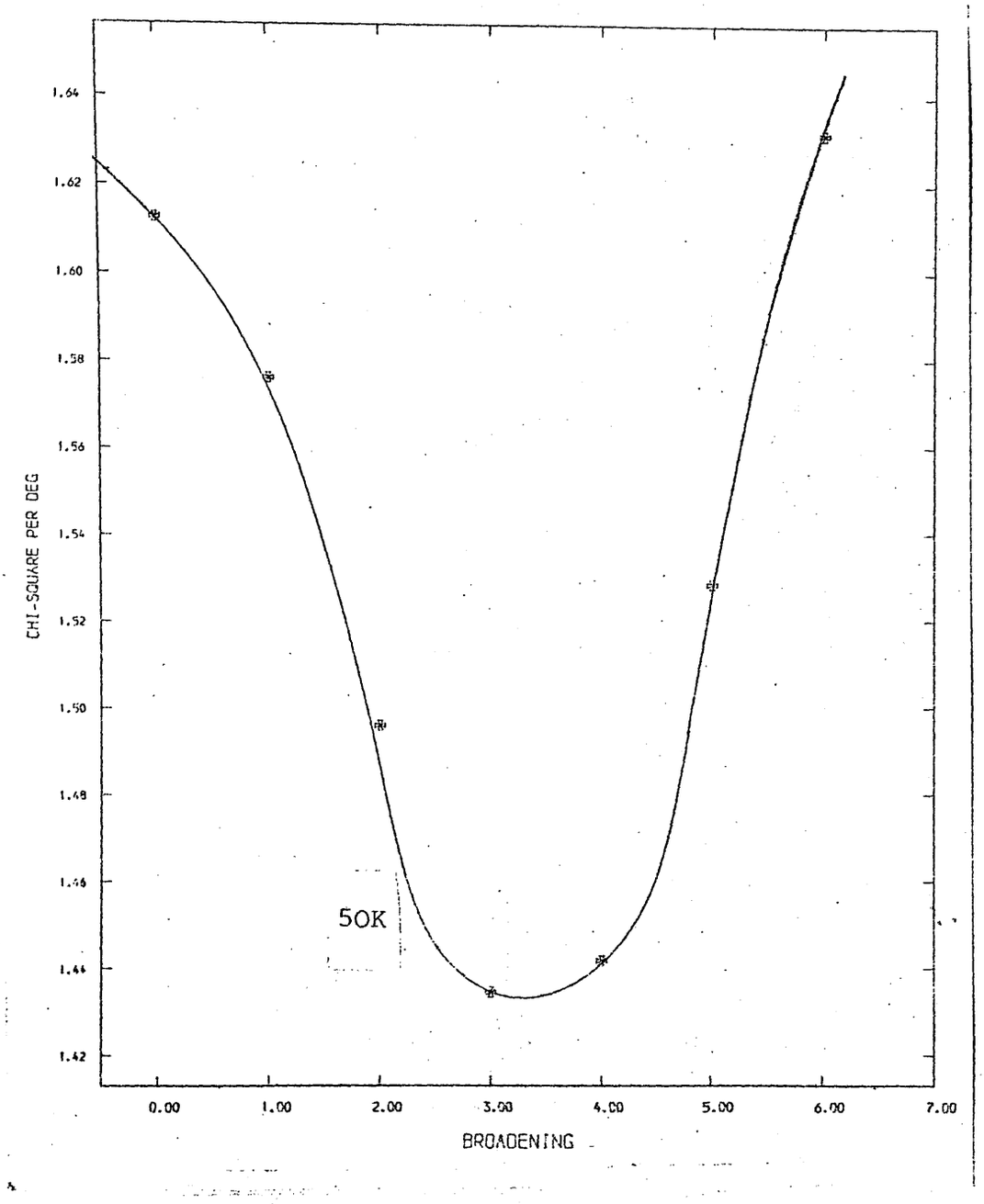

Figure 8.6: The variation of CHI-SQUARED with positron GAUSSIAN WIDTH at 50K for the specimen of polycrystalline cadmium deformed at room temperature.

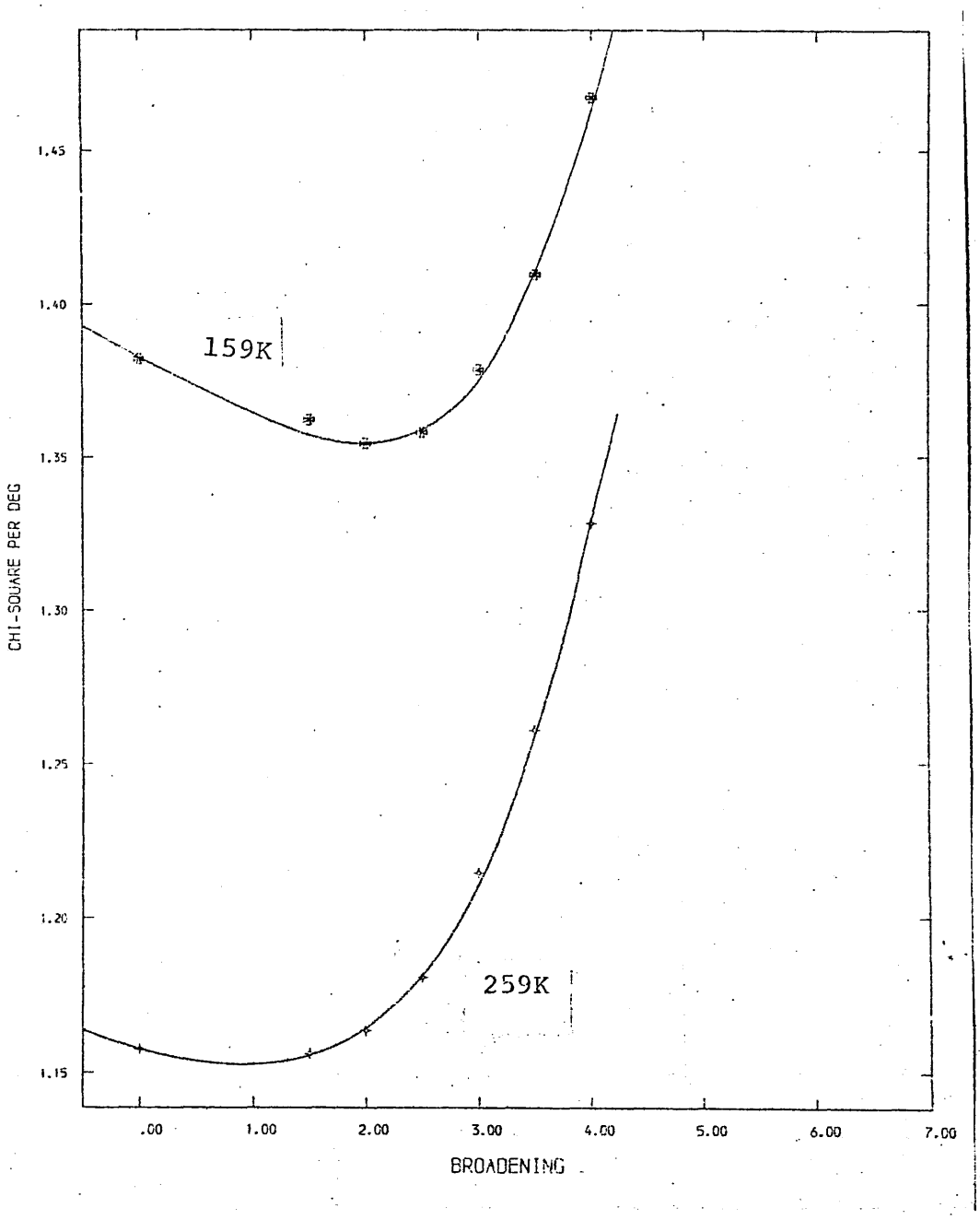

Figure 8.7: The variation of CHI-SQUARED with positron GAUSSIAN WIDTH at 159K and 259K for the specimen of polycrystalline cadmium deformed at room temperature.

The optimum value of σ obtained for the low temperature region (4.2K-130K), where it is suggested that indirect positron trapping in vacancies applies, can be seen to be smaller than that normally obtained for saturation trapping in such defects. This is consistent with the F-parameter observed in this region if it is assumed that partial trapping between vacancies and dislocations obtains at 4.2K. Employing the lineshape parameter value corresponding to the plateau (150K-200K) as that characteristic of dislocation trapping and the characteristic vacancy value from the annealed study, a trapping fraction of 30 % is suggested for vacancies at 4.2K.

The optimum value of σ obtained from the temperature region 140K-200K suggests that σ=2 applies to dislocations. As the temperature is raised above 200K, the magnitude of the positron broadening function suggested as well as the definition of the associated minimum are reduced. This indicates that the fraction of annihilations which take place from dislocations decreases at the expense of annealed state annihilations as the dislocations are thermally re-arranged.

CHAPTER 9: CONCLUDING REMARKS

In this study hitherto unpredicted evidence of the orientational dependence of the response to temperature of the positron annihilation lineshape parameter in annealed single crystal specimens of the h.c.p. metals cadmium and zinc has been presented.

It was found that, in the pre-vacancy regions of both of these metals, the temperature dependence of the lineshape parameter exhibited an orientation effect opposite to that expected on the basis of thermal expansion alone. It is felt that these findings, in respect of their pre-vacancy anisotropies, are not necessarily in conflict with the generally accepted version of the two-state trapping model as applied to the positron annihilation characteristics i.e. the "linear-rise" model. While no such orientational dependence is predicted by this model, the combination of the lattice thermal expansion anisotropy with that of the relevant phonon spectra may go some way towards its explanation.

However, the appearance of a plateau towards the top of the pre-vacancy region for the $[10\bar{1}0]$ direction of cadmium does not enhance the plausibility of this explanation. Such a pre-vacancy feature lends itself to interpretation rather to the self-trapping or to a thermal

activation model than to that of the response of the free positron to the combined linear effects of lattice vibrations and thermal expansion. While no such plateau was apparent for the hexagonal axis of cadmium nor was one detectable for either orientation of single crystal zinc, the inability of the "linear-rise" model to account for its presence for the basal plane of cadmium casts serious doubt on the appropriateness of this model.

The sensitivity of the deduced monovacancy formation enthalpies to the assumptions made in the application of the trapping model to positron annihilation data was pointed out and it was reported that distinct values of this enthalpy for single crystal cadmium arose from the fact that the orientational nature of the lineshape parameter temperature dependence required the use of two separate models. The characteristic temperature technique for this same material yielded monovacancy formation enthalpy values which were in much closer mutual agreement than those derived from the trapping models. This agreement reflects the uncertainty inherent in the characteristic temperature technique.

For the case of oriented single crystal specimens of zinc, optimum fits were provided for both the crystallographic orientations by the "linear-rise" model with $\chi = 0$. Nevertheless, a distinct orientational nature was revealed in the enthalpy values deduced from the two directions, a finding which is in clear conflict with the

thermodynamic nature of the monovacancy formation enthalpy. The application of the characteristic temperature technique to these zinc data yielded values which, within the uncertainty of the technique, are mutually consistent. In order to investigate the repeatability of the trapping model results, a further series of measurements was undertaken on the single crystal zinc specimen. The emergent enthalpies were in agreement with those previously deduced from the trapping model.

As a result of convolution analysis conducted on the spectra arising from the studies of single crystal cadmium and zinc it was concluded that the inclusion of a zero-point broadening function in the convolution model, while useful for cases where close to 100 % positron trapping obtains, does not yield clear indications of the process dominant in the pre-vacancy region. The evidence which does emerge from such a study of these two h.c.p. metals, suggests that some degree of positron localisation obtains to the pre-vacancy region and moreover that the extent of this localisation seems to be larger for the $[10\bar{1}0]$ direction of both metals. This orientational dependence in the pre-vacancy region contrasts with the case obtaining at the high and low temperature extremes. At these extremes no detectable orientational effect on the reduced chi-squared versus σ relationships was found. Further, in the low and high temperature domains the reduced chi-squared versus σ relationships are well-defined and the optimum values of σ obtained exhibit internal consistency.

An attempt was made, for the data arising from the single crystal cadmium study, to refine this convolution technique in order to effect its more successful application to cases of partial trapping. The success of this attempt was, however, limited to the temperature range from 350K to 500K and thus no significant enhancement of the understanding of the pre-vacancy processes was thereby obtained. These limitations to the success of the analysis technique are thought to reflect the shortcomings of the assumptions made as to the annihilation process in the pre-vacancy region.

It was concluded, on the basis of lineshape parameter results and of the convolution analysis, that as a result of a 33 % thickness compression on a polycrystalline specimen of cadmium at liquid nitrogen temperatures, several distinct types of positron trap are created. It is thought that annealing of these defects occur at temperatures above 120K. Evidence of the re-arrangement of dislocations was observed in the temperature region extending from 250K to 300K. Indirect positron trapping into vacancy-like defects and trapping by dislocations was proposed to explain the behaviour of the lineshape parameter for a polycrystalline specimen of cadmium compressed by 21 % at room temperature over the temperature range 4.2K to 300K.

It was concluded that the discrepencies in the monovacancy formation enthalpies which arose between distinct crystallographic directions of the h.c.p. metals cadmium and zinc are a reflection of the inability of the trapping model, as it is currently applied to explain the orientational nature of the temperature dependences here reported. This inadequacy is thought to be a reflection of the lack of understanding of the temperature dependence of positron annihilation in metals.

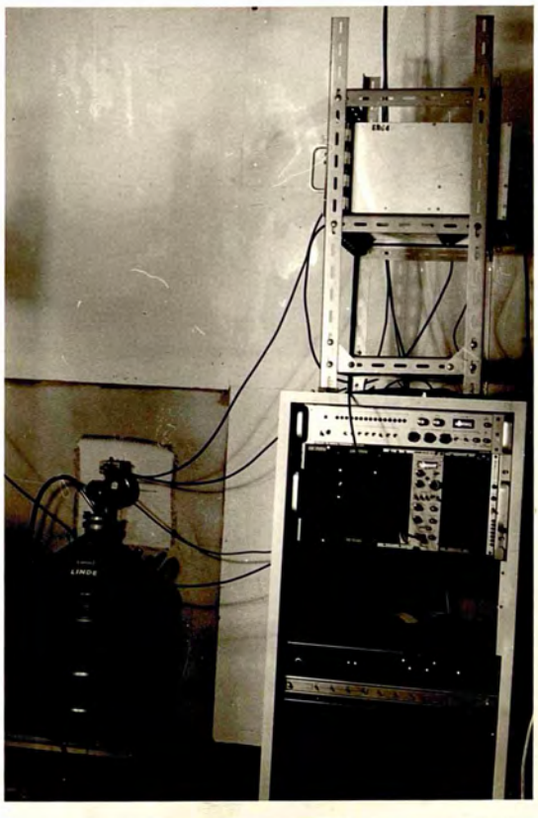

APPENDIX

As can be seen from figure 6.20 and the following two figures the values of the reduced chi-squared obtained depart significantly from unity and do not obviously indicate satisfactory fits. It was subsequently discovered that these values were produced as a result of a change in the compiler used at the University of London Computer Centre. It was found that if the minimisation routine was used in compiled form, values of chi-squared closely approaching unity were obtained. If however, the program was attached in uncompiled form by the user, as was the case during the single crystal cadmium analysis, higher values of the reduced chi-squared resulted. Close inspection of the final values of the minimisation variables produced by the two compiler variants revealed that no minimisation end-point movement had resulted and accordingly, that the parameter values corresponding to these higher chi-squared values are representative of optimum fits to the data.

BIBLIOGRAPHY

[1]P.A.M.Dirac,Proc. Camb. Phil. Soc. 26 361 (1930)

[2]C.D.Anderson,Phys. Rev., 41 405 (1932)

[3]R.Beringer,C.G.Montgomery,Phys. Rev., 61 (1942)

[4]S.de Benedetti,C.E.Cowon,W.R.Kronneker,H.Primakoff, Phys. Rev.,77 205 (1950)

[5]P.R.Wallace,Solid State Physics ed.F.Seitz,D.Turnbull (Academic Press,New York,1960) Vol.10,p1

[6]A.T.Stewart,Positron Annihilation (New York: Academic Press,1967)eds:A.T.Stewart,L.O.Roellig p17

[7]R.N.West,Positron studies of Condensed Matter (Taylor and Francis,London,1974)

[8]A.Seeger,J. Phys. F:Metal Physics, 3 248(1973)

[9]Proc. Fourth Int. Conf. on Positron Annihilation Halsingor,Denmark 1976.

[10]V.B.Berestetskii,E.M.Lifshitz,L.P.Pitaevskii,: Relativistic Quantum Theory(Pergamon,Oxford,1971)

[11]H.Weisberg,S.Berko Phys. Rev., 154 249(1967)

[12]P.Hautojarvi, A.Tamminen,P.Jauho Phys. Rev. Lett., 24 459(1970)

[13]B.T.A.McKee,A.Jost,I.K.MacKenzie Can. J. Phys., 50 415(1972)

[14]O.Ore,J.L.Powell Phys. Rev., 75 1696(1949)

[15]A.K.Akheizer,V.B.Berestetskii:Quantum Electrodynamics (Interscience Publishers, New York,1965)

[16]G.E.Lee-Whiting Phys. Rev., 91 1557(1955)

[17]S.M.Kim,A.T.Stewart,J.P.Carbotte Phys. Rev. Lett., 18 385(1967)

[18]J.P.Carbotte,H.L.Aurora Can. J. Phys., 45 387(1967)

[19]E.J.Woll,J.P.Carbotte Phys. Rev., 164 985(1967)

[20]A.Perkins,J.P.Carbotte Phys. Rev. B1 101(1970)

[21]P.Kubica,A.T.Stewart Phys. Rev. Lett., 34 852(1975)

[22]H.J.Mikeska Phys. Lett., 24 402(1967)

[23]S.M.Kim,W.L.Buyers J. Phys. F:Metal Physics, 6 L67(1976)

[24]K.P.Singh,R.N.West J. Phys. F:Metal Physics,6 L267(1976)

[25]C.J.Majumdar Phys. Rev., 149 406(1966)

[26]D.R Hamman Phys. Rev., 146 277(1966)

[27]W.Brandt,R.Paulin Phys. Rev. B15 2511(1977)

[28]W.Brandt Applied Phys., 5 1(1974)

[29]A.P.Mills Jnr.,L.Pfieffer Phys. Rev. Lett., 36 1389(1976)

[30]A.P.Mills Jnr.,L.Pfieffer Phys. Lett., 63 118(1977)

[31]B.Bergersen,E.Pajanne,P.Kubica,M.J.Stott,C.H.Hodges Sol. St.Comm., 15 1377(1977)

[32]R.E.Bell Nucl. Instrum. Methods, 55 1(1966)

[33]D.A.Gedcke,W.J.McDonald Nucl. Instrum. Methods, 58 253(1968)

[34]D.A.Gedcke,C.W.Williams:Ortec Information Sheet-High Resolution Time Spectroscopy",1 Scintillation Detectors (1968)

[35]H.R.Myllyla Nucl. Instrum. Methods, 148 267 (1978)

[36]P.Kirkegaard,M.Eldrup Computer Phys. Commun., 3 240(1972)

[37]P.Kirkegaard,M.Eldrup Computer Phys. Commun., 7 401(1974)

[38]V.H.C.Crisp,I.K.MacKenzie,R.N.West J. Phys. E 6 1191(1973)

[39]D.Knapton,B.T.A.McKee Proc. Second Int. Conf. on Positron Annihilation, Kingston, Ontario, 1971.

[40]S.Berko,J.J.Mader Applied Phys., 5 287(1975)

[41]A.T.Stewart Can. J. Phys., 35 168(1957)

[42]S.Berko,J.S.Plaskett Applied Phys., 5 287(1975)

[43]R.A.Ferrel Rev. mod. Phys., 28 308(1956)

[44]B.T.A.McKee,W.Triftshauser,A.T.Stewart Phys. Rev. Lett., 28 358(1972)

[45]W.Triftshauser,J.D.McGervey Applied Phys., 5 177(1975)

[46]R.Colombino,B.Fiscella,L.Trossi Nuovo Cim., 27B 589(1963)

[47]H.P.Hotz,J.M.Mathieson,J.P.Hurley Phys. Rev., 170 351(1968)

[48]K.Rama Reddy,R.A.Carrigan Nuovo Cim., 66B 105(1970)

[49]I.K.MacKenzie Phys. Lett.,A30 115(1969)

[50]I.K.MacKenzie,J.A.Eady,R.R.Gingerich Phys. Lett.,A33 279(1970)

[51]I.K.MacKenzie,T.W.Craig,B.T.A.McKee Phys. Lett.,A36 227(1971)

[52]K.Shizuma Nucl. Instrum. Methods, 150 447(1978)

[53]D.P.Kerr,S.Dannefaer,G.W.Dean,B.G.Hogg Can. J. Phys., 56 1453(1978)

[54]J.L.Campbell Applied Phys., 13 365(1977)

[55]C.H.Hodges Phys. Rev. Lett., 25 284(1970)

[56]A.G.Gould,R.N.West,B.G.Hogg Can. J. Phys., 50 2294(1972)

[57]P.Kubica,M.J.Stott J. Phys. F:Metal Physics, 4 1974(1969)

[58]M.J.Stott,P.Kubica Phys. Rev. B11 1(1975)

[59]M.J.Stott,R.N.West J. Phys. F:Metal Physics, 8 635(1978)

[60]C.H.Hodges,M.J.Stott Phys. Rev. B7 73(1973)

[61]H.T.Jamieson,B.T.A.McKee,A.T.Stewart Applied Phys., 4 79(1974)

[62]G.Lang,S.de Benedetti Phys. Rev., 108 257(1957)

[63]W.Brandt,J.Reinheimer Phys. Lett., A35 109(1971)

[64]P.Bhattacharyya,K.S.Singwi Phys. Rev. Lett., 29 22(1972)

[65]R.N.West Sol. St. Comm., 9 1417(1971)

[66]S.Kahana Phys. Rev., 129 1622(1963)

[67]J.P.Carbotte Phys. Rev.,155 197(1967)

[68]A.Seeger Cryst. Latt. Defects, 4 221(1973)

[69]A.S.Nowick,R.Feder Phys. Rev. B5 1238(1972)

[70]R.Feder,A.S.Nowick Phys. Rev., 109 1959(1958)

[71]R.O.Simmons,R.W.Baluffi J. appl. Phys., 31 2284(1960)

[72]A.Seeger,H.Mehrer:Vacancies and Interstitials in Metals, eds. A.Seeger,D.Schumacher,W.Schilling,J.Diehl (Amsterdam,North Holland,1970)

[73]S.Berko,J.C.Erskine Phys. Rev. Lett., 19 307(1967)

[74]I.K.MacKenzie,G.F.O.Langstroth,B.T.A.McKee,C.G.White Can. J. Phys., 42 1837(1964)

[75]I.K.MacKenzie,T.L.Khoo,A.B.McDonald,B.T.A.McKee Phys. Rev. Lett., 19 946(1967)

[76]B.Bergersen,M.J.Stott Sol. St. Comm., 7 1203(1969)

[77]D.C.Connors,R.N.West Phys. Lett. A30 24(1969)

[78]W.Brandt: Positron Annihilation (New York: Academic Press,1967) eds:A.T.Stewart,L.O.Roellig

[79]M.Bertolaccini,A.Bisi,G.Gambarini,L.Zappa J. Phys. C:Solid State Physics, 4 734(1971)

[80]P.C.Lichtenberger,C.W.Schulte,I.K.MacKenzie Applied Phys., 6 305(1975)

[81]A.Seeger Applied Phys., 7 85(1975)

[82]A.Seeger Applied Phys., 7 257(1975)

[83]A.Seeger Phys. Lett. A40 135(1972)

[84]C.H.Hodges,H.Trinkhaus Sol. St. Comm., 18 857(1976)

[85]C.H.Leung,T.McMullen,M.J.Stott J. Phys. F:Metal Physics, 6 1063(1976)

[86]J.H.Kusmiss,C.D.Esseltine,C.L.Snead Jnr.,A.N.Goland Phys. Lett. A32 175(1970)

[87]C.L.Snead Jnr.,A.N.Goland,J.H.Kusmiss,H.C.Huang,R.Meade Phys. Rev. B3 225(1971)

[88]C.H.Hodges J. Phys. F:Metal Physics, 4 L230(1974)

[89]B.Bergersen,D.W.Taylor Can. J. Phys., 52 1594(1974)

[90]T.McMullen,B.Hede J. Phys. F:Metal Physics, 5 669(1975)

[91]A.Seeger Phys. Lett. A41 267(1972)

[92]B.Bergersen,T.McMullen Sol. St. Comm., 24 421(1977)

[93]T.McMullen J. Phys. F:Metal Physics, 7 3041(1977)

[94]T.McMullen J. Phys. F:Metal Physics, 8 87(1978)

[95]D.C.Connors,V.H.C.Crisp,R.N.West J. Phys. F:Metal Physics, 1 355(1971)

[96]G.M.Hood,R.J.Schultz J. Phys. F:Metal Physics, 10 545(1980)

[97]K.Shizuma,E.Hashimoto,Y.Yoshizawa,T.Kino J. Phys. F:Metal Physics, 11 2461(1981)

[98]G.M.Hood,R.J.Schultz J. Nucl. Mat., 69-70 607(1978)

[99]P.Audit,H.M.Gilder J. Nucl. Mat., 69-70 641(1978)

[100]H.M.Gilder,D.Lazarus Phys. Rev. B11 4916(1975)

[101]S.Mantl,W.Kesternich,W.Triftshauser J. Nucl. Mat., 69-70 593(1978)

[102]M.J.Fluss,L.C.Smedskjaer,M.K.Chason,D.G.Legnini, R.W.Siegel Phys. Rev. B17 3444(1978)

[103]M.J.Stott J. Nucl. Mat., 69-70 593(1978)

[104]R.P.Gupta,R.W.Siegel Phys. Rev. Lett., 39 1212(1977)

[105]S.Nanao,K.Kuribayashi,S.Tanigawa,M.Mori,M.Doyama J. Phys. F:Metal Physics, 3 L5(1973)

[106]S.Nanao,K.Kuribayashi,S.Tanigawa,M.Doyama J. Phys. F: Metal Physics, 7 1403(1977)

[107]L.C.Smedskjaer,M.J.Fluss,R.W.Siegel,M.K.Chason,D.G. Legnini J. Phys. F:Metal Physics, 10 559(1980)

[108]P.Rice-Evans,T.Hlaing,D.B.Rees J. Phys. F:Metal Physics, 6 1079(1976)

[109]S.Nanao,K.Kuribayashi,S.Tanigawa,M.Doyama J. Phys. F: Metal Physics, 3 L225(1973)

[110]G.M.Hood,B.T.A.McKee J. Phys. F:Metal Physics, 8 1457 (1978)

[111]K.Kuribayashi,S.Tanigawa,S.Nanao,M.Doyama Sol. St. Comm., 12 1179(1973)

[112]I.K.MacKenzie,P.C.Lichtenberger Applied Phys., 9 331 (1976)

[113]R.O.Simmons,R.W.Baluffi Phys. Rev., 129 1533(1963)

[114]S.M.Kim,W.J.L.Buyers J. Phys. F:Metal Physics, 8 L1Ø3 (1978)

[115]A.Seeger Applied Phys., 4 183(1974)

[116]I.Chaglar:Positron Annihilation in Pure and Defected Metals,Ph.D. Thesis, University of London(1978)

[117]J.L.Campbell,C.W.Schulte Applied Phys., 21 19(198Ø)

[118]D.P.Kerr,P.D.Fellows,D.J.Sullivan,R.N.West Phys. Lett. A61 418(1977)

[119]I.K.MacKenzie,P.C.Lichtenberger,J.L.Campbell Can. J. Phys., 52 1389(1974)

[12Ø]P.J.Schultz,K.G.Lynn,I.K.MacKenzie,Y.C.Jean,C.L.Snead Jnr. Phys. Rev. Lett., 44 1629(198Ø)

[121]C.F.Coleman Applied Phys., 18 87(1979)

[122]D.P.Kerr,P.D.Fellows,D.J.Sullivan,R.N.West Phys. Lett. A61 418(1977)

[123]H.H.Jorch,J.L.Campbell Nucl. Instrum. Methods, 143 551 (1977)

[124]I.Chaglar,P.Rice-Evans,F.A.R.el Khangi,A.A.Berry Nucl. Instrum. Methods, 187 581(1981)

[125]C.Duawe,L.Dorikens-Vanpraet,M.Dorikens Sol. St. Comm.,11 717(1972)

[126]T.E.Jackman,P.C.Lichtenberger,C.W.Schulte Applied Phys., 5 259(1974)

[127]S.Dannefaer,D.P.Kerr Nucl. Instrum. Methods, 131 119(1975)

[128]R.N.West ,R.E.Borland,J.R.A.Cooper,N.E.Cusack Proc.Phys.Soc. 92 195(1967)

[129]J.A.Arias-Limonta,P.G.Varlashkin Phys. Rev. B1 142(1970)

[130]T.E.Jackman,C.W.Schulte,J.L.Campbell,P.C.Lichtenberger, I.K.MacKenzie,M.R.Wormold J. Phys. F:Metal Physics, 4 L1(1974)

[131]P.Hautojarvi Sol. St. Comm., 11 1049(1972)

[132]F.A.R.el Khangi:Positron Annihilation in Metals,Ph.D. Thesis, University of London(1980)

[133]P.Rice-Evans,I.Chaglar,F.A.R.el Khangi Phys. Lett. A81 480(1981)

[134]M.J.McGetrick:Resolution of Lattice Defects in Metals by Positron Annihilation,Ph.D. Thesis,University of London(1981)

[135]D.Herlach,H.Stoll,W.Trost,H.Metz,T.E.Jackman,K.Maier, H.E.Schaefer,A.Seeger Applied Phys., 12 59(1977)

[136]P.Rice-Evans,I.Chaglar,F.A.R.el Khangi,M.A.Moghimi Proc. Fifth Int. Conf. on Positron Annihilation, eds:R.R.Hasiguti,K.Fujiwara(Japanese Inst. of Metals,Sendai,Japan,1979), 9A-V-3

[137]L.C.Smedskjaer,D.G.Legnini,R.W.Siegel J. Phys. F: Metal Physics, 10 L1(1980)

[138]I.K.MacKenzie,J.Fabian Can. J. Phys., 58 1635(1980)

[139] P.Rice-Evans,I.Chaglar,F.A.R.el Khangi,M.A.Moghimi Fifth Int. Conf. on Positron Annihilation, eds:R.R.Hasiguti,K.Fujiwara(Japanese Inst. of Metals,Sendai,Japan,1979), 9A-V-3'

[140] P.Rice-Evans,I.Chaglar,F.A.R.el Khangi Phys. Rev. Lett., 40 716(1978)

[141] P.Rice-Evans,I.Chaglar,F.A.R.el Khangi,A.A.Berry Phys. Rev. Lett., 47 271(1981)

[142] L.C.Smedskjaer,M.J.Fluss,M.K.Chason,D.G.Legnini,R.W. Siegel J. Phys. F:Metal Physics, 7 1261(1977)

[143] D.E.Gray ed.American Institute of Physics Handbook (McGraw-Hill,New York 1972) 3rd edition

[144] R.N.West:Positrons in Solids(Springer-Verlag,Munich, 1979)ed.P.Huatojarvi

[145] R.Feder,A.S.Nowick Phys. Rev. B5 1244(1972)

[146] J.P.Simon,P.Vostry,J.Hillairet,V.Levy Pil. Mag., 31 145 (1975)

[147] P.Minchin,A.Meyer,W.H.Young J. Phys. F:Metal Physics, 4 2117(1974)

[148] Y.C.Jean,K.G.Lynn,A.N.Goland Phys. Rev. B23 5719(1981)

[149] W.Puff,P.Mascher,P.Kindl,H.Sormann Applied Phys., A27 257(1982)

[150] M.Hasegawa,M.J.Stott,W.H.Young J. Phys. F:Metal Physics, 9 1(1979)

[151] C.Janot,B.George Phys. Rev. B12 2212(1975)

[152] N.W.Ashcroft,N.D.Mermin:Solid State Physics(Holt,Reinhart and Winston, New York,1976)

[153]C.Kittel:Introduction to Solid State Physics(Wiley, New York,1976) 5th edition

[154]O.Mogensen,K,Petersen Phys. Lett. A30 542(1969)

[155]G.Kontrym-Sznajd,H.Stachowiak Applied Phys., 5 361(1975)

[156]C.J.Smithells:Metals Reference Book (Butterworths, London,1962)3rd edition Voll,p225

[157]L.Granatelli,K.G.Lynn,J.C.Bilello Phys. Rev. B25 3073(1982)

[158]G.Borgonovi,G.Cagliotti,J.J.Antal Phys. Rev., 132 683(1963)

[159]J.P.Simon,P.Vostry,J.Hillairet,P.Vajda Phys. Stat. Sol. B64 277(1974)

[160]H.M.Gilder,G.N.Wallmark Phys. Rev., 182 771(1969)

[161]D.Schumacher:Vacancies and Interstitials in Metals, eds. A.Seeger,D.Schumacher,W.Schilling,J.Diehl (Amsterdam,North Holland,1970)

[162]M.I.Current,H.M.Gilder Phys. Rev. B16 2386(1977)

[163]R.Balzer,H.Sigvaldson J. Phys. F:Metal Physics, 9 171(1979)

[164]M.Doyama,R.R.Hasiguti Cryst. Latt. Defects, 4 139(1973)

[165]P.C.Lichtenberger:Annihilation Spectroscopy of Defected Metals using Germanium Detectors,Ph.D. Thesis, University of Waterloo(1974).

[166]G.Faraci,E.Turrisi Nuovo Cim., 58B 308(1968)

[167]J.Jackman private comm.

[168]S.Kupca,B.G.Hogg,D.P.Kerr Phys. Lett.,A77 281(1980)

[169]I.K.MacKenzie Phys. Rev. B16 4705(1977)

[170]J.V.Sharp,A.Mitchell,J.W.Christian Acta Met. 13
965(1965)